Quantification of Red Blood Cell Adhesion using Holographic Optical Tweezers and Single Cell Force Spectroscopy

Dissertation
zur Erlangung des Grades
des Doktors der Naturwissenschaften
der Naturwissenschaftlich-Technischen Fakultät II
-Physik und Mechatronik-
der Universität des Saarlandes

von

Patrick Steffen

Saarbrücken

2012

Tag des Kolloquiums: 17.09.2012

Dekan: Prof. Dr. Helmut Seidel

Mitglieder des Prüfungsausschusses:

Vorsitzender: Prof. Dr.-Ing. Michael Möller
1. Berichterstatter: Prof. Dr. Christian Wagner
2. Berichterstatter: apl. Prof. Dr. Ingolf Bernhardt
3. Berichterstatter: Dr. Chaouqi Misbah
Akademischer Mitarbeiter: Dr. Martin Straub

Abstract

In this work the adhesion processes of red blood cells are investigated by means of a combined approach of holographic optical tweezers and microfluidics and are quantified by means of single cell force spectroscopy. In general, there are two different mechanisms that trigger red blood cells to aggregate: specific aggregation after stimulation with certain messengers and non-specific aggregation due to the presence of surrounding macromolecules. Both mechanisms are investigated in this work.
The former occurs during blood coagulation in which a released messenger, lysophophatidic acid, triggers the red blood cells to aggregate. Holographic optical tweezers and microfluidics resolved key features of this adhesion process. Single-cell force spectroscopy quantified the occurring adhesion process to amount to 100 pN. With this value the adhesion mechanism is identified to be of importance in the later stages of blood coagulation and thrombosis and supports the assumption that red blood cells actively participate in thrombus solidification.
The second investigated aggregation process is caused by macromolecules present in the blood plasma. To resolve the ongoing question of whether this aggregation is caused by an absorption and resulting bridging of macromolecules (bridging model) or by an osmotic pressure of the surrounding macromolecules (depletion model), single cell force spectroscopy is utilized to measure the interaction energies and adhesion forces of two adhering cells. With this approach, an existing theory in favor of the depletion model is confirmed, resulting in the conclusion that the aggregation of red blood cells is rather depletion-induced than bridging-induced.

Kurzzusammenfassung

In dieser Arbeit werden optische Pinzetten, Microfludiken und die Methode der Einzel-Zell Spektroskopie genutzt, um zwei Adhäsions-Phänomene roter Blutzellen zu untersuchen und zu quantifizieren. Bei den untersuchten Adhäsionsarten handelt es sich zum einen um eine spezifisch ausgelöste Adhäsion einzelner Blutzellen nach Stimulation mit einem gewissen Botenstoff und eine unspezifisch auftretende Adhäsion infolge osmotischen Drucks umgebender Makro-Moleküle. Der erste Prozess findet während der Blutgerinnung statt, wenn aktivierte Blutplätchen Botenstoffe aussenden, die in der roten Blutzelle Prozesse auslösen die vermutet werden eine direkte Adhäsion der Zellen untereinander zur Folge zu haben. Mittels optischer Pinzetten und Mikrofluidiken konnte das Auftreten der Adhäsion statistisch belegt und mittels der Einzel-Zell Spektroskopie auch quantifiziert werden. Die Messungen belegen, dass sich im Mittel die Stärke der Adhäsion auf 100 pN beläuft. Dieser Wert scheint groß genug um physiologisch im späteren Verlauf der Blutgerinnung zur Stabilität des Blutgerinnsels beizutragen.
Der zweite untersuchte Adhäsions-Prozess stellt die Rouleauxbildung dar. Im statischen Blut oder bei geringen Scherraten neigen rote Blutzellen dazu lineare Aggre-

gate zu bilden die dem Abbild von Geldrollen ähneln. Die hier zugrunde liegenden Mechanismen sind bis heute nicht restlos geklärt. Es haben sich zwei Theorien entwickelt die verschiedene Ursachen für dir Rouleauxbildung postulieren. Zum einen das so genannte Bridging Modell, welches eine Absorption von Makromolekühlen in der Membran und der damit verbunden Überbrückung zu benachbarten Zellen als Ursache der Adhäsion sieht. Zum anderen das so genannte Depletion Modell, in welchem der osmotische Druck, infolge von Verarmung von Makromolekühlen als Ursache der Adhäsion angesehen wird. Es wird in dieser Arbeit die Einzel-Zell Spektroskopie verwendet um die ersten direkten Zell-Zell Adhäsionmessungen von roten Blutzellen in ihrer natrlichen, discozoiden Form durchzuführen. Die Ergebnisse der Messung stehen in sehr guter Übereinstimmung mit den aus dem Depletion Modell vorhergesagten Ergebnissen. Basierend auf diesen Ergebnissen ist eine Depletion induzierte Adhäsion der roten Blutzellen bei der Ursache der Rouleaux Bildung als am wahrscheinlichsten anzusehen.

Contents

1 Introduction

Interdisciplinary work of biology, medicine and physics have become more important over the past. Accordingly, disciplines such as biophysics or medical physics pushed themselves to the fore front. Questions involved in these areas exhibit such a large complexity that a quantitatively accurate description of the underlying physical processes required the development of modern numerical and experimental methods. One of the areas of research currently using methods provided by physics is the field of blood coagulation. Thrombosis develops in the arterial as well as in the venous circulatory system and occasionally has fatal clinical ramifications [120]. Acute arterial thrombosis is the main cause of myocardial infarction or apoplectic stroke and are therefore the reason for the most frequent causes of death in the Western World. To this day, the involved processes are not fully understood. Nonetheless, a comprehensive understanding is crucial for the development of effective medical treatments. At this present day, arterial thrombosis is treated with medication that focuses on the blood platelets (thrombocytes), whereas venous thrombosis is treated with medication that focuses on certain proteins involved in the clotting process. However, an undesirable side effect, as a direct consequence of the inhibited clotting process, is long bleeding times. In general, it is distinguished between white and red thromboses. A white thrombus consists of a polymerized fibrin mesh, a protein that is generated from fibrinogen in the blood coagulation cascade. A red thrombus (see Fig. 1.1a) additionally possesses a huge amount of red blood cells (erythrocytes), that are trapped in the fibrin mesh; a fact that is not surprising, considering the circumstance that $40 - 50\,\%$ of the blood volume consist of red blood cells. This dissertation deals with with the following question: "What if the red blood cells in a thrombus are subjected to adhesion forces among themselves?" Such aggregates have been known to exist for a long time. In static blood or at very low shear rates in the vascular system red blood cells form linear aggregates, known as rouleaux, which look similar to a stack of coins (see Fig. 1.1b). Erythrocyte aggregation is the main determinant of blood viscosity. At low shear rates large rouleaux form and cause a large viscosity. With increasing shear rates the rouleaux break and the viscosity consequently decreases (see Fig. 1.1c). The mechanism responsible for rouleaux formation still has not been fully understood yet and will also be investigated in this work in chapter 7. The adhesion process in the rouleaux formation is assumed to be completely reversible and probably does not play a significant role in the cardiovascular system. However, during

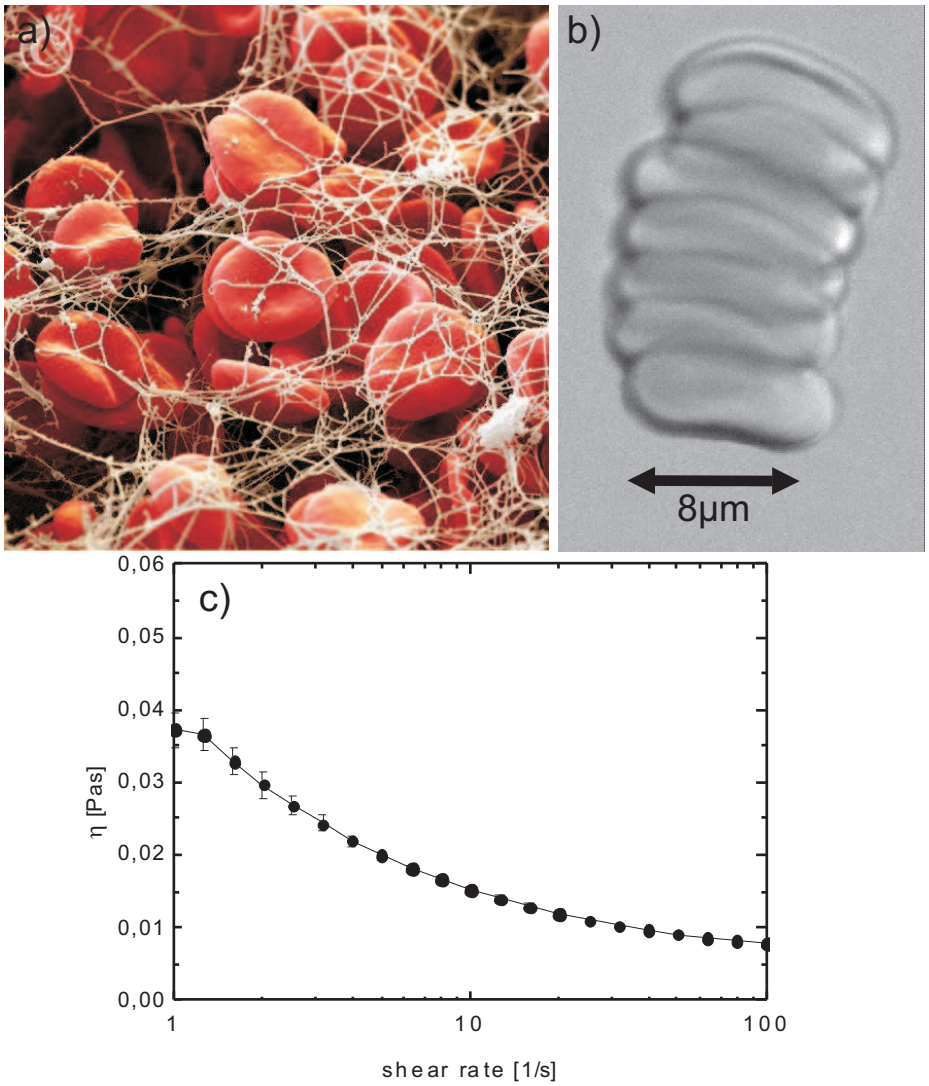

Figure 1.1: a) Colored SEM photograph of a red thrombus.(Source: Science Photo Library) b) Snapshot of a rouleaux of 7 RBCs in a dextran solution. c) Dependence of blood viscosity η on the applied shear rate. Illustration of the shear thinning properties of blood

blood coagulation and thrombus formation, an inter cellular adhesion of red blood cells would be important for both, a deeper understanding of the clotting process and for new approaches to medical treatments. Recently, Kaestner et al. [97] suggested a signaling cascade that hypothesiszed such an active adhesion of red blood cells after stimulating with physiological substances released during blood coagulation. A test

of this hypothesis is part of chapter 6. In this chapter, holographic optical tweezers were used to either validate or refute this hypothesis. The results of these measurements strongly support the signaling cascade. To value the occurring adhesion to be of significance for the in vivo situation, it has to be strong enough. Therefore, it was quantified in further experiments by means of single cell force spectroscopy. The results indicate that the inter cellular adhesion of red blood cells after stimulation is strong enough and therefore could be actively supportive for blood clot solidification.

2 Literature Survey

2.1 Lysophosphatidic Acid-Induced Adhesion of Red Blood Cells

Kaestner and Bernhardt hypothesized a Ca^{2+} influx via a non-selective cation channel (NSC) [43, 93] which is permeable to different mono and bivalent cations such as Na^{+},Ka^{+} or also Ca^{2+}. This channel is opened by physiological concentrations of prostaglandin E_2 (PGE_2) and lysophosphatidic acid (LPA) [92, 97, 98]. The influx of Ca^{2+} takes centre stage in their studies. The increased intracellular Ca^{2+}-concentration acts as a trigger for mainly two processes. Firstly, another calcium-dependent channel is opened by the increased calcium level; this channel is known as the Gardos channel [71]. Through this channel, intracellular potassium effluxes out of the cell, followed by a shrinkage of the cell [113, 109]. The second, more important, process is that due to the elevated intracellular Ca^{2+} concentration the lipid scramblase protein is activated which has a profound consequence: The breakdown of the asymmetrical lipid distribution between both leaflets [14, 185, 183, 189, 49]. In this way, the negatively charged phospholipid phosphatidylserin (PS), usually exclusively present in the inner leaflet, is transported into the outer leaflet [133]. This PS-exposure is hypothesized to take centre stage in the hypothesized adhesion of red blood cells. Christele Closse et al. [46] also showed that the PS-exposure is the key player in the adhesion of RBCs on endothelium cells. They activated the RBCs with the calcium ionophore A23187 in order to artificially increase the intracellular calcium concentration. The consecutive rise in the intracellular calcium levels resulted in an expression of PS in the outer leaflet followed by an increased adhesiveness of the RBCs on the endothelium. Manodori et al. [123] also investigated the influence of PS-exposure on the adhesiveness of RBCs on endothelium cells. Similar to Closse et al., Manodori et al. also used a calcium ionophore (A23187) to increase the intracellular Ca^{2+}-concentration and to transport the PS to the outer leaflet. In these studies the enhanced adhesiveness is believed to be of physiological significance in diseases such as the sickle cell disease.
Chung et al. [45] also hypothesized an active participation of RBCs in thrombus formation. In their studies they showed that the treatment of RBCs with lysophosphatidic acid (LPA) leads to a PS-exposure and a generation of PS-bearing micro

vesicles in a concentration-dependent manner. The smaller the concentration used, the smaller the fraction of cells that expose PS in their outer leaflet. The higher the concentration the more microvesicles release from the surface. Above a concentration of $10\,\mu M$ LPA the cells undergo a shape transformation from discocytes to echinocytes due to the loss of surface area as a direct consequence of the vesiculation.

Much work has already been conducted on the hypothesize of an active participation of RBCs in thrombus formation. However, a direct investigation of the involved adhesion forces in order to check this hypothesis is still missing. Therefore, the aim of this work is to investigate the adhesion phenomenon among RBCs on the single cellular level. Optical tweezers as well as single cell force spectroscopy are used to check this hypothesis and to quantify the occurring adhesion in terms of adhesion strength. With the quantification a statement toward physiological significance can be made.

2.2 Depletion-Induced Adhesion of Red Blood Cells

The rouleaux formation, in which RBCs form large aggregates that look similar to a stack of coins, has been known for a long time and it is already known that this aggregation is caused by macromolecules in the solution (e.g. fibrinogen or dextran). However, the deeper mechanism as to how these macromolecules induce this adhesion still remains unclear. There are two different models in order to explain the macromolecule induced adhesion of RBCs: the Bridging model and the Depletion model. Conclusive data for both theories exist, but most of the data is derived by indirect measuring methods. Buxbaum et al. [32] for instance used a dual micropipet approach to manipulate cells and spherical vesicles into position for contact. After contact, the red cells encapsulated the small vesicle to an extent that depended on the concentration of macromolecules in the solution. They calculated surface affinities with the use of a minimum free energy analysis and knowledge of the RBC membrane elastic properties. With this approach, surface affinities (i.e. interaction energies) were measured for RBCs in various solutions of dextran. These measurements were the first quantitative data on the dextran-induced adhesion of red blood cells but were also subjected to large error bars due to optical abberations and pressure fluctuations. Neu et al. [131] tried to numerically model the dextran-induced adhesion of RBCs based on this experimental data and they developed a theory for the depletion induced aggregation of RBCs. In their approach they describe the calculation of the interaction energy between RBC in polymer solutions. The model combines electrostatic repulsion due to RBC surface charge with osmotic attractive forces due to polymer depletion near the RBC surface. The effects of polymer concentration and polymer

physicochemical properties on depletion layer thickness and on polymer penetration into the RBC glycocalyx are considered for 40 to 500kDa dextran. Their simulations result into bell-shaped interaction-concentration curves. Although, the experimental data from Buxbaum et al. matches the predicted curve of Neu et al., the large error bars and the lack of data points prevent a conclusive statement of the validity of their model. Further data rely on RBC aggregation rely on indirect methods like rheology [149] or sedimentation rate experiments [150]. These methods all suffer from the indirect nature of the principle of measurement.

In this work, for the fiorst time, the interaction energy of two single RBCs is directly measured by means of single cell force spectroscopy in various concentrations of dextran 70 and dextran 150 in order to check for the validity of the numerical derived predictions for the interaction energies. By confirming or denying the theoretical curve, a step toward the unravelling of the deeper mechanism involved in macromolecule induced adhesion of RBCs can be made.

3 Optical Tweezers

As early as the 17th century, Johannes Kepler observed that the tail of a comet is always directed away from the sun. He postulated the cause for this phenomenon to be the radiation pressure of the light which was the first indication of the impact of light on matter. With the invention of the laser several centuries later, it was possible to use the pure power of light in order to trap small objects. Optical tweezers (OT) were born. Arthur Ashkin was the first to realize optical traps [5, 10, 11, 7]. These traps were levitation traps which were able to trap single particles due to radiation pressure against the gravitational force. In subsequent studies he developed counter propagating two-beam traps which illustrated the framework for todays laser based atom traps and cooling methods [44, 42].
The invention of high focusing microscope objectives facilitated the realization of a special form of optical traps that are referred to as optical tweezers (OT) [6, 8].
OT turned out to be a versatile tool for several applications in physics, chemistry and foremost biology [22, 168, 108]. They serve as an accurate measuring tool for forces between 0.1 fN [74, 142] and 100 pN [73, 115] and as a as positioning tool [166]. By means of optical tweezers microscopic objects can be trapped via a high focused laser beam. Optical tweezers are called as such because an object can not only be trapped but also be moved in a controlled manner. With these traps, dielectric particles as well as living cells can be manipulated. The outstanding advantage of optical tweezers is, especially for biological purposes, that mechanical forces are not exerted onto the cell, i.e. a contamination of the investigated cell can be excluded *a priori*. Hence, OT are minimal invasive to the manipulation of living cells.

3.1 Basics of Optical Forces

This paragraph will introduce the basics of interactions between light and matter for a deeper understanding of the acting forces in optical tweezers. Accordingly, the required physical quantities will be introduced. The Poynting vector $\vec{S}$ describes the energy flux of an electromagnetic wave. It results from the vector product of the electric field intensity vector $\vec{E}$ and the magnetic field intensity vector $\vec{B}$:

$$\vec{S} = \frac{1}{\mu_0} \vec{E} \times \vec{B} \tag{3.1}$$

in which μ_0 depicts the magnetic permeability ($\mu_0 = 1,25663706 \cdot 10^{-6}\mathrm{kg}/(\mathrm{A}^2\mathrm{s}^2)$). In case $\vec{E}$ and $\vec{B}$ are perpendicular, the direction of $\vec{S}$ equals the direction of propagation of the energy flux, while the absolute value of $\vec{S}$ equals the actual energy density of the electromagnetic wave. The intensity of an electromagnetic wave is described by the timely weighted average of the absolute value of the Ponyting vector:

$$I = \langle \left| \vec{S} \right| \rangle \tag{3.2}$$

The absolute value of momentum $\vec{p}$ of an electromagnetic wave is determined by the energy W of the wave and the speed of light c:

$$p = \frac{W}{c} \tag{3.3}$$

Therefore the force resulting from change of momentum is characterized by:

$$F = \left| \vec{F} \right| = \frac{dp}{dt} = \frac{1}{c}\frac{dW}{dt} = \frac{P}{c} \tag{3.4}$$

in which P determines the radiation power. Hence, it is possible to exert a force onto a physical object with pure power of radiation. Due to the extreme small values of the momentum of a single photon ($10^{-28}\mathrm{kgm/s}$), a tremendous amount of photons is required to produce a large enough absolute value of force, equivalent to a very high radiation intensity. The invention of the LASER (**L**ight **A**mplification by **S**timulated **E**mission of **R**adiation) provided a large enough source of photons with high intensity. In general, two different forces in optical tweezers are distinguished. There are scattering forces and gradient forces. The former always act in the direction of beam propagation and are caused by the scattering of the photons at the particle. The latter originate from the inhomogeneity of the electromagnetic field of the focused laser beam. The theoretical description of both forces will be described in more detail in the following subsections. In dependency of the size of the trapped particle and the wavelength of the used laser beam, one has to distinguish between different regimes in the theoretical description of the optical forces.

3.2 Theoretical Models

Different theories concerning the theoretical description of the optical forces acting in optical tweezers have been developed for different size regimes of the trapped particles. In the following sections, the different theories will be introduced with regard to the size of the trapped particle.

3.2.1 Ray Optics Model

The Ray Optics Model is valid for particles that are much larger than the wavelength of the used laser. According to this model "the basic operation of optical tweezers can be explained by the momentum transfer associated with the redirection of light at a dielectric interface" [64]. In this limiting case the optical forces can be described by simple Ray Optics equations [9, 8]. According to Snell's law, the light rays will be refracted at the transition of two media with different optical densities. For the angle between axis of incidence and refracted rays applies:

$$n_p sin(\alpha_p) = n_m sin(\alpha_m). \tag{3.5}$$

where n_p and n_m are the refractive indices of particle and surrounding medium, respectively. The single rays of a focused laser beam are refracted while passing through an object according to the above mentioned law. The change in direction of the momentum of light causes a change of momentum of the object according to the conservation of momentum. As a result, the produced force is proportional to the intensity of light. Figure 3.1 shows a sketch of the optical forces produced by a laser laser beam passing through a spherical particle. In case the refractive index of the particle exceeds the refractive index of the surrounding medium ($n_p > n_m$), the addition of all partial momenta and Newton's 2nd law yield a returning force directed towards the greatest intensity gradient; i.e. towards the focal point of the objective. Objects in the range of influence of the laser beam will be dragged towards the focal point of the objective, no matter what their relative position to the focal point might be. In case the refractive index of the particle is less than the refractive index of the surrounding medium ($n_p < n_m$) all particles will be pushed out of the focus. In this case, no stable trap is generated. i.e. it is an inevitable condition that the trapped particle has a larger refractive index compared to the surrounding solution. Taking a closer look at the ray profile of the used laser beam, one will see that it has a Gaussian shape with high intensity in the centre and diminishing intensity going towards the borders. When a particle is trapped in such an intensity profile, the photons at the border of the Gaussian profile will mainly produce the gradient force since they hit the particle under a certain angle, different from zero. The photons from the centre of the beam will mainly produce a scattering force, because they hit the particle under an angle of zero degrees, resulting in no change of the direction of the momentum. Some photons will be backscattered which results in a high scattering force on the particle. In order to produce a strong trap, strategies have to be developed to reduce the scattering force and to increase the gradient forces. One way to increase the gradient force is to expand the beam to overfill the back aperture of the used objective (see Figure 3.2). By doing so the intensity difference between border and center will be less, although

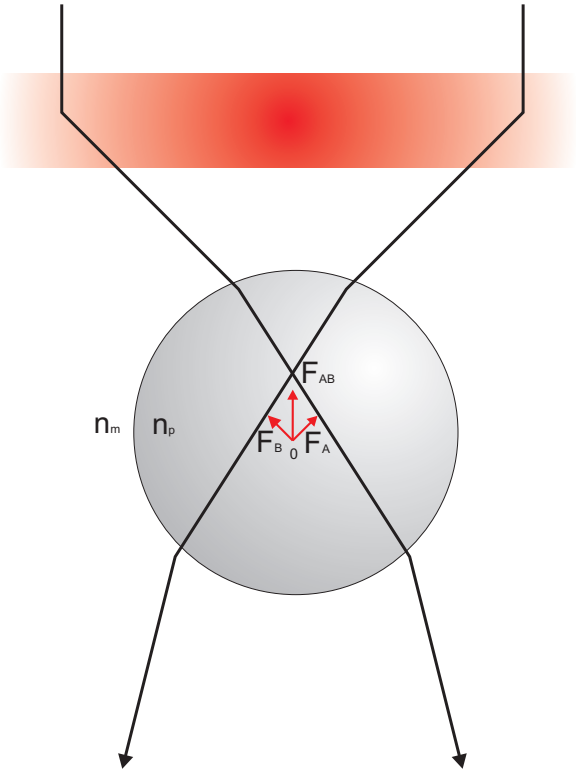

Figure 3.1: Optical forces acting on a particle (refractive index n_P) trapped in a solution (refractive index n_m) with optical tweezers. The Gaussian distributed rays A and B are first focused by an objective and refracted while passing through a transparent particle. The refraction of rays causes a change of the momentum of the photons. Due to conservation of momentum, these changes of momentum of the photons have to be compensated by the particle, whose momentum changes in the opposite direction. According to Newtons 2nd law, a net force F_{AB} towards the focal point of the objective results from the superposition of the forces F_A and F_B.

this method requires higher laser powers since power is lost due to the overfilling. A different approach is to use a ray profile that has zero intensity at the center and maximum intensity at the border. Such an intensity profile is called a "Doughnut" profile. Taking multiple reflections into account, a possible beam course is illustrated in Figure 3.3.

R and T determine the Fresnel coefficients for reflection and transmission. The arising force due to this multiple reflections can only be developed in a row. According to [9] gradient force sums up to:

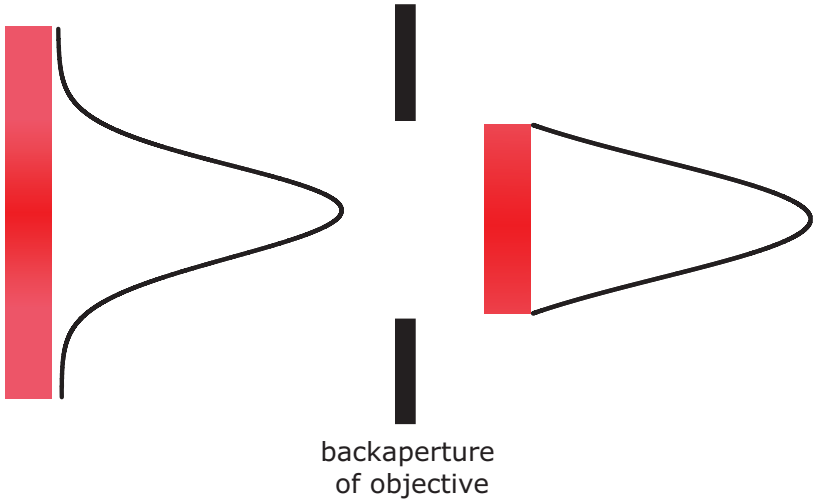

Figure 3.2: Overfilling of the back aperture in order to increase the influence of the rays at the boundaries of the laser to increase the gradient forces.

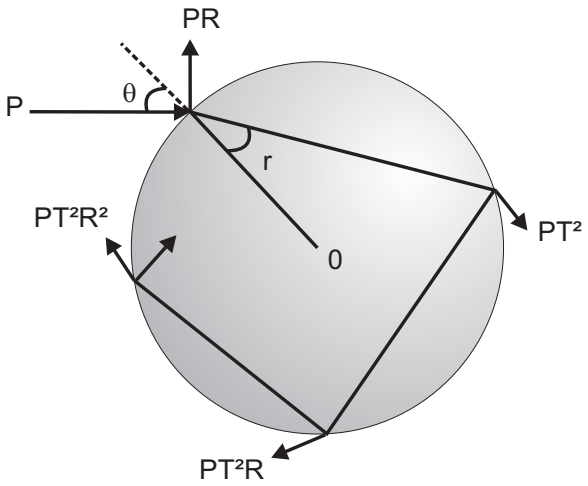

Figure 3.3: Multiple reflections inside a particle result in different reflection and transmission coefficients.

$$F_G = \frac{nP}{c}[Rsin(2\theta) - \frac{T^2(sin(2\theta - 2r) + Rsin(2\theta))}{1 + R^2 + 2Rcos(2r)}] \tag{3.6}$$

while the scattering force results in:

$$F_G = \frac{nP}{c}[1 + Rcos(2\theta)) - \frac{T^2(cos(2\theta - 2r) + Rcos(2\theta))}{1 + R^2 + 2Rcos(2r)}] \tag{3.7}$$

Here, n determines the refractive index of the particle, P the laser power and r the radius of the particle. This formula can be reduced by introducing a quality factor Q (which essentially is the bracket term), which gives:

$$F = Q\frac{P}{c} \tag{3.8}$$

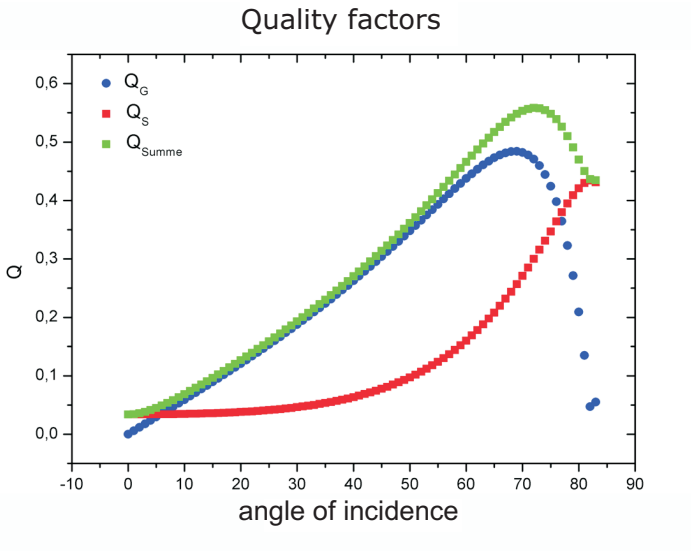

Figure 3.4: Quality factors Q_G, G_S and Q_{Sum} of the gradient, scattering and complete force in dependence of the angle of incidence.

Thus, in principle it is possible to deduce the acting forces of an optical trap with simple ray optics. Taking a closer look at the quality factor Q, the need for an objective with high numerical aperture is obvious. In Fig. 3.4 the quality factors of gradient and scattering forces are plotted against the angle of incidence of the laser beam. A maximum of quality is reached with an angle of incidence of about 70°. This implies that a maximum gradient force (i.e. the strongest optical trap) is reached with an angle of incidence of 70°. Only objectives with high numerical apertures provide such a strong focusing and are consequently used to built an optical trap.

3.2.2 Electromagnetic Field Model

In case of small object diameters, where the diameter of the object is smaller than the wavelength of the laser beam ($d << \lambda$), the mode of operation of optical tweezers is explained as follows [176, 51]. In this scenario, a dielectric particle can be seen as a punctual dipole [78]. Furthermore, as pointed out in the introduction, two different forces act on the particle, the scattering force and the gradient force. In this regime simple formulas can be found to calculate these forces. The scattering force results from the scattering of the photons on the spherical particle. The particle itself has a scattering cross section in dependence of radius r, relative refraction index $m = \frac{n_p}{n_m}$ and wavelength of the laser beam [8]:

$$\sigma_s = \frac{128\pi^5 r^6}{3\lambda^4}(\frac{m^2-1}{m^2+2})^2 \tag{3.9}$$

Fractions of photons get scattered by entering and exiting the particle [8]. Hence, a momentum transfer from photons to particle takes place. With the cross section area σ_s of the particle the scattering force arises to:

$$F_{scat} = \frac{\sigma_s n_m}{c}\langle\vec{S}\rangle \tag{3.10}$$

The scattering force acts in the direction of beam propagation and consequently destabilizes the optical trap. For this reason optical tweezers would only work limited with a scattering force only. Actually, the first realizations of optical trap were so-called levitation traps [5, 10, 11, 7] in which the counter-balancing force to the scattering force was gravity. This kind of optical trap had severe disadvantages and hence needed to be advanced. It was Arthur Ashkin who first developed optical tweezers that used the gradient force as counter-balancing force. The laser beam has a Gaussian shape in the x and the y direction, therefore it exhibits a gradient in the x and the y direction. On top of that, the laser beam is focused very steeply via an objective of high numerical aperture, resulting in a large gradient in z-direction in the region of the focal point of the objective. A dielectric particle exhibits a polarisability α:

$$\alpha = n_m^2 r^3(\frac{m^2-1}{m^2+2}) \tag{3.11}$$

This polarisability is the measure of the change in a molecules' electron distribution in response to an applied electric field $\vec{E}$. The inhomogeneity of the electric field in the laser beam induces a dipole moment in the dielectric particle. An electric dipole set into an inhomogeneous electric field will not only orientated towards the region of highest intensity, but also be dragged towards it (see Fig. 3.5). This is because one pole of the dipole is closer to the region of highest intensity than the other pole,

therefore sensing a stronger electric field. This explains that the direction of the the gradient force is towards the focal point of the objective, since there is the point of maximum field intensity. With a given polarisability α the gradient force amount to:

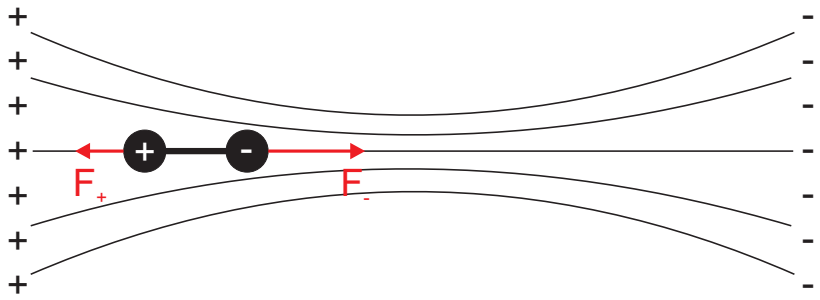

Figure 3.5: Dipole in an inhomogeneous electric field. The minus pole of the dipole is closer to the region of highest intensity than the plus pole and therefore is sensing a stronger electric field. Consequently, the attractive force on the minus pole exceeds the repulsing force on the plus pole, resulting in a net force on the dipole directed towards the point of highest field intensity.

$$\vec{F}_{grad} = \frac{\alpha}{2}\vec{\nabla}\langle\vec{E}^2\rangle \tag{3.12}$$

As pointed out earlier, the scattering force and the gradient force are opponent forces which only result in a stable optical trap when the gradient force exceeds the scattering force. Since the gradient force directly depends on the degree of focusing (the stronger the focusing the larger the gradient force) the need for an objective of high numerical aperture, again, is obvious.

3.2.3 Intermediate Regime

When the particle diameter and the used laser wavelength are comparable, both aforementioned theoretical descriptions fail to explain the occurring radiation forces. The polarization of the particle is no longer homogeneous and therefore the theory of Rayleigh needs to be corrected by higher order terms [151, 152, 153] or dipole-dipole coupling [35, 36]. These corrections exhibit a large complexity, and thus, are not discussed in this dissertation. The interested reader however, is referred to the aforementioned literature.

3.3 Holographic Optical Tweezers

Holographic optical tweezers use computer-generated holograms to create arbitrary configurations of single-beam optical traps useful for capturing, moving and transforming objects. By a combination of beam-splitting, mode forming, and adaptive wavefront correction, holographic traps can exert precisely specified and characterized forces on objects ranging in size from a few nanometres to hundreds of micrometres. With nanometre-scale spatial resolution and real-time reconfigurability, holographic optical traps offer extraordinary access to the microscopic world and have already found applications in fundamental research and industrial applications.

3.3.1 Holography

Light, aside from its frequency that determines its colour, possesses further important parameters: The amplitude and the phase. In normal photography, one is exclusively restricted to recording the amplitude, which is easily assembled over the intensity of light. Therefore, the information about the phase, and with it the information about the three-dimensionality of the object, is lost. In contrast, holography records the amplitude, as well as the phase information about an object. The phase information is not as easily accessible as the amplitude and requires a specific recording process (see Fig. 3.6a), in which the object is illuminated with a coherent light source and the reflected light from the object is subsequently overlayed with a reference beam that has not hit the object. The produced interference pattern is recorded onto a photo plate. In the reconstruction process (see Fig. 3.6b) the photo plate is illuminated with the same coherent light as in the recording process. In this way a three-dimensional picture of the object arises: a so-called hologram. The key difference to normal photography is the storing of the information about the phase of an object. The control over the phase of a light beam is crucial for the development of holographic optical tweezers in which holograms are used to display desired three dimensional images of optical traps into the specimen chamber. In this particular setup only the phase holograms were used in which only the phase of the laser beam is modified and not its amplitude.

3.3.2 Phase-Modulation

Central to the hologram generation and with this the generation of multiple optical traps is the so-called phase-modulation. This phase modulation is achieved with a so-called phase modulator and it resembles the above described photo plate and generates the interference pattern of an recorded object. It consists of liquid crystals, whose optical attributes can be controlled over the applied voltage. The technical details

are described in chapter 5.1.3. The basic idea of holographic optical tweezers is to generate a phase pattern on the phase modulator in such a way that after illumination with a laser beam a desired pattern of optical traps emerge in the focal plane of the

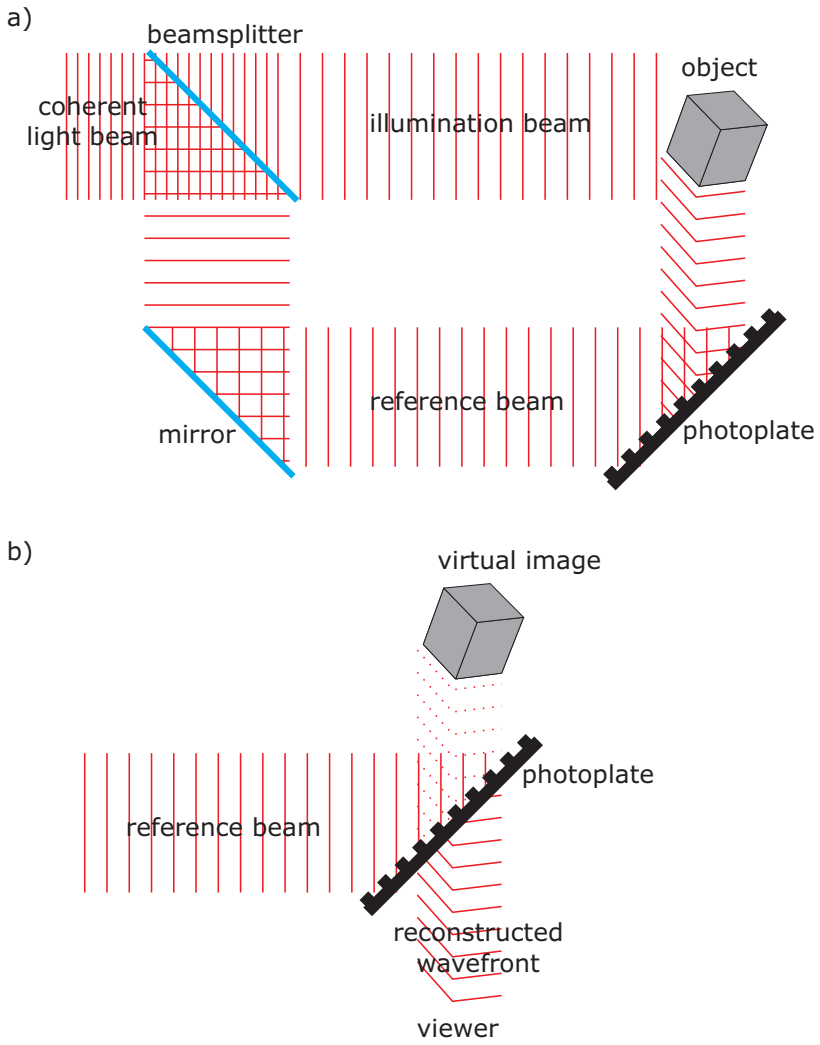

Figure 3.6: a) Hologram-recording: A coherent light beam is separated into two beams. One of them (illumination beam) is directed to the object and the reflected beams from the object are directed to a photo plate where they interfere with the second beam (reference beam). The interference pattern is saved on the photo plate accordingly. b) After illumination of the photo plate with the same wavelength as in the recording process a three dimensional picture of the recorded object develops.

objective. Fig. 3.7 shows examples of generated interference patterns applied onto the phase modulator and its corresponding imaged optical traps in the focal plane of the objective. As mentioned above the modification of the laser beam is a pure phase

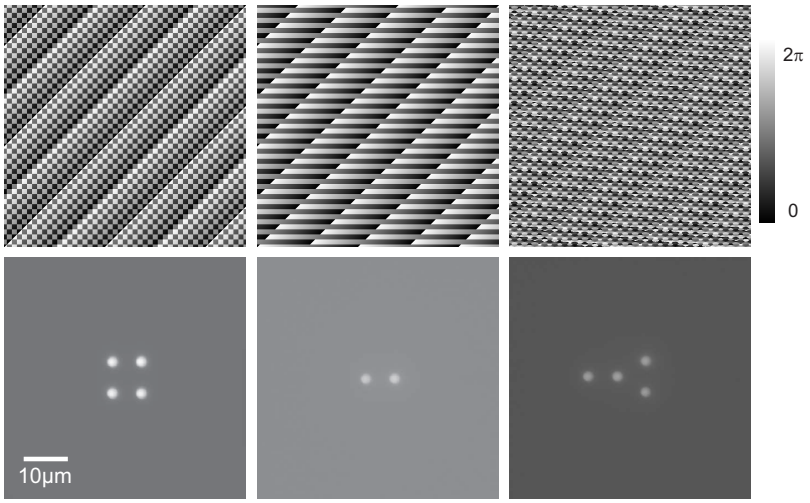

Figure 3.7: Phase holograms and their corresponding imaged optical traps in the focal plane of the objective.

modulation, i.e. the amplitude of the laser beam remains unaffected. The greatest advantage of this approach is that the applied interference patterns can be changed in real time since the phase modulator can be computer-controlled. With each applied interference pattern the orientation and number of traps can be changed in the focal plane of the objective. Therefore, a full two dimensional movability is gained and thus can be used for various applications.

3.3.3 Prism Superposition

The calculation of the interference patterns is a key point in holographic optical tweezers. There are several available algorithms with different beneficial effects, each of them suited for different applications. In this work, the interference patterns have been calculated by the use of the so-called prism-superposition algorithm. Fig. 3.8 shows the basic idea of this algorithm. When a prism with the opening angle α is inserted into the beam path of a laser, the phase of the laser beam is modified in relation to the actual thickness of the prism. Due to the fact that only a phase shift in between the interval of 0 to 2π resembles a physical difference, a large (thick) prism can be treated as a superposition of several smaller ones. As a result, the smaller prisms are only able to change phase of the laser beam with a maximum value of

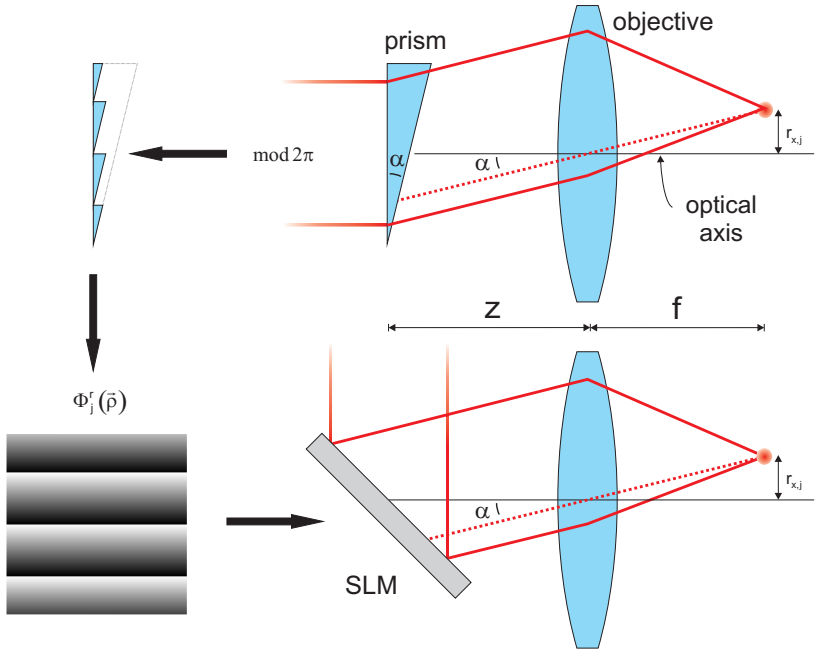

Figure 3.8: Upper left: replacement of one large prism via several smaller ones. Upper right: changed beam coarse due to an inserted prism. Lower left: example of a phase hologram. Lower right: beam coarse with phase modulator.

2π. In total the prism generates a refraction of the laser beam from its original axis. After passing the prism, the laser beam hit the objective consistently under a certain angle. This angle results in a focusing of the light that is slightly displaced from its focal point without prism. A change of the thickness and angle of the inserted prism results in a movement of the focus in the focal plane of the objective. Therefore, a two-dimensional movability of the generated trap is gained. In order to generate several optical traps, a superposition of several prisms is needed.

3.4 Calibration of Optical Tweezers

Even though optical tweezers have not been used to measure absolute forces in this work, the following section will shortly introduce the calibration of optical tweezers. Optical tweezers, realized via a laser beam, generate a harmonic potential in which a particle is trapped. The potential has the following shape:

$$U(x) = \frac{1}{2}kx^2 \tag{3.13}$$

in which k determines the trap stiffness or trap strength and x gives the displacement of the particle out of the center of the trap. When using optical tweezers as a tool to measure small forces, the trap stiffness has to be determined by a calibration measurement. There are several different calibration methods in order to determine the trap stiffness as accurately as possible. Dependent on the trap strength, different calibration methods turned out to be more or less advantageous [132]. There are calibration procedures involving Brownian motion and procedures involving drag forces. The so-called viscous drag-method is one of the most common methods to determine the trap stiffness and will be discussed in more detail below. In this method, a known force is applied onto the particle, resulting in a displacement of the particle out of the trap's center. Because the applied force is known, with

$$F = kx \tag{3.14}$$

the trap stiffness can be determined by measuring the displacement of the particle out of the center of the trap. A possible kwon force is the Stokes friction:

$$F_S = 6\pi\eta r v. \tag{3.15}$$

This friction force arises when a sphere with radius r is dragged through a viscous medium (viscosity η) with the velocity v. In the calibration measurement the surrounding fluid is moved via a piezo stage and the particle remains, trapped in the optical tweezers, static. Given a laminar flow (i.e. the velocities have to be sufficiently small) the following balance of forces can be established:

$$6\pi\eta r v = kx \tag{3.16}$$

Therefore, with the knowledge of radius r, viscosity η, velocity v and displacement x of the particle the trap stiffness can be determined.

3.5 Microfluidics

A microfluidic device can be identified by the fact that it has one or more channels with at least one dimension less than 1 mm. Common fluids used in microfluidic devices include whole blood samples, bacterial cell suspensions, protein or antibody solutions and various buffers. Microfluidic devices can be used to obtain a variety of interesting measurements including molecular diffusion coefficients [99, 100], pH values [179, 121], and enzyme reaction kinetics [76, 55]. The use of microfluidic devices to conduct biomedical research and create clinically useful technologies has a number of significant advantages. Because the volume of fluids within these channels

is very small, usually several nanolitres, the amount of reagents and analytes used is quite small. This is especially significant for expensive reagents. The fabrications techniques used to construct microfluidic devices, are relatively inexpensive and are discussed in section 3.5.2.

3.5.1 Navier-Stokes Equation

The flow of a simple fluids is described by the laws of hydrodynamic. The flow of fluid through a control volume can be described by the Navier-Stokes equation. This equation can be derived from the principles of conservation of mass, momentum and energy. The conservation of mass equation states that at all times (for incompressible, steady flow) the mass entering the control volume is equal to the mass leaving the control volume,

$$\frac{\partial \rho}{\partial t} + \nabla(\rho u) = 0 \tag{3.17}$$

where ρ is the fluid density, t is time and u is the local fluid velocity. This equation is also often called the 'continuity equation' because it is based on the assumption that the fluid medium is continuous. As an analog to Newton's second law of motion, the Navier-Stokes equation states that due to the conservation of momentum the change in momentum within the control volume is equal to the sum of the forces acting on the control volume,

$$\rho(\frac{\partial}{\partial t} + u\nabla)u = -grad(p) + \rho g + \eta \Delta u \tag{3.18}$$

where p is the pressure, g the gravitational force and η the viscosity. In everyday life the quantity of fluid is such that flow velocities are "high" and viscosities are "small". In microfluidics, on the contrary, one has to deal with small fluid amounts and slow velocities. In this regime, most things simplify due to the reduction of the physical dimensions. A normalization of all length units to a unit length L as well as all time units to a unit time T leads to:

$$t = t\prime T, \qquad u = u\prime \frac{L}{T}, \qquad \nabla = \frac{\nabla\prime}{L}, \qquad p = p\prime(\frac{L}{T})^2\rho. \tag{3.19}$$

in which $t\prime$,$u\prime$ and $p\prime$ are dimensionless units. With this conversion the Navier-Stokes equation without any gravity part is transformed into [50]:

$$\frac{u\prime}{t\prime} + (u\prime\nabla\prime)u\prime = -\nabla\prime p\prime + \frac{1}{R_e}\Delta u\prime \tag{3.20}$$

with the dimensionless Reynolds number:

$$R_e = \frac{\rho L U}{\eta} \qquad with \qquad U = \frac{L}{T} \tag{3.21}$$

U has the dimension of a velocity. More precisely, U describes the mean velocity averaged over a distance L. The latter is the most relevant length scale in the fluid system. The physical meaning of R_e is obvious after extension with L^2U:

$$R_e = \frac{\rho L^3 U^2}{\eta L^2 U} = \frac{2E_{kin}}{W_{friction}} \tag{3.22}$$

The nominator gives twice the kinetic energy of a given volume L^3, traveling with velocity U, while the denominator describes the friction energy that is dissipated when the volume L^3 is moved the distance L. The Reynolds number characterizes the tendency of a fluid to behave turbulently or to behave laminarly. For every flowing system one can calculate a Reynolds number and predict a turbulent or laminar behavior. With large Reynolds numbers, inertia forces are dominant and a turbulent flow develops. However, with smaller Reynolds numbers friction forces become dominant and a laminar flow develops. In normal fluid systems (water pipes) the transition from the laminar to the turbulent regimes takes place at a Reynolds number of about 2300 [50]. Yet, this so-called critical Reynolds number cannot be treated as sharp transition point, but strongly depends on the flow geometry.
Usually, in microfluidics a rectangular channel geometry is present that requires for correction in the formula for the Reynolds number, since the above derived law was calculated for spherical channel geometries. The hydraulic diameter of

$$\frac{4A}{U} \tag{3.23}$$

where U determines the circumference and A the cross section of the channel, is used to transform the rectangular channel geometry to an equivalent spherical geometry. Therefore, the corrected Reynolds number for a rectangular channel is:

$$R_e = \frac{2\rho u b h}{\eta(b+h).} \tag{3.24}$$

The flow of a fluid through a microfluidic channel can also be characterized by this Reynolds number. With this equation the behaviour of the fluid in a microfluidic channel can be predicted, given the knowledge of the velocity and the channel dimensions. Because the dimensions of the channel will be in the µm-regime the Reynolds number will remain very small ($R_e << 1$) with any reasonable velocity. Hence, in

microfluidics almost always a laminar flow is observed. In fact, the only way of mixing is via diffusion; however, this way of mixing is a rather slow process. The equation of diffusion is given by

$$\langle y^2 \rangle = 2Dt \tag{3.25}$$

in which D is the diffusion constant, t the time and y the mean diffusion length. Taking reasonable values for the diffusion constant (e.g. $0,4\mu m^2/s$ for calcium) it can be estimated that the maximum diffusion length after 1 cm with a fluid velocity of 1 cm/s is only about 28 µm. Since the dimensions of the used microfluidic are about 200 µm the mixing due to diffusion can be neglected and can be used to produce a shapr concentration gradient inside a single channel. Interestingly, to overcome this laminar flow through the development of micro-mixing techniques is of current interest in various studies [33, 118, 72] since it resembles an obstacle for various applications of microfluidics. However, in this work the laminar flow is essential for the conducted experiments.

3.5.2 Microfluidic Design

Polydimethylsiloxane (PDMS), as an elastomer, is known for its mold-release properties and ability to replicate features down to the nanoscale and excellent elastic properties. It has come to be the most widely used material in microfluidic device fabrication due to its many advantages in fabrication ease [68], physical properties, and economy. The process outlined here and in Fig. 3.9 presumes the work is being conducted in a clean environment; the use of a clean room is not absolutely necessary except for the most demanding fabrication requirements. However, avoiding surface contamination is essential. The first step in microfluidics manufacturing an appropriate mold. In case of larger dimensions, a mechanical manufactured mold for casting the PDMS structure is sufficient. In case of smaller dimensions the usage of photolithographic methods is required to produce a mold. Typically, the mold is a negative mold, with the PDMS poured into it and filling the regions left open by the mold. The next step is to mix the fluid PDMS with a hardener agent and to fill it into the mold. After a heating period of 1 h at a temperature of 75 $°C$ the PDMS is solid and can be peeled out of the mold. In order to conduct the microfluidic device with a fluid reservoir, holes are punched into the channel as seen is Fig. 3.9c). The final step in the manufacturing process is the bonding of the microfluidic device to a glass substrate. In oder to reduce its hydrophobicity the most common approach is to expose the surface to be bonded to oxygen plasma for about 1 min. The PDMS is then placed in less than a minute on a glass substrate.
In order to investigate the adhesion of red blood cells in a time-resolved manner, a microfluidic device was designed and constructed. It has a y-shape and consists of

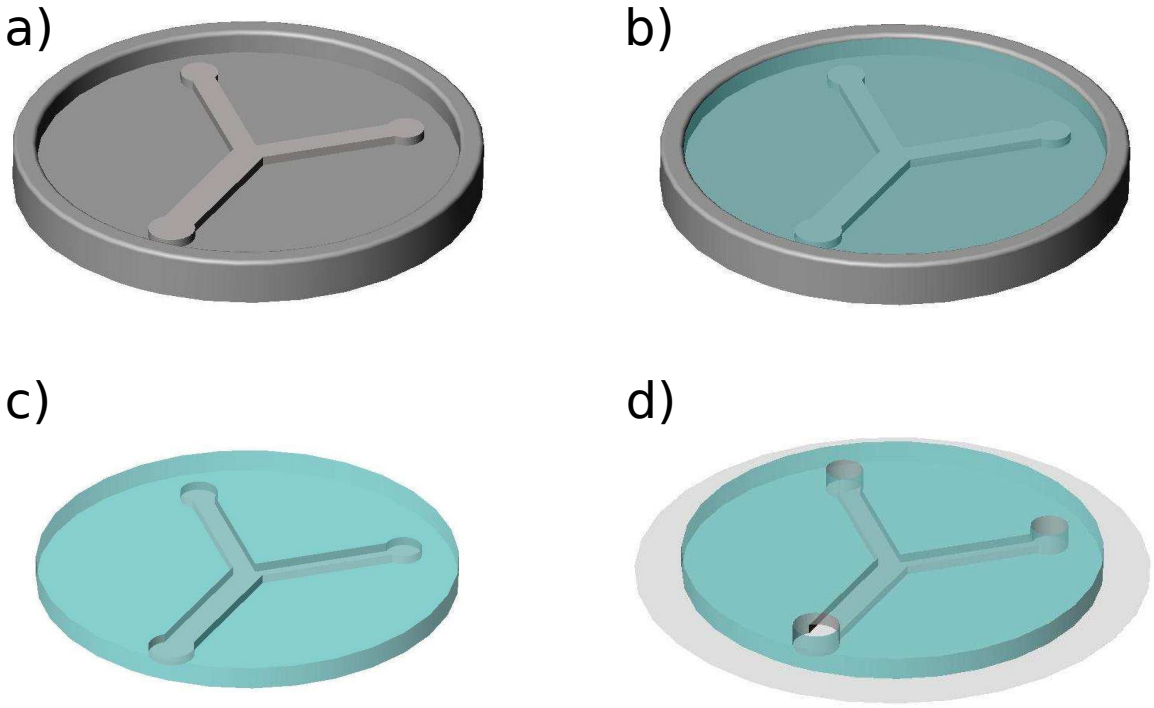

Figure 3.9: a) Mold b) Mold filled with PDMS c) PMDS with punching holes d) PDMS device bonded to a glass substrate

two inlets and one outlet (3.10a and b). The flow is driven by gravity (see Fig. 3.10d). The laminar flow and the y-shape of the microfluidic device allow for the generation of a sharp concentration gradient between the upper and lower part of the channel outlet. In Fig. 3.10c this concentration gradient is illustrated with two different dyes. With the help of optical tweezers the cells can be moved from one solution to another in a very fast and controllable manner. This approach enables the recording of the kinetics of the processes. For instance, when a cell is moved from a salt solution into a messenger containing solution the signaling processes, like calcium uptake, can be recorded.

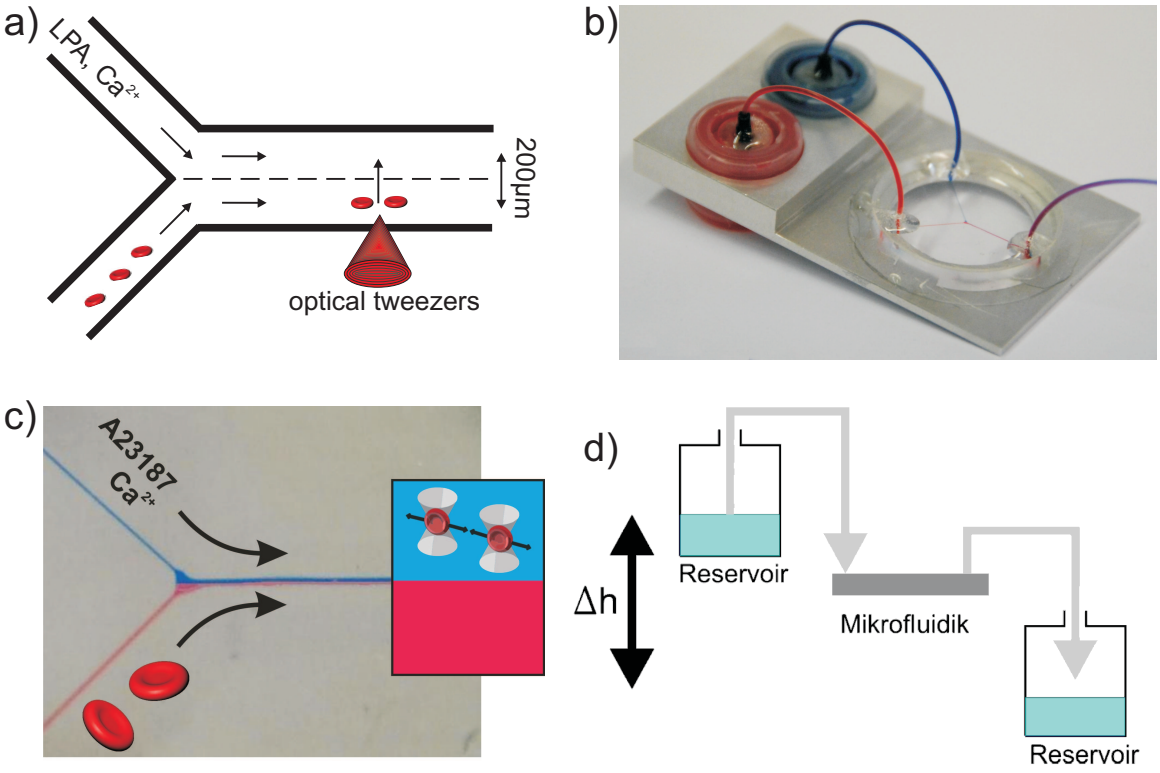

Figure 3.10: a) Sketch of the Y-shape of microfluidic device. Two fluid inlets for RBCs and stimulants. Both channels unify into one large channel in which, due to the laminar flow, a concentration gradient is established between upper and lower part of the channel.b) Picture of the microfluidic device filled with two dyes. c) Illustration of the laminar flow inside the microfluidic channel. d) Gravitational driven flow.

3.6 Summary

In this chapter the theoretical basics of the working principle of optical tweezers (OT) were introduced. Basically, optical tweezers are highly focused laser beams. The high focus is realized by an objective of high numerical aperture. Depending on the diameter d of the trapped particles three different theoretical regimes are differed. For small wavelengths ($d << \lambda$) the so-called Rayleigh theory is valid in which the particle exhibits a homogeneous polarization. This theory is based on the electromagnetic scattering theory. For large particle sizes ($d >> \lambda$), the so-called ray optics regime is valid in which the optical forces can be derived by simple ray optics. In the case of intermediate diameters a theoretical description becomes difficult. In general, in

all theories the arising forces can be divided into two groups: scattering forces and gradient forces. The scattering force acts in the direction of beam propagation and is caused by the scattering of the photons whereas the gradient force is always directed towards the centre of the used objective because there is the point of highest field intensity. Therefore, a particle can be trapped in the centre of an objective, given the gradient force exceeds the scattering force.
If the potential of the OT is harmonic, the repulsing force is linear and can be described by $F = -kx$; i.e. the optical trap acts as a Hookean spring. This fact is the most important part in most of the applications of OT, where they serve as an accurate measuring tool for very small forces. Crucial for these measurements is an accurate determination of the spring constant via a calibration measurement, that have been introduced in this chapter. The most important calibration method used in this work is the viscous drag method in which a particle is dragged through a viscous medium with a known speed. By measuring the displacement of the particle out of the centre of the trap and the velocity, the particles' diameter and the viscosity of the medium the spring constant can be calculated. After the explanation of the formation of single traps the concept of holographic optical tweezers (HOT) was introduced, a tool to create multiple optical traps by separating the laser beam into several sub-rays. First, the general concept of holography was introduced since being a crucial part in the hologram generation in HOT. It was shown how a phase-modulator creates phase holograms that influence the laser beam in such a way that after passing the microscope objective a desired number and a desired orientation of traps emerge in the focal plane of the objective. These phase holograms can be computer controlled and enable a 2-dimensional movability of the generated traps in the focal plane of the objective.
After introducing the working principles of OT and HOT, the combined approach of microfluidics and HOT were described. The basics of microfluidics were introduced as well as the particular microfludic design. The main difference in microfluidics compared to large fluid systems is that the behaviour of the flow changes significantly. While large fluid systems are dominated by inertia and consequently arising turbulences, microfluidics are dominated by friction forces and laminar flows. The particular shape and properties of the microfluidic used in this work have been introduced and its advantages and disadvantages were discussed.

After introducing OT, HOT and microfluidics, the next chapter will introduce Single Cell Force Spectroscopy, the second used method in this work.

4 Single Cell Force Spectroscopy

A broad spectrum of biological processes requires controlled cell adhesion, including assembly of tissues and the nervous system, cellular communication, inflammation and wound healing, tumor metastasis, cell culturing, and viral and bacterial infection. Despite being well-informed about cell adhesion in general, many questions remain obscure due to its multiple facets and complexity. In the past, the strength of the adhesion of a cell to a substrate was studied using simple washing assays [104]. Washing assays have proven to be a versatile and useful tool, but they fail to quantify the occurring adhesion forces. In order to estimate the force to which cells are subjected, various assays that are based on the regulated flow of media have been implemented, including spinning-disk [70] and flow-chamber [101, 15] assays. Unfortunately, the shear force that is exerted on the cells in these assays strongly depends on parameters such as cell shape, cell size and how the cell is attached to the substrate. Therefore shear force can only be estimated. For a more controlled and quantitative approach to measurements of adhesion strength, single-cell methods are needed. In the past, mainly three different approaches to single-cell force spectroscopy (SCFS) assays have been developed to measure the strength of cell adhesion down to single-molecule level. In all three assays optical microscopes are used to observe the cell while force measurements are made, but differ in how cells are manipulated and how forces are determined. The oldest method uses micro pipettes to grab cells. The detachment force is measured using a bio-membrane force probe, which can gauge force between 10^{-2} pN and 100 pN [61]. The bio-membrane force apparatus is a pressurized red blood cell and the force is measured determining the deflection of the membrane. A second approach also uses a pipette to hold a cell while the strength of interactions between the cell and a functionalized bead are determined using optical tweezers. The laser trap allows three dimensional positioning of the bead with nanometre precision and force measurement from 10^{-2} pN to 200 pN [115]. In the third method a cell is attached to a cantilever of an atomic force microscope (Fig. 4.1a)). By combining atomic force microscopy (AFM) and optical microscopy, cells can be positioned in order for cellular interactions to be assessed at a given location on a functionalized surface, tissue or on another cell [17]. The deflection of the cantilever is utilized to measure interaction forces. Among SCFS approaches, the AFM-based technique allows for the widest practical force range, from 10 pN to 10^6 pN.

4.1 SCFS Setup and Experimentation

The basic experimental AFM-type set-up for SCFS is rather straightforward. An AFM that is equipped with a fluid chamber allows measurements to be made in aqueous environments under controlled temperatures. Suspended cells are added to the fluid chamber and allowed to settle. Thereafter, a single cell is captured by gently pressing a functionalized AFM cantilever onto it. This transforms the living cell into a probe which is brought into contact with functionalized surfaces or other cells at a set point force and for a specific contact time. Subsequently, the cantilever is withdrawn at a constant speed detaching the cell from its adhesion place. During the separation process, the cantilever deflection, which is proportional to the vertical force that exists between the cell and substrate, is recorded in a force-distance curve (Fig. 4.1b). This curve provides the information about the adhesion process. The challenge, however, lies in interpreting these curves because various specific, as well as unspecific adhesion processes, can occur simultaneously.

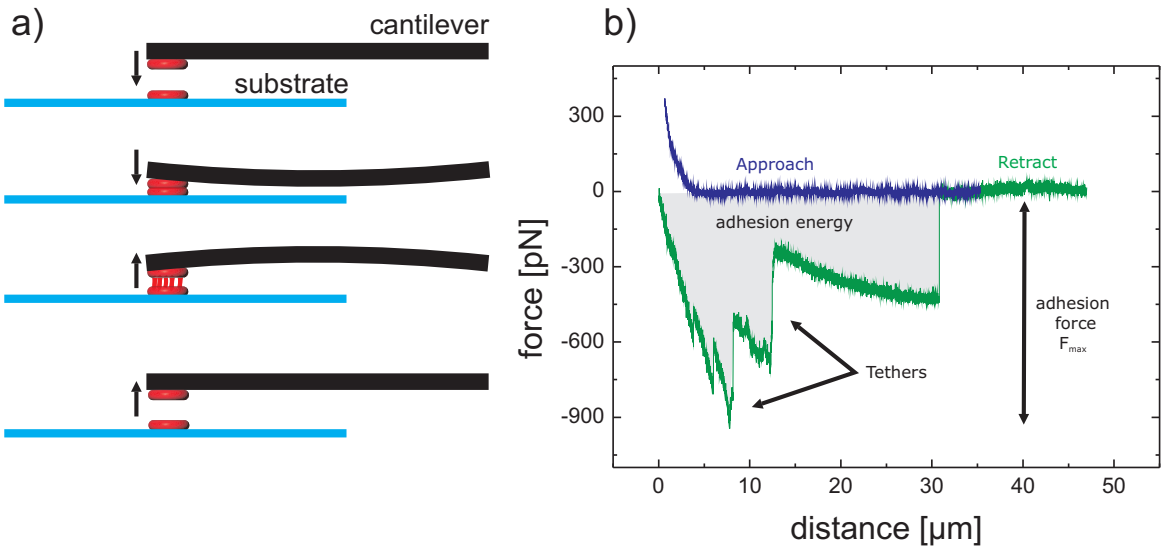

Figure 4.1: a) Sketch of the working principle of SCFS. b) Example of a force distance curve.

4.1.1 Interpretation of Cell-Adhesion Signals

The detachment of a cell from a substrate or another cell is described by the force-distance retraction curve (green curve in Fig. 4.1b). During the initial phase, the retraction of the cantilever inverts the force that is acting on the cell from pushing

to pulling. As the overall pulling force increases forces that are acting at individual cell-cell adhesion points increase. If many adhesion points act together, the applied detachment force will be sufficiently enough to mechanically deform the cell cortex. For very flexible cells (i.e. red blood cells) this deformation can be significant. The binding strengths of the receptors or adhesion points, as well as their number and geometric placement, determine at what force the cell will start to detach. The largest adhesion force that is recorded, called the maximum unbinding force F_{max}, represents the maximum strength of cell substrate or cell-cell binding. The work that is required to detach the cells can also be used to describe the adhesion strength of the cell. It is computed from the area that is enclosed by the retraction forcedistance curve (Fig. 4.1b). It is therefore important to consider that the detachment force is a composition of many different properties of the cell [20]. These include cell elasticity, membrane tension, membrane properties and cell geometry. After the cell starts to detach from the substrate, individual force steps can be seen (Fig. 4.1b). During this phase, the receptor or focal binding point can detach from the cell membrane and is pulled away from the cell membrane. Another phenomenon that leads to a stepwise release in the force distance curve is the so-called tether formation, in which a membrane tube is pulled out of the membrane. In cell-cell adhesion experiments with highly flexible cells and occurring tether formation, retraction distances that approach 100 µm are required to fully separate cells [18, 146, 172]. The CellHesion module from JPK-Instruments is the only available commercial atomic force microscope that is capable of measuring spectroscopic with a maximum pulling length of 100 µm. Because RBCs are known for their extraordinary flexibility and their tendency to form tethers, the use of this AFM was essential.

4.1.2 Cantilevers

Terminology regarding cantilevers can be confusing. The large piece of silicon is called the “chip”, and is a support for tweezer handling. The “cantilever” itself is normally in the range of $100 - 500$ µm long. The “tip” is the projection that is usually used for scanning. Often however, the term “cantilever” is used when the “chip” or “tip” is actually meant. Normally, the tip attached to the cantilever cannot be seen without a microscope. Many types of cantilevers for various applications are available and differ in several properties. In single cell force spectroscopy, tip-less cantilevers (see Fig. 4.2) that do not exhibit a tip are often used. At the place of the tip one binds a single cell that somewhat replaces the tip. The most important property is the spring constant that refers to the flexibility of the lever. Depending on the strength of the measured adhesion force an appropriate spring constant has to be chosen to gain the highest force sensitivity and accuracy. Further important properties are the geometry of the cantilever and, of course, the material.

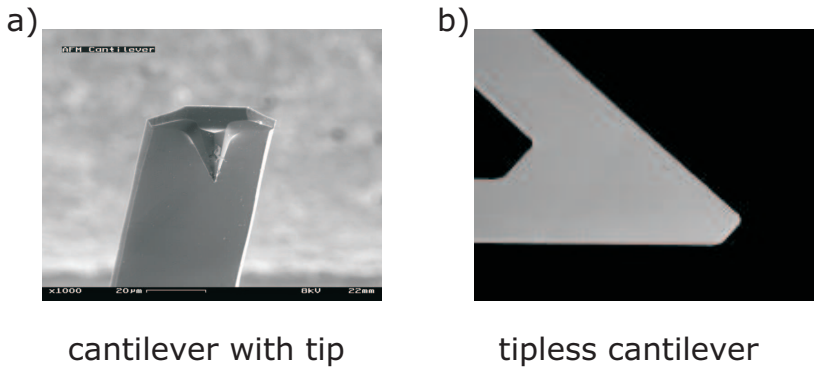

Figure 4.2: a) cantilever with tip b) tip less cantilever [180]

4.1.3 Attaching Cells to the Cantilever

A crucial step in single cell force spectroscopy is the binding of the cell to the cantilever. The cantilever must be coated with a molecule that allows for the binding of the cell. Therefore, the adhesion of the cell to the coated cantilever must exceed the adhesion of the cell to the surface of the petri dish. In the following subsections different possibilities to bind a cell to the cantilever will be introduced and discussed.

Concanavalin A

One approach is to coat the cantilever with the lectin Concanavalin A (ConA) which binds D-glucose and α-D-mannose sugar moieties at the cell surface. With this approach a non-specific strong binding is achieved between the cell and cantilever. The functionalization process is a multi-step process. Initially the cantilever should be activated by UV treatment or plasma cleaning. Cantilevers are then successively coated with biotinylated BSA, streptavidin and finally biotinylated ConA.

Cell-Tak

BD *Cell Tak*^{TM} (BD Biosciences, 354240) is a strong tissue adhesive consisting of marine mussel proteins which can also be used to glue a cell on a cantilever. The binding is of non-specific nature and is assumed not to activate any cells. There are two different protocols to use Cell-Tak: the hand spread protocol and the adsorption protocol. Both protocols have been used in this work. Each of them has their advantages but also their disadvantages. The protocols are described in more detail in the materials section. In general, the hand spread protocol turned out to be the more convenient one, because with it, it was easier to bind a cell to the cantilever. The disadvantage of this method is discussed in section 7.4.2.

4.2 Thermal noise calibration

In order to relate cantilever deflections to forces one has to calibrate the cantilever. The most common method to calibrate flexible cantilevers is the so-called thermal noise method [125, 31]. The thermal noise method for calibrating AFM cantilevers dates back to 1993 [85]. It uses the equipartition theorem to relate the measured thermal noise in the AFM cantilever deflection signal to the spring constant in the cantilever, which was assumed to behave like an ideal spring. The equipartition theorem states that the thermal energy present in all terms in the Hamiltonian of a system that are quadratically dependent on a generalized coordinate is equal to $\frac{k_B T}{2}$, where k_B is Boltzmann's constant and T is the absolute temperature (in Kelvin). If one can treat the cantilever as an ideal spring of constant k, a measurement of the thermal noise $< x^2 >$ in its position allows the spring constant to be determined as:

$$k = \frac{k_B T}{\langle x^2 \rangle} \tag{4.1}$$

Butt and Jaschke [31] recognized that because a cantilever spring is not an ideal Hookian spring, its potential energy is not simply $\frac{kx^2}{2}$. In order to relate the cantilever spring constant to the noise in its end position, one must express the Hamiltonian of the cantilever spring in terms of its normal modes. A series of improvements led to the correct calibration formula:

$$k = 0.8174 \frac{k_B T}{s^2 P} [\frac{1 - (\frac{3D}{2L}) \tan(\Phi)}{1 - (\frac{2D}{L}) \tan(\Phi)}]^2 \tag{4.2}$$

where the numerical factor 0.8174 is a result of the geometry of the cantilever spring, s is a sensitivity calibration factor, P is the positional noise power isolated in the fundamental resonant mode only, D is the height of the tip, L is the cantilever length (more correctly, the distance from the base of the cantilever to the tip) and the term in square brackets accounts for the cantilever tilt relative to the substrate and the geometry of the optical-lever detection scheme commonly used in commercial AFMs. This "thermal calibration formula", first presented in [84] will be used in this study. The thermal noise method is limited by the sensitivity of the device used to measure the noise in the deflection signal: stiffer cantilevers suffer less thermal vibration. Since the expected adhesion forces are small, very flexible cantilevers have to be used within this study which justifies the usage of the thermal noise method for calibration.

4.3 Parameter settings

In most SCFS studies the strength of the adhesion between two cells or a cell and a substrate depends on parameters such as contact time, contact area, cantilever velocity and set point force. Generally, retraction curves show that higher detachment forces are the result of an increased number of adhesive interactions. Therefore, these parameters have to be carefully taken into consideration depending on the investigated phenomenon. The following subsections will shortly introduce the influence of these parameters.

4.3.1 Force Set Point

The set point force is the force with which the cells are squeezed together in order to bring them into contact. The set point force is used as an indicator to decide when the cells come close enough to be in "physical" contact. This means that the cantilever is lowered until it touches the cell when the cantilever consistently begins to bend. When the bending of the cantilever exceeds a certain value, the set point force is reached. The fact that the set point force is used as an indicator for "physical" contact prevents the user from reducing it below a critical value. A to small set point force would result in many errors in the approaching process. When the cantilever bends due to friction forces of the surrounding medium, this would mistakenly be interpreted as a contact of the cantilever with the cell. In general, it is not recommended to lower the value below 100 pN. On the contrary, a large value of the set point force inevitably increases the contact area between the cells resulting in larger measured adhesion forces. Every investigated phenomenon should be checked for the influence of the set point force in order to exclude any influences of the measured adhesion forces on the chosen set point.

4.3.2 Cantilever Velocity

The velocity of the cantilever while approaching and retracting also has the potential to influence the measured adhesion forces. Due to viscous effects, an additional drag can bend the cantilever which requires correction afterwards. Another problem is the confinement of the displaced fluid between cantilever and petri dish surface. When the cantilever is retracted too fast, an low-pressure develops because the fluid does not have enough time to enter the confinement between cantilever and surface. This is especially a problem in more viscous media such as dextran solutions. Furthermore, the measured unbinding forces are not a fundamental property of a ligand-receptor pair but depend on the cantilever velocity: If the velocity is sufficiently slow, there is time for thermal fluctuations to drive the system over the energy barrier, and the

unbinding force will be small [60]. On the contrary, when the velocity is high enough, thermal fluctuations do not have enough time to break the bond. In conclusion, in every measurement the influence of the cantilever velocity should be checked.

4.3.3 Contact Time

The dependence on the contact time is the most intuitive one. The longer the cells are in contact, the more time the ligands have to connect with their receptors. Furthermore the contact area can increase over time since the cells are given more time to connect. Additionally, artificial effects like nonspecific adhesion can lead to an increase of the measured adhesion force. In order to overcome this obstacle, it is helpful to know the time scales in which the investigated adhesion process takes place.

4.4 Current Limitations of SCFS and Perspectives

SCFS measurements do have some limitations. Adhesion measurements that involve single cells are time consuming since only one cell can be characterized at a time. For statistical reasons, many detachment-forcedistance curves must be recorded, which limit the length of the contact times that can reasonably be assayed. Furthermore, the almost unavoidable thermal drift in AFM complicates long-contact-time experiments ($> 20\,\mathrm{min}$) and the tight adhesion of cells after longer contact times ($> 1\,\mathrm{h}$) exceeds the capability of the system. Thus, SCFS is currently restricted to short contact times that range from milliseconds to minutes [79]. SCSF represents a rather new technique that is still in its infancy and thus still needs to mature. The use of SCFS has much potential for development. This potential is based on the versatility of SCFS and the enormous variety of biological and medical applications to which it can be applied.

4.5 Summary

In this chapter the method atomic force microscopy based Single Cell Force Spectroscopy (SCFS) was introduced. This method displays a relatively new technique to measure adhesion forces between single cells. Thereby, a cantilever without a tip is coated appropriately to glue a cell onto it. This cell on the cantilever is now lowered onto another cell being fixed at the bottom. After bringing them into close contact the cantilever is retracted and the adhesion force is measured by measuring the deflection of the cantilever. In order to measure adhesion forces as accurately as possible several things have to be accounted for. Foremost, the appropriate cantilever has to be chosen (the stiffness of the cantilever has to be in the correct order of magnitude for the investigated cell adhesion). After that, the cantilever has to be calibrated. The Thermal noise method, as a widely-used calibration method, was introduced. In this calibration method the equipartition theorem is used to relate the measured thermal noise in the AFM cantilever deflection signal to the spring constant in the cantilever which was assumed to behave like an ideal spring. With this method the spring constant of the used cantilever can be determined quite accurately. After the calibration, several additional things have to be taken into account during the measurements. Parameters like set point force, cantilever velocity and contact time have been discussed for their potential to artificially pollute the measuring signal. The binding of the cell onto the cantilever resembles another crucial point in SCFS. There are a variety of different functionalization protocols available for all sorts of cells. In this chapter the two available protocols to bind RBCs to a cantilever were discussed. Since SCFS is a relatively new technique there is still room for improvements. Therefore, in the end of the chapter the current limitations and the perspectives of SCFS were discussed.

In the next chapter the experimental realization of OT,HOT, microfluidics and SCFS will be described.

5 Setup

5.1 Optical Tweezers

Figure 5.1 shows the holographic optical tweezers setup used for the optical tweezers measurements. In this chapter, the single parts of the setup will be described in more detail.

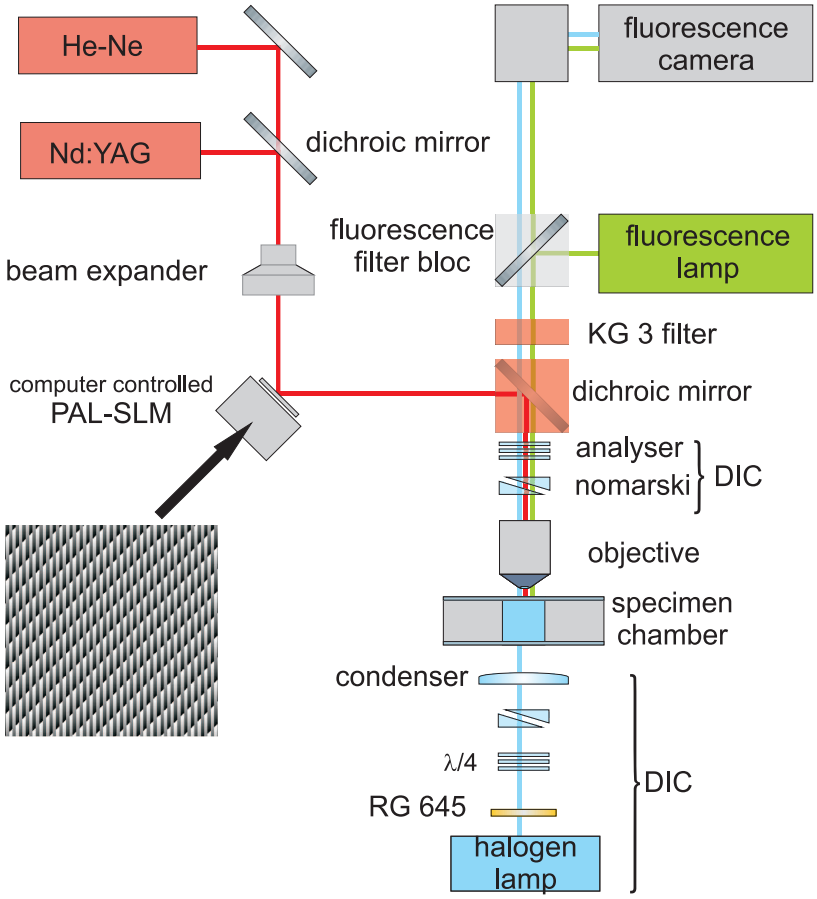

Figure 5.1: Schematic picture of the holographic optical tweezers setup. For detailed description see text.

5.1.1 Laser

The laser used for realizing the optical tweezers is a diode-pumped Nd:YAG solid-state laser (*Ventus*). The laser works with a wavelength of 1064nm (near infrared, NIR) and possesses and Gaussian transversal electromagnetic ground mode (TEM_{00}). Maximum power in continuous operation mode is 1500mW. For coarse alignment of the optics the Nd:YAG laser was overlayed with a He-Ne-laser in order to simplify the adjustment of the optical tweezers. The power supply unit was positioned separately from the anti-vibration table in order to protect the tweezers from acoustic vibrations. In order to protect the user's eyes from the infrared laser, several KG 3 filter were placed before camera and eyepiece.

5.1.2 Beam Expander

The beam diameter of the laser amounts to 2.5mm and the beam divergence adds up to less than 1mrad. A beam expanding system of a BM.X type (*Linos Photonics GMbH*) was used for optimal filling of the spatial light modulator (see below). With the help of the beam expander the beam was expanded to 20mm in diameter. All optics are coated with an anti-reflection layer designed for a wavelength of 1064nm. With the help of several mirror optics, the laser is directed onto the spatial light modulator (PAL-SLM). Another advantage of the beam expander system is the possibility to change the beam divergence of the laser. By changing the beam divergence the optical trap can be moved along the optical axis. This is very important because normal objectives used in microscopy are designed for visible light, and as a result, using 1064nm the position of the trap will not match the plane of observation of the objective. With the adjustment of the beam divergence one can correct for this chromatic aberration. Without this adjustment of the beam divergence it would never be possible to display a trapped particle sharp.

5.1.3 PAL-SLM

The heart of the holographic optical tweezers is a PAL-SLM (parallel aligned liquid crystal spatial light modulator) PPM X8267-15 from *Hamamatsu Photonics*. The mode of operation is explained shortly. The intensity distribution of the writing laser with a wavelength of $\lambda = 690\,\mathrm{nm}$ is modulated over an electronically addressable liquid crystal display with 768×768 pixels. The XGA-signal of the phase holograms is applied to this LCD via an output of the graphic board of the controlling computer. The intensity distribution of the writing laser arises through inter connective optics over an layer of amorphous silica (α-Si:H) in the actual PAL-SLM. The spatial filtering of the connective optics removes higher frequencies and the pixel structure of the LCD

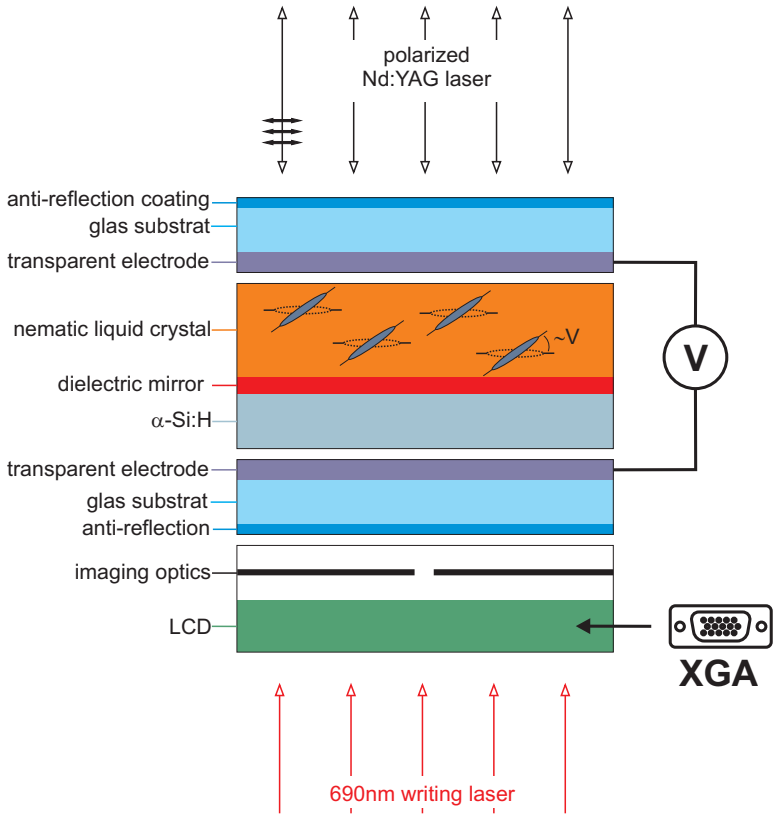

Figure 5.2: Schematic picture of the PAL-SLM. For detailed description see text.

can be minimized. The PAL-SLM is structured shown in Fig. 5.2. A dielectric mirror is sandwiched between a liquid crystal and an a-Si:H layer in order to enhance the reflective performance of the device and cope with variations of the readout light wavelength. The liquid crystal directions are all parallel to each other in the PAL-SLM. On application of voltage the molecules simply tilt with essentially no rotation about the optical axis. This causes phase modulation of the light polarized along the original direction of the directors, while the orthogonally polarized light is essentially unaffected. The Nd-YAG-Laser is reflected on the dielectric mirror in a very efficient way and finally exits the PAL-SLM again. To summarize, the light of the Nd-YAG experiences a phase shift while passing the PAL-SLM in dependence of the applied voltage. Through this phase shift the phase front of the laser beam modulated in such a way that after passing the objective a desired pattern of traps (i.e. number and orientation of traps) emerges in the focal plane of the objective. In chapter 3.3 this is explained in more detail.

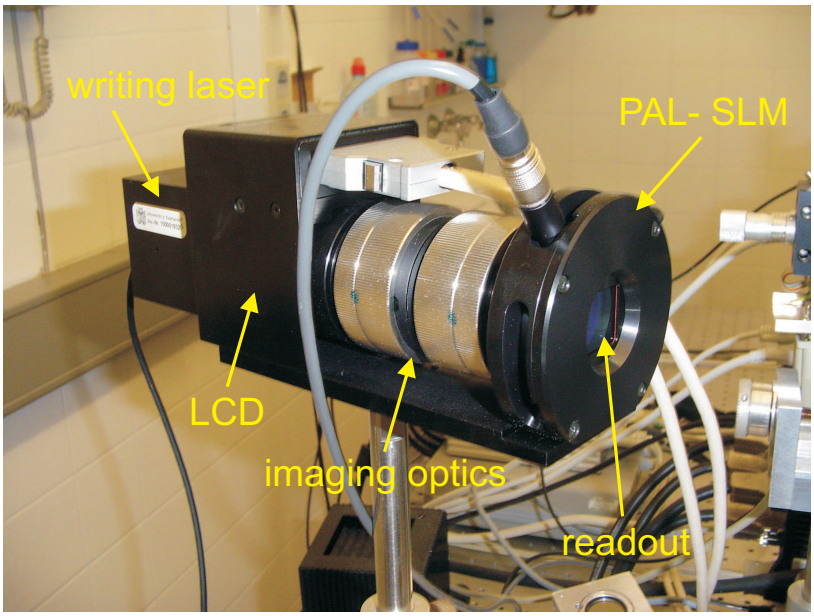

Figure 5.3: PAL-SLM with the main parts: witting laser, LCD, imaging optics and readout surface

5.1.4 Damping Table

The complete setup is placed on an active anti-vibration table (*Vario, Halccyonics GmbH*) in order to filter all external vibration sources. Thereby, frequencies in the range of 10Hz to 100Hz can be damped reliably with an efficiency of over 98%. Problematic are low frequency vibrations in the range of 1Hz (e.g. vibrations of the building). In order to cope with this, the whole setup was placed in the basement.

5.1.5 Fluorescence Camera

The fluorescence camera used, equipped with a CCD-sensor, is a digital camera from Roper Scientific Inc. (Cascade 512F). The energy of the incident light is assigned via the internal photo effect onto the electrons of a semiconductor. These free electrons are dispatched by an applied voltage, whereby the number of separated electrons is directly proportional to the light intensity. The CCD-chip is 512×512 pixel large with a total size of $16 \times 16\mu m$. A 2.5-magnification lens is placed in front of the camera. With the 60-times magnification of the objective and the 2.5-magnification lens in front of the camera this setup sum up to a total magnification of 150. In order to avoid any vibrations due to the cooling fan, the camera is equipped with a standard CPU-water-cooling system. For fluorescence measurements the camera is

additionally equipped with an avalanche amplifier, therefore, the separated electrons are preamplifier before being read out.

5.1.6 Objective

The objective used is an infinity corrected CFP Plan Fluor oil-immersion-objective (Nikon Corp.) with a 60 time magnification and a maximum numerical aperture of $N_A = 1.25$. The numerical aperture is adjustable via a sub stage iris diaphragm between the values of $N_A = 0.5$ to $N_A = 1.25$. The maximum diaphragm opening is 8mm in diameter.

5.1.7 Microscope

The objective is part of an inverted microscope (TE2000, Nikon), displaying an crucial part of the optical tweezers. The microscope features two filter carousels, enabling the separation of the beam paths of optical tweezers and fluorescence illumination pathways. The internal structure of the microscope and the beam paths are displayed in Fig. 5.4 With the help of the upper filter carousel and a filter block with a dichroic

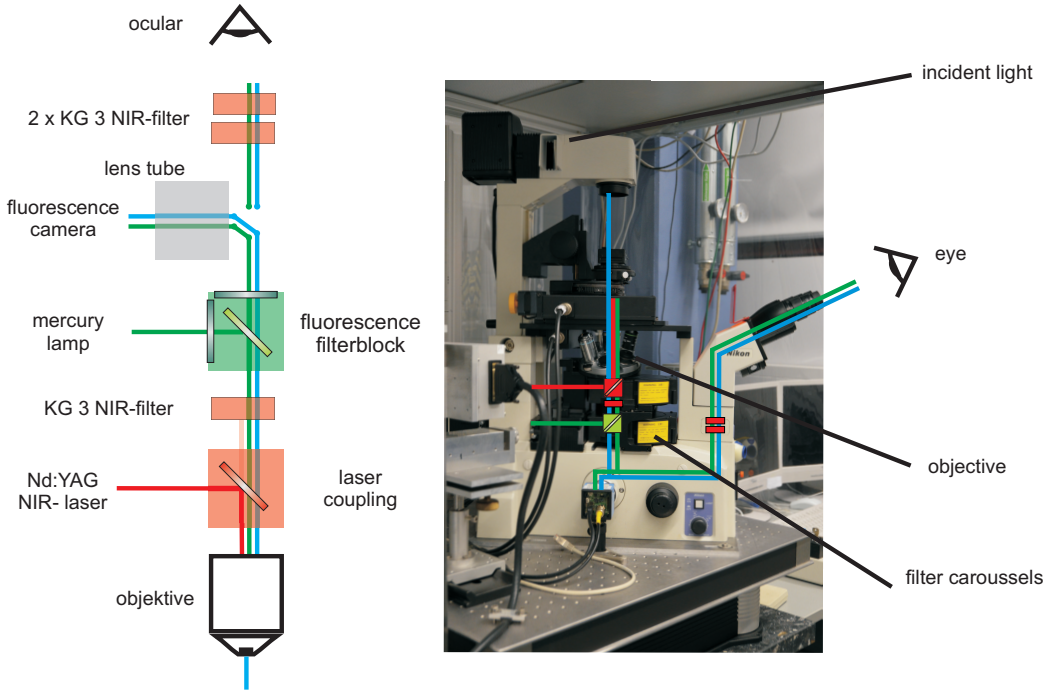

Figure 5.4: Left: imaging optics: internal structure of microscope and the filter carousels. Right: microscope with beam coarse.

mirror, the laser beam is coupled into the microscope objective. The dichroic mirror reflect up to 99, 9% of the laser beam up into the microscope objective. Because not all the laser intensity is reflected a KG-3 NIR filter (*Edmund Optics*) has to be inserted in front of the camera in order to protect it from the high laser intensity. To protect the eyes of the user, the same filters have to be inserted in front of the ocular lens. The lower filter carousel enables the coupling of a fluorescence unit with excitation, dircoidic and emission filters. The illumination source of the fluorescence unit is a mercury lamp from which the desired excitation wavelength is filtered via an excitation filter. The selected wavelength is then guided up the the objective with the help of the dicroidic mirror. In the specimen chamber this light stimulates the specimen to emit light with, in most of the cases, a longer wavelgenth (Stokes-Shift). This shift in wavelength enables to be sent through the dicroidic mirror (the mirror is transparent for this particular wavelength) onto the fluorescence camera.

5.1.8 Differential Interference Contrast Microscopy

The microscope used is a differential interference contrast microscope (DIC). The specialty of this microscope is significant better imaging of phase objects (i.e. objects that only change the phase of a passing light ray but not is intensity). The parts of the DIC are shown in Fig. 5.5: main parts of the DIC are an incident light unit

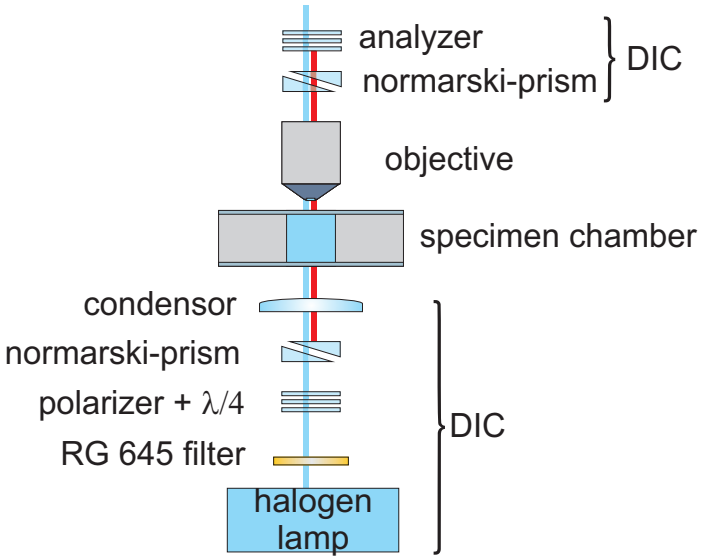

Figure 5.5: Structure and functional principle of differential interference contract microscopy. Main parts are polarizer with $\lambda/4$ plate, nomarski-prism, condenser, objective and analyzer.

(halogen lamp), a polarizer with $\lambda/4$ plate, two Nomarski-prisms and an analyzer. The unpolarized light from the halogen lamp is transformed into linear polarized light via the polarizer. The linear polarized light passes through the $\lambda/4$ plate and is converted into elliptical, circular or linear polarized light depending on the relative position of the preceding polarizer. The subsequent Nomarski prism is a type of prism made of two layers of a crystalline substance, such as quartz, which, due to the variation of refractive index depending on the polarization of the light, splits the light according to its polarization. Therefore, the polarized light enters the first Nomarski prism and is separated into two rays polarized at 90° to each other (see Fig. 5.6). The two rays are focused by the condenser for passage through the sample. The two

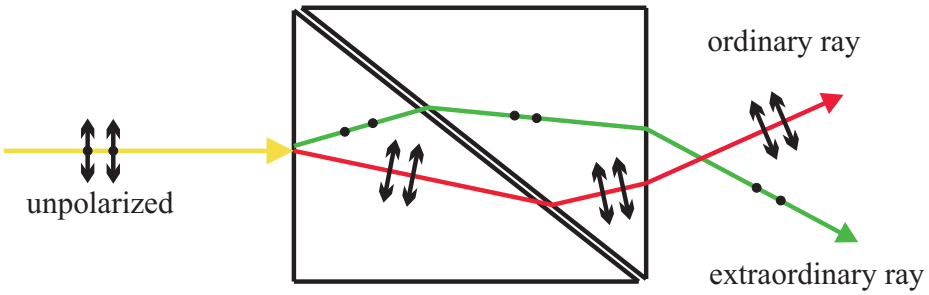

Figure 5.6: Functional principle of a Nomarski-prism: An unpolarized ray hits on the prism and due to the birefringence of the material is separated into two rays with perpendicular polarizations. One of the rays behaves like a normal ray passing a prism (referred to as the ordinary ray), while the other one does not behave like a normal ray and is reflected under a different angle (referred to as the extraordinary ray).

rays are focused in order to pass through two adjacent points in the sample, around 0.2µm apart. The separation is normally similar to the resolution of the microscope. They will experience different optical path lengths where the areas differ in refractive index or thickness. This causes a change in phase of one ray relative to the other due to the delay experienced by the wave in the optically denser or thicker material. After passing through the sample, the rays travel through the objective lens and are focused for the second Nomarski prism. The second prism recombines the two rays into one polarized at 135°. The combination of the rays leads to interference, brightening or darkening the image at that point according to the optical path difference. A RG 645 filter (transmission only for $\lambda > 645$ nm) was inserted into the illumination unit because red blood cells risk being harmed from illumination by short wavelengths.

5.1.9 Microfluidic

The PDMS microfluidic was manufactured with an appropriate mold that was mechanically produced. The microfluidic is shown in Fig. 5.7. It exhibits a Y-shape and it consist of two inlets and one outlet while each channel width is about 200 µm. The flow is driven by gravity. The laminar flow and the y-shape of the microfluidic

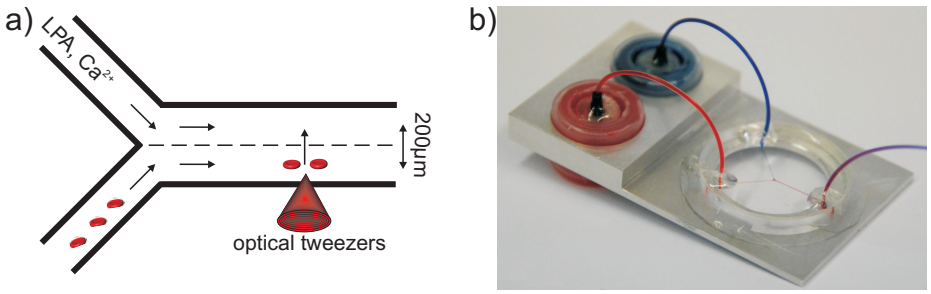

Figure 5.7: a) Sketch of the y-shaped microfluidic. b) photograph of the microfluidic, holder and reservoirs.

device allow for the generation of a sharp concentration gradient which can be established between the upper and lower part of the channel outlet. Because PDMS is transparent to a broad spectrum of the visible and infrared light, the interior is accessible for optical tweezers. Simultaneously, normal and fluorescence microscopy can be conducted in order to control the experiment.

5.2 Single Cell Force Spectroscopy

Fig. 5.8 shows the Nano-Wizard 2 Afm with integrated CellHesion module that was used for the single cell spectroscopy measurements.

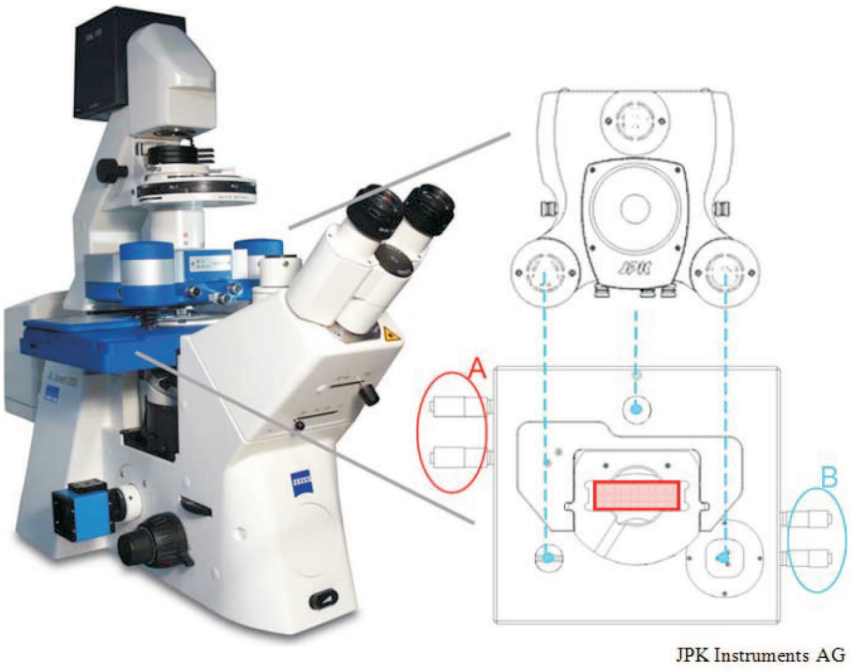

Figure 5.8: The Nanowizard AFM setup mounted on an inverted optical microscope. The stage and AFm head are sketched separately. The micropositioners to move the sample, represented by a red glass slide, are surrounded in red (A) and the micropositioners to move the AFM head are surrounded in blue (B).

5.2.1 AFM

The basic setup of an AFM is very simple on the face of it. A micrometre-sized, flexible cantilever is scanned over a surface while its deformations (i.e. deflections) are simultaneously recorded. The data acquisition is realized by reflecting a laser beam at the cantilever rear and recording the position of the reflected signal by a position-sensitive detector (see Fig. 5.9). When the cantilever bends due to a force, the laser spot will move on the 4-quadrant photo diode and this movement is converted into a force by calibrations method. In the experiments of this work, the height precision of the cantilever is maintained by three closed loops through high-speed capacitive

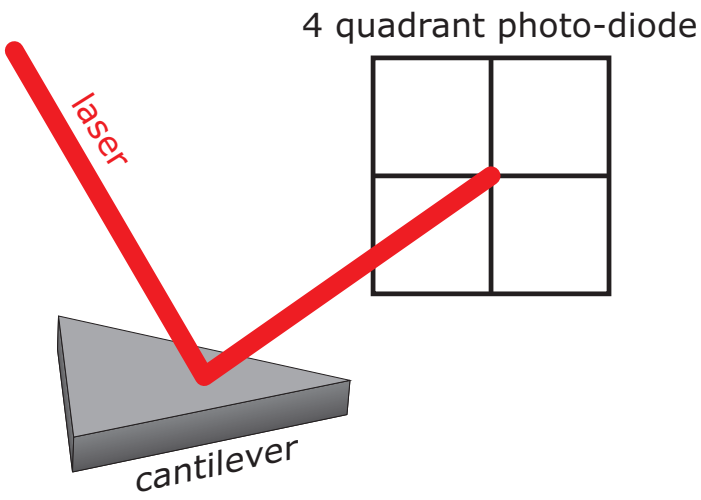

Figure 5.9: Measuring principle of the deflection (and the corresponding adhesion force) of a cantilever via the reflection of a laser on the rear of the cantilever. The movement of the laser beam is accurately measured with a 4-quadrant photo diode.

sensor feedback piezo elements in the AFM head, one for each direction (piezo ranges : $x, y = 100\,\mu\text{m}$, $z = 15\,\mu\text{m}$).

Figure 5.10: Image of the Nanowizard 2 life science setup from JPK Instruments.

5.2.2 CellHesion Module

In order to design this AFM for live cell adhesion measurements the AFM has to be modified because cells often exhibit a certain flexibility and a cell size that is of about several µm the normal z-range of 15 µm is not sufficient for cell-cell adhesion measurements or for the detachment of cells from the substrate. Therefore, the Nanowizzard AFM is equipped with three further piezo elements of 100 µm z-range with sub-nm precision which move the sample towards or away from the cantilever, instead of moving the AFM head (CellHesion module).

5.2.3 Microscope

In order to optically visualize the studied objects, the AFM system is installed onto an inverted microscope (Axiovert200, Zeiss), allowing a simultaneous operation of AFM and standard microscopy, such as phase contrast and fluorescence microscopy.

5.2.4 Petri Dish Heater

In order to conduct measurements under controlled temperature conditions, the Petri Dish Heater (Fig. 5.11 was installed into the setup. The Biocell is a petri dish holder that utilizes a thermostat in order to heat the sample to a defined temperature. In this way, measurements at $37°C$ could be conducted.

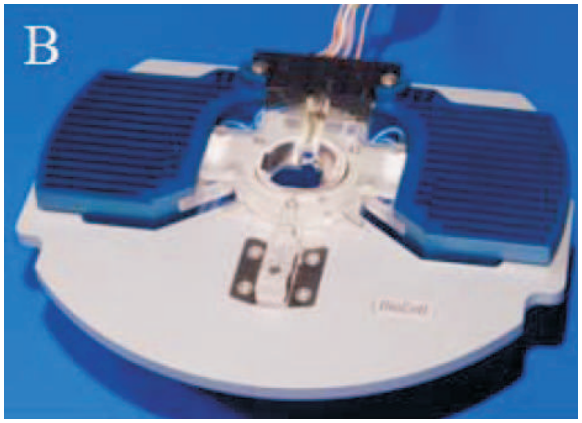

Figure 5.11: The petri dish heater controls the temperature of the sample.

5.3 Summary

In this chapter the experiment built of all the used methods, including optical tweezers (OT), holographic optical tweezers (HOT) and single cell force spectroscopy (SCFS) was described. The framework for every OT is a stable source of photons, which is realized by a laser beam. In order to exclude any optical damage in the investigated cells a infrared Nd-YAG laser was used, because the wavelength of 1064 nm resembles a compromise between low absorption coefficients of hemoglobin (the main constituent inside the RBC) and low absorption coefficients of water.
The central part of the HOT is the phase modulator PAL-SLM (PPM X8267-15, Hamamatsu Photonics). Onto this phase modulator specifically designed and calculated phase patterns are applied in order to modify the trapping laser beam. The phase front of the trapping beam is modified in such a way that a desired number and orientation of traps are generated.
The HOT was integrated into a inverted fluorescence microscope (TE2000, Nikon Corp.) equipped with two filter carousels and a differential interference module. This special build of the microscope combines the advantages of normal fluorescence microscopy with differential interference microscopy and therefore resembles an adequate tool to investigate RBCs.
In the second part of this chapter the experimental realization of SCFS was described. The heart of this technique is an atomic force microscope (Nanowizard2, JPK Instruments) placed onto an inverted microscope (Axiovert200, Zeiss). Cell-cell adhesion measurements often require large z-pulling lengths. Therefore, the AFM is additionally equipped with an CellHesion module (JPK Instruments), with three further piezo elements of 100 µm z-range with sub-nm precision, which moves the sample towards or away from the cantilever, instead of moving the AFM head. Additionally, a petri dish heater enables the controlled setting of the sample temperature. This is of importance when performing measurements under body temperature.

6 LPA-Induced Adhesion of Red Blood Cells

6.1 Introduction

There are many different types of cells in the cardiovascular system of the human body: endothelial cells and smooth muscle cells in the vessel walls, white blood cells (leukocytes), blood platelets (thrombocytes) and RBCs (RBC) (erythrocytes). The latter represents the largest fraction of blood cells among all blood cells: about 90% of all cells are RBCs. This large number of RBCs accounts for $40 - 50\%$ of the blood volume (the haematocrit value). In addition, they play a crucial role in the circulatory system, in which the function of the RBCs' enclosed hemoglobin is essential. Hemoglobin is able to bind oxygen in the lung cappilaries and release it again in the tissue cappilaries. RBCs do not have intracellular compartments such as endoplasmatic reticula, Golgi apparatuses or cell nuclei. Therefore, RBCs are not able to synthezize or modify new proteins. They do not exibit mitochondria; the demand for energy is gained through anaerobe respiration. Due to the relative simple build of the RBCs as biomembranes filled with hemoglobin containing cytoplasma, the RBCs often serve as a model system to answer various questions with regards to cell biology and pyhsics of soft matter. For expample, the asymmetric distribution of phospholipids in a lipid bilayer was first discoverd in the membrane of an RBC [159]. They also serve as model system for investigating the movability of membrane lipids and proteins in lipid bilayers [128] and for the characterisation of the underlying spectrin network [192, 141] which supllied a deeper insight into the function of the glycocalyx. Furthermore, the mechanical properties of biomembranes were intensively investiged in the past [62].
The blood coagulation process is a complex process that involves many collective players and factors. In a brief manner, the coagulation process starts with the activation of blood platelets (e.g. at a damaged vessel wall). Those activated platelets release several messengers and growth factors in order to recruit other cells to participate in blood clot formation. Therefore, coagulation is governed by a complex cascade and it requires a number of essential enzymes and cofactors, so-called coagulation factors, and is finalized by the formation of the thrombus [120]. The platelets themselves play

the most important role in the coagulation process, inside those platelets the so called scramblase protein is activated. This scramblase activation results in a degradation of the asymmetrical distribution of phospholipids in the lipid bilayer and the negatively charged phospholipid phosphatidylserine (PS) is exposed in the outer leaflet of the platelet membrane. This PS is suspected to play an important role in blood coagulation, since it may provide a catalytic surface for prothrombinase complexes [45]. Obviously, RBCs are a major part of the thrombus, but it is commonly believed that they are simply trapped in the fibrin network due to their prevalence in the blood [34]. Therefore, the role of RBCs is always assumed to be completely passive. As early as a century ago, the first clinical studies described a correlation between a decreased concentration of RBCs, i.e. haematocrit value, and longer bleeding times [56]. These early results have been confirmed by a number of clinical investigations [2, 83]. Considering the high percentage of erythrocytes in the blood and the clinical indications, it is evident that a profound understanding of the role of RBCs in clotting is crucial. However, an adhesion of RBCs to platelets - and not to each other- was assumed to be of principal importance [83]. Andrews and Low [2] described that activated platelets induce scramblase activity in RBCs as well, and they concluded that the additional presence of PS on the outer leaflet of the RBC should support the prothrombinatic activity of the platelets or support the signaling cascade for the thrombus formation. In some studies, it was shown that the phosphatidylserine-exposing RBCs adhere to endothelial cells [46, 123]. In general, PS-exposure and non-reversible adhesion of RBCs is known to happen in some diseases such as malaria or sickle cell disease [106, 188]. However a co-adhesion of healthy RBCs was not assumed until recently. Kaestner et al. [97] suggested a signaling cascade that predicts an active participation of RBCs in blood clot formation. Flow cytometry (FACS) and patch clamp techniques could confirm the theory of an activation of a non-selective calcium channel across which, after activation via messengers, extracellular calcium can enter the cell, resulting in an activation of a signaling cascade that, in the end, is expected to lead to an active co-adhesion among RBCs. In first studies [165, 90, 133, 134] the active co-adhesion of RBCs could be shown; however, statistically significant and quantitative data is still lacking. Therefore, in this work the adhesion process of RBCs was investigated with respect to the point: statistical investigation and quantification of the occurring adhesion.

6.2 Structure of RBC-Membrane

6.2.1 Membrane

The membrane of RBCs consists of lipids (41%), proteins (52%) and carbohydrates (7%) [77]. Subgroups of the lipids are neutral lipids, cholesterol, phospholipids and glycolipids. The membrane lipids consist of a polar and hydrophilic headgroup and a non-polar tailgroup (one or several hydrocarbon chains). Those hydrocarbon chains orient each other due to the hydrophobic interaction. According to the valid Fluid-Mosaic modell [161] the RBC membrane consists of a lipid double-layer in fluid-crystalic status, in which proteins are embedded 6.1. The carbohydrates of the cell

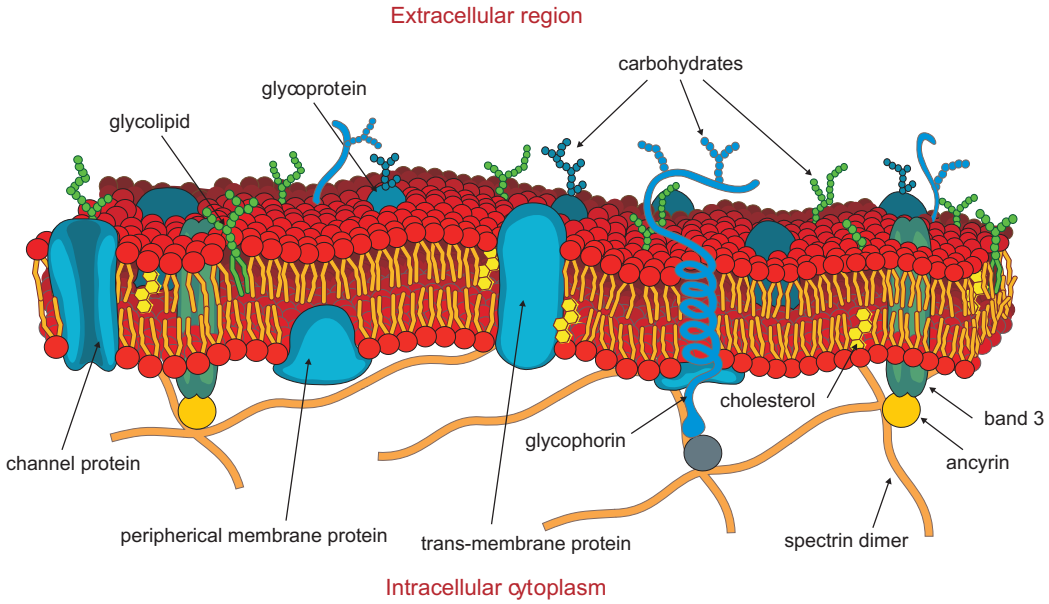

Figure 6.1: Schematic build of the cell membrane ([181]).

membrane are exclusively present on the outer leaflet and contain a large amount of sialic acid, a negatively charged sugar. These glycolipids or glycoproteins form the so called glycocalyx, a 5nm thick layer attached to the cell membrane. The negative charge of the outer membrane surface prevents an aggregation under physiological conditions. The lipids and proteins are able to diffuse laterally within leaflet of the membrane as long as this is not prohibited by specific interactions [174]. A transversal movement, i.e. a movement of a lipid from one leaflet to the other, is unlikely. Normally, this is only possible under the active help of special proteins, so called flippases, and hydrolysis of adenosin triphosphate (ATP) to adenosin diphosphate (ADP) and to phosphate. The phospholipids of RBCs and other human cells

(e.g. leukocytes, thrombocytes and fibroblasts) are asymmetrically distributed across the cell membrane. Cholinphospholipids, sphingomyelin (Sph) and phosphatidylcholin are exclusively present in the outer leaflet, whereas phosphatidylserine (PS) and phospahtidylethanolamin (PE) are exclusively present in the inner leaflet of the cell membrane [53, 189, 13]. This asymmetry can be abolished by the activation of the flippase [194].
Cell proteins are divided into trans-membrane proteins and peripheral proteins. Peripheral proteins are located on the membrane surface, where they are covalently bound or non-covalently bound to the cytoskeleton proteins. On the contrary, the trans-membrane proteins, with their long hydrophobic tails, are embedded into the membrane and can even penetrate the membrane. Therefore, these proteins can serve as receptors and take transport functions.
A network of spektrin forms the cytosol-sided cytoskeleton [1]. The cytoskeleton is responsible for the elastic properties of the cells and their robust shape. It is also responsible for the ability of RBCs to cross narrow capillaries that are even smaller than their mean diameter.

6.2.2 Cell Shapes

The inner solution of RBCs do not involve any structure and therefore the shape of the RBCs solely depend on the physical and chemical state of their membranes. It is commonly believed that the shapes, for given membranes, that are formed correspond to the minimum value of the membrane elastic energy. This energy can, in general, be decomposed into the sum of the stretching, shear and bending energy [62]. It is also a general property of membranes that more energy is needed to stretch them than to cause shear deformation or bending. Consequently, the shape established by a flaccid cell corresponds to the minimum value of the sum of the shear and bending energy terms, where the membrane area is practically constant. The primary extrinsic factor in cell deformability is the surface area-to-volume ratio which establishes the minimum-caliber vessel into which a cell can deform (without rupturing). Normally, RBCs are biconcave discs with a mean radius of $7.5 - 8\,\mu m$ and a mean thickness of $1.5 - 2\,\mu m$ (see Fig. 6.2a)). The biconcave shape, with its large surface area to volume ratio, enhances the gas exchange. When the physical or chemical state of the membrane changes, RBCs can also be present in different shapes, such as echinocytes (Fig. 6.2b)), stomatocytes ((Fig. 6.2c)) and spherocytes (Fig. 6.2d). The other cell shapes arise according to the ambient conditions. For example, RBCs change their shape into an echinocytic shape after direct contact to glass (so-called glass effect) [59]. Depending on the ionic strength of the solution all the other shapes are achievable. The exact processes involved in this shape transformation are still not fully understood. It is assumed that changes in the extension of the inner and

outer leaflet of the bilayer membrane, via asymmetrical incorporation of lipids, are responsible for the shape changes of the RBCs [160, 114, 52].

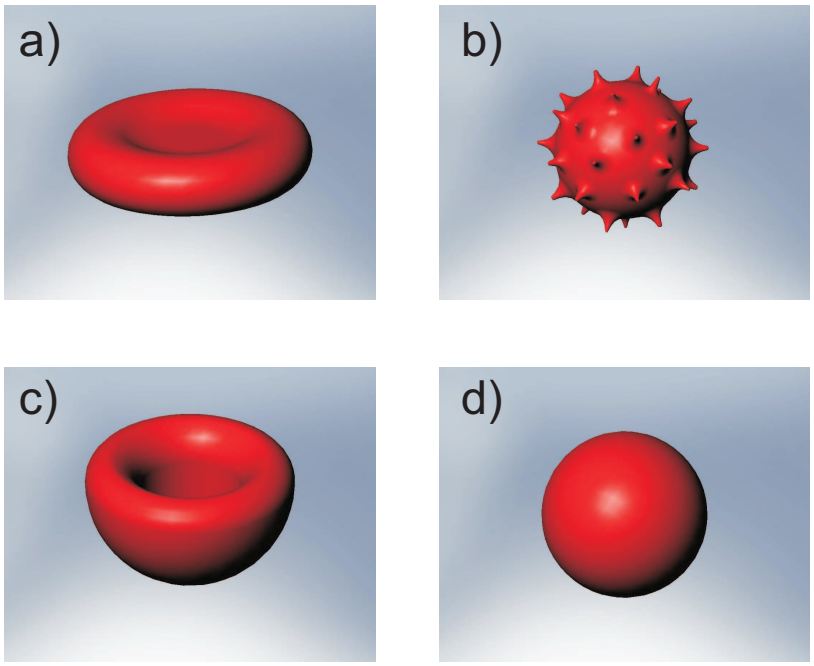

Figure 6.2: Different RBC cell-shapes: a) Discocyte b) Echinocyte c) Stomatocyte d) Spherocyte

6.2.3 Transporting Systems

Due to the structure of the lipid-bilayer with its hydrophilic heads and its hydrophobic tails, the membrane constitutes a permeability barrier for certain substances while being permeable for other substances. Most notably, water, O_2 and CO_2 as well as smaller, polar uncharged molecules such as urea and ethanol are able to diffuse across the cell membrane along a concentration gradient. On the contrary, larger molecules, like sugar, are not able to diffuse across the membrane. Moreover, for charged molecules, even smaller inorganic ions, the membrane is practically impermeable. In order to supply the internal cell compartment with a defined amount of those molecules, the cell uses transport mechanisms incorporated into the cell membrane. Available transport mechanisms are ion channels, transporters and pumps.
Ion channels are water-filled trans-membrane proteins which carry polar amino acids into the inner part. Thereby, polar particles and ions are able to diffuse along their

electrochemical gradients, either into the cell or out of the cell. In this case no energy has to be provided (passive transport). Most of the channels only open after activation by a certain signal. Voltage-controlled channels only open after a change of the trans-membrane potential, ligand-controlled channels after binding of a messenger substance and mechanic controlled channels open after a mechanical stimulus like pressure or shearing.
The ion transport via pumps, like the Na^+/K^+-pump or the Ca^{2+}-pump is called an active transport. In this transport metabolic energy will be consumed in order to transport ions and molecules against their electrochemical gradient into or out of the cell. Hereby, the energy is supplied by hydrolysis of adenosine triphosphate (ATP) to adenosine diphosphate (ADP) and to phosphate. The Ca^{2+}-pump is the only active and outward directed pump in the RBC. These active Ca^{2+} outward pumps are responsible for the extremely low concentration of free Ca^{2+} inside the cell of about $60\mathrm{n}M$ (The concentration of Ca^{2+} in the extracellular medium is in the $\mathrm{m}M$ range). Among the transporters one distinguishes between so-called uni-porter, which only transports a single substance, and Co-transporter, which transport several substances at the same time. The uni-porter belongs to the passive transporters; they open as a result of certain stimuli (e.g. an electrical voltage, a mechanical tension, etc.). Co-transporters transport molecules or ion against their electrochemical gradient via stoichiometric coupling to another transported ion. This ion is transported along an electrochemical gradient via an active pump under the consumption of metabolic energy. Through the coupling, an unfavorable transport mechanism is replaced by a more favorable one. Dependent on the direction of the transport one calls them symporter or antiporter, according to whether the substances are transported in the same direction or in opposite directions.
In general, the transport mechanisms of the RBC are rather complex. Most of the time, a variety of different mechanisms are involved in the transportation of particular substances. Fig. 6.3 illustrates the variety and complexity of the transport mechanism in the RBCs.

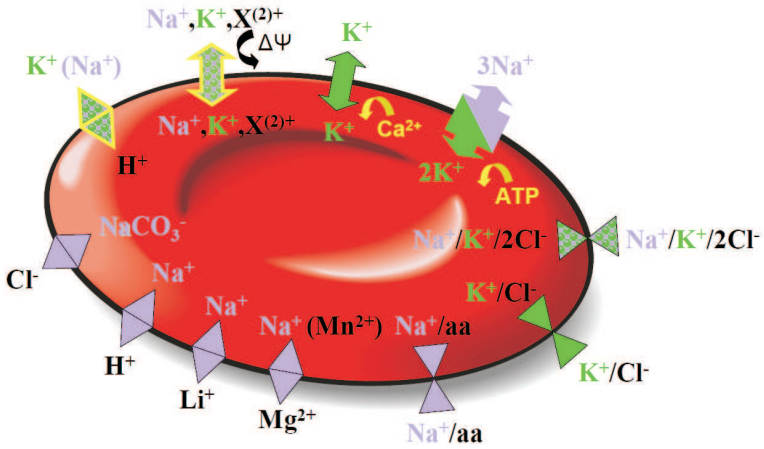

Figure 6.3: Transport mechanisms of human RBCs for Na^+ and K^+ [133].

6.3 Signalling Cascade

Kaestner and Bernhardt suggested a Ca^{2+} influx via an non-selective cation channel (NSC) [43, 93] which is permeable for different mono and bivalent cations such as Na^+,Ka^+ or also Ca^{2+}. This channel is activated by positive [93, 94] as well as negative membrane potentials. Furthermore, this channel can also be activated under physiological conditions with nicotine, acethylcholine and carbachol [16]. Apart from that, it has been shown that this channel is also suspected to be opened by physiological concentrations of prostaglandin E_2 (PGE_2) and lysophosphatidic acid (LPA) [92, 97, 98]. LPA and PGE_2 are local mediators that are released by activated platelets in the blood clotting process [162] but also from RBCs themselves under mechanical stress [139]. Fig. 6.4 shows the proposed model of the active participation of RBCs in thrombus formation or solidification. The cascade starts with the activation of blood platelets [120] that subsequently release mediators such as PGE_2 or LPA. Those messengers open the NSC, and extracellular Ca^{2+} enter the cell. The increased intracellular Ca^{2+}-concentration acts as a trigger for mainly two processes. Firstly, another calcium-dependent channel gets opened by the increased calcium level; this channel is known as the Gardos channel [71]. Through this channel, intracellular potassium effluxes out of the cell, followed by a shrinkage of the cell [113, 109]. The second, more important, process is that due to the elevated intracellular Ca^{2+} concentration the lipid scramblase protein is activated which has a profound consequence: The breakdown of the asymmetrical lipid distribution between both leaflets [14, 185, 183, 189, 49]. In this way, the negatively charged phospholipid phosphatidylserin (PS), usually exclusively present in the inner leaflet, is transported

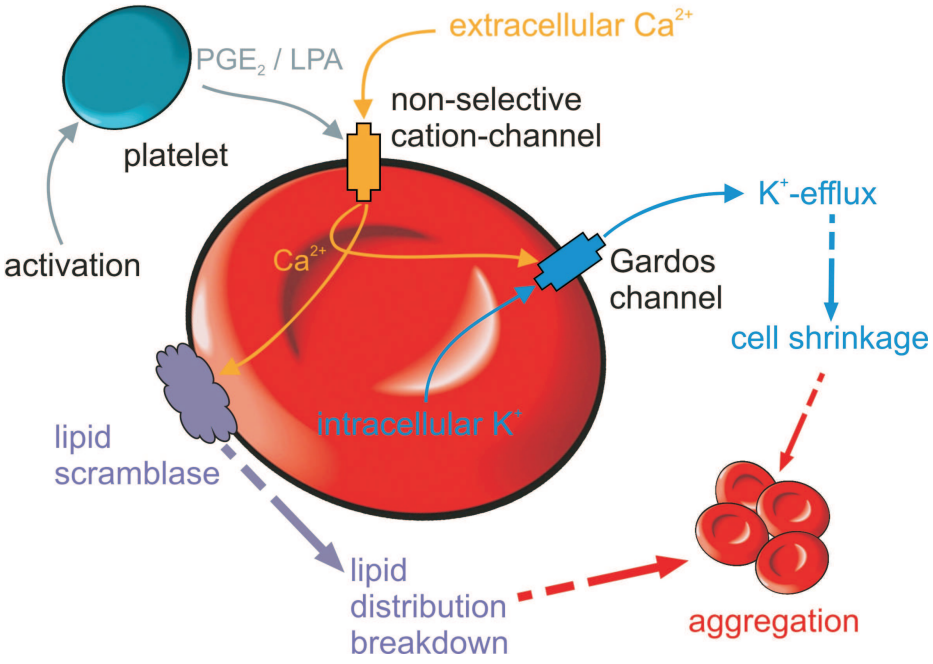

Figure 6.4: Signaling Cascade of the LPA induced adhesion of RBCs.

into the outer leaflet [133]. This PS-exposure in the outer leaflet is suspected to play a crucial role in the expected adhesion process [194]. However, the molecular identities (i.e. the deeper adhesion mechanism) still remain obscure. At low intracellular Ca^{2+}-concentrations, the asymmetrical distribution of phospholipids is maintained by an active transportation of phospholipids into the inner leaflet. The responsible transport protein is the so called translocase [159, 13]. Due to the elevated Ca^{2+} concentrations the translocase is inhibited. However, the inhibition of the translocase alone can not be responsible for the breakdown of the phospholipid distribution, since without active transport (i.e. with scramblase), it would take very long for measurable amounts of phospholipids to be present in the outer leaflet. Hence, the scramblase activation can be seen as key process in the breakdown of the phospholipid asymmetry. The process of Ca^{2+} elevation and its consequences, the scramblase activation and translocase inhibition, are known for platelets in the blood clotting process after activation as well as in apoptotic cells [140, 186]. Furthermore, a scramblase activation is also reported in lymphocytes [184]. The PS exposure after a Ca^{2+} rise inside the RBC can be detected via labelling of the PS with Annexin V and the consequences of this exposure can be investigated under greater detail. In studies with endothelium cells it could be shown that this increased intracellular Ca^{2+} concentration and the consequent exposure of PS leads to an increased adhesion of RBCs to endothelium

cells [46]. Furthermore, this is thought to be a reason for the increased adhesion of RBCs to endothelium cells in the sickle cell disease [188, 123]. Aside from the sickle cell disease, there are a various number of processes that are related to PS exposure in the outer leaflet. There are hints [194, 189, 193] that in blood clotting, cell adhesion, cell fusion [175] and phagocytosis apoptotic cells are accompanied by the expression of PS on the outer leaflet [171, 157, 127, 193]. In principle, RBCs are not able to undergo apoptosis because they are lacking the common parts involved in apoptosis such as mitochondria and nucleus. However, due to the similarity of the involved processes the term eryptosis has been established to describe these phenomena in RBCs [107]. It is controversial whether the Ca^{2+} influx is causal for the PS exposure or not. While Kaestner and Bernhardt detected a clear correlation between the two of them [98], Chung et al. reported from a mostly Ca^{2+}-independent process [45].

6.3.1 Substances

A23187

A23187 is one of the few known naturally occurring compounds capable of transporting divalent cations across biological membranes [143]. Ion transport by A23187 is mediated by a dimeric form of the molecule that complexes the cation. A23187 exhibits a high selectivity for Ca^{2+} and elicits a wide range of pharmacological responses: e.g., platelet aggregation [190], insulin release [187] and increased cardiac contractility [82]. Fig. 6.5 shows the working principle of A23187. The A23187 molecules get incorporated into the membrane and make them permeable for Ca^{2+}. In the course of time, more and more Ca^{2+} is transported from the exterior to the interior of the cell. The Ca^{2+} rise inside the cells can be visualized with fluorescence microscopy by using a calcium sensitive fluorescent dye (e.g. Fluo-4). The A2387 will be used ion this work to artificially increase the intracellular calcium concentration in order to perform control measurements (see section 6.4.4).

EDTA

Ethylenediaminetetraacetic acid, widely abbreviated as EDTA is a polyamino carboxylic acid and a colourless, water-soluble solid. It is widely used to dissolve limescale. Its usefulness arises because of its role as a hexadentate ligand and chelating agent, i.e. its ability to "sequester" metal ions such as Ca^{2+} and Fe^{3+}. After being bound by EDTA, metal ions remain in solution but exhibit diminished reactivity. In this work EDTA is used for control measurements where the influence of the Ca^{2+} is investigated. The EDTA chelates the Ca^{2+} in the solution and therefore suppresses the influence of it.

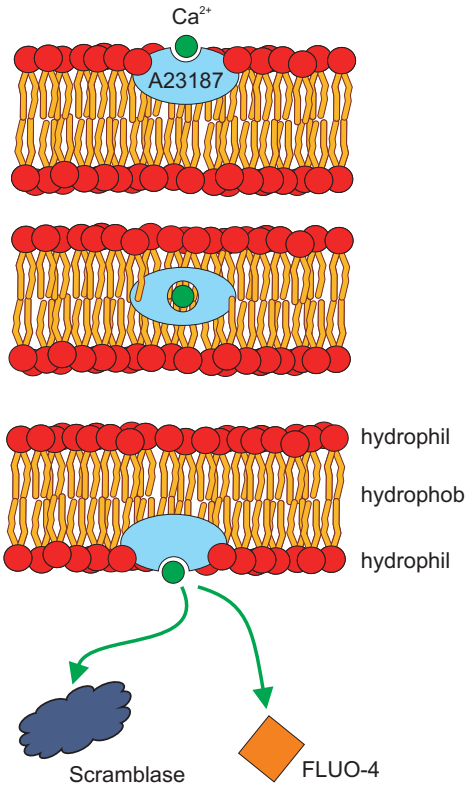

Figure 6.5: Sketch of the function principle of A23187. The A23187 molecules get incorporated into the membrane and make them permeable for Ca^{2+}. In coarse of time more and more Ca^{2+} is transported from the exterior to the interior of the cell.

Fluo4

In order to visualize the Ca^{2+} rise a calcium sensitive fluorescent dye has to be used. The measurement of concentrations, however, is generally seen as rather problematic because of the auto-fluorescence or absorption properties of the intracellular milieu. Fluo-4 turns out to be the preferable indicator because its excitation and emission properties is least influenced by hemoglobin and it is the only dye for which excitation light did not lead to significant auto-fluorescence of the RBCs. Fluo-4, is an improved version of the calcium indicator, Fluo-3. It is commonly used as the non-fluorescent acetoxymethyl ester (Fluo-4 AM) which is cleaved inside the cell to give the free, fluorescent Fluo-4. It loads faster, is brighter at equivalent concentrations and is well-excited by the 488 nm. Unfortunately, concentrations can not be determined quantitatively with Fluo-4 because the binding of the Fluo-4 to the Ca^{2+} is only

accompanied with an increase in fluorescence intensity, but not with a shift in the exciting spectrum.

6.4 Results

All measurements have been conducted with fresh blood samples from at least 3 apparently healthy donors. For details about the materials or methods used the interested reader is referred to the materials section in the materials section.

6.4.1 Microfluidic Approach to RBC Adhesion

In order to provide a controlled yet interchangeable solvent environment, a microfluidic polydimethylsiloxane (PDMS) cell was constructed by standard soft lithography (Fig. 6.6a). The cell consists of two inlets from which either the cells in the HIS solution (see appendix A), LPA (used concentrations $2.5\,\mu M - 10\,\mu M$) or the ionophore A23187 (final concentration of $40\,\mu M$) could be applied. The flow was driven by a hydrostatic pressure difference that allowed for fine tuning. After injection of a new sample, the flow could be brought approximately to rest by eliminating the pressure difference. As described in section 3.5.2 behind the y-junction, the flow remained laminar, and the two solutions did not mix, except for very slow diffusion. With the optical tweezers, access to the microfluidic chamber was achieved and given small flow rates one can trap two RBCs (see Fig. 6.6a). Thus, the cells could be transferred from one solvent condition to another in a rapid and controlled manner. Since the cells were loaded with fluo-4 the calcium concentration inside the cell could be controlled and monitored in real time. In the blood flow, cell-cell contact times are rather short when RBCs "bum" into each other. To mimic this physiological condition, two cells were grabbed with the laser foci (compare Fig. 6.6) and moved back and forth as depicted in Fig. 6.6c. With this, the length of time for cells to adhere to each other could be determined, if they adhered.

6.4.2 Petri Dish Measurements

The same measurements were also conducted in a petri dish as follows: RBCs were incubated for 10 min with either A23187 or LPA in the presence of Ca^{2+} (for concentration values, please refer to the figure legends), followed by a fast sequence of adhesion tests between various cells. There were more than 50 cells tested in each experiment; the total number of tested cells amounted to more than 250.

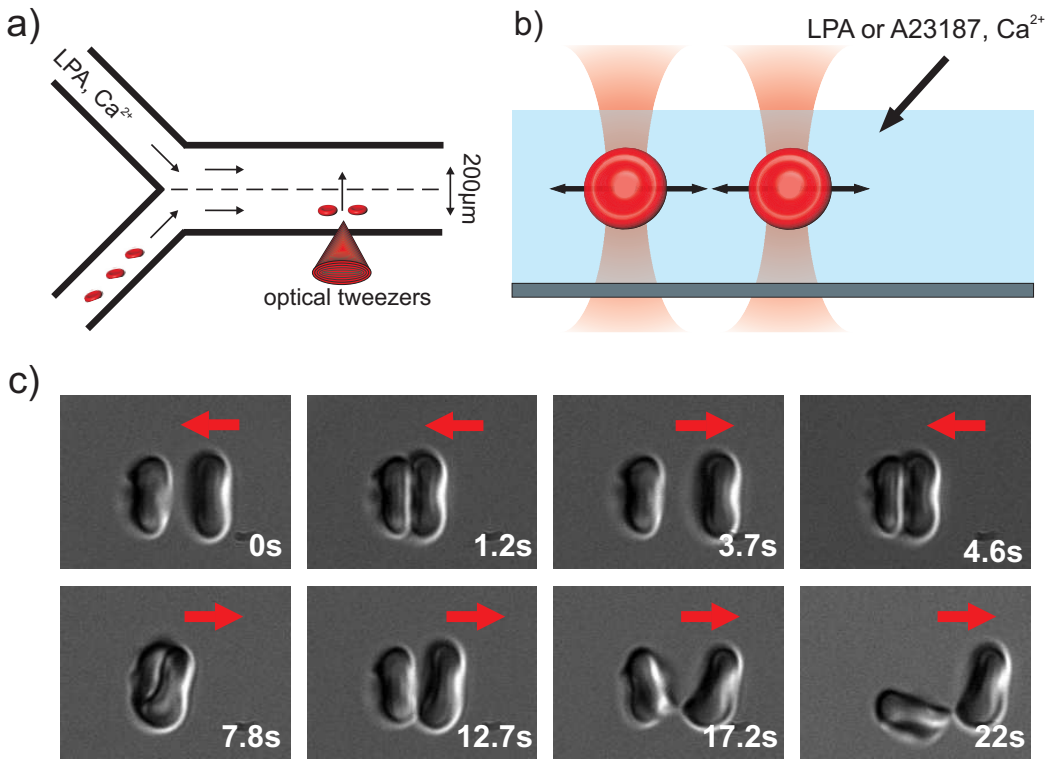

Figure 6.6: Probing for adhesion between RBCs after LPA or A23187 stimulation. a) Sketch of the microfluidic working principle. b) A sketch of the oscillatory movement of two trapped cells. c) Representative images of an adhesion measurement of two RBCs held by 4 optical traps. During a recording period of 22 sec, the cells were moved back and forth as indicated by the red arrows. (Images are 16 µm × 12 µm)

6.4.3 Red Blood Cell Stimulation with LPA

As pointed out in the Introduction, RBCs can be stimulated by LPA, and this has been proposed to contribute to the active participation of RBCs in the later stage of thrombus formation. In order to test for altered inter cellular adhesion behaviour under different conditions cells were treated with various solutions and were investigated in microfluidics, holographic optical tweezers accordingly. Upon stimulation with 2.5 µM LPA, the RBCs adhered to each other as visualized in an image sequence in Fig. 6.6c), respectively. During the stimulation procedure, most of the RBCs remained in their discocyte shape. To exclude any dependencies on the interaction surface due to the anisotropic shape of the cells, we aimed for another condition using spherocytes [96]. This was realized by increasing the LPA concentration to 10 µM,

which is still within the physiologically observed range. The separation force could not be determined by the HOT approach because it exceeds the force of the laser tweezers, which, in this particular setup, amounts to $15 - 25\,\mathrm{pN}$. Consequently, at this stage, the adhesion force could only be qualified to be larger than this. Nevertheless, with this approach a statement about the general behaviour of the treated RBCs and the adhesion statistics could be reached. Cells under five different conditions were tested: (i) HIS-solution (see appendix A), (ii) HIS-solution containing $2\,\mathrm{m}M$ Ca^{2+} and $10\,\mu M$ LPA, (iii) HIS-solution containing $2\,\mathrm{m}M$ Ca^{2+} and $2.5\mu M$ LPA, (iv) HIS-solution containing $2\,\mathrm{m}M$ Ca^{2+} and no LPA, and finally (v) HIS-solution containing $2\,\mathrm{m}M$ EDTA and $10\,\mu M$ LPA. We used at least 60 cells per condition. The results are summarized in Fig. 6.7. The great advantage of the microfluidic approach is that, in

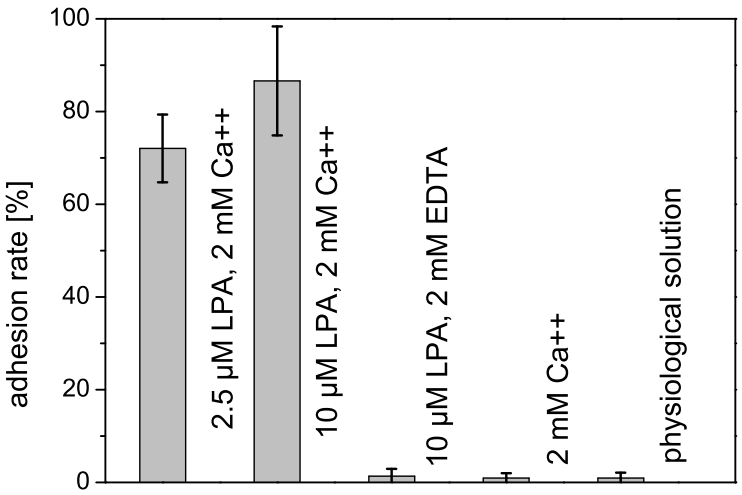

Figure 6.7: Results of the LPA measurements conducted in the microfluidic chamber and the Petri dish. The gray bars represent the percentage of cells that showed adhesion. The overall number of cells tested was 60 cells per measurement. In the presence of LPA and Ca^{2+}, a significant number of cells showed adhesion, whereas in the control experiments, only a very small portion of the cells showed an adhesion. The results of the student's t-test, compared to the control measurement (HIS-solution), are indicated at the top of each bar.

parallel, the Ca^{2+} uptake of the cells can be followed up by Fluo-4 imaging (the cells

were loaded with Fluo-4), as the trace in Fig. 6.8 shows for the stimulation with LPA. By this the course of the calcium uptake can be investigated and more importantly it can be controlled how many cells react with a calcium influx and how many of those change their adhesion behaviour. As can be seen in Fig. 6.8 more than 100 s are required after stimulation until the calcium influxes into the cells. However, the time to calcium peak varied significantly from cell to cell. Therefore, all the adhesion tests were run after a calcium peak. The RBC stimulation with LPA (2.5 μM as well as

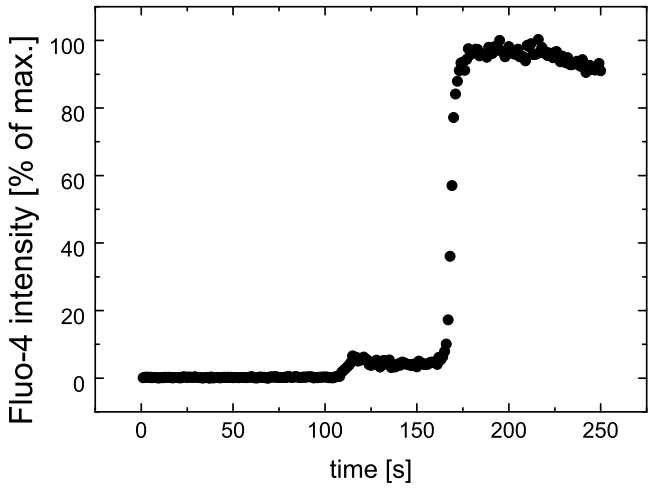

Figure 6.8: The relative fluorescence signal of a representative RBC in the upper microfluidic channel; t = 0 s is the time when the cell was moved into the LPA solution. The inset shows a schematic picture of the microfluidic chamber used.

10 μM) in the presence of extracellular Ca^{2+} led to an immediate qualitative change in the adhesion behaviour: cells stuck irreversibly to each other. In case of treatment with 2.5 μM about 72 % of the cells tested showed an irreversible adhesion. In the case of 10 μM, which still represents a physiological concentration near or inside a blood clot [57], the adhesion rate went even up to more than 90 %. In the control measurement where the extracellular Ca^{2+} was chelated by EDTA and in the control measurements without any RBC treatment, almost no adhesion events could be seen. In additional measurements performed by Bernhardt et al. [133], it was investigated that LPA treatment, as predicted, leads to a PS staining in the outer leaflet of the cell membrane (see. Fig. 6.9). In order to check for the role of the calcium in this adhesion process measurements with a calcium ionophore were conducted, which will

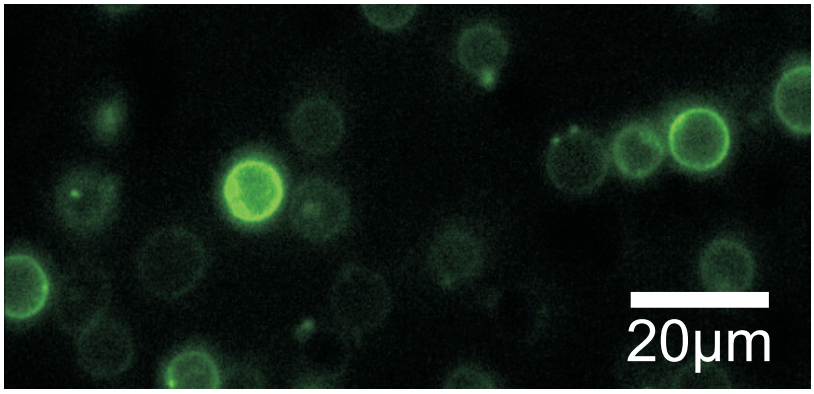

Figure 6.9: A fluorescence image of LPA-treated (2.5 μM) RBCs after annexin 5-FITC staining. The annexin 5 binding indicates the presence of PS on the outer membrane leaflet of the cells. [166]

be the focus of interest in the next subsection.

6.4.4 Approaching Signaling Entities

The initial stimulation experiments using LPA revealed that an LPA-induced Ca^{2+} influx leads to inter cellular RBC adhesion. To test whether this is a pure Ca^{2+} effect or if the presence of LPA is required, experiments were performed using the Ca^{2+} ionophore A23187 as an artificial tool to increase the intracellular Ca^{2+} concentration (see Fig. 6.5). A23187 increases the ability of bivalent ions to pass through the cell membrane[189, 46, 123]. Due to its high selectivity for Ca^{2+}, it is commonly used increasing the intracellular concentration of Ca^{2+} [169]. Virtually all cells react with a calcium influx after treatment with A23187 which makes it an excellent tool to test the signalling entities in this case. Hence, the cells were treated with a certain concentration of A23187 (up to 40 μM). Again these measurements were carried out in the microfluidic as well as in the petri dish. In the microfluidic approach, after transferring them into the A23187 containing solution, the Fluo-4 fluorescence signal increased almost immediately, i.e., faster than after application with LPA. The Ca^{2+} influx into the cell is depicted in Fig. 6.10. With the help of the microfluidic approach it could be noticed that the calcium increase in the cells was much faster compared to case of LPA treatment. The reasons for this behaviour can be found in the artificiality of the permeability after treatment with A23187. During the Ca^{2+} increase, the cells undergo a shape transformation from discocytes to spherocytes via an intermediate step of echinocytes. This shape transformation has been reported in several studies [46, 133] and is a known side effect of the A23187 treatment, especially

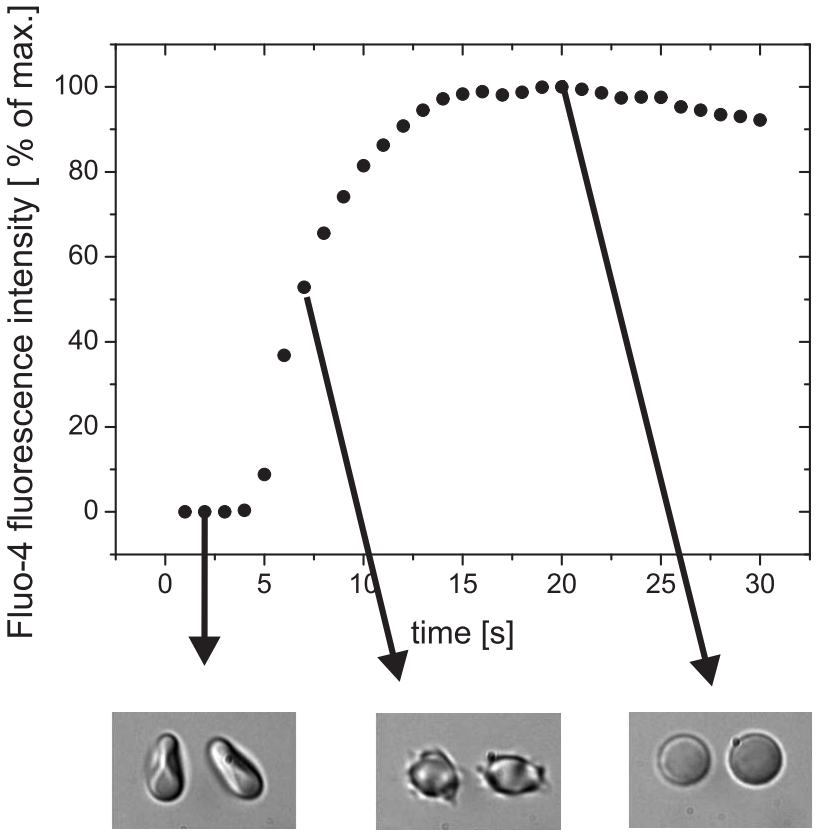

Figure 6.10: The relative fluorescence signal of a representative RBC in the upper channel of the microfluidic system; t = 0 s is the time when the cell reaches the A23187 solution. The Ca^{2+} increase happens almost instantaneously. The decrease in signal after 15 s is due to photo bleaching. The RBCs undergo a shape transformation from discocytes (left) via echinocytes (middle) to spherocytes (right) after transfer into the A23187 buffer solution in the upper channel.

with higher concentrations. This shape transformation is caused by a vesiculation of PS containing vesicles and a consequent loss of membrane area [45]. Testing for adhesion was performed using a procedure identical to the LPA experiments performed in the following four media: (i) HIS-solution (see appendix A), (ii) HIS-solution containing $2\,\mathrm{m}M$ Ca^{2+} and $40\,\mu M$ A23187, (iii) HIS-solution containing $2\,\mathrm{m}M$ Ca^{2+} and no A23187, and (iv) HIS-solution containing $2\,\mathrm{m}M$ EDTA and $40\,\mu M$ A23187. The results are summarized in Fig. 6.11. Intercellular adhesion was significantly increased compared to the controls only when the intracellular Ca^{2+} concentration was increased. In the case of RBC treatment with $40\,\mu M$ A23187 the adhesion rate

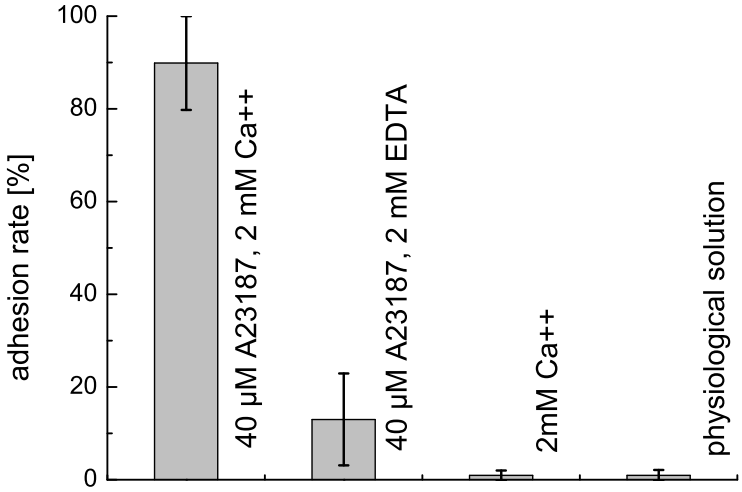

Figure 6.11: The results of the ionophore measurements conducted in the microfluidic chamber and a Petri dish. The black bars represent the percentage of cells that showed adhesion. The number of cells tested was about 60 per measurement. In the presence of A23187 and Ca^{2+}, about 90 % of the cells tested adhered, whereas in the control experiments, less than 3 % of the cells adhered. The results of the student's t-test, compared to the control measurement (HIS-solution), are indicated at the top of each bar.

increased up to almost 90 %. Experiments with lower concentrations resulted in much lower adhesion rates, which is most probably due to the concentration-time dependence of the PS exposure in RBCs after A23187 treatment. Nguyen et al. showed that dependent on the concentration used for these measurements, it can take up to hours until a significant amount of cells represent a PS exposure [133]. With increasing A23187 concentrations the time reduces significantly. Since the combined approach of optical tweezers and microfludic do not allow for an observation time of more than a couple of minutes; in those measurements a larger concentration of A23187 had to be used in order to speed up the PS-exposure. One might argue that the investigated adhesion could be an artifact due to the high concentrations of ionophore, but in control measurements where all the extracellular Ca^{2+} was chelated by EDTA, only a small increase in the adhesion rate could be found. In the control measurements without any RBC treatment, as in the measurements with the LPA, no adhesion at

all could be found among two RBCs. Bernhardt et al. [133] also found a PS staining after A23187 treatment (see Fig. 6.12) indicating a presence of PS in the outer leaflet of the RBC membrane.

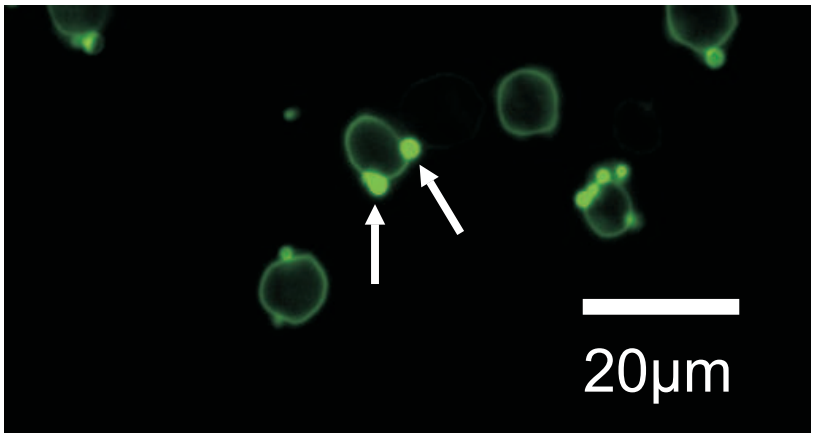

Figure 6.12: A fluorescence image of annexin 5-FITC-labeled RBCs. The cells were treated with A23187, and exposure of PS at the cell surface was clearly identified. A vesiculation of the cells was also observed (indicated by arrows). [166]

The drawback of this approach is the force limitation of the optical tweezers which forbid the exact force determination. Therefore, in order to quantify the occurring adhesion more precisely a different approach was chosen. With AFM based single cell force spectroscopy (SCFS) the adhesion forces were measured, which will be in the focus of the attention of the next paragraphs.

6.4.5 Quantification of the Intracellular Adhesion

To allow a discussion of a physiological (or pathophysiological) relevance of the described adhesion process, one needs to determine the separation force. As described above, the separation force exceeds the abilities of the HOT. Therefore, single-cell force spectroscopy [67] was utilized to determine the force. For further information about the SCFS-technique, see chapter 4.

Cantilever Functionalisation

For these measurements the adsorption protocol (see appendix A.2.4) of $Cell-Tak^{TM}$ (BD Biosciences) turned out to be the most efficient functionalization protocol for binding a RBC to the cantilever.

Measuring Parameters

The cells were captured with the manual lowering of the cantilever and a gently movement of the cantilever while carefully retracting the cantilever. In all the measurements the setpoint force was set to a low value of 200 pN in order to exclude any influence of additional adhesion sources. The contact time was varied between 0 s and 120 s in preliminary experiments, but since no strong dependence on the contact time was found, it was set to 0 s for all the experiments. The pulling velocity of the cantilever was set to 5 µm/s in order to compromise between fast experiments and small velocity influence on the adhesion measurements. During spectroscopy experiments the deflection of the cantilever was monitored in real time using an built-in feature of the SPM software. The cantilevers used were tipples TL-1 with nominal spring constant of 0.03 N/m from Nanoworld. Cell morphology was monitored using phase contrast microscopy. A further functionalisation of the petri dish surface was not necessary since the RBCs stuck to the surface without any treatment.

Measurements

In the following section, two different measurements were conducted: control measurements in which the cells remained untreated, and measurements in which the cells were treated with a concentration of 2.5 µM LPA. A concentration of 2.5 µM was chosen for most of the measurements because it resembles most physiological concentrations. Later on, further measurements with 10 µM LPA were conducted as well to check for the influence of the cell shape on the measured forces. Fig. 6.13a shows two example curves of measurements with 2.5 µM LPA treated cells (red) and untreated cells (green). In most of the measurements, a significantly changed adhesion behaviour was observable after the treatment with LPA. Whereas the measured forces in the case of untreated cells barely exceeded 20 pN, in the case of LPA treatment this measured force went up to even more than 300 pN in some cases. However, the the measured forces strongly varied from cell to cell. In total, more than 50 cells were tested for each case and the results are summarized in Fig. 6.13a and c. The mean value of the maximum unbinding force of untreated RBCs (control, green) amounted to 28.8 ± 8.9 pN (s.d.) (n=71), whereas in the LPA experiments, the mean value of the maximum unbinding force amounted to a much higher value of 100 ± 84 pN (s.d.) (n=193, from three different donors), indicating a severe difference in adhesion behavior of untreated and LPA-stimulated RBCs. The occurrence of the small adhesion forces in the control measurements require further discussion since the measured forces in the control were large enough to be seen in the optical tweezers measurements, but have never been seen there. The reason for these forces most probably lie in the different measuring technique of the SCFS. It is an inherent part of the single-cell force

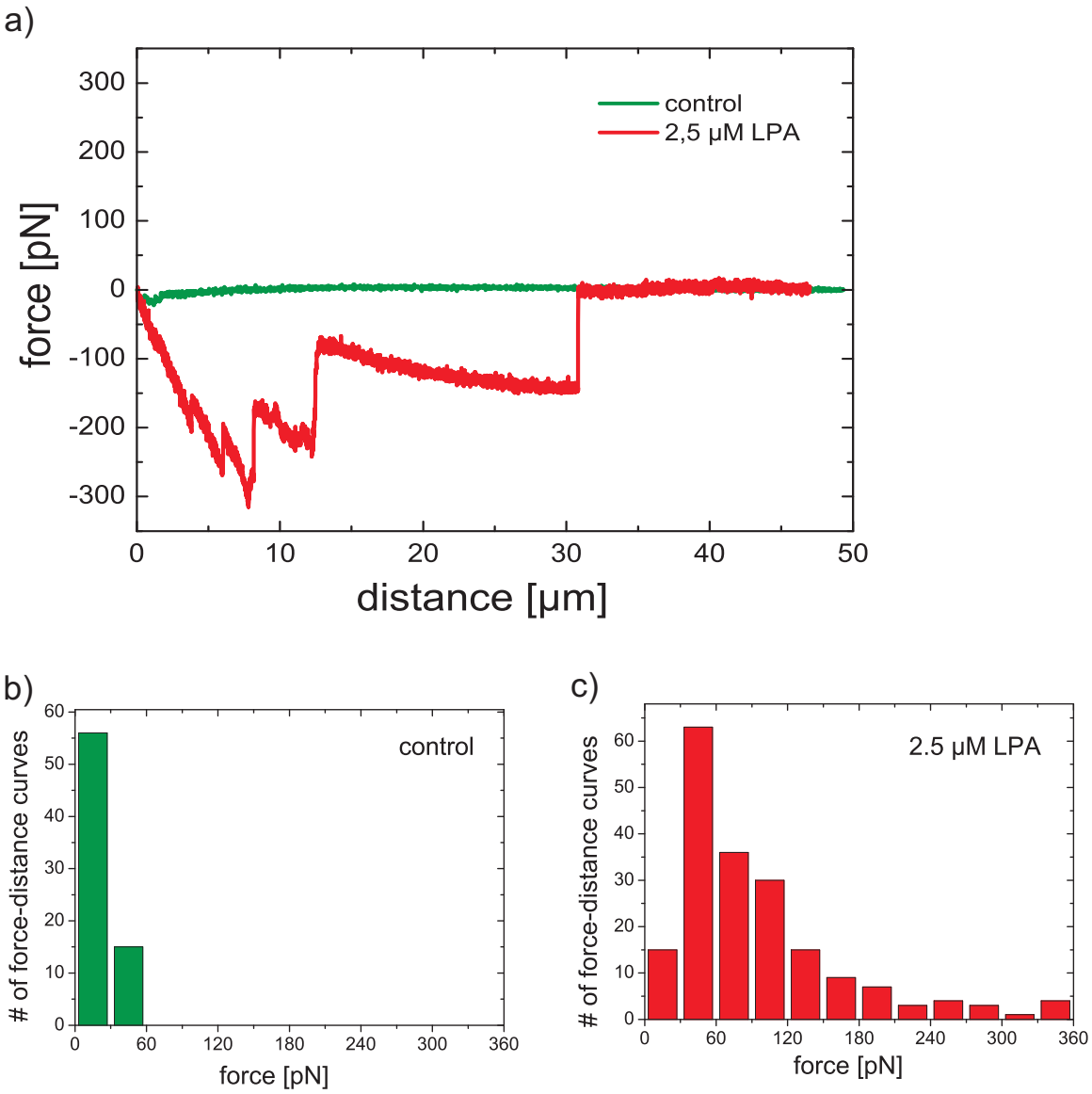

Figure 6.13: a) Shows the combined plot of an example force-distance-curve of a control(green) and an LPA measurement (red). b) The statistics of measured adhesion forces in the control measurement (without LPA treatment) c) Recorded data of the measured forces for LPA treated RBCs.

spectroscopy procedure that cells need to be brought into contact by a certain force application (i.e. a certain force set point). Due to the preset force set point or due to misalignment of the two cells and the resulting cell-cantilever or cell-surface contacts

a small adhesion force is measured. Since the absolute value measured in the LPA measurements is much larger than this value, theses force artifacts can be neglected. A step-wise release plotted in Fig. 6.13a was typical for all the LPA treated cells

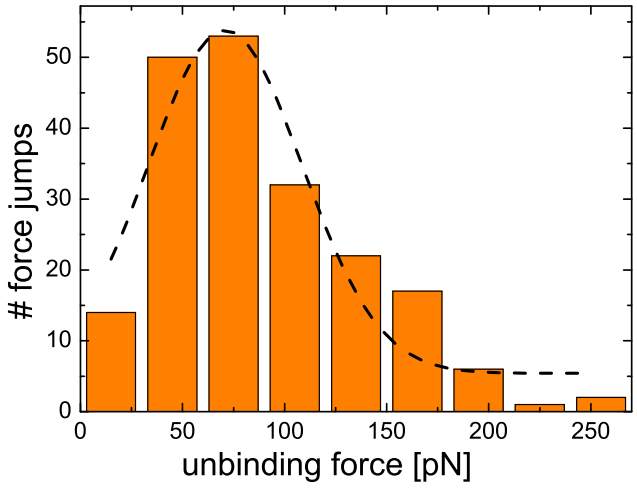

Figure 6.14: A histogram of the unbinding force of a single tether within the procedure visualized in Fig. 6.13 (red curve). The dotted line depicts a Gaussian approximation of the bars.

measured. Each step in this force-distance diagram corresponds to a single rupture of a so called membrane-tether. Since such force jumps can be an indicator for specific binding points, an the jump heights of all force jumps was analyzed. Fig. 6.14 depicts a histogram of all force jumps. A Gaussian distribution of of the adhesion forces of the single jumps could be found, but it could not conclusively confirm an involvement of specific binding points.

6.4.6 Effects of Spherical Shape on Adhesion Behavior

In order to check whether the cell shape has an effect on the adhesion properties of the RBCs measurements with $10\,\mu M$ LPA were conducted. It is known that larger LPA concentrations cause shape transformation from discocytes to spherocytes (see Fig. 6.2d). The cells undergo a vesiculation process in which PS containing vesicles are expelled from the membrane, resulting in a loss of membrane area. This leads to a change in the area to volume ratio of the cells and the spherical shape arises. The open question was how and to what extend this shape transformation has an

impact on the measured adhesion forces. As can be seen in Fig. 6.15 this treatment leads to a change in the shape of the force distance curves. The treatment results in a significant shorter interaction length (i.e. tether length is much shorter). Fig. 6.16

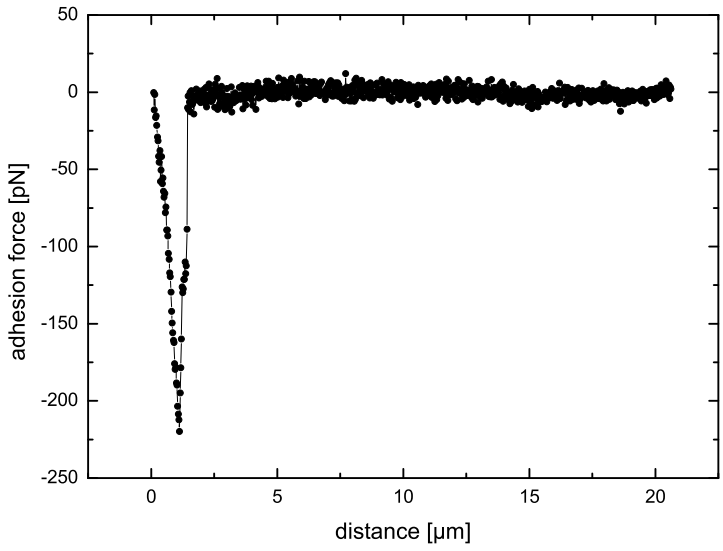

Figure 6.15: Force distance diagram of a RBC-RBC interaction after treatment with $10\mu M$ LPA.

shows a comparison of the tether lengths measured in case of $2.5\,\mu M$ and $10\,\mu M$ LPA treatment. In the case of $2.5\,\mu M$ one gets much shorter tether lengths compared to the case when $10\,\mu M$ LPA was used. The total value of adhesion force remains more or less the same about the value measured in the measurements with $2.5\,\mu M$ LPA, indicating that the adhesion process (in terms of adhesion strength) has not been affected by the higher concentration of LPA. The difference in adhesion behavior can easily be explained. Due to the cell shape change from discocytes to spherocytes the cell looses most of its flexibility; i.e. the discocytic cells are much more flexible. Therefore, given the same adhesion force between two cells the discocytes can form much larger tethers until the membrane tension has reached the critical value which causes disaggregation. In the case of the $10\,\mu M$ LPA treated RBCs, with their smaller flexibility, this critical value is reached faster. Hence, the tether length has to decrease in this case.

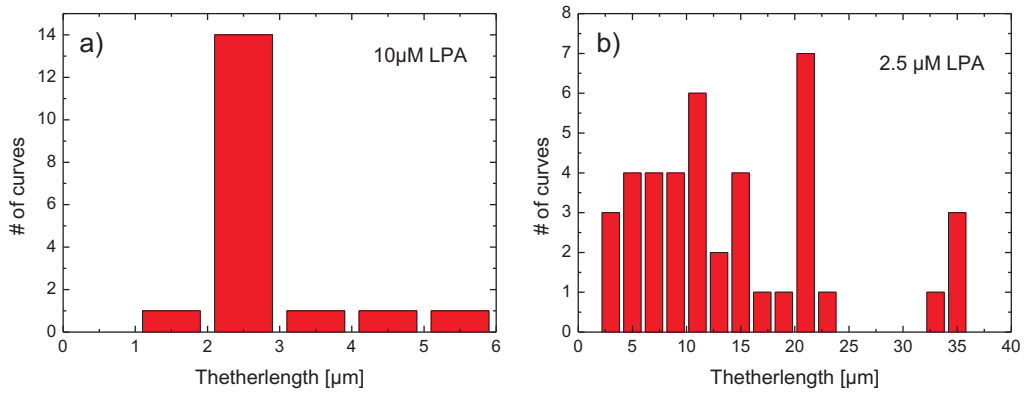

Figure 6.16: a) Histogram of the measured tether length in case of 10 μM LPA treatment. b) Histogram of the measured tether length in case of 2.5 μM LPA treatment.

6.5 Discussion

6.5.1 LPA Stimulation Leads to Inter-Cellular Adhesion

It is an established fact that the stimulation of RBCs with LPA leads to a Ca^{2+} influx through an non-selective voltage dependent channel (NSVDC) [97, 92]. It is further known that the increased intracellular Ca^{2+} results in the stimulation of the Ca^{2+}-activated K^+ channel (Gardos channel) [71, 81] and the activation of the lipid scramblase [189, 77]. Based on these mechanisms, an increased aggregation tendency of stimulated RBCs has been hypothesized [97, 191]. Concentrations of 2.5 μM and 10 μM LPA were chosen because they seemed to be within the common range of concentrations used with other cell types [54, 126] in addition to RBCs [45]. Moreover, this concentration is comparable to the local LPA concentration in the immediate surroundings of activated platelets, e.g., inside a blood clot [57, 69]. While the choice of the LPA concentration did not seem to have any significant effect on the adhesion rate itself, it had an impact on the shape of the RBCs. This relationship is discussed in the next section. After an intracellular Ca^{2+} increase was observed by fluorescence imaging, the setup mode was switched to white light for better HOT operation. Then, the cells were brought into contact and adhered to each other immediately. Because the time for the Ca^{2+} increase varied from cell to cell, which is in agreement with previous investigations [97, 98], the time between the initial stimulation of the cell and the final adhesion varied between 10 s and 140 s, yielding an average value of 72.75 $\pm$ 46.79 (s.d.). This time range already indicates

that under normal physiological conditions, the activation of RBCs is not compatible with an active process contributing to the initiation of a blood clot, but once caught in the fibrin network, the RBCs may actively support clot formation. In addition, to test the necessity of the presence of Ca^{2+} during LPA stimulation, the negative control experiments excluded any interplay between the infrared trapping laser and the adhesion process.

6.5.2 Signaling Components

Because LPA is a phospholipid derivative, the extent to which it is directly involved in the adhesion process was examined. Although the concentration used was clearly below the critical micelle concentration (70 μM - 1 mM) [57], which might induce detergent-like effects, LPA is likely to be incorporated into the membrane. From the initial intercellular adhesion after LPA stimulation (Fig. 6.7), one may propose the following alternative explanations: (i) LPA is directly responsible for the adhesion, (ii) LPA and the Ca^{2+} influx are both necessary to mediate adhesion, and (iii) LPA simply triggers the Ca^{2+} influx, and the Ca^{2+} signaling alone is sufficient to induce adhesion. Option (i) can be excluded immediately because it was tested as a control in the initial set of experiments (Fig. 6.7). In order to discriminate between options (ii) and (iii), experiments where A23187, a Ca^{2+} ionophore, was added to the RBCs were performed. As shown in Fig. 6.11, the increased intracellular Ca^{2+} concentration is the dominant signal initiating the adhesion. The Ca^{2+} entry under LPA stimulation is channel-mediated, although the molecular identity of the channel remains unclear [91]. Because LPA is not the major entity in the adhesion process, an alternative molecule or a combination of several entities downstream of the Ca^{2+} signal must control the response. Proteins that are known to be activated in RBCs by an increase in intracellular Ca^{2+} concentration are the Gardos channel, the lipid scramblase, the cysteine protease calpain [19, 155] and the Ca^{2+} pump. Although all the proteins are Ca^{2+}-activated, their sensitivity to Ca^{2+} differs. To determine in which order and under what conditions the aforementioned players activate, it is referred to the Ca^{2+} concentration with the half maximal effect (EC_{50}). It would therefore be desirable to quantitatively measure the Ca^{2+} concentration in an individual RBC. Unfortunately, this is not possible due to the failure of ratiometric Ca^{2+} sensors in RBCs [98]. Instead, EC_{50} values determined in different studies [112, 173, 21, 111] and the cellular responses that have been observed in the present study are compared. The smallest EC_{50} for Ca^{2+} is obviously that of the Ca^{2+} pump that keeps the resting Ca^{2+} concentration in RBCs well below 100nM [112]. With any increase in the intracellular Ca^{2+} concentration, the Ca^{2+} pump will activate. Although the V_{max} of the Ca^{2+} pump was determined in cell populations to be patient- and sample-dependent in a range of 8 to 20 mmol/(l$cells$ h) [173], the pump activity per cell varies tremendously

[173] . This variation explains the broad time range observed between the start of LPA stimulation and the Ca^{2+} increase. While the pump can counterbalance the LPA-induced Ca^{2+} influx for a short time period, during the application of A23187, the amount of Ca^{2+} entering the cell exceeds the V_{max} capacity of the Ca^{2+} pump for all cells. At a Ca^{2+} concentration of 400nM, the flippase transporting PS actively from the outer membrane leaflet to the inner one is inhibited [21]. Once the Ca^{2+} influx exceeds the transport capacity of the Ca^{2+} pump, the first player that will be activated is the Gardos channel, with an EC_{50} of 4.7µM [111]. As can be seen for the shape transitions upon A23187 stimulation shown in Fig. 6.10, cells turn (transiently) into echinocytes as a consequence of KCl loss triggered by K^+ efflux through the Gardos channel. For LPA stimulation, the situation is different: due to the activation of the non-selective cation channel by LPA, a Na^+ influx and, consequently, NaCl uptake counterbalances the KCl loss initiated by the Gardos channel, producing an osmotic equilibrium. For a 2.5 µM LPA stimulation, this equilibrium [95] is reached, whereas for a 10 µM LPA stimulation, the effect of the NaCl uptake overwhelms the KCl loss, resulting in the formation of spherocytes. The next entity to be activated upon Ca^{2+} entry is the scramblase, with an EC_{50} of 29 µM [167]. Scramblase activity was demonstrated by probing for PS in the outer membrane leaflet using annexin V-FITC staining. Staining was present after both LPA and A23187 stimulation, as depicted in Figs. 6.9 and 6.12, respectively. Calpain is activated with an EC_{50} of 40 µM, which is very close to the EC_{50} of the scramblase [129]. Under both stimulation conditions (LPA and A23187), a vesiculation that has been shown to be associated with the activation of calpain [19] was observed, which cleaves spectrin and actin and therefore leads to the breakdown of the cytoskeleton. This is in good agreement with a recent report on exovesiculation by Cueff et al. [47]. However, the vesiculation was much more pronounced under A23187 stimulation than under LPA stimulation, as depicted in the representative images in Fig. 6.9 and Fig. 6.12, respectively. Therefore, it is suggested that the Ca^{2+} concentration after stimulation with 2.5µM LPA is smaller compared to the A23187 stimulation and might be in the range of EC_{50} of calpain. For A23187 stimulation, a shape change from echinocytes to spherocytes occurs (compare Fig. 6.10), which is mediated by the encapsulation of microvesicles. However, the occurrence of PS on the outside of the cell makes it a good candidate for initiating the adhesion process. This could be due to simple Ca^{2+}-PS-cross-bridging and/or a more complex process involving adhesion proteins. Further evidence for both options comes from aggregation studies of PS vesicles [137, 110], where aggregation occurs in solutions of physiological ionic strength containing Ca^{2+} in the mM concentration range. The dependence on high Ca^{2+} concentrations and evidence from further studies reporting enhanced aggregation of PS liposomes in the presence of polymers [12] suggest that additional membrane constituents in the RBC contribute to the aggregation process. This leads to other Ca^{2+}-dependent proteins

in RBCs, such as PKC_α [75, 103] or the nitric oxide synthase [105, 122]. Further research is required to address the question of the molecular identity of the additional components in the adhesion process. Analyzing the stepwise unbinding (compare Fig. 6.13a) when RBCs are separated from each other, a Gaussian distribution of the force centered at 71.9 pN was observed (Fig. 6.14). Such a distribution suggests the formation of tethers and specific bonds between the RBCs that are released one by one during the separation process.

6.5.3 Relevance to in Vivo Conditions

The LPA concentration of between 2.5 and 10 μM is a physiologically relevant concentration that is likely to occur locally after platelet activation. Upon stimulation with such an LPA concentration, RBCs adhere irreversibly to each other. The separation force of approximately 100 pN (determined by single cell force spectroscopy) is in a range that is of relevance in the vasculature [163]. As mentioned previously, due to the time course of the Ca^{2+} increase, an initiation of a blood clot based on intercellular RBC adhesion is regarded to be irrelevant under physiological conditions. However, once caught in the fibrin network of a blood clot, the adhesion process observed here in vitro may support the solidification of the clot. This notion is supported by the aforementioned experimental and clinical investigations reporting a prolongation of bleeding time in subjects with low RBC counts [80, 116, 97, 120]. Evidence that the adhesion process described in this work may play a role in vivo was recently provided by Chung and coworkers [135]. In this study, an increase in intracellular Ca^{2+} of RBCs associated with a PS exposure was be related to prothrombotic activity in vivo in a venous thrombosis rat model.
Under pathophysiological conditions, inter cellular RBC adhesion after Ca^{2+} influx seems to have a more pronounced effect. An example is the vasco-occlusive crisis of sickle cell disease patients. Here, the Ca^{2+} influx is mediated by the NMDA-receptor, which has been found to be abundant in RBCs [122]. This study provides a link between the increased prevalence of the NMDA-receptor in sickle cell disease patients [23] and the symptoms of the vasco-occlusive crisis. Further examples where disorders in the ion homeostasis of RBCs are associated with thrombotic events are malaria [119] and thalassemia [58, 170]. Therefore, it is proposed that the Ca^{2+} increase, independent of the entry pathway, followed by PS exposure and RBC aggregation is a general mechanism that may become relevant under pathological conditions.

6.6 Summary

In this chapter, a combined approach of holographic optical tweezers and microfluidics was utilized to test the present hypothesis whether the physiological stimulant lysophosphatidic acid (LPA) induces an intercellular adhesion among RBCs. The hypothesis could be confirmed by these measurements. Thereby, the cells were loaded with the calcium sensitive dye Fluo-4 in order to detect a calcium rise in the cells after LPA treatment. This calcium rise could be identified to be crucial for the occurring intercellular adhesion. A microfluidic was used to stimulated the RBCs in a time-controlled and time-resolved manner. By this the identification of calcium as a key player could be achieved. By this approach, a large number of cells could be tested and it could be concluded that LPA treatment, in fact, leads to an inter cellular adhesion of red blood cells. Unfortunately, the occurring adhesion exceeded the force abilities of the optical tweezers and only a lower limit of adhesion forces could be declared. In order to quantitatively study this adhesion process, single cell force spectroscopy was utilized. In this method a single cell is attached to a cantilever and is lowered onto another cell. The adhesion forces are measured by measuring the deflection of the cantilever while retracting it. With this approach the intercellular adhesion could be quantified to amount to $100 \pm 84\,\mathrm{pN}$ in strength. Concerning the question of physiological significance the results of holographic optical tweezers and single cell force spectroscopy were combined and it could be concluded that the LPA induced inter cellular adhesion of RBCs could be of importance in the later stage of blood clotting and actively contributes to blood clot solidification.

In the next chapter another adhesion process of RBCs, induced by macromolecules, is investigated by means of SCFS.

7 Depletion-Induced Adhesion of Red Blood Cells

7.1 Introduction

Human red blood cells have a tendency to form aggregates that look similar to a stack of coins [39, 40, 63, 136]. These linear structures are called rouleaux. Fig. 7.1 shows a single rouleau in autologous plasma consisting of 7 individual RBCs. The number of RBCs per rouleau can vary and branching between two rouleaux can occur. The picture of the aggregate shown in Fig. 7.1 was taken under static conditions meaning that no flow was applied to the sample. The attractive forces involved in the creation process of rouleaux are relatively weak. Hence, it is possible to dissolve rouleaux into smaller fractions or even into single cells by applying a sufficient shear forces [148, 156]. In general the rouleaux formation of RBCs is assumed to be a reversible process, in contrast to blood coagulation in which irreversible aggregates are formed. In both coagulation and aggregation, the fibrinogen plays a crucial role [136]. In coagulation it is converted into fibrin that is polymerized to form a mesh in which platelets and RBCs are trapped [29]. Unlike in coagulation, fibrinogen remains soluble during aggregation. Here, fibrinogen acts as a macromolecule that is responsible for the RBC aggregation. The processes involved in this macromolecule-induced aggregation are the main focuses of this chapter.

7.2 Mechanism of Red Blood Cell Aggregation

As outlined in the introduction, RBCs form aggregates in static blood, characterized by a face-to-face morphology, similar to a stack of coins, termed rouleaux. This aggregation is caused by the presence of macromolecules, such as fibrinogen in blood plasma. Similar rouleaux formation can also be induced by re-suspending the RBCs in physiological solutions containing neutral macromolecules such as dextran [144] (DEX). However, without any macromolecules, e.g. RBCs in a simple salt solution, no aggregation occurs. The fibrinogen mediated aggregation of RBCs increases consistently with increasing fibrinogen concentration [124], whereas the dextran-mediated aggregation of RBCs reaches a maximum at a certain dextran concentration. The

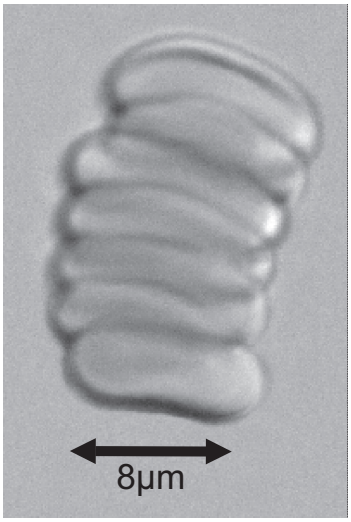

Figure 7.1: Snapshot of a rouleaux of 7 RBCs in a dextran solution. b) A sketch of the working principle of single cell force spectroscopy (SCFS).

strength of the aggregation depends not only on the dextran concentration, but also on the molecular weight of the dextran (i.e., the radius of gyration of the dextran) [27, 40]. To this day, the mechanisms involved in RBC aggregation have not been fully understood. There are two coexisting models that try to explain the rouleaux formation of RBCs: the bridging model and the depletion model. In the bridging model, it is assumed that fibrinogen or dextran molecules non-specifically adsorb onto the cell membrane and form a "bridge" to the adjacent cell [27]. In contrast, the depletion model proposes the opposite. In this model, aggregation occurs because the concentration of macromolecules near a RBC surface in close proximity is depleted compared to the concentration of the bulk phase, resulting in a net "depletion" force. In the next paragraphs the two models are explained in more detail.

7.2.1 The Bridging Model

The bridging model assumes that large macromolecules adsorb onto the cell surface and thereby bridge two adjacent cells. When these bridging forces exceed the disaggregation forces such as electrostatic repulsion, membrane strain and mechanical shearing, aggregation occurs [26, 27, 38, 40, 164]. More precisely, studies that focused on the inter-cellular distance [39] of two adjacent cells revealed that the inter-cellular distance is less than the size of the hydrated molecules. This led to the assumption that the terminal portions of the flexible polymers are adsorbed onto the surfaces of adjacent cells, resulting in a cell-cell adhesion (see Fig. 7.2). Thereby, the cell-cell dis-

tance increases with increasing polymer size but is always smaller than the diameter of the hydrated polymer [37].

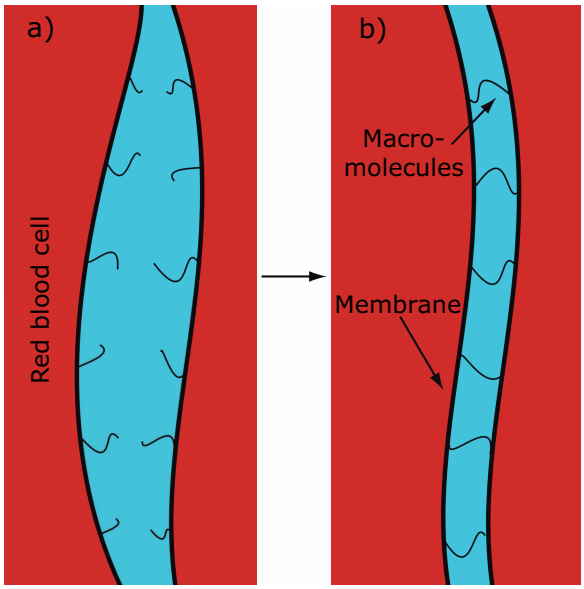

Figure 7.2: Schematic illustration of how macromolecular bridging leads to intercellular adhesion. Macromolecules adsorb onto the RBC-membrane and are able two bridge the adjacent cell.

7.2.2 The Depletion Model

In the depletion model aggregation occurs because the concentration of macromolecules near a RBC surfaces in close proximity is depleted compared to the concentration of the bulk phase, resulting in a net "depletion" force. A first explanation of depletion forces was given by Asakura and Oosawa [4], who discovered that the presence of small spheres (i.e., macromolecules) can induce effective forces between two larger particles if the distance between them is small enough. The origin of these forces is purely entropic. When two large plates are immersed in a solution of rigid spherical macromolecules and the distance between the inner surfaces of these two plates is smaller than the diameter of solute macromolecules, none of these macromolecules can enter the space between the plates and this space becomes a phase of the pure solvent. Therefore, a force equivalent to the osmotic pressure of the solution of macromolecules acts on the outer surfaces of these plates. Such a force also appears between two spherical particles, if the distance between the two large particles decreases to less than the size of the surrounding macromolecules (Fig. 7.3). In such a sys-

tem a so-called depletion layer surrounds the large particles where the centres of the smaller particles cannot enter. Consistently, in that depletion layer the concentration of macromolecules becomes depleted compared to that of the bulk. The thickness of this depletion layer equals the radius of the smaller particles. When overlapping between two depletion layers occurs, an additional free volume is available for the smaller particles causing an increase in entropy and hence an increase in Helmholtz's free energy leading to an effective osmotic pressure causing an attractive force between the large particles. In diluted solutions below the overlap concentration [48], polymers can be treated as rigid spheres with a radius $d_2/2$ matching the radius of gyration of the polymer [138].

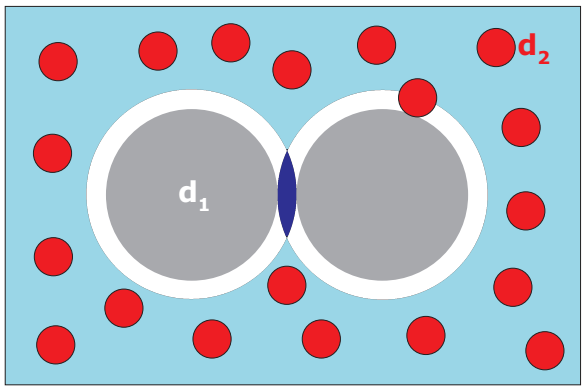

Figure 7.3: Illustration of the depletion phenomenon in a binary colloidal system. The depletion layer of the colloids with diameter d_1 (grey) are marked white. When two depletion layers overlap, a volume $\delta V > 0$ (dark blue) is released, which is additionally available for the the smaller colloids (macromolecules, red) with diameter d_2.

7.2.3 Bridging Versus Depletion

In the past, there have been studies in support of both theories. Studies in favour of the bridging model deal with either aggregation induced by nonspecific binding of macromolecules [28, 37] or by specific binding sites or mechanisms [117]. However, the determination of macromolecular adsorption of polymers and proteins to RBCs are subject to a lot of potential artifacts and, consequently, the interpretation of existing data is difficult [86, 87]. Despite numerous efforts to quantify macromolecular binding, conclusive data is still lacking. On the other hand, several studies favouring the depletion model over the bridging model have been published [3, 30, 131]. Neu et al. [131] adopted the depletion concept and applied it on the aggregation of red blood

cells and developed a theoretical description of the acting forces. They also predicted quantitative values of the affinities and interaction energies. The next section will describe this theory in more detail.

7.3 Theoretical Description of Depletion Based Aggregation of RBCs

In order to develop a conclusive theory of the RBC aggregation due to non-adsorbing macromolecules, one has to define the nature of the cell-cell interaction. First and for most, the nature of the interaction forces depends on the surfaces of the adhering objects. In the case of RBCs, the surface of the RBCs is strongly influenced by the glycocalyx, which consists of a complex layer of proteins and glycoproteins and bears a negative charge that is primarily caused by ionized sialic acid groups [158]. Therefore, one has to take the possibility into account that the RBCs also interact via steric interaction due to the overlapping glycocalyces. Due to the high electrostatic repulsion, cell-cell distances at which minimal interaction energies occur (i.e. maximum adhesion strength) are always greater than twice the thickness of the glycocalyx [131]. Thus, steric interactions can be neglected for the case of RBCs and in the following only depletion and electrostatic repulsion will be considered. Van der Waals interactions can be neglected as well since they are two orders of magnitude smaller than the aforementioned mentioned interaction energies.

7.3.1 Depletion Interaction

In order to estimate the depletion forces between two surfaces, one has to calculate the product between change of the volume of the depletion zone and the osmotic pressure drop. Assuming a step profile for the free polymer (see Fig. 7.4) [65, 178], the depletion interaction energy per area w_D can be calculated as a function of the cell-cell separation d:

$$w_D = -\Pi(2\Delta - d) \tag{7.1}$$

when $d/2 < \Delta$ and equals zero for $d/2 > \Delta$. To calculate the osmotic pressure Π, a viral equation can be employed by neglecting coefficients higher than the second viral coefficient (B_2) since the concentrations relevant for RBC aggregation are comparably small [131]:

$$\Pi = \frac{RT}{M_2} c_2 + B_2 (c_2)^2 = - - \frac{\mu_1 - \mu_1^0}{\nu_1} \tag{7.2}$$

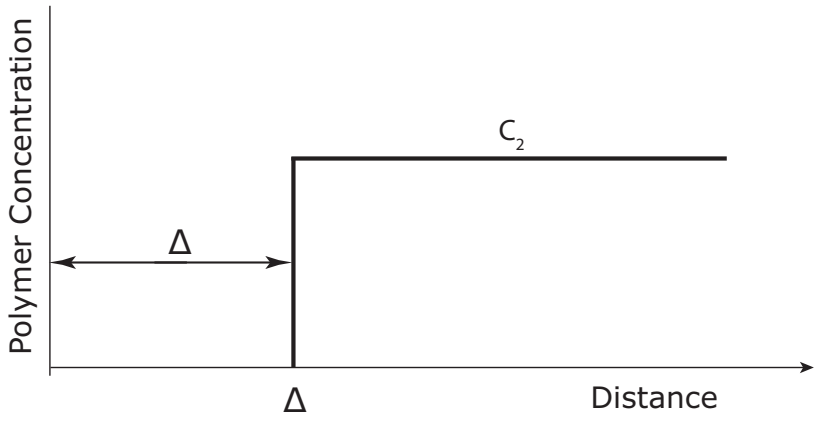

Figure 7.4: Schematic concentration-distance diagram of a step profile near a hard surface to calculate the depletion interaction energy.

where R, T, ν_1 and M_2 are the gas constant, the absolute temperature, the molecular volume of the solvent, and the molecular mass of the polymer. The chemical potential of the solvent in the polymer solution is μ_1 and is μ_1^0 in a free solution; c_2 represents the bulk polymer concentration. In general, the examination of depletions layers requires distinguishing between "har" and "soft" or "hairy" surfaces. Hard surfaces are considered smooth and do not allow polymer penetration, whereas soft and hairy surfaces do allow polymer penetration. As will be shown later the resulting depletion interaction energies can be quite different in both cases. RBC surface are characterized by a soft and hairy structure (glycocalyx) with attached macromolecules that can be penetrated in part or entirely by the free polymer in solution [131, 89, 178]. Fig. 7.5 shows the changed concentration-distance diagram in the case of a soft and hairy surfaces. The segment densities of the attached layer (e.g. the cell-glycocalyx, subscript a) and the free polymer (subscript 2) are indicated by Φ, the glycocalyx thickness by δ, and the penetration depth of the free polymer into the attached layer by p. In the case of a perfectly hard surfaces the penetration depth would be zero (see Fig. 7.5) and in case of a perfectly soft surface the penetration depth would be as large as the glycocalyx thickness δ. The depletion interaction energy w_D can be estimated by assuming a step profile for the free polymer as shown in Fig. 7.6 [65, 178].

$$-2\Pi(\Delta - \frac{d}{2} + \delta - p) \tag{7.3}$$

when $(d/2-\delta+p) < \Delta$ and zero for $(d/2-\delta+p) > \Delta$. Given the fact that the depletion layer thickness, the glycocalyx layer thickness and the penetration of the free polymer into the glycocalyx are known, the depletion energy can be calculated by equation 7.3. The glycocalyx layer thickness of RBCs has already been investigated and amounts to 5 nm in thickness. The depletion layer thickness as well as the penetration depth of the polymer into the glycocalyx will be discussed in the following subsections.

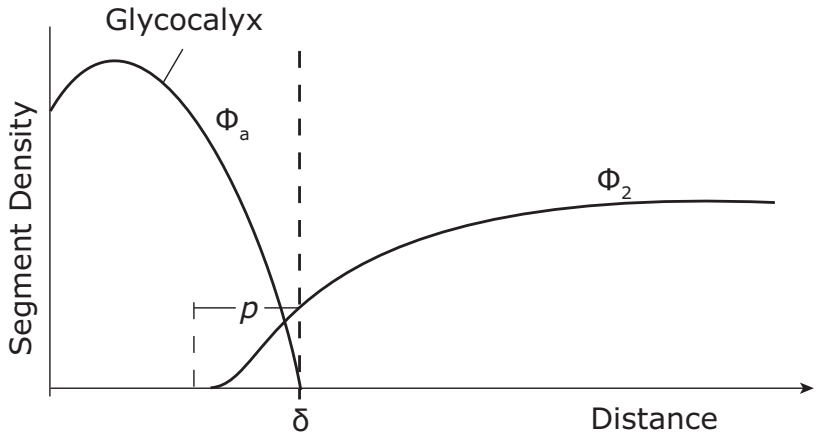

Figure 7.5: Illustration of the concentration-distance profile near a RBC soft surface in the presence of a depleted polymer. Φ_a and Φ_2 are the segment density of the glycocalyx and the depleted polymer, δ is the thickness of the glycocalyx, and p is the penetration depth of the free polymer into the glycocalyx

7.3.2 Depletion Layer Thickness

In this section an analytical expression that was derived by Vincent et al. [177] will be introduced. This approach is based upon calculating the equilibrium between the compressional or elastic free energy and the osmotic force experienced by polymer chains at a non adsorbing surface. It yields the depletion layer thickness as a function of the bulk polymer concentration c_2 and the molecular mass of the polymer M_2:

$$\Delta = -\frac{1}{2}\frac{\Pi}{D} + \frac{1}{2}\sqrt{(\frac{\Pi}{D})^2 + 4\Delta_0^2} \tag{7.4}$$

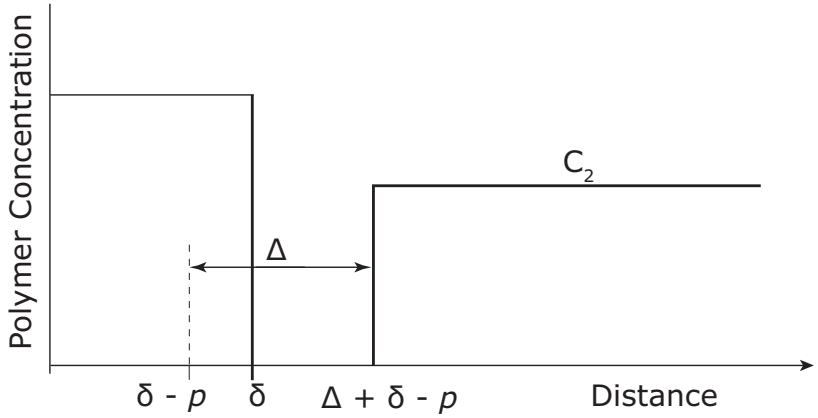

Figure 7.6: Concentration-distance step profiles near a soft surface (e.g. RBC surface) as an approach to calculate depletion interaction energy. δ is the thickness of the glycocalyx, p is the penetration depth of the free polymer into the glycocalyx and c_2 is the bulk concentration of the free polymer in the surrounding solution.

where Π is the osmotic pressure of the bulk polymer solution. The parameter D is a function of the bulk polymer concentration c_2 and is given by:

$$D = \frac{2k_BT}{\Delta_0^2}\left(\frac{c_2N_a}{M_2}\right)^{2/3} \tag{7.5}$$

where k_B and N_a are the Boltzmann constant and Avogadro number. Δ_0 is the depletion thickness for vanishing polymer concentration and is equal to $1.4\,R_g$, where R_g is the polymer's radius of gyration. Fig. 7.7 presents calculated depletion layer thicknesses for dextran and poly(ethylene glycol), PEG [131]. Dextran and PEG are both flexible, non-ionic and water-soluble molecules that are known to induce RBC aggregation above a certain threshold molecular mass [24, 27, 40, 130]. Dextran and PEG are available in several molecular mass fractions and their physiochemical properties have been studied extensively. Hence, those substances are perfect substances to test the feasibility of a theoretical model for RBC aggregation. In Fig. 7.7, it can be seen that the depletion layer thickness for different dextrans and PEG decreases only slightly with increasing concentrations up to 10 mg/ml, while at higher concentration

the depletion layer thickness decreases rapidly. For dextrans with different molecular masses the depletion layer thickness increases with increasing molecular mass and hence with increasing size of the polymer or radius of gyration. However, there are additional factors that can influence the largeness of the depletion layer thickness, such as the physiochemical properties of the polymers.

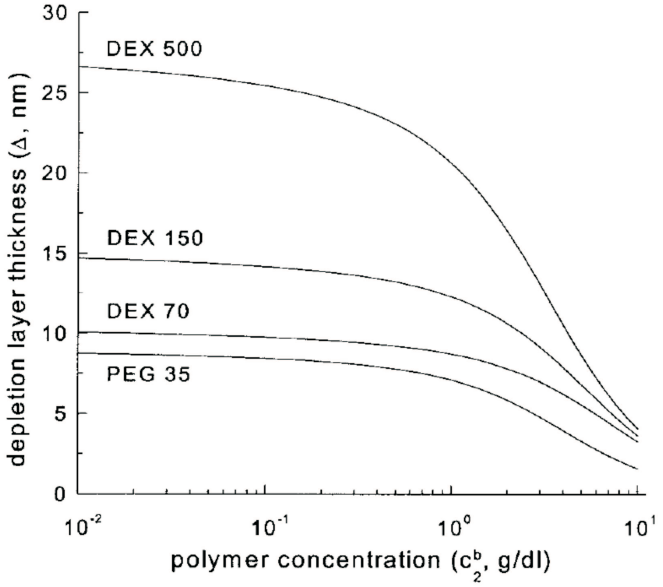

Figure 7.7: Theoretical dependence of the depletion layer thickness Δ on the bulk phase polymer concentration c_2 for dextrans with molecular masses of 70 kDa, 150 kDa and 500 kDa and PEG with a molecular mass of 35 kDa. Neu et al. 2002. "Depletion-mediated Red Blood Cell Aggregation in Polymer Solutions" *Biophysical Journal* 83:2482-2490

7.3.3 Macromolecular Penetration into the Glycocalyx

The last parameter to be taken care of in order to quantitatively describe the RBC depletion interaction energy is the penetration depth of polymers into the glycocalyx. Intuitively, the penetration depth of the free polymer into the attached layer (glycocalyx) should depend on the concentration, the polymer type and the molecular size of the used polymer. The penetration depth should be larger for smaller molecules and for higher concentrations due to increasing osmotic pressure. One possible approach to calculate the penetration depth of the free polymer is to assume that the penetration of the polymer proceeds until the local osmotic pressure developed in the

attached layer is balanced by the osmotic pressure of the bulk solution [178]. For such an approach one needs to know the exact concentration-distance diagram of the glycocalyx of the RBC. In Fig. 7.8 a simple concentration-distance model is shown,

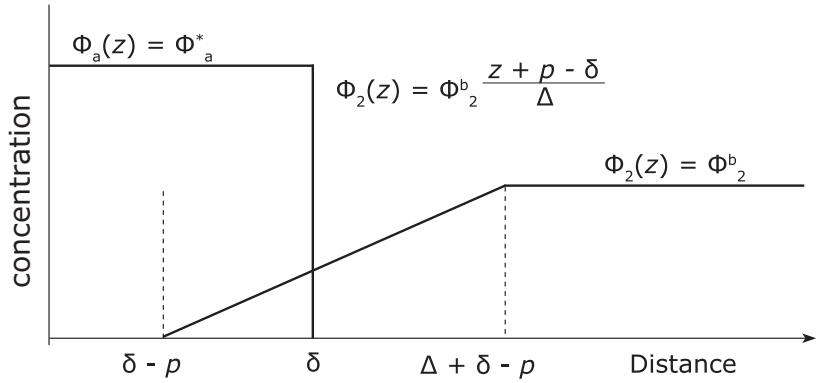

Figure 7.8: Illustration of concentration-distance profiles near a surface having a soft layer in which a uniform profile of attached macromolecules is assumed and a linear depletion layer profile for the polymer in solution. Subscript a and 2 determine the attached soft layer and the free polymer. z indicates the distance from the surface. From: Rad, S. and B. Neu 2009. "Impact of Cellular Properties on Red Blood Cell Affinity in Plasma-Like Suspensions" *European Physical Journal* E30:135-140 [147]

in which a uniform profile of attached macromolecules is assumed for the glycocalyx [178]:

$$\Phi_a(z) = \Phi_a^* \tag{7.6}$$

and a linear profile of the depleted polymer in solution [178]:

$$\Phi_2(z) = \frac{\Phi_2^b}{\Delta}(z + p - \delta) \tag{7.7}$$

When the glycocalyx is approached, the volume fraction of the polymer decreases from Φ_2^b at $\Delta + \delta - p$ to zero at $\delta - p$. Using these profiles, the penetration p can be calculated [178]:

$$p = \frac{\Pi \nu_1 \Delta}{k_B \Phi_a^* \Phi_2} \tag{7.8}$$

in which ν_1 determines the molecular volume of the solvent and Φ_a^* is given by:

$$\Phi_a^* = (1 - 2\chi)\Phi_a \tag{7.9}$$

where Φ_a determines the volume fraction of the attached macromolecules in the glycocalyx and χ is the Flory interaction parameter for the polymer and solvent [66]. Thus, for $\chi = 0$, Φ_a^* corresponds to the volume fraction of polymer in the glycocalyx. The influence of the volume fraction on the polymer penetration is shown in Fig. 7.9. In these studies Neu et al. assumed that the glycocalyx thickness was 5nm and

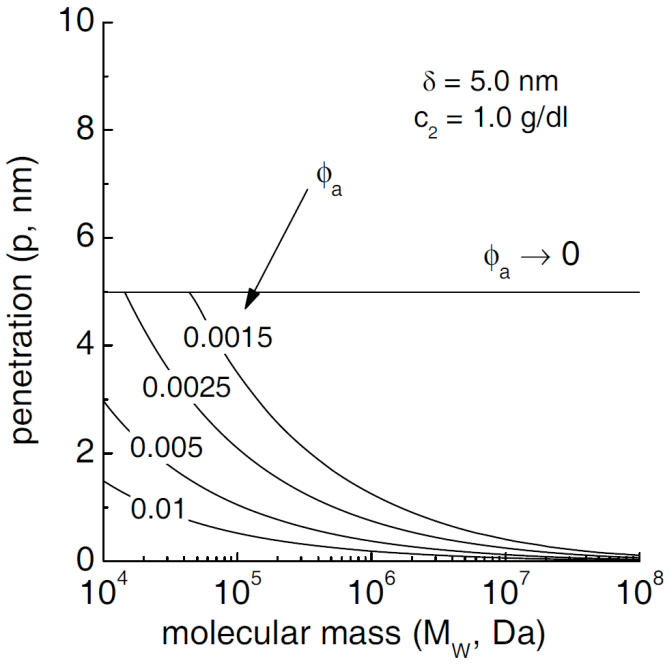

Figure 7.9: Effect of molecular mass on polymer penetration into the glycocalyx for differnet glycocalyx volume fraction Φ_a assuming a constant bulk polymer concentration of 10 mg/ml and a glycocalyx layer thickness of 5nm. From: Rad, S. and B. Neu 2009. "Impact of Cellular Properties on Red Blood Cell Affinity in Plasma-Like Suspensions" *European Physical Journal* E30:135-140 [147]

the bulk polymer concentration was 10mg/ml. The result of the study revealed that varying the glycocalyx volume fraction between 0 for a perfectly soft surface to 1 for a perfectly hard surface results in a distinct dependence of penetration on molecular mass, although this approach is not perfectly consistent because in it δ is assumed to be independent of bulk polymer concentration. A more realistic approach would be that the attached surface layer (e.g. glycocalyx) would collapse under a large osmotic pressure of bulk polymers [89]. Unfortunately, it is difficult to apply such an approach to RBC surfaces, since little is known about the physiochemical properties

of the glycocalyx, especially the interaction of the glycocalyx with different polymers. Regarding the aforementioned lack of information about the glycocalyx, an alternative approach would be to estimate the concentration dependence of the penetration depth via an exponential approach [131]:

$$p = \delta(1 - \exp(-\frac{c_2}{c_p})) \tag{7.10}$$

where c_p is the penetration constant of the polymer in solution (i.e. when c_p equals c_2 p is 63 % of δ). Again in this approach δ is assumed to be independent of bulk polymer concentration. Hence, p is basically a linear function of the polymer concentration are comparably small to c_p and asymtotically approaches δ at high concentrations. In a first approximation, c_2 can be assumed to be constant. However, for a more accurate description it would be necessary to express c_2 as a function of the used polymer type and polymer concentration.

7.3.4 Electrostatic Repulsion

Because the surfaces of RBCs is negatively charged electrostatic repulsion has to be taken into account additionally. The electrostatic free energy between two cells can be calculated by simply considering an isothermal charging process:

$$E = \frac{1}{2} \int_0^d \int_0^\rho \Psi(\rho, z) d\rho dz \tag{7.11}$$

where Ψ is the electro statical potential between the cells which is dependent on the charge density ρ. In order to calculate the electrostatic interaction energy between two cells, the free energy of two cells at a separation distance d has to be calculated, followed by the deduction of the free energy of two single cells (i.e. $d \to \infty$). In the case of RBCs, the Poisson-Boltzmann equation has to be solved in order to calculate the electrostatic potential Ψ. A linear approximation can be employed for the problem under consideration since it is usually suitable for the moderate electrical potentials encountered for various cells [30]. Assuming an evenly distributed constant surface charge of both cells within the glycocalyx, Ψ can be calculated for a single cell surface and for two cells at separation distance d. On top of that, it is even possible to simplify this approach by approximating the electrostatic potential between two cells as a superposition of the potential of two single cells. This approximation is legitimate since the Debye length (κ^{-1}) is small compared to both the glycocalyx thickness δ and the cell-cell distance d. Using these simplifications the electrostatic interaction

energy w_E is:

$$w_E = \frac{\sigma^2}{\delta^2 \epsilon \epsilon_0 \kappa^3} \begin{cases} \sinh(\kappa\delta)(\exp(\kappa\delta - \kappa d) - \exp(-\kappa d)) & d < 2\delta \\ (2\kappa\delta - \kappa d) - (\exp(-\kappa\delta) + 1)\sinh(\kappa\delta - \kappa d) - \sinh(\kappa\delta)\exp(-\kappa d) & d > 2\delta \end{cases} \tag{7.12}$$

where ϵ and ϵ_0 are the relative permittivity of the solvent and the permittivity of vacuum, and σ is the surface charge density.

7.3.5 Red Blood Cell Adhesion Energy in Polymer Solutions

With the depletion energy calculated above and electrostatic interaction energy it is possible to calculate the total interaction energy w_T of two adhering RBCs [131].

$$w_T = w_D + w_E \tag{7.13}$$

Neu et al. computed the effects of bulk phase polymer concentration on interaction energy. Fig. 7.10a shows a computation of the interaction energy with the assumption that the penetration depth is equal to the glycocalyx thickness and thus the penetration depth is independent of polymer concentration, whereas Fig. 7.10b shows the computed interaction energies when setting the interaction energy to zero. As one clearly can see, both assumption result in a completely different shape of the concentration-interaction energy curves. Hence, the penetration of polymers into the attached layer of proteins on the RBC is of a crucial nature when it comes to calculating the interaction energy. Within the concentration range shown in Fig. 7.10a, polymer penetration into the glycocalyx results in energy-polymer concentration relations that are bell-shaped and concave to the concentration axis. At first sight these bell-shaped curves are a bit confusing; when considering depletion interaction, one expects a consecutive increase in the interaction energy with increasing polymer concentration. The reason for these bell-shape nature of the curves lies in the increasing penetration depth of the polymers into the glycocalyx with increasing bulk polymer concentration (see equation 7.10) and in the decreasing depletion layer thickness with increasing bulk polymer concentration (see Fig. 7.7). For instance the dextran 70 (70 kDa) has a radius of gyration of about 8 nm. With the increasing penetration depth of the polymer into the glycocalyx (which has a thickness of 5 nm) the polymers gain the possibility to overcome the depletion barrier of the two surfaces' adhering surfaces. Due to the high osmotic pressure and the large penetration depth the polymers are allowed to "pass" through the depleted region between the two surfaces and hence the interaction energy decreases. Fig. 7.10a shows that smaller molecules result in higher interaction energies since the greater osmotic pressure difference outweighs the influence of the larger depletion layer for the larger molecules. Since the inter-

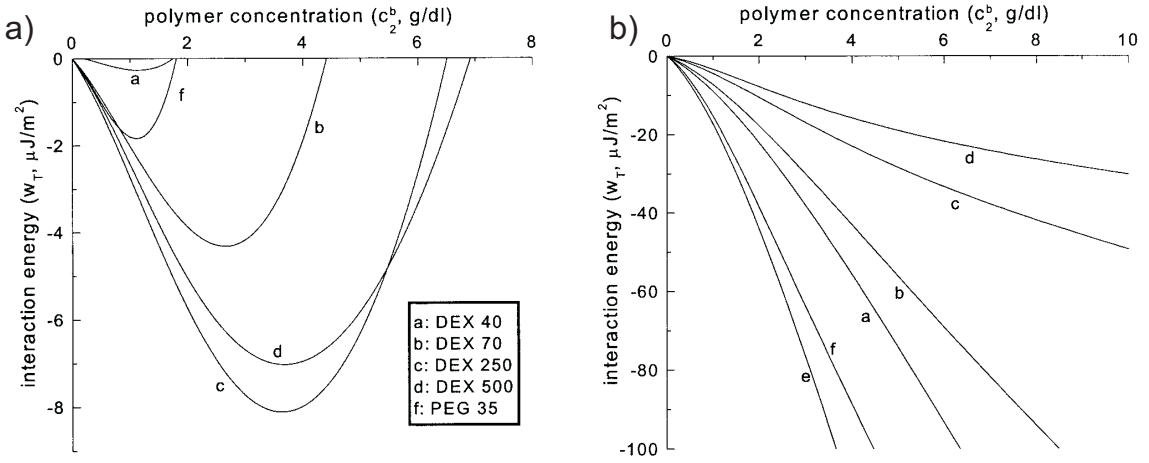

Figure 7.10: a) Effect of bulk phase polymer concentration on total interaction energy for RBCs suspended in various molecular mass fractions of dextran and PEG when penetration constant p is equal to δ and thus all polymers fully penetrate the glycocalyx. (a) dextran 40 kDa, (b) dextran 70 kDa, (c) dextran 250 kDa, (d) dextran 500 kDa, (e) PEG 35 kDa b) Effect of bulk phase polymer concentration on total interaction energy for RBCs suspended in various molecular mass fractions of dextran and PEG when penetration constant p is set equal to zero and thus no polymers penetrate the glycocalyx. (a) dextran 40 kDa, (b) dextran 70 kDa, (c) dextran 250 kDa, (d) dextran 500 kDa, (e) PEG 35 kDa From: B. Neu and H.J. Meiselman. 2002. "Depletion-Mediated Red Blood Cell Aggregation in Polymer Solutions" *Biophysical Journal* 83:2482-2490 [131].

action energies show a strong dependence on the penetration depth of the polymers into the glycocalyx, one has to carefully determine the actual penetration depth of the polymers into the glycocalyx. In order to find the correct value for the penetration depth, Neu et al. used data from Buxbaum et al. [32] to fit the penetration depth to the measured data of surface affinities (see Fig. 7.11). In this study Buxbaum et al. used a micro pipette based approach to measure the surface affinities of two adhering RBCs in various concentrations of dextran. They measured the extent of encapsulation of an RBC membrane sphere by an intact RBC. In order to quantitatively compare these experimental findings with the developed theoretical model, Neu et al. varied the penetration constant c_p until the calculated peak interaction energy for dextran 70 kDa or dextran 150 kDa equaled the value reported by Buxbaum et al (i.e., c_p was the only parameter varied). This equality occurred at $c_p = 0.7$ g/dl for dextran 70 kDa and $c_p = 7.5$ g/dl for dextran 150 kDa. By taking a look at the data

from Buxbaum et al. it can be seen that the total number of data points (i.e. the number of measured concentrations) remained limited. Additionally, the results were obtained by the micropipette aspiration technique which greatly suffers from large error bars due to abberations and inaccurate sucking pressure determination. Therefore in the present study the interaction energy of two adhering RBCs in dextran solution will be re-measured with more data points and more accuracy. The tool that was utilized to measure the interaction energy between two RBCs in their natural, discocytic form was the relatively new technique of single cell force spectroscopy.

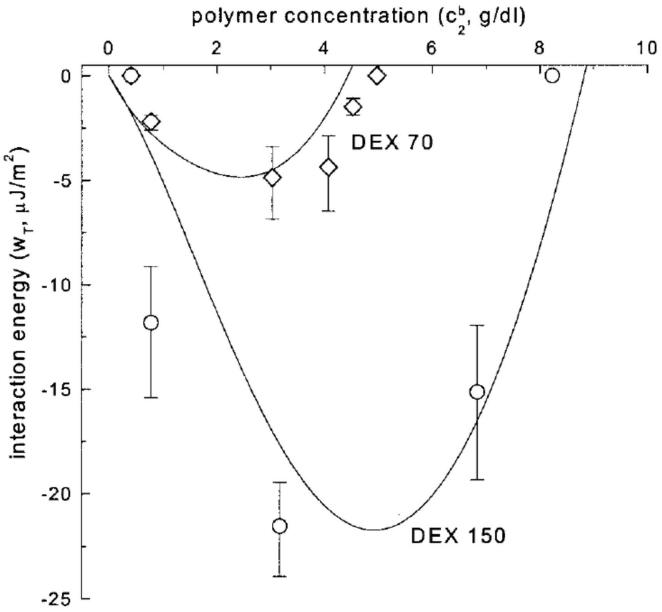

Figure 7.11: Comparisons between calculated (solid lines) and experimental values of interaction energy (w_T) for RBC suspended in various concentrations of dextran 70 kDa (DEX70) and dextran 150 kDa (DEX150) From: B. Neu and H.J. Meiselman. 2002. "Depletion-Mediated Red Blood Cell Aggregation in Polymer Solutions" *Biophysical Journal* 83:2482-2490 [131].

7.4 Results

In the present study, we used the technique of single cell force spectroscopy (SCFS, see chapter 4) to measure the interaction energies between human red blood cells as functions of the molecular mass and concentration of dextran. The dextrans used were dextran70 (DEX70 with a molecular weight of 70 kDa), and dextran150 (DEX150 with a molecular weight of 150 kDa) from Sigma-Aldrich. The measurements where conducted at the single cellular level and were compared to the predicted values of Neu et al. [131].

7.4.1 Preparation

Red Blood Cells

Fresh blood from healthy donors was obtained by a fingertip needle prick and was obtained within one day of the experiment. The cells were washed three times by centrifugation (800 g, 3 min) in PBS. The buffy coat and plasma were removed by aspiration.

Functionalization

Cell Tak^{TM} (BD Science) was used to bind a cell to the cantilever. The hand spread protocol was used, in which the cantilever was incubated in a Cell Tak^{TM} drop. After 2 min, the Cell Tak^{TM} solution was carefully removed; this was followed by a 3 min wait time to allow the acetic acid to evaporate from the cantilever. Rinsing the cantilever with ethanol and PBS (Phosphate-Buffered Saline) completed the functionalization protocol. Functionalization of the surface (to immobilize the cell on the surface) was not necessary because untreated RBCs have a high affinity to untreated surfaces.

Cantilever Calibration

The spring constant of the cantilever was determined using the common thermal noise method [125, 31] (the cantilevers used were MLCT-O cantilevers with spring constants on the order of 0.01 N/m, Bruker).

Measurement Protocol

To attach an RBC to the cantilever, the cantilever was lowered manually until a preset force set point F_{set} was reached, indicating contact between the cantilever and the cell. The cantilever was withdrawn continuously at low speed until the cell was no longer

in contact with the surface. After the cell was attached to the cantilever, the cell was positioned on top of another cell that lay on the bottom of the petri dish. After cell capture, the cantilever was lowered onto another cell, and the adhesion force and adhesion energy were measured. The retraction curve is typically characterized by the maximum force required to separate the cells from each other and adhesion energies are calculated by computing the area under the retraction curve of the force distance curve. The interaction energies (more precisely, the interaction energy densities of two RBCs) are calculated by dividing the measured adhesion energies by the contact areas of the adhering cells using a value of $50.24\,\mu m^2$ derived from the mean radius of RBCs.

7.4.2 BSA Treatment

The present study is exclusively concerned with adhesion that is caused by the presence of dextran molecules in the solution. Hence, any further source of adhesion (e.g., adhesion of the upper RBC to the cover slip or the lower RBC to the cantilever surface or Cell-Tak) had to be excluded. For larger and stiffer cells (than RBCs) such undesired adhesion events are rarely observed. However, RBCs have a height of just 2 µm,

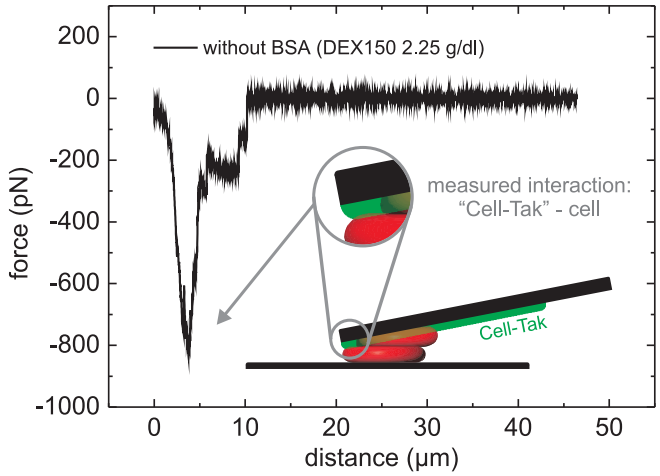

Figure 7.12: Without BSA treatment, undesired adhesion events occur whose origin is not the investigated depletion effect; e.g., the cells hit concentrically and the lower cell touches the Cell-Tak (i.e., a stronger adhesion force is measured because of the strong adhesiveness of the Cell-Tak).

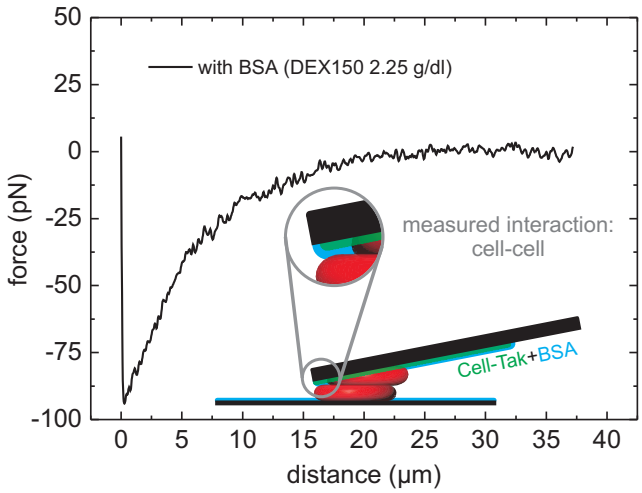

Figure 7.13: With BSA treatment, the Cell-Tak is completely passivated and the influence of those undesired adhesion events is minimized, as the change in shape and magnitude of the measured force curve document.

and this is an experimental difficulty; even with optimum (concentric) alignment, such binding to the surface was often observed in our first experiments. An example of those undesired adhesion events is shown in Fig. 7.12. The measured adhesion forces were much higher than any reasonable estimate for dextran-induced adhesion. To overcome this problem, 0.1 g/dl BSA (Bovine Serum Albumin) was added to the solution after attaching the RBC to the cantilever. BSA could potentially induce an additional depletion interaction; however because the radius of gyration of BSA is only 3 nm [154] and the concentration is fairly small, the additional depletion interaction due to the presence of BSA can be neglected. The effects of BSA treatment on RBCs (e.g., on cell geometry or mechanical properties) have been studied intensively [102, 88, 182]. However, any effect of the BSA treatment on the measured interaction energy can be neglected for the investigated adhesion because this adhesion is purely physical (i.e., we assume that there no adhesion proteins are involved that could possibly be blocked by the incorporation of BSA into the RBC membrane). The only purpose of the BSA is to passivate the surfaces of the cantilever and the petri dish. Thus, only the RBC surfaces contribute to the measured adhesion force arising from the depletion effect. Fig. 7.13 shows an example force curve after BSA treatment of the cantilever and the petri dish. The shape and magnitude of the force distance curve changes significantly. The extraordinary flexibility of RBCs allows them to stay in

contact over large withdrawing distances after adhering, as done in the measurements with BSA (Fig. 7.13).

7.4.3 Parameter Settings

In the next step, the parameter set point force F_{set}, cantilever velocity v, and contact time τ of the cantilever were adjusted. These adjustments were necessary because the viscosity of the solvent increases and due to the dextran possible non-Newtonian effects could affect the results of the measurements. In fact, the following subsections will demonstrate the necessity for these control measurements.

Setpoint Force

As described in the methods section, a set point force has to be chosen prior to a measurement in order to get a feedback when the two cells are in physical contact. The set point can be varied over large values from 50 pN up several nN depending on the investigated cell type. For red blood cells, with their extreme flexibility, a small value is expected to be sufficient to produce a large enough contact area. Fig. 7.14 shows the interaction energy as a function of F_{set} for dextran 70 (DEX70), dextran 150 (DEX150) and a control measurement without dextran (control). In all measurements a very small influence of the chosen set point is recognizable. Only in the case of very small set point forces (< 100 pN) can an increase in interaction energy with increasing set point be seen (data not shown). Above 100 pN the influence of the choice of F_{set} on the measured interaction energy is negligible and was set to $F_{set} = 300$ pN for the remaining measurements.

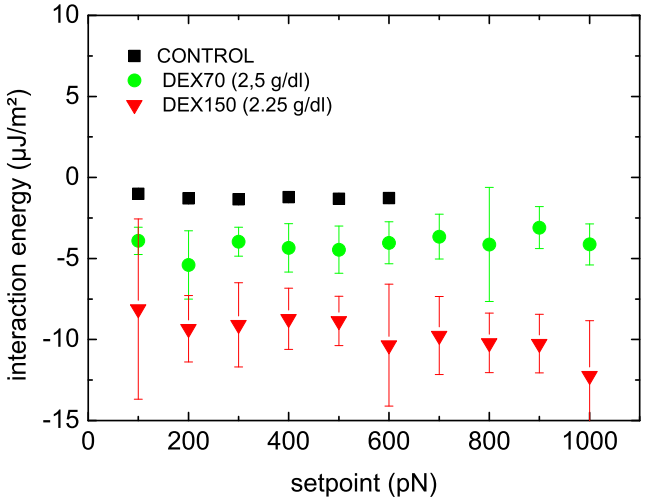

Figure 7.14: Shows the dependence of the measured adhesion energy on the chosen force set point F_{set}. In all measurements, no significant dependence on F_{set} was observed.

Contact Time

It will be shown that the data can be described well with a depletion model, but it is also known that macromolecular "bridging" between the RBCs can occur when the cells are in contact for a longer time [25]. Bronkhorst et al. [25] discovered that the time constant for those possible cross bridges is in the order of seconds. The contact time was varied from $\tau = 0\,\mathrm{s}$ (i.e. i.e. the cells will be in physical contact for less than 0.2 s) to $\tau = 30\,\mathrm{s}$ to resolve the influence of the parameter τ (Fig. 7.15). Large contact times lead to increased adhesion energies and increased error bars. Both can be indications for bridging events. Therefore, we attempted to minimize the contact time by setting τ to 0 s. Depending on the cantilever velocity, the RBCs will be in "physical" contact for a longer time because due to their flexibility, the RBCs can stay in contact over distances of several μm. Hence, to minimize the actual contact time (to exclude bridging effects), the cantilever velocity had to be sufficiently high. This ensures that the measured interaction energies are purely depletion-induced.

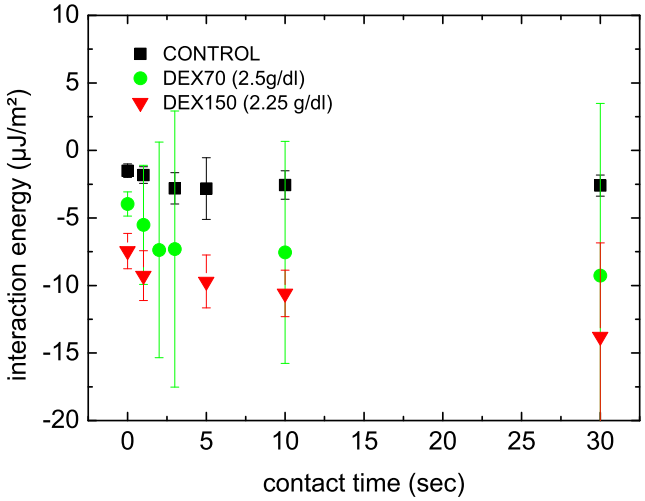

Figure 7.15: Dependence of the measured adhesion energy on the chosen contact time τ of both cells. Increasing contact time leads to an increase in interaction energy and error bars.

Cantilever Velocity

Fig. 7.16 shows the dependence of the cantilever velocity v on the measured interaction energies. In the control measurements, no influence of the velocity could be seen. On the contrary, a dependence of the velocity could be observed in the dextran measurements. It is probable that higher interaction energies lead to larger viscoelastic effects while deforming the RBCs. The RBCs are deformed to greater extent, and this leads to higher apparent interaction energies. Up to a certain velocity, the effect of velocity can be neglected; e.g., for DEX70 this effect begins at velocities only higher than $9\,\mu$m/s. At high velocities, in the DEX150 measurements, this effect can be significant; however, for moderate velocities, this effect is still less than the error in the measurement. As mentioned above, it is necessary to minimize the contact time such that any bridging effects can be excluded; i.e., the cantilever velocity may not be too small. Therefore, in all measurements, the cantilever velocity was chosen as $v = 5\,\mu$m/s.

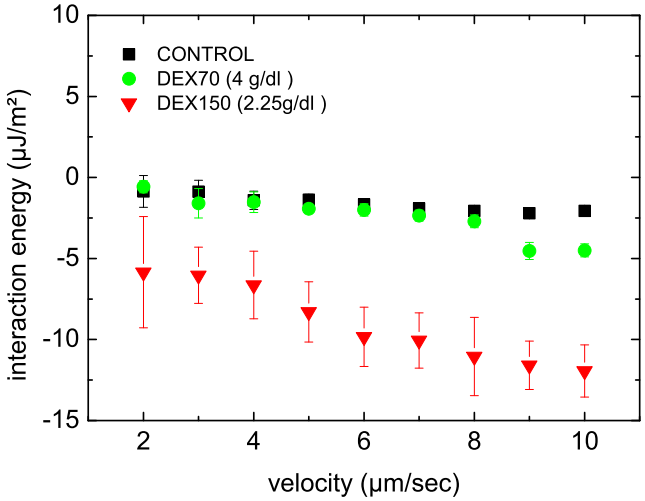

Figure 7.16: Shows the dependence of the measured adhesion energy on the chosen velocity v of the cantilever. At higher velocities in the DEX150 measurements a dependence on the cantilever velocity was observed, but for moderate velocities this dependence is still less than the error in the measurement.

7.4.4 Adhesion Forces and Adhesion Energies of RBCs

After finding the correct parameters for set point, contact time and velocity the depletion-induced adhesion of two RBCs can be measured. In the following measurements, the concentration of dextran 70 kDa and dextran 150 kDa was varied and the resulting adhesion force was measured with SCFS. Each data point represents an average of 100 force curves for the same cell. In this way a statistic could be produced in order to minimize artificial effects, such as bridging, that occurs from time to time. Fig. 7.17a and b show the dependence of the adhesion force and the interaction energy on the concentration of the dextran used.

7.5 Discussion

7.5.1 Dextran-Induced Adhesion of RBCs

There are no conclusive data on the absolute value of dextran-induced adhesion forces between RBCs available in the literature. The reason for this is that all previously conducted measurements were of an indirect nature, such as electrophoretic mobility

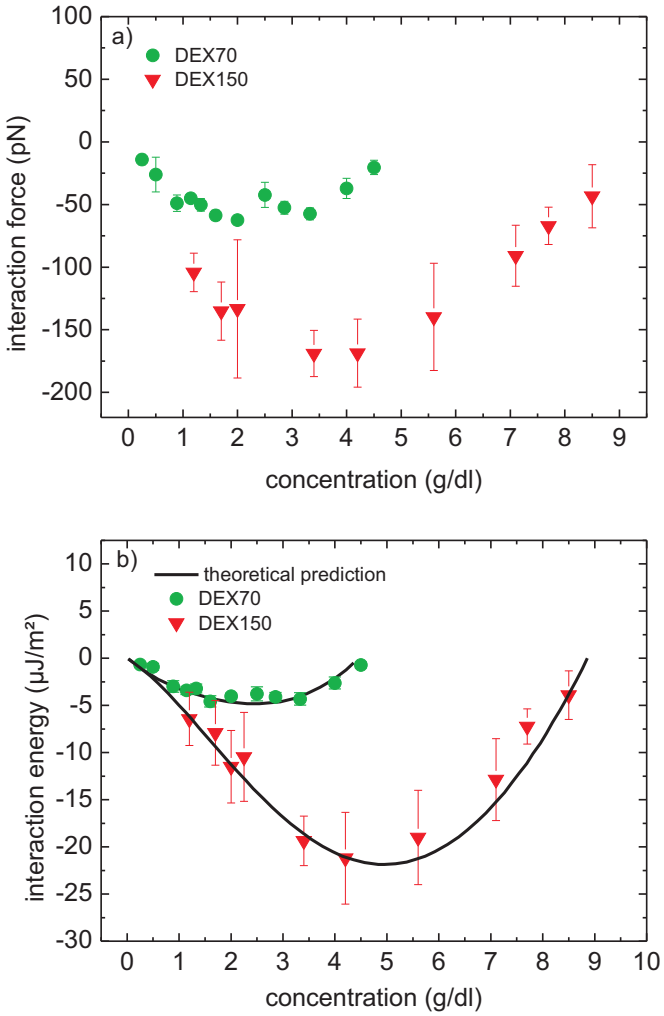

Figure 7.17: a) The measured adhesion forces of the dextrans (triangles: dextran 70, squares: dextran 150) and the concentrations used [145]. The maximum interaction strengths were observed at 2g/dl (dextran 70) and 4g/dl (dextran 150). b) Dependence of the interaction energy of two red blood cells on the concentrations of two dextran types (triangles: dextran 70, squares: dextran 150). The solid line represents the curve calculated by Neu et al. [131].

measurements [26], sedimentation rate experiments [150], low shear viscosity experiments [149], flow chamber experiments [41] or light reflectometry measurements [163];

they did not involve single cells. The measured values for the adhesion forces, however, seem reasonable since they are large enough to "survive" low shear rates but will not be large enough to form a rouleaux under high shear rates. For instance Snabre et al. [163] estimate the disaggregation force between 2 RBCs in a dextran 70 solution to be in the order of $5 - 25$ pN. A comparison of the measured adhesion forces (for dextran 70, see Fig. 7.17a) with the estimated forces of Snabre et al. shows that the results are in agreement with the qualitative results from the indirect measuring techniques [41, 163]. The more important parameter to check the correctness of the experiments is the adhesion energy because there exist some data in literature and even a theory was developed to predict absolute values for adhesion energies [131]. The solid line in Fig. 7.17b represents the predicted values of Neu et al. The measured values are in excellent agreement with those numerically derived values.

7.5.2 Bridging vs. Depletion

With the excellent agreement of the SCFS measurements with the theoretical description give more rise to the assumption that the driving force in rouleaux formation is rather depletion induced than bridging induced. However, as could be seen in the contact time dependence measurements the adhesion energies increase with increasing contact time. This could be due to bridging, but to little data is present to conclusively decide that. With the present data it appears that the rouleaux formation, at least at the beginning, is purely depletion-mediated.

7.6 Summary

In this chapter the macromolecule-induced adhesion of RBCs was investigated by means of single cell force spectroscopy. In the past, there was a big debate regarding the so-called rouleaux formation in static blood. Two different theories have been introduced that to some extend exclude each other: The depletion theory in which an osmotic pressure of depleted macromolecules are causal for the rouleaux formation and the so called Bridging model in which the macromolecules adsorb to the surface of the cells and actively "bridge" the adjacent cell. There are studies in favour of both theories and today it is not yet fully understood. For the depletion theory a theoretical description is available but the experimental data to confirm this theory are few and far between. Furthermore, experiments in which the adhesion force of two single RBCs is measured have never been conducted before. Therefore, in this work the SCFS was utilized to measure the interaction of two single red blood cells and to compare the measured results with the depletion model derived prediction for the interaction energies. The adhesion of RBCs was studied for two different macromolecules (dextran 70 and dextran 150) and the measured interaction energies are in excellent agreement with the ones predicted by the depletion theory. Therefore, based on this data, it can be concluded that the rouleaux formation is rather depletion-mediated than bridging-mediated. However, for longer contact times of the cells additional enhanced interaction energies could suggest and influence of bridging in the later stage of adhesion [25].

8 Summary

In this work different adhesion phenomenona of red blood cells (RBC) are in the center of interest. RBC aggregation has already been known for a long time and is the main determinant of blood viscosity. Additionally, there are hints that RBC aggregation could play a role in thrombus formation and thrombus solidification. In order to quantify the different adhesion phenomenona, accurate force measuring tools are required. Optical tweezers (OT) are a versatile tool for several applications in physics, chemistry and foremost biology [22, 168, 108] because microscopic objects can be trapped via a high focused laser beam. As an accurate measuring tool OTs are used to determine very small forces [74, 142, 73, 115] and furthermore they serve as a positioning tool [166]. The consecutive development of OT to holographic optical tweezers (HOT) enabled the ability to trap and move multiple particles at the same time. This property features HOT with unprecedented flexibility and thus makes them a perfect tool to investigate cell-cell adhesion.
Atomic force microscopy based single cell force spectroscopy (SCFS,) is rather a new technique to measure adhesion forces and adhesion energies. This technique allows the capture of a single cell by gently pressing a functionalized AFM cantilever onto it. In addition, it transforms the living cell into a probe which is brought into contact with functionalized surfaces or other cells at a set point force and for a specific contact time. Subsequently, the cantilever is withdrawn at a constant speed detaching the cell from its adhesion place. During the separation process, the cantilever deflection, which is proportional to the vertical force that exists between the cell and substrate, is recorded in a force-distance curve. This curve provides all the information about the adhesion process.
The first investigated mechanism is a new hypothesized adhesion among red blood cells. A co-adhesion of healthy RBCs was recently proposed by Kaestner et al. [97]. They suggested a signaling cascade which predicts an active participation of RBCs in blood clot formation. In their theory an activation of a non-selective calcium channel is assumed across which, after an activation via messengers, extracellular calcium can enter the cell. Consequently, this results in an activation of a signaling cascade that involves several processes which in the end are expected to induce an active co-adhesion among RBCs. In preliminary studies [165, 90, 133] active co-adhesion of RBCs were shown but statistically significant and quantitative data are still lacking. Therefore, in this work the adhesion process of RBCs is investigated with respect to

the point: statistical investigation and quantification of the occurring adhesion. A combined approach of microfluidics and holographic optical tweezers are used to test the hypothesis statistically. The arising adhesion exceeds the force capabilities of optical tweezers, thus single cell force spectroscopy is used to quantitatively investigate this adhesion phenomenon. This approach quantifies the inter-cellular adhesion to amount to $100 \pm 84\,\mathrm{pN}$ in strength. Concerning the question of physiological significance, the results of HOT and SCFS are combined and it is concluded that the LPA-induced inter-cellular adhesion of RBCs is of importance in the later stages of blood clotting and actively contributes to blood clot solidification.
The second investigated adhesion phenomenon among red blood cells is the so-called rouleaux formation. In static blood or physiologically at low shear rates, red blood cells form linear aggregates that look like a stack of coins. The involved processes of this formation and the underlying adhesion mechanism are not fully understood yet. Two different models developed to explain the origin of the adhesion. First, the bridging model that assumes the absorption of macromolecules onto the cell membrane resulting in bridging to adjacent cells and second, the depletion model that account the osmotic pressure of surrounding macromolecules to be responsible for the adhesion. Since these theories propose quite the opposite, there is a ongoing debate among advocates for both. There are data in favour of both theories but all of them are indirect measurements and not actual cell-cell interaction measurements. In this work, the first direct cell-cell adhesion measurement of RBCs in their natural, discocytic shape was conducted to test which of the theories is most likely to be the cause for the aggregation. This has never been done before and it is shown that the measured interaction energies are in excellent agreement with the ones predicted by the depletion theory. Therefore, based on this data, it can be concluded that the rouleaux formation is rather depletion-mediated than bridging-mediated. However, for longer contact times of the cells additional enhanced interaction energies could suggest an influence of bridging in the later stages of adhesion, but could not be conclusively confirmed. The results of this work represent an important step towards the unraveling of the true origin of rouleaux formation.

A Materials and Methods

A.1 Materials

notation	amount	manufacturer
NaCl, KCl, $CaCl_2$		Sigma / Roth
NaOH		Sigma
Glukose		Sigma
DEX70, Dextran, M_W=$70 \cdot 10^3$	100 mg	Sigma
DEX150, Dextran, M_W=$150 \cdot 10^3$	100 mg	Sigma
PBS (Phosphate Buffered Saline), Lsung	500ml	Invitrogen
HEPES		Roth
FLUO-4 AM-Ester	10x50 µg	Molecular Probes
A23187, 4-Bromo-Calcium Ionophore, powder	1 mg	Sigma
Lysophosphatidsure (Oleoyl-L-α-Lysophosphatidic Acid Sodium Salt)	1 mg	Sigma
Pluronic F-127	1 ml	Invitrogen
CellTak	1 ml	BD
BSA	10 g	Polysciences

A.2 Methods

The following section will deal with the methological procedures and protocols that have been used in this work.

A.2.1 RBC Preparation and Fluorescence Microscopy

For experiments using the optical tweezers and microfluidics, fresh blood from healthy donors was obtained by a fingertip needle prick, while for annexin V-FITC fluorescence measurements, human venous blood was drawn from healthy donors. Heparin or EDTA was used as an anticoagulant. The blood was obtained within one day of the experiment from the Institute of Clinical Hematology and Transfusion Medicine of the Saarland University Hospital. The cells were washed three times by centrifugation (800 g, 3 min) in a HEPES buffered solution of physiological ionic strength

(HIS-solution) containing the following (in mM): 145 NaCl, 7.5 KCl, 10 glucose and 10 HEPES, pH 7.4, at room temperature. The buffy coat and plasma were removed by aspiration. For Ca^{2+} imaging, RBCs were loaded with 5µM Fluo-4 AM (Molecular Probes, Eugene, USA) from a 1mM stock solution in Dimethyl sulfoxide (DMSO) with 20 % Pluronic (F-127, Molecular Probes). Loading was performed in 1 ml of PIS-solution at an RBC haematocrit of approximately 1% for 1 h at 37° C. The cells were washed by centrifugation once more and equilibrated for de-esterification for 15min. LPA, prepared from a stock solution of 1 mM in distilled water, and the Ca^{2+} ionophore A23187, prepared from a stock solution of 1mMin ethanol, were obtained from Sigma Aldrich (St. Louis, USA). To investigate phosphatidylserine (PS) exposure, cells were stained with annexinV-FITC (Molecular Probes). Annexin V-FITC was delivered in a unit size of 500 µl containing 25 mM HEPES, 140 mM NaCl, 1 mM EDTA, pH 7.4, and 0.1 % bovine serum albumin. Five hundred microliters of annexin binding buffer (10 mM HEPES, 140 mM NaCl, 2.5 mM $CaCl_2$, pH 7.4) was added to 1 µl of washed, packed RBCs previously treated with LPA or A23187. Afterwards, 5µl annexin V-FITC was added, and the cells were gently mixed. The probes were incubated at room temperature in the dark for 15 min and then washed 2 times in 1 ml of annexin binding buffer (800 g, 3 min). Finally, the cells were re-suspended in 500µl of annexin binding buffer and used for microscopy. The measurements were obtained from images taken with a CCD camera (CCD97, Photometrics, USA).

A.2.2 Loading of RBCs with Fluo-4

Fresh blood from apparently healthy donors was taken at the day of the experiment by a finger needle prick. Approximately $50 - 100$ µl was resuspended in 1 ml HIS solution and was centrifuged at $800 - 2000\,g$ at room temperature. The excess end was removed by a sucking pump. In this way all other cell types such as thrombocytes and leukocytes were removed from the blood sample. This “washing” process was conducted 3 times. Fluo-4 ester was present in 1 mM diluted in Pluronic F-127. The incubation of the RBCs took place at a approximated hematocrit value of 1%, with a Fluo-4 concentration of 4 µM and at 37°C. Then the cells were gently shaken for the incubation time of 1h. In order to remove the rest of the Fluo-4 after the incubation, the cells were washed for 2 times as described above.

A.2.3 Statistical Significance

A Student’s t-test was used to test the results obtained from the adhesion experiments for statistical significance. Statistical significance of the data were defined as follows: p ¿ 0.05 (n.s.), p ? 0.05 (*); p ? 0.01 (**), p ? 0.001 (***).

A.2.4 Cell Tak Functionalization Protocol

Hand Spread Protocol

Incubate the centilever for several seconds in a 50 µl drop of BD Cell Tak stock solution and let the acidic acid evaporate from the cantilever. Wash the cantilever with ethanol and water. Storage is not recommended.

Adsorption Protocol

Incubate the cantilever in a 50 µl drop of 1:30 dillution of BD Cell Tak (in 0.1 M sodium bicarbonate, ph 8) for at least 20 min. Wash with water. It is important to know that the adsorption begins immediately upon changing the pH. Therefore, the dilution is to be dispended within 10 min. the functionalized cantilevers can be stored for up to 2 weeks at $2 - 8°C$ (air dried).

A.2.5 ConA Functionalization Protocol

1) Activate/clean cantilevers by UV activation or plasma cleaning.
2) Incubate cantilever in a 50 µl drop of 0.5mg/ml biotin-BSA (in 0.1 M sodium bicarbonate $pH = 8.6$)- overnight, $37°C$
3) Incubate cantilever in a 50 µl drop of streptavidin (0.5 mg/ml in PBS) 30 min, room temperature
4) Incubate cantilever in a 50 µl drop of biotin-ConA (0.2 mg/ml in PBS) 30 min, room temperature

Between each step the cantilever should be washed 3 times in excess volume of PBS. The functionalized cantilevers can be stored up to one week at $4°C$

A.2.6 Dextran Preparation

The desired amount of dextran was weighed in a small container. After that, a desired amount of PBS was added to to powder. In order to not destroy the long chains of dextran the container had to be gently shaked and warmed until all the dextran powder was soluted.

A.2.7 Solutions

HIS-solution: 145 mM NaCl, 10 mM Glukose, 10 mM HEPES, 7, 5 mM KCl pH 7,4 at room temperature mit NaOH
4-Bromo-Calcium Ionophore A23187: 1 mM in Ethanol

FLUO-4 AM: 1 mM in Pluronic F-127
Lysophosphatidic acid: 500 µM in deionisied water

A.2.8 PDMS Manufacturing Protocol

The classic choice of PDMS for microfluidics is *Dow and Cornings* Sylgard 184, a two-part system with mix ratio of cross-linker/curing agent A: siloxane B=1:10. The fluid PDMS was filled into the cleaned mold and was degassed by applying underpressure. Thereafter the fluid PDMS was heated at $100°C$ for $1\,h$. After the heating period the PDMS was pealed out of the mold and the inlets for the hoses were punched. An exposure to O_2-plasma for 30 s prepared the PDSM for the binding to a coverslip. The injection of the supply hoses concluded the microfluidic manufacturing protocol.

Publications

P. Steffen, A. Jung, D.B. Nguyen, T. Müller, I. Bernhardt and C. Wagner. *Stimulation of human red blood cells leads to Ca^{2+}-mediated intercellular adhesion*, Cell Calcium **50** (2011) 54-61.

L. Kaestner, P. Steffen, D.B. Nguyen, J. Wang, L.Wagner-Britz, A. Jung, C. Wagner., I. Bernhardt *Lysophosphatidic acid induced red blood cell aggregation in vitro*, Bioelectrochemistry (2011) http://dx.doi.org/10.1016/j.bbr.2011.03.031

D.B. Nguyen, L.Wagner-Britz, Sara Maia, P. Steffen, C. Wagner, L. Kaestner and I. Bernhardt. *Regulation of Phosphatidylserine Exposure in Red Blood Cells*, Cell Calcium **28** (2011) 847-856.

P. Steffen, C. Verdier and C. Wagner. *Quantification of Depletion Induced Adhesion of Red Blood Cells*, (2012) submitted.

Cell Calcium 50 (2011) 54–61

Contents lists available at ScienceDirect

Cell Calcium

journal homepage: www.elsevier.com/locate/ceca

Stimulation of human red blood cells leads to Ca^{2+}-mediated intercellular adhesion

Patrick Steffen[a], Achim Jung[a], Duc Bach Nguyen[b], Torsten Müller[c], Ingolf Bernhardt[b], Lars Kaestner[d,*], Christian Wagner[a,**]

[a] Experimental Physics Department, Saarland University, 66123 Saarbruecken, Germany
[b] Biophysics, Saarland University, 66123 Saarbruecken, Germany
[c] JPK Instruments AG, Bouchéstrasse 12, 12435 Berlin, Germany
[d] Molecular Cell Biology, Saarland University, 66421 Homburg, Germany

ARTICLE INFO

Article history:
Received 1 February 2011
Received in revised form 30 April 2011
Accepted 3 May 2011
Available online 25 May 2011

Keywords:
Blood clot
Calcium signaling
Lysophosphatidic acid
Red blood cells
Single-cell force spectroscopy

ABSTRACT

Red blood cells (RBCs) are a major component of blood clots, which form physiologically as a response to injury or pathologically in thrombosis. The active participation of RBCs in thrombus solidification has been previously proposed but not yet experimentally proven. Holographic optical tweezers and single-cell force spectroscopy were used to study potential cell–cell adhesion between RBCs. Irreversible intercellular adhesion of RBCs could be induced by stimulation with lysophosphatidic acid (LPA), a compound known to be released by activated platelets. We identified Ca^{2+} as an essential player in the signaling cascade by directly inducing Ca^{2+} influx using A23187. Elevation of the internal Ca^{2+} concentration leads to an intercellular adhesion of RBCs similar to that induced by LPA stimulation. Using single-cell force spectroscopy, the adhesion of the RBCs was identified to be approximately 100 pN, a value large enough to be of significance inside a blood clot or in pathological situations like the vasco-occlusive crisis in sickle cell disease patients.

1. Introduction

Previous studies of the interactions between red blood cells (RBCs) have relied on either hydrodynamic interactions [1] or interactions mediated by plasma macromolecules. Co-adhesion of RBCs under physiological conditions is known as rouleaux formation. These structures might be generated either by plasma polymers bridging between the cells [2,3] or, more likely, by depletion forces. The adhesion energies are small enough to allow for breakage in the shear flow, and the effect is thought to be reversible, even if some controversial data exist [4]. This reversibility is crucial for the ability of RBCs to cross capillary sections that are smaller than the cell diameter. However, in several pathologies, such as sickle cell disease or thalassemia, an increased propensity for red blood cell–cell adhesion has been observed [5]. Clot formation is a collective phenomenon based on the interplay of many components. In current models, the contribution of RBCs to the clotting process is thought to be purely passive, i.e., they are simply caged in the fibrin network due to their prevalence in the blood. Based on experimental and clinical studies that have shown a correlation between decreased hematocrit values and longer bleeding times [6–8] and their own experiments, Andrews and Low summarized the evidence for active participation of RBCs in thrombus formation. Kaestner et al. [9] proposed a signaling mechanism based on Ca^{2+} entry via a nonselective voltage-dependent cation (NSVDC) channel that is permeable to mono- and bivalent cations like Na^+, K^+ and Ca^{2+} [10,11]. This channel has been shown to be activated by prostaglandin E_2 (PGE_2), lysophosphatidic acid (LPA) [9,12] and by the mechanical deformations that occur when RBCs pass through capillaries smaller than their resting diameter [13]. PGE_2 and LPA are extracellular, local mediators that are released both by platelets after their activation within the coagulation cascade and by RBCs themselves under mechanical Ca^{2+} stress [14]. The aim of this study was to test the hypothesis that intercellular RBC adhesion can occur directly (without participation of platelets). To perform this at the level of individual cells, we used the complementary methods of non-invasive holographic optical tweezers (HOT) [15], using the momentum of light and single-cell force spectroscopy to quantify the occurring adhesion.

* Corresponding author at: Institute for Molecular Cell Biology, Building 61, 66421 Homburg/Saar, Germany. Tel.: +49 6841 1626 103; fax: +49 6841 1626 104.
** Corresponding author at: Experimental Physics Department, Building E 2 6, 66123 Saarbruecken, Germany. Tel.: +49 681 302 3003; fax: +49 681 302 4676.
E-mail addresses: lars_kaestner@me.com (L. Kaestner), c.wagner@mx.uni-saarland.de (C. Wagner).

0143-4160/$ – see front matter © 2011 Elsevier Ltd. All rights reserved.
doi:10.1016/j.ceca.2011.05.002

2. Materials and methods

2.1. RBC preparation and fluorescence microscopy

For experiments using the optical tweezers and microfluidics, fresh blood from healthy donors was obtained by a fingertip needle prick, while for annexin V-FITC fluorescence measurements, human venous blood was drawn from healthy donors. Heparin or EDTA was used as an anticoagulant. The blood was obtained within one day of the experiment from the Institute of Clinical Haematology and Transfusion Medicine of the Saarland University Hospital. The cells were washed three times by centrifugation (2000 × *g*, 3 min) in a HEPES buffered solution of physiological ionic strength (PIS-solution) containing the following (in mM): 145 NaCl, 7.5 KCl, 10 glucose and 10 HEPES, pH 7.4, at room temperature. The buffy coat and plasma were removed by aspiration. For Ca^{2+} imaging, RBCs were loaded with 5 μM Fluo-4 AM (Molecular Probes, Eugene, USA) from a 1 mM stock solution in Dimethyl sulfoxide (DMSO) with 20% Pluronic (F-127, Molecular Probes). Loading was performed in 1 mL of PIS-solution at an RBC haematocrit of approximately 1% for 1 h at 37 °C. The cells were washed by centrifugation once more and equilibrated for de-esterification for 15 min. LPA, prepared from a stock solution of 1 mM in distilled water, and the Ca^{2+} ionophore A23187, prepared from a stock solution of 1 mM in ethanol, were obtained from Sigma Aldrich (St. Louis, USA). To investigate phosphatidylserine (PS) exposure, cells were stained with annexin V-FITC (Molecular Probes). Annexin V-FITC was delivered in a unit size of 500 μL containing 25 mM HEPES, 140 mM NaCl, 1 mM EDTA, pH 7.4, and 0.1% bovine serum albumin. Five hundred microliters of annexin binding buffer (10 mM HEPES, 140 mM NaCl, 2.5 mM $CaCl_2$, pH 7.4) was added to 1 μL of washed, packed RBCs previously treated with LPA or A23187. Afterwards, 5 μL annexin V-FITC was added, and the cells were mixed gently. The probes were incubated at room temperature in the dark for 15 min and then washed 2 times in 1 mL of annexin binding buffer (2000 × *g*, 3 min). Finally, the cells were re-suspended in 500 μL of annexin binding buffer and used for microscopy. The measurements were obtained from images taken with a CCD camera (CCD97, Photometrics, USA).

2.2. Holographic optical tweezers (HOT)

A schematic drawing of our experimental setup is shown in supplemental Fig. S1a. A Nd:YAG infrared laser (Ventus, Laser Quantum, Stockport, UK) with a beam width of 2.5 mm was coupled for coarse alignment with a visible He–Ne laser via a dichroic mirror. The latter was switched off during the experiments. Both beams were expanded five-fold (BM.X, Linos Photonics, Göttingen, Germany) to overfill the 8 mm back aperture of the microscope objective (CFI Plan Fluor 60× oil immersion, Nikon Corp., Tokyo, Japan). The optics were integrated into an inverted fluorescence microscope (TE-2000, Nikon Corp.). This allowed for combined trapping and fluorescence or differential interference contrast (DIC) measurements. Images were taken with an electron multiplication CCD camera (Cascade 512F, Roper Scientific, Trenton, USA) with a typical frame rate of 100 Hz. To reduce vibrations, the original cooling fan was replaced with water-cooling components. In addition, the optical setup was placed on active vibration isolation elements (Vario Series, Halcyonics, Göttingen, Germany). The phase of the laser's electric field was modified using a spatial light modulator (PPM X8267-15, Hamamatsu Photonics, Hamamatsu City, Japan) to create the desired trap pattern in the focal plane of the microscope objective. In order to test for RBC adhesion after stimulation, a suitable configuration of independently movable optical traps was created (see the schematic sketch in Fig. 1a). The laser power in each trap was approximately 5 mW. Cells could be moved against one another by replaying a series of

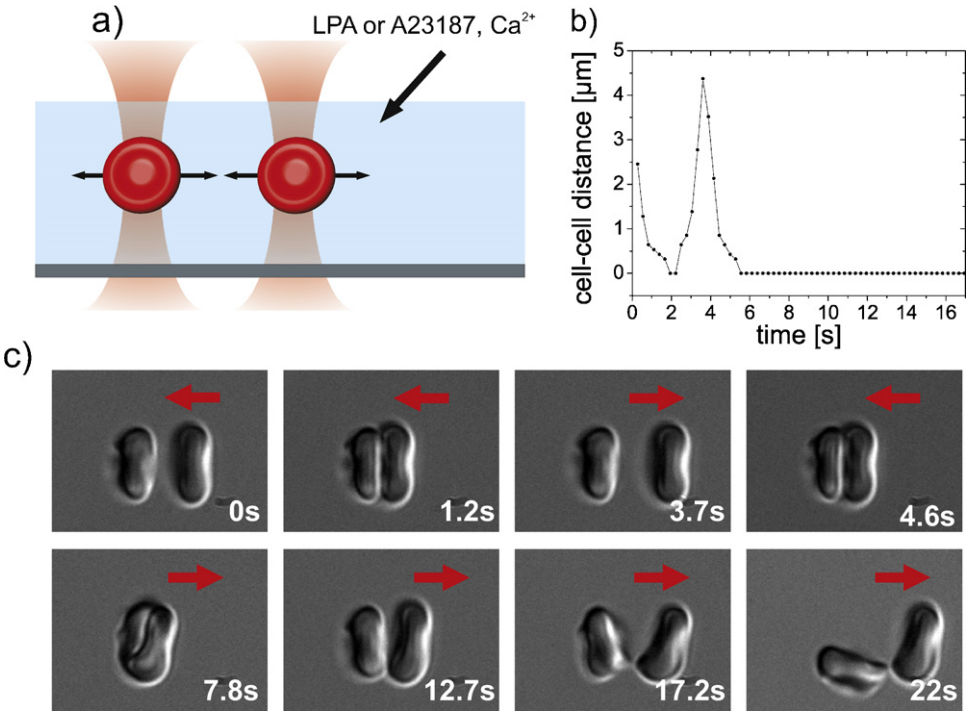

Fig. 1. Probing for adhesion between RBCs after LPA stimulation. Panel (a) represents a sketch of the oscillatory movement of two trapped cells. The actual cell–cell distance over the course of the adhesion test is depicted in panel (b). The graph depicts the separation distance of two red blood cells, as determined using edge detection, over the course of the experiment. Cells were preincubated with 2.5 μM LPA for 5 min. After adhesion occurred at around 6 s, the distance between the cells remained zero. Panel (c) depicts representative images of an adhesion measurement of two RBCs held by 4 optical traps. During a recording period of 26 s, the cells were moved back and forth as indicated by the red arrows. The full video can be seen in supplemental material. (For interpretation of the references to color in this figure legend, the reader is referred to the web version of the article.)

kinoforms on the computer-controlled spatial light modulator. As an example, supplemental Fig. S1b shows a quadrotrap in parallel and perpendicular configuration for RBC arrangement along with the corresponding kinoforms.

2.3. Microfluidics

In order to provide a controlled yet interchangeable solvent environment, a microfluidic polydimethylsiloxane (PDMS) cell was constructed by standard soft lithography (inset in Fig. 2). The cell consists of two inlets from which either the cells in the buffer solutions or LPA or the ionophore A23187 (final concentration of 40 μM) could be applied. The flow was driven by a hydrostatic pressure difference that allowed for fine tuning. After injection of a new sample, the flow could be brought approximately to rest by eliminating the pressure difference. Behind the y-junction, the flow remained laminar, and the two solutions did not mix, except for very slow diffusion. The RBCs could then be captured by the HOT and transferred to the new environment. Thus, the cells could be transferred from one solvent condition to another in a rapid and controlled manner. The same measurements were also conducted in a Petri dish as follows: RBCs were incubated for 10 min with either A23187 or LPA in the presence of Ca^{2+} (for concentration values, please refer to the figure legends), followed by a fast sequence of adhesion tests between various cells. There were more than 50 cells in each experiment; the total number of tested cells amounted to 250.

2.4. Single-cell force spectroscopy

In order to quantify the occurring cell–cell adhesion, an atomic force microscope (AFM) (CellHesion 200 with increased pulling range up to 100 μm, JPK Instruments, Germany) was used to conduct single-cell force spectroscopy measurements. In these measurements, a single RBC was attached to an AFM cantilever with the help of an appropriate adhesive. Cell-Tak™ (BD Biosciences) turned out to be the most efficient adhesive for binding RBCs to the cantilever. A stock solution of 2.4 mg/mL was diluted 1:30 according to instructions from BD. The cantilevers were incubated for at least 30 min at room temperature and used after rinsing with PIS solution. After the cell capture (CellTak™ functionalized cantilevers brought in contact with a 0.2 nN force for 10 s), the approach- and retraction speed were set to 5 μm/s. The pulling range varied between 30 and 50 μm, and the contact time varied from 0 to 120 s. During spectroscopy experiments, the deflection of the cantilever was monitored in real time using a built-in feature of the AFM software. The spring constant of the cantilever was determined by the common thermal noise method. The cantilevers used were tipples TL1 with a nominal spring constant of 0.03 N/m (Nanoworld). The cell morphology was monitored using phase contrast microscopy. In the course of the experiment, the cantilever with the attached cell was lowered onto another cell attached to the substrate, which was coated with 0.005% poly-L-lysine, until a preset defined constant force was reached and kept stationary for a defined contact time. The conditions during contact were determined by the choice of the particular closed-loop mode, specifically at a constant piezo position, after reaching a prescribed maximum pushing force of 400 pN. Subsequently, the cantilever was withdrawn at a constant speed. During approach and retraction, the cantilever deflected as a consequence of the acting forces. This deflection, which is proportional to the acting forces, was recorded in force–distance curves. The retraction curve was typically characterized by the maximum force required to separate the cells from each other, referred to as the maximum unbinding force F_{max}.

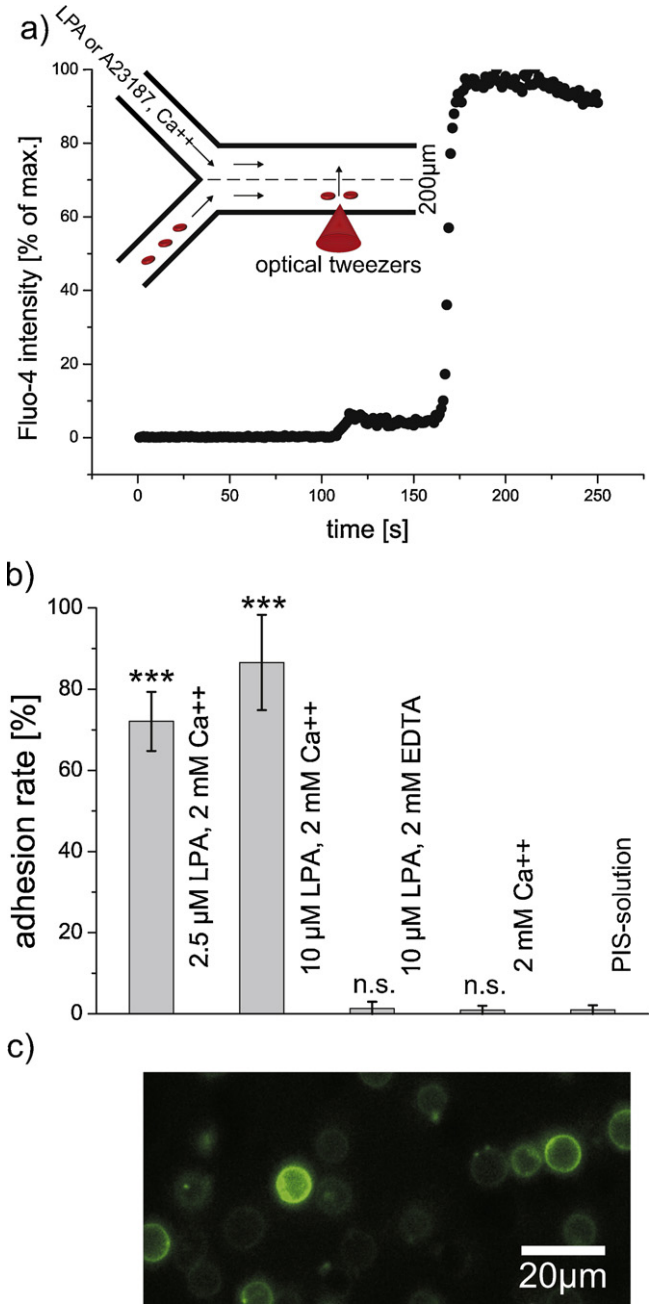

Fig. 2. The response of RBCs to LPA. (a) The relative fluorescence signal of a representative RBC in the upper microfluidic channel; $t = 0$ s is the time when the cell was moved into the LPA solution. The inset shows a schematic picture of the microfluidic chamber used. (b) Results of the LPA measurements conducted in the microfluidic chamber and the Petri dish. The grey bars represent the percentage of cells that showed adhesion. The overall number of cells tested was 60 cells per measurement. In the presence of LPA and Ca^{2+}, a significant number of cells showed adhesion, whereas in the control experiments, only a very small portion of the cells showed an adhesion. The results of the Student's *t*-test, compared to the control measurement (PIS-solution), are indicated at the top of each bar. (c) A fluorescence image of LPA-treated (2.5 μM) RBCs after annexin V-FITC staining. The annexin V binding indicates the presence of PS on the outer membrane leaflet of the cells.

2.5. Statistical significance

A Student's *t*-test was used to test the results obtained from the adhesion experiments for statistical significance. Statistical significance of the data was defined as follows: $p > 0.05$ (n.s.), $p \leq 0.05$ (*); $p \leq 0.01$ (**), $p \leq 0.001$ (***).

3. Results

3.1. Red blood cell stimulation with LPA

As pointed out in Section 1, RBCs can be stimulated by LPA, and this has been proposed to contribute to the active participation of RBCs in the later stage of thrombus formation. In order to test for altered intercellular adhesion behavior, we set up holographic optical tweezers (for details, refer to supplemental Fig. S1). In the blood flow, cell–cell contact times are rather short when RBCs "bump" into each other. To mimic this physiological condition, two cells were grabbed with the laser foci (compare Fig. 1c) and moved back and forth as depicted in Fig. 1a and supplemental movie SM1, in a cyclical manner. Upon stimulation with 2.5 μM LPA, the RBCs adhered to each other as plotted and visualized in an image sequence in Fig. 1b and c, respectively (the movie is available in supplemental material). During the stimulation procedure, most of the RBCs remained in their discocyte shape. The separation force could not be determined by the HOT approach because it exceeds the force of the laser tweezers. In this configuration, 72% of the cells tested showed such an irreversible adhesion (grey bars in Fig. 2b). To exclude any dependencies on the interaction surface due to the anisotropic shape of the cells, we aimed for another condition using spherocytes. This was realized by increasing the LPA concentration to 10 μM, which is still within the physiologically observed range. In parallel to the adhesion experiments, the Ca^{2+} uptake of the cells was followed up by Fluo-4 imaging, as the trace in Fig. 2a shows for the stimulation with LPA. Additionally, a microfluidic system, schematically plotted as an inset in Fig. 2a, allowed a fast change of media by moving the RBCs using the holographic optical tweezers from one "channel" to the other. In this way, we tested cells under five different conditions: (i) PIS-solution, (ii) PIS-solution containing 2 mM Ca^{2+} and 10 μM LPA, (iii) PIS-solution containing 2 mM Ca^{2+} and 2.5 μM LPA, (iv) PIS-solution containing 2 mM Ca^{2+} and no LPA, and finally (v) PIS-solution containing 2 mM EDTA and 10 μM LPA. We used at least 60 cells per condition. The results are summarized in Fig. 2b. The RBC stimulation with LPA (2.5 μM as well as 10 μM) in the presence of extracellular Ca^{2+} led to an immediate qualitative change in the adhesion behavior: cells irreversibly stuck to each other. Additionally, RBCs were stained with an annexin V-FITC conjugate to probe for phosphatidylserine (PS) exposure of the RBCs by means of fluorescence microscopy. In Fig. 2c, we show that the 2.5 μM LPA-induced Ca^{2+} influx indeed was associated with PS transport from the inner leaflet to the outer leaflet of the RBC membrane. This staining was not observed in cells treated with conditions (i), (iv) and (v).

3.2. Approaching the signaling entities

The initial stimulation experiments using LPA revealed that an LPA-induced Ca^{2+} influx leads to intercellular RBC adhesion. To test whether this is a pure Ca^{2+} effect or if the presence of LPA is required, experiments were performed using the Ca^{2+} ionophore A23187 as an artificial tool to increase the intracellular Ca^{2+} concentration. After transferring the Fluo-4 loaded RBCs to the A23187 solution, the Fluo-4 fluorescence signal increased almost immediately, i.e., faster than after application with LPA. The Ca^{2+} influx into the cell is depicted in Fig. 3a. As illustrated in Fig. 3b, during the Ca^{2+} increase, the cells undergo a shape transformation from discocytes to spherocytes via an intermediate step of echinocytes. Testing for adhesion was performed using a procedure identical to the LPA experiments performed in the following four media: (i) PIS-solution, (ii) PIS-solution containing 2 mM Ca^{2+} and 40 μM A23187, (iii) PIS-solution containing 2 mM Ca^{2+} and no A23187, and (iv) PIS-solution containing 2 mM EDTA and 40 μM A23187. The results are summarized in Fig. 3c. Intercellular adhesion was significantly

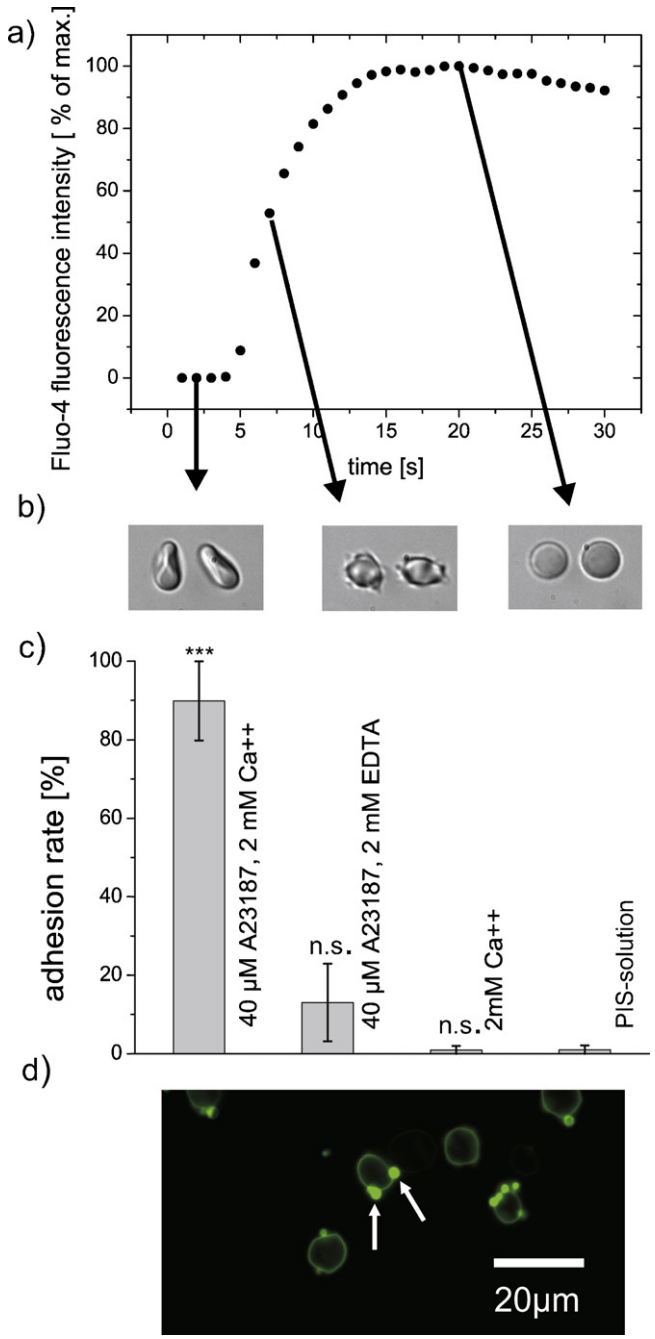

Fig. 3. Measurements with the Ca^{2+} ionophore A23187. (a) The relative fluorescence signal of a representative RBC in the upper channel of the microfluidic system; $t = 0$ s is the time when the cell reached the A23187 solution. The Ca^{2+} increase happens almost instantaneously. The decrease in signal after 15 s is due to photobleaching. (b) The RBCs undergo a shape transformation from discocytes (left) via echinocytes (middle) to spherocytes (right) after transfer into the A23187 buffer solution in the upper channel. (c) The results of the ionophore measurements conducted in the microfluidic chamber and a Petri dish. The black bars represent the percentage of cells that showed adhesion. The number of cells tested was about 60 per measurement. In the presence of A23187 and Ca^{2+}, about 90% of the cells tested adhered, whereas in the control experiments, less than 3% of the cells adhered. The results of the Student's *t*-test, compared to the control measurement (PIS-solution), are indicated at the top of each bar. (d) A fluorescence image of annexin V-FITC-labeled RBCs. The cells were treated with A23187, and exposure of PS at the cell surface was clearly identified. A vesiculation of the cells was also observed (indicated by arrows).

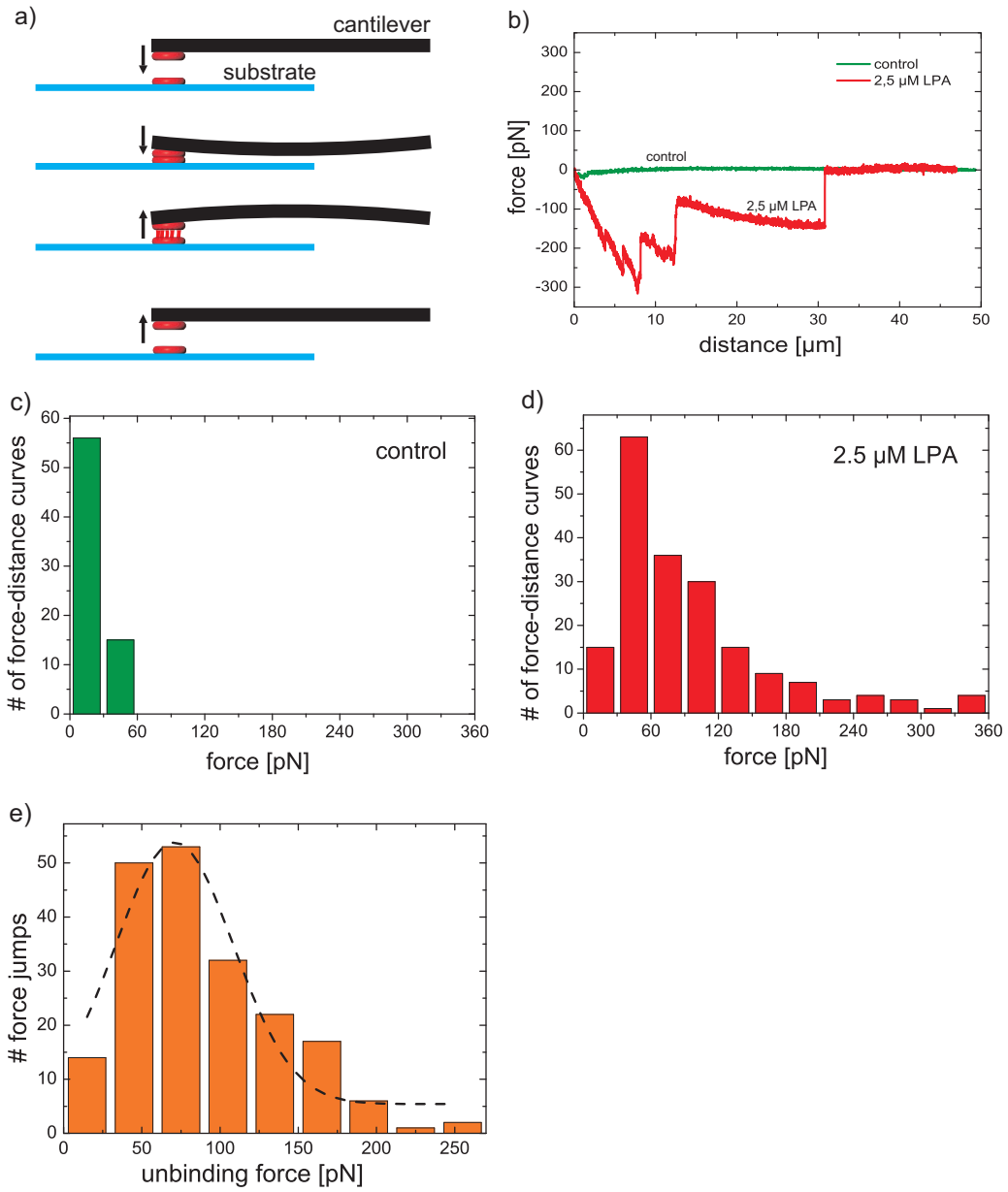

Fig. 4. Force quantification using atomic force spectroscopy (AFS). Panel (a) shows the working principle of the AFS. One cell is attached to a cantilever, while another one is attached to the surface. Over the course of the experiment, the cells are brought into contact and are withdrawn again. The adhesion force of the two cells can be measured by measuring the deflection of the cantilever. Panel (b) shows the combined plot of an example force–distance-curve of a control (green) and an LPA measurement (red). Panel (c) and panel (d) depict the statistics of the measured forces in the controls and LPA measurements, respectively. Panel (e) provides a histogram of the unbinding force of a single tether within the procedure visualized in panels (a) and (b). The dotted line depicts a Gaussian approximation of the bars. (For interpretation of the references to color in this figure legend, the reader is referred to the web version of the article.)

increased compared to the controls only when the intracellular Ca^{2+} concentration was increased. There have been controversial reports about PS transition to the outer membrane leaflet that claim merely coincidental increase in Ca^{2+} that is not related to the PS exposure [16,17]. Therefore, RBCs were stained with annexin-V-FITC conjugates in order to visualize PS exposure on the surface of RBCs. As depicted in Fig. 3d, treatment with A23187 in the presence of extracellular Ca^{2+} leads to a clear annexin-V binding (PS staining) on the outer leaflet of the membranes. Under all the other conditions (i), (iii), and (iv), no such staining could be observed.

3.3. Quantification of the intracellular adhesion

To allow a discussion of a physiological (or pathophysiological) relevance of the described adhesion process, one needs to determine the separation force. As described above, the separation force exceeds the abilities of the HOT. Therefore, single-cell force spectroscopy [18] was utilized for determination of the force. Two different measurements were conducted: control measurements in which the cells remained untreated and measurements in which the cells were treated with a concentration of 2.5 µM LPA. Example curves for both experiments are depicted in Fig. 4b. It is an inherent part of the single-cell force spectroscopy procedure that cells need to be brought in contact by a certain force application (step 2 in Fig. 4a). In the control measurements, it was only possible to detect a weak interaction between the cells, whereas in the LPA measurements, a pronounced adhesion of the red blood cells could be observed. The step-wise release plotted in Fig. 4b (step 3 in Fig. 4a) was typical for all the cells measured. All results of the measurements are collected into histograms summarized in Fig. 4c and

d. The mean value of the maximum unbinding force of untreated red blood cells amounted to 28.8 ± 8.9 pN (s.d.) (n = 71), whereas in the LPA experiments, the mean value of the maximum unbinding force amounted to a much higher value of 100 ± 84 pN (s.d.) (n = 193, from three different donors) indicating a severe difference in adhesion behavior of untreated and LPA-stimulated RBCs.

4. Discussion

4.1. LPA stimulation leads to intercellular adhesion

It is an established fact that the stimulation of RBCs with LPA leads to a Ca^{2+} influx through an NSVDC channel [9,12]. It is further known that the increased intracellular Ca^{2+} results in the stimulation of the Ca^{2+}-activated K^+ channel (Gardos channel) [19,20] and the activation of the lipid scramblase [21,22] (see below for further discussion). Based on these mechanisms, an increased aggregation tendency of stimulated RBCs has been hypothesized [9,23]. The development of the HOT provides a tool for testing this hypothesis at the cellular level. Concentrations of 2.5 μM and 10 μM LPA were chosen because they seemed to be within the common range of concentrations used with other cell types [24,25] in addition to RBCs [17]. Moreover, this concentration is comparable to the local LPA concentration in the immediate surroundings of activated platelets, e.g., inside a blood clot [26,27]. While the choice of the LPA concentration did not seem to have any significant effect on the adhesion rate itself, it had an impact on the shape of the RBCs. This relationship is discussed in the next section. After an intracellular Ca^{2+} increase was observed by fluorescence imaging, the setup mode was switched to white light for better HOT operation. Then, the cells were brought into contact and adhered to each other immediately. Because the time for the Ca^{2+} increase varied from cell to cell, which is in agreement with previous investigations [9,28], the time between the initial stimulation of the cell and the final adhesion varied between 10 and 140 s, yielding an average value of 72.75 ± 46.79 s (s.d.). This time range already indicates that under normal physiological conditions, the activation of RBCs is not compatible with an active process contributing to the initiation of a blood clot, but once caught in the fibrin network, the RBCs may actively support clot formation. In addition, to test the necessity of the presence of Ca^{2+} during LPA stimulation, the negative control experiments excluded any interplay between the infrared trapping laser and the adhesion process.

4.2. Signaling components

Because LPA is a phospholipid derivative, we examined the extent to which it is directly involved in the adhesion process. Although the concentration used was clearly below the critical micelle concentration (70 μM–1 mM) [26], which might induce detergent-like effects, LPA is likely to be incorporated into the membrane. From the initial intercellular adhesion after LPA stimulation (Fig. 2b), one may propose the following alternative explanations: (i) LPA is directly responsible for the adhesion, (ii) LPA and the Ca^{2+} influx are both necessary to mediate adhesion, and (iii) LPA simply triggers the Ca^{2+} influx, and the Ca^{2+} signaling alone is sufficient to induce adhesion. Option (i) can be excluded immediately because it was tested as a control in the initial set of experiments (Fig. 2b). In order to discriminate between options (ii) and (iii), experiments where A23187, a Ca^{2+} ionophore, was added to the RBCs were performed. As shown in Fig. 3, the increased intracellular Ca^{2+} concentration is the dominant signal initiating the adhesion. The Ca^{2+} entry under LPA stimulation is channel-mediated, although the molecular identity of the channel remains unclear [29]. Because LPA is not the major entity in the adhesion process, an alternative molecule or a combination of several entities downstream of the Ca^{2+} signal must control the response. Proteins that are known to be activated in RBCs by an increase in intracellular Ca^{2+} concentration are the Gardos channel, the lipid scramblase, the cysteine protease calpain [30,31] and the Ca^{2+} pump. Although all the proteins are Ca^{2+}-activated, their sensitivity to Ca^{2+} differs. To determine in which order and under what conditions the above mentioned players activate, we refer to the Ca^{2+} concentration with the half maximal effect (EC_{50}). It would therefore be desirable to quantitatively measure the Ca^{2+} concentration in an individual RBC. Unfortunately, this is not possible due to the failure of ratiometric Ca^{2+} sensors in RBCs [28]. Instead, we compare EC_{50} values determined in different studies with the cellular responses we observed in the present study. The smallest EC_{50} for Ca^{2+} is obviously that of the Ca^{2+} pump that keeps the resting Ca^{2+} concentration in RBCs well below 100 nM [32]. With any increase in the intracellular Ca^{2+} concentration, the Ca^{2+} pump will activate. Although the V_{max} of the Ca^{2+} pump was determined in cell populations to be patient- and sample-dependent in a range of 8–20 mmol/(l_{cells} h) [32], the pump activity per cell varies tremendously [33]. This variation explains the broad time range observed between the start of LPA stimulation and the Ca^{2+} increase. While the pump can counterbalance the LPA-induced Ca^{2+} influx for a short time period, during the application of A23187, the amount of Ca^{2+} entering the cell exceeds the V_{max} capacity of the Ca^{2+} pump for all cells. At a Ca^{2+} concentration of 400 nM, the flippase transporting PS actively from the outer membrane leaflet to the inner one is inhibited [34]. Once the Ca^{2+} influx exceeds the transport capacity of the Ca^{2+} pump, the first player that will be activated is the Gardos channel, with an EC_{50} of 4.7 μM [35]. As we can see for the shape transitions upon A23187 stimulation shown in Fig. 3b, cells turn (transiently) into echinocytes as a consequence of KCl loss triggered by K^+ efflux through the Gardos channel. For LPA stimulation, the situation is different: due to the activation of the non-selective cation channel by LPA, a Na^+ influx and, consequently, NaCl uptake counterbalances the KCl loss initiated by the Gardos channel, producing an osmotic equilibrium. For a 2.5 μM LPA stimulation, this equilibrium [36] is reached, whereas for a 10 μM LPA stimulation, the effect of the NaCl uptake overwhelms the KCl loss, resulting in the formation of spherocytes. The next entity to be activated upon Ca^{2+} entry is the scramblase, with an EC_{50} of 29 μM [37]. Scramblase activity was demonstrated by probing for PS in the outer membrane leaflet using annexin V-FITC staining. Staining was present after both LPA and A23187 stimulation, as depicted in Fig. 3c and d, respectively. Calpain is activated with an EC_{50} of 40 μM, which is very close to the EC_{50} of the scramblase [38]. Under both stimulation conditions (LPA and A23187), we observed vesiculation that has been shown to be associated with the activation of calpain [30], which cleaves spectrin and actin and therefore leads to the breakdown of the cytoskeleton. This is in good agreement with a recent report on exovesiculation by Cueff et al. [39]. However, the vesiculation was much more pronounced under A23187 stimulation than under LPA stimulation, as depicted in the representative images in Figs. 3d and 2c, respectively. Therefore, we suggest that the Ca^{2+} concentration after stimulation with 2.5 μM LPA is smaller compared to the A23187 stimulation and might be in the range of EC_{50} of calpain. For A23187 stimulation, a shape change from echinocytes to spherocytes occurs (compare Fig. 3a and b), which is mediated by the encapsulation of microvesicles. However, the occurrence of PS on the outside of the cell makes it a good candidate for initiating the adhesion process. This could be due to simple Ca^{2+}–PS cross-bridging and/or a more complex process involving adhesion proteins. Further evidence for both options comes from aggregation studies of PS vesicles [40,41], where aggregation occurs in solutions of physiological ionic strength containing Ca^{2+} in the mM concentration range. The dependence on high Ca^{2+} concentrations and evidence from further studies reporting enhanced

aggregation of PS liposomes in the presence of polymers [42] suggest that additional membrane constituents in the RBC contribute to the aggregation process. This leads to other Ca^{2+}-dependent proteins in RBCs, such as PKC_{α} [43,44] or the nitric oxide synthase [45,46]. Further research is required to address the question of the molecular identity of the additional components in the adhesion process. Analyzing the stepwise unbinding (compare Fig. 4b) when RBCs are separated from each other (corresponding to step 3 in Fig. 4a), we found a Gaussian distribution of the force centered at 71.9 pN (Fig. 4e). Such a distribution suggests the formation of tethers and specific bonds between the RBCs that are released one by one during the separation process.

4.3. Relevance to in vivo conditions

The LPA concentration of between 2.5 and 10 μM is a physiologically relevant concentration that is likely to occur locally after platelet activation. Upon stimulation with such an LPA concentration, RBCs adhere irreversibly to each other. The separation force of approximately 100 pN (determined by single cell force spectroscopy) is in a range that is of relevance in the vasculature [47]. As mentioned previously, due to the time course of the Ca^{2+} increase, we regard an initiation of a blood clot based on intercellular RBC adhesion to be irrelevant under physiological conditions. However, once caught in the fibrin network of a blood clot, the adhesion process observed here in vitro may support the solidification of the clot. This notion is supported by the aforementioned experimental and clinical investigations reporting a prolongation of bleeding time in subjects with low RBC counts [7–9,48]. Evidence that the adhesion process described in this paper may play a role in vivo was recently provided by Chung and coworkers [49]. In this study, an increase in intracellular Ca^{2+} of RBCs associated with a PS exposure was related to prothrombotic activity in vivo in a venous thrombosis rat model. Under pathophysiological conditions, intercellular RBC adhesion after Ca^{2+} influx seems to have a more pronounced effect. An example is the vasco-occlusive crisis of sickle cell disease (SCD) patients. Here, the Ca^{2+} influx is mediated by the NMDA-receptor, which has been found to be abundant in RBCs [46]. Our study provides a link between the increased prevalence of the NMDA-receptor in SCD patients [50] and the symptoms of the vasco-occlusive crisis. Further examples where disorders in the ion homeostasis of RBCs are associated with thrombotic events are malaria [51] and thalassemia [52,53]. Therefore, we propose that the Ca^{2+} increase, independent of the entry pathway, followed by PS exposure and RBC aggregation is a general mechanism that may become relevant under pathological conditions.

Conflict of interest statement

All authors have no conflicts of interest to declare.

Acknowledgements

This work has been supported by the DFG Graduate School, GRK 1276 and the Ministry of Economy and Sciences of the Saarland. The study was approved by the ethics committee of the Medical Association of the Saarland (reference number 132/08).

Appendix A. Supplementary data

Supplementary data associated with this article can be found, in the online version, at doi:10.1016/j.ceca.2011.05.002.

References

[1] J.L. McWhirter, H. Noguchi, G. Gompper, Flow-induced clustering and alignment of vesicles and red blood cells in microcapillaries, Proc. Natl. Acad. Sci. U.S.A. 106 (2009) 6039–6043.
[2] P. Snabre, G.H. Grossmann, P. Mills, Effects of dextran polydispersity on red blood-cell aggregation, Colloid Polym. Sci. 263 (1985) 478–483.
[3] A. Pribush, D. Zilberman-Kravits, N. Meyerstein, The mechanism of the dextran-induced red blood cell aggregation, Eur. Biophys. J. 36 (2007) 85–94.
[4] E. Evans, Detailed mechanics of membrane-membrane adhesion and separation. 1. Continuum of molecular cross-bridged. 2. Discrete kinetically trapped molecular cross-bridges, Biophys. J. 48 (1985) 175–192.
[5] K.I. Ataga, M.D. Cappellini, E.A. Rachmilewitz, Beta-thalassaemia and sickle cell anaemia as paradigms of hypercoagulability, Br. J. Haematol. 139 (2007) 3–13.
[6] W.W. Duke, The relation of blood platelets to hemorrhagic disease, JAMA 55 (1910) 1185–1192.
[7] A.J. Hellem, C.F. Borchgrevink, S.B. Ames, The role of red cells in haemostasis: the relation between haematocrit, bleeding time and platelet adhesiveness, Br. J. Haematol. 7 (1961) 42–50.
[8] M. Livio, E. Gotti, D. Marchesi, G. Mecca, G. Remuzzi, G. de Gaetano, Uraemic bleeding: role of anaemia and beneficial effect of red cell transfusions, Lancet 2 (1982) 1013–1015.
[9] L. Kaestner, W. Tabellion, P. Lipp, I. Bernhardt, Prostaglandin E_2 activates channel-mediated calcium entry in human erythrocytes: an indication for a blood clot formation supporting process, Thromb. Haemost. 92 (2004) 1269–1272.
[10] L. Kaestner, C. Bollensdorff, I. Bernhardt, Non-selective voltage-activated cation channel in the human red blood cell membrane, Biochim. Biophys. Acta 1417 (1999) 9–15.
[11] L. Kaestner, P. Christophersen, I. Bernhardt, P. Bennekou, The non-selective voltage-activated cation channel in the human red blood cell membrane: reconciliation between two conflicting reports and further characterisation, Bioelectrochemistry 52 (2000) 117–125.
[12] L. Kaestner, I. Bernhardt, Ion channels in the human red blood cell membrane: their further investigation and physiological relevance, Bioelectrochemistry 55 (2002) 71–74.
[13] A. Dyrda, U. Cytlak, A. Ciuraszkiewicz, A. Lipinska, A. Cueff, G. Bouyer, S. Egee, P. Bennekou, V.L. Lew, S.L.Y. Thomas, Local membrane deformations activate Ca^{2+}-dependent K^+ and anionic currents in intact human red blood cells, PLoS One 5 (2010) e9447.
[14] T. Oonishi, K. Sakashita, N. Ishioka, N. Suematsu, H. Shio, N. Uyesaka, Production of prostaglandins E_1 and E_2 by adult human red blood cells, Prostaglandins Other Lipid Mediat. 56 (1998) 89–101.
[15] K. Dholakia, G. Spalding, M. MacDonald, Optical tweezers: the next generation, Phys. World 15 (2002) 31–35.
[16] P.A. Lang, S. Kaiser, S. Myssina, T. Wieder, F. Lang, S.M. Huber, Role of Ca^{2+}-activated K^+ channels in human erythrocyte apoptosis, Am. J. Physiol. Cell Physiol. 285 (2003) C1553–C1560.
[17] S.M. Chung, O.N. Bae, K.M. Lim, J.Y. Noh, M.Y. Lee, Y.S. Jung, J.H. Chung, Lysophosphatidic acid induces thrombogenic activity through phosphatidylserine exposure and procoagulant microvesicle generation in human erythrocytes, Arterioscler. Thromb. Vasc. Biol. 27 (2007) 414–421.
[18] J. Friedrichs, J. Helenius, D.J. Muller, Quantifying cellular adhesion to extracellular matrix components by single-cell force spectroscopy, Nat. Protoc. 5 (2010) 1353–1361.
[19] G. Gardos, The function of calcium in the potassium permeability of human erythrocytes, Biochim. Biophys. Acta 30 (1958) 653–654.
[20] J.F. Hoffman, W. Joiner, K. Nehrke, O. Potapova, K. Foye, A. Wickrema, The hSK4 (KCNN4) isoform is the Ca^{2+}-activated K^+ channel (Gardos channel) in human red blood cells, Proc. Natl. Acad. Sci. U.S.A. 100 (2003) 7366–7371.
[21] L.A. Woon, J.W. Holland, E.P. Kable, B.D. Roufogalis, Ca^{2+} sensitivity of phospholipid scrambling in human red cell ghosts, Cell Calcium 25 (1999) 313–320.
[22] C.W.M. Haest, Distribution and movement of membrane lipids, in: Red Cell Membrane Transport in Health and Disease, Springer Verlag, Berlin, 2003, pp. 1–26.
[23] L. Yang, D.A. Andrews, P.S. Low, Lysophosphatidic acid opens a Ca^{2+} channel in human erythrocytes, Blood 95 (2000) 2420–2425.
[24] R. Dixon, K. Young, N. Brunskill, Lysophosphatidic acid-induced calcium mobilization and proliferation in kidney proximal tubular cells, Am. J. Physiol. 276 (1999) F191–F198.
[25] K. Meerschaert, V. De Corte, Y. De Ville, J. Vandekerckhove, J. Gettemans, Gelsolin and functionally similar actin-binding proteins are regulated by lysophosphatidic acid, EMBO J. 17 (1998) 5923–5932.
[26] T. Eichholtz, K. Jalink, I. Fahrenfort, W.H. Moolenaar, The bioactive phospholipid lysophosphatidic acid is released from activated platelets, Biochem. J. 291 (1993) 677–680.
[27] F. Gaits, O. Fourcade, F. LeBalle, G. Gueguen, B. Gaige, A. GassamaDiagne, J. Fauvel, J. Salles, G. Mauco, M. Simon, H. Chap, Lysophosphatidic acid as a phospholipid mediator: pathways of synthesis, FEBS Lett. 410 (1997) 54–58.
[28] L. Kaestner, W. Tabellion, E. Weiss, I. Bernhardt, P. Lipp, Calcium imaging of individual erythrocytes: problems and approaches, Cell Calcium 39 (2006) 13–19.
[29] L. Kaestner, Cation channels in erythrocytes – historical and future perspective, Open Biol. J. 4 (2011) 27–34.
[30] C. Berg, I. Engels, A. Rothbart, K. Lauber, A. Renz, S. Schlosser, K. Schulze-Osthoff, S. Wesselborg, Human mature red blood cells express caspase-3 and caspase-

8, but are devoid of mitochondrial regulators of apoptosis, Cell Death Differ. 8 (2001) 1197–1206.
[31] H.J. Schatzmann, ATP-dependent Ca^{2+}-extrusion from human red cells, Experientia 22 (1966) 364–365.
[32] T. Tiffert, R.M. Bookchin, V.L. Lew, Calcium homeostasis in normal and abnormal human red cells, in: Red Cell Membrane Transport in Health and Disease, Springer Verlag, Berlin, 2003, pp. 373–405.
[33] V.L. Lew, N. Daw, D. Perdomo, Z. Etzion, R.M. Bookchin, T. Tiffert, Distribution of plasma membrane Ca^{2+} pump activity in normal human red blood cells, Blood 102 (2003) 4206–4213.
[34] M. Bitbol, P. Fellmann, A. Zachowski, P.F. Devaux, Ion regulation of phosphatidylserine and phosphatidylethanolamine outside inside translocation in human-erythrocytes, Biochim. Biophys. Acta 904 (1987) 268–282.
[35] T. Leinders, R.G.D.M. Vankleef, H.P.M. Vijverberg, Single Ca(2+)-activated K^+ channels in human erythrocytes: Ca^{2+} dependence of opening frequency but not of open lifetimes, Biochim. Biophys. Acta 1112 (1992) 67–74.
[36] L. Kaestner, A. Juzeniene, J. Moan, Erythrocytes – the "house elves" of photodynamic therapy, Photochem. Photobiol. Sci. 3 (2004) 981–989.
[37] J.G. Stout, Q.S. Zhou, T. Wiedmer, P.J. Sims, Change in conformation of plasma membrane phospholipid scramblase induced by occupancy of its Ca^{2+} building site, Biochemistry 37 (1998) 14860–14866.
[38] T. Murakami, M. Hatanaka, T. Murachi, The cytosol of human-erythrocytes contains a highly Ca^{2+}-sensitive thiol protease (calpain I) and its specific inhibitor protein (calpastatin), J. Biochem. 90 (1981) 1809–1816.
[39] A. Cueff, R. Seear, A. Dyrda, G. Bouyer, S. Egee, A. Esposito, J. Skepper, T. Tiffert, V.L. Lew, S.L. Thomas, Effects of elevated intracellular calcium on the osmotic fragility of human red blood cells, Cell Calcium 47 (2010) 29–36.
[40] J. Lansman, D.H. Haynes, Kinetics of a Ca^{2+}-triggered membrane aggregation reaction of phospholipid membranes, Biochim. Biophys. Acta 394 (1975) 335–347.
[41] S. Ohki, N. Duzgunes, K. Leonards, Phospholipid vesicle aggregation: effect of monovalent and divalent ions, Biochemistry 21 (1982) 2127–2133.
[42] M. Babincova, E. Machova, Dextran enhances calcium-induced aggregation of phosphatidylserine liposomes: possible implications for exocytosis, Physiol. Res. 48 (1999) 319–321.
[43] R.B. Govekar, S.M. Zingde, Protein kinase C isoforms in human erythrocytes, Ann. Hematol. 80 (2001) 531–534.
[44] B.A. Klarl, P.A. Lang, D.S. Kempe, O.M. Niemoeller, A. Akel, M. Sobiesiak, K. Eisele, M. Podolski, S.M. Huber, T. Wieder, F. Lang, Protein kinase C mediates erythrocyte "programmed cell death" following glucose depletion, Am. J. Physiol. Cell Physiol. 290 (2006) C244–253.
[45] P. Kleinbongard, R. Schulz, M. Muench, T. Rassaf, T. Lauer, A. Goedecke, M. Kelm, Red blood cells express a functional endothelial nitric oxide synthase, Eur. Heart J. 27 (2006) 127.
[46] A. Makhro, J. Wang, J. Vogel, A.A. Boldyrev, M. Gassmann, L. Kaestner, A. Bogdanova, Functional NMDA receptors in rat erythrocytes, Am. J. Physiol. Cell Physiol. 298 (2010), doi:10.1152/ajpcell.00407.2009.
[47] P. Snabre, M. Bitbol, P. Mills, Cell disaggregation behavior in shear, Biophys. J. 51 (1987) 795–807.
[48] N. Mackman, Triggers, targets and treatments for thrombosis, Nature 451 (2008) 914–918.
[49] J.Y. Noh, K.M. Lim, O.N. Bae, S.M. Chung, S.W. Lee, K.M. Joo, S.D. Lee, J.H. Chung, Procoagulant and prothrombotic activation of human erythrocytes by phosphatidic acid, Am. J. Physiol. Heart Circ. Physiol. 299 (2010) H347–H355.
[50] A. Bogdanova, A. Makhro, J. Goede, J. Wang, A. Boldyrev, M. Gassmann, L. Kaestner, NMDA receptors in mammalian erythrocytes, Clin. Biochem. 42 (2009) 1858–1859.
[51] V. Luvira, S. Chamnanchanunt, V. Thanachartwet, W. Phumratanaprapin, A. Viriyavejakul, Cerebral venous sinus thrombosis in severe malaria, Southeast Asian J. Trop. Med. Public Health 40 (2009) 893–897.
[52] A. Eldor, E.A. Rachmilewitz, The hypercoagulable state in thalassemia, Blood 99 (2002) 36–43.
[53] A.T. Taher, Z.K. Otrock, I. Uthman, M.D. Cappellini, Thalassemia and hypercoagulability, Blood Rev. 22 (2008) 283–292.

Quantification of Depletion Induced Adhesion of Red Blood Cells

P. Steffen[1],C. Verdier[2], C. Wagner[1]
[1] *Experimental Physics, Saarland University, 66041 Saarbreucken, Germany*
[2] *CNRS - Université de Grenoble I, UMR5588, Laboratoire Interdisciplinaire de Physique (LIPhy) 38041 Grenoble, France*

Red blood cells (RBC) are known to form aggregates in the form of rouleaux due to the presence of plasma proteins under physiological conditions. The formation of rouleaux can also be induced *in vitro* by the addition of macromolecules to the RBC suspension. Current data on the adhesion strength between red blood cells in their natural discocyte shapes mostly originate from indirect measurements such as flow chamber experiments, but data is lacking at the single cell level. Here, we present measurements on the dextran-induced aggregation of red blood cells using atomic force microscopy-based single cell force spectroscopy (SCFS). The effects of dextran concentration and molecular weight on the interaction energy of adhering RBCs were determined. The results are in excellent agreement with a model based on the depletion effect and previous experimental studies.

PACS numbers: 87.17.Rt,87.64.Dz,87.15.nr

Non-pathological aggregation of RBCs or "rouleaux formation" (Fig.1a) *in vivo* is frequently observed and caused by the fibrinogen in plasma [1]. These aggregates are reversibly formed and can be dispersed by moderate shear rates. Thus, the shear thinning viscosity of blood is determined to a large extent by the formation and breaking of these aggregates. Irreversible red blood cell aggregation could be a microcirculatory risk factor and indicative of disease because irreversible aggregates can be observed in diseases such as malaria, multiple myeloma, inflammation [2] or in pathological thrombus formation [3]. Reversible rouleaux formation can also be induced by resuspending the RBCs in physiological solutions containing neutral macromolecules such as dextran (DEX) [4]. The fibrinogen mediated aggregation of RBCs increases consistently with increasing fibrinogen concentration [5], whereas the dextran-mediated aggregation of RBCs reaches a maximum at a certain dextran concentration. The strength of the aggregation depends not only on the dextran concentration, but also on the molecular weight of the dextran (i.e., the radius of gyration of the dextran) [6, 7]. Previously, two different models have been developped to explain the aggregation of RBCs in polymer solutions: the Cross-Bridging model and the Depletion model. The Bridging model has been favored for a long time and has been proposed for plasma protein and neutral dextran macromolecule-induced RBC aggregation [8]. In this model, it is assumed that fibrinogen or dextran molecules non-specifically adsorb onto the cell membrane and form a "bridge" to the adjacent cell. However, over the most recent decade, more and more evidence has been observed in favor of the depletion model [9–13]. A first explanation of depletion forces was given by Asakura and Oosawa [14], who discovered that the presence of small spheres (i.e., macromolecules) can induce effective forces between two larger particles if the distance between them is small enough. The origin of these forces is purely entropic. If the distance between the two large particles decreases to less than the size of the surrounding macromolecules, these macromolecules are expelled from the region between the particles. Consistently, the concentration of macromolecules becomes depleted in this region compared to that of the bulk, and an effective osmotic pressure causing an attraction between the large particles occurs. Neu et al. [9] applied this concept of depletion-induced adhesion to red blood cells and developped a theoretical description of the interaction energy between two red blood cells in terms of the molecular weight and concentration of the dextran used. These results were compared with former measurements reported by Buxbaum et al. [15] based on the micropipette aspiration technique. Neu et al. were able to adapt their model parameters consistently to the experimental data of Buxbaum et al., but the number of data points remained limited.

FIGURE CAPTIONS

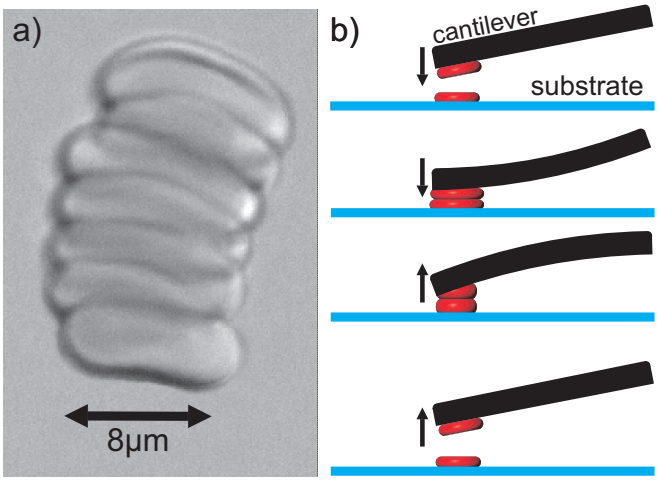

In the present study, we used the technique of single cell force spectroscopy (SCFS) (Fig.1b) to measure the interaction energies between human red blood cells as functions of the molecular weight and concentration

FIG. 1: a) Snapshot of a rouleau of 7 RBCs in a dextran solution. b) A sketch of the working principle of single cell force spectroscopy (SCFS). A single cell is attached to the pre-functionalized cantilever and is lowered onto another cell, which is fixed at the bottom. The adhesion force and adhesion energy are measured while withdrawing the cells.

of dextran at the single cellular level and compared them to the predicted values of Neu et al.[9]. The used dextrans were dxtran70 (DEX70 with a molecular weight of 70kDa) and dextran150(DEX150 with a molecular weight of 150kDa) from Sigma-Aldrich. In SCFS a single RBC is attached to a cantilever, while another cell is attached to the surface of the petri dish. Both cells are now brought into close contact and during the withdrawing of the cantilever the adhesion force between both cells is measured via the deflection of the cantilever (see Fig.1b). An atomic force microscope (AFM) (Nanowizard 2, equipped with the CellHesion Module with an increased pulling range of 100µm, JPK Instruments, Germany) was used to conduct single cell force spectroscopy measurements [16]. The spring constant of the cantilever was determined using the common thermal noise method (the cantilevers used were MLCT-O cantilevers with spring constants on the order of 0.01N/m, Bruker). Fresh blood from healthy donors was taken using a finger prick. The blood was obtained within one day of the experiment. The cells were washed three times by centrifugation (2000g, 3min) in a phosphate-buffered solution of physiological ionic strength. In the course of the experiment, a single RBC was attached to an AFM cantilever by appropriate functionalization. Cell Tak^{TM} (BD Science) was used to bind a cell to the cantilever. A protocol was used, in which the cantilever was incubated in a Cell Tak^{TM} drop. After 2min, the Cell Tak^{TM} solution was carefully removed; this was followed by a 3min waiting period to allow the acetic acid from teh Cell-Tak^{TM} to evaporate from the cantilever. Rinsing the cantilever with ethanol and PBS (Phosphate-Buffered Saline, 137mM/l $NaCl$, 2.7mM/l KCl, 10mM/l $Na_2HPO_4 2H_2O$, 2mM/l KH_2PO_4, $pH = 7.4$) completed the functionalization protocol. To attach a RBC to the cantilever, the latter was lowered manually until a preset cantilever deflection (i.e. force setpoint F_{set}) was reached, indicating contact between the cantilever and the cell. The cantilever was withdrawn continuously at low speed until the cell was no longer in contact with the surface. After the cell had been attached to the cantilever, the cell was placed on top of another cell that lay on the bottom of the petri dish. Functionalization of the plastic petri dish (PS, Polystyrol), to immobilize the bottom cell, was not necessary because RBCs adhered to the surface without any further treatment. While withdrawing (or retracting) the cantilever the adhesion force and adhesion energy were measured. The retraction curve is typically characterized by the maximum force required to separate the cells from each other and adhesion energy is calculated by computing the area under the retraction curve of the force distance curve. The interaction energies (or, more precisely, the interaction energy densities of two RBCs) are calculated by dividing the measured adhesion energies by the contact areas of the adhering cells using a value of 50.24µm^2 derived from the mean radius of RBCs. The present study

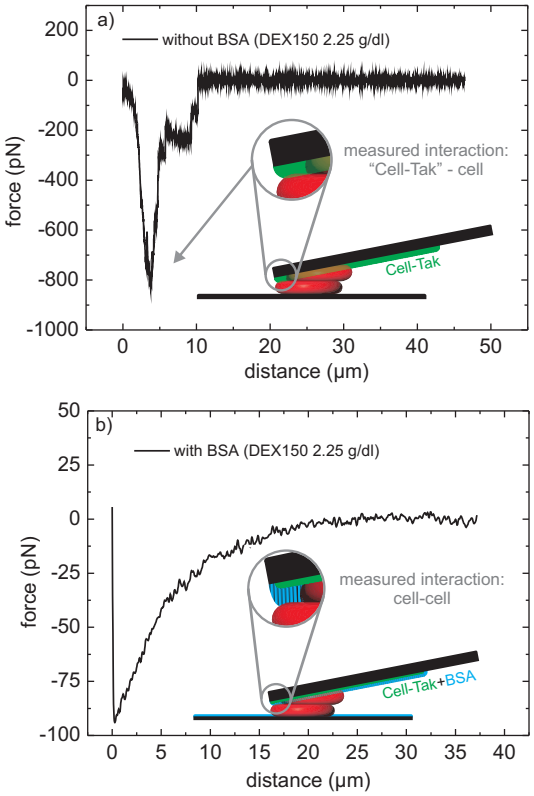

FIG. 2: a) and b) show the effects of BSA treatment (see the text for details). Without BSA treatment, undesired adhesion events occur whose origin is not the investigated depletion effect; e.g., the cells don't hit concentrically and the lower cell touches the Cell-Tak (i.e., a stonger adhesion force is measured because of the strong adhesiveness of the Cell-Tak). With BSA treatment, the Cell-Tak is completely passivated and the influence of those undesired adhesion events is minimized, as the changes in shape and magnitude of the measured force curve document.

is exclusively concerned with adhesion that is caused by the presence of dextran molecules in the solution. Hence, any further source of adhesion (e.g., adhesion of the lower RBC to the Cell-Tak coated surface of the cantilever, see Fig.2a) had to be excluded. For larger and stiffer cells, compared to RBCs, such undesired

adhesion events are rarely observed. For RBCs that have a height of just 2µm, and this is an experimental difficulty; even with optimum (concentric) alignment, such binding to the surface was often observed in our first experiments. An example of those undesired adhesion events is shown in Fig.2a. The measured adhesion forces were much higher than any reasonable estimate for dextran-induced adhesion. To overcome this problem, 0.1g/dl BSA (Bovine Serum Albumin) was added to the solution after attaching the RBC to the cantilever. BSA could potentially induce an additional depletion interaction; however because the radius of gyration of BSA is only 3nm [17] and the concentration is fairly small, the additional depletion interaction due to the presence of BSA can be neglected. The effects of BSA treatment on RBCs (e.g., on cell geometry or mechanical properties) have been studied intensively [18–20]. However, any effect of the BSA treatment on the measured interaction energy can be neglected for the investigated adhesion because this adhesion is purely physical (i.e., we assume that there no adhesion proteins are involved that could possibly be blocked by the incorporation of BSA into the RBC membrane). In agreement with the literature, we found that in most of the cases, both the cells on the petri dish as well as on the cantilever remained in their physiological, discocyte shape. The only purpose of the BSA is to passivate the surfaces of the cantilever and the petri dish. Thus, only the RBC surfaces contribute to the measured adhesion force arising from the depletion effect. Fig.2b shows an example force curve after BSA treatment of the cantilever and the petri dish. The shape and magnitude of the force distance curve changes significantly. The extraordinary flexibility of RBCs allows them to stay in contact over large withdrawing distances after adhering, as one can see in the measurements with BSA (Fig.2b).

In the next step, the parameter setpoint force F_{set}, cantilever velocity v, and contact time τ of the cantilever were adjusted. Fig.3a shows the interaction energy as a function of F_{set} for DEX70, DEX150 and a measurement without dextran (control). The influence of the choice of F_{set} on the measured interaction energy is negligible and was set to $F_{set} = 300$pN for the remaining measurements. We will show below that we can describe our data well with a depletion model, but it is also known that macromolecular "bridging" between the RBCs can occur when the cells are in contact for a longer time [21]. Bronkhorst et al.[21] discovered that the time constant for those possible cross bridges is on the order of seconds. We varied the contact time from $\tau = 0$s to $\tau = 30$s to resolve the influence of the parameter τ (Fig.3b). Large contact times lead to increased adhesion energies and increased error bars. Both can be indications for bridging events. Therefore, we attempted to minimize the contact time by setting τ to 0s. Depending on the cantilever velocity, the RBCs will be in "physical" contact for a longer time because due to their flexibility, the RBCs can stay in contact over distances of several

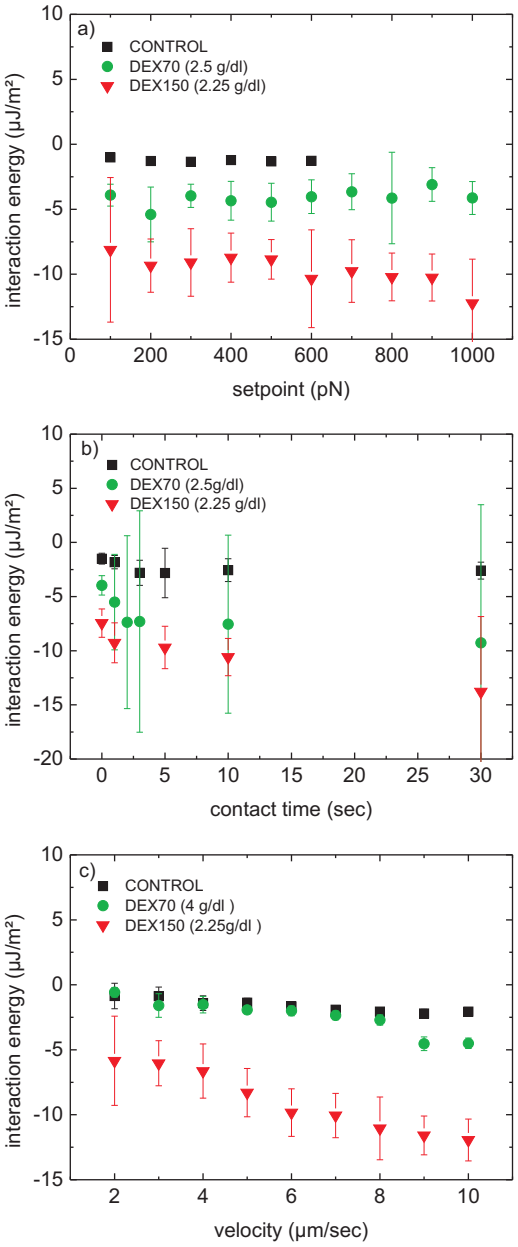

FIG. 3: Parameter measurements: a) shows the dependence of the measured adhesion energy on the chosen force setpoint F_{set}. In all measurements, no significant dependence on F_{set} was observed. b) shows the dependence of the measured adhesion energy on the chosen contact time τ of both cells. Increasing contact time leads to an increase in interaction energy and error bars. c) shows the dependence of the measured adhesion energy on the chosen withdrawal velocity v of the cantilever. At higher velocities in the DEX150 measurements a dependence on the cantilever velocity was observed, but for moderate velocities this dependence was still less than the error in the measurement.

μm. Hence, to minimize the actual contact time (to exclude bridging effects), the cantilever velocity had to be sufficiently high. This ensures that the measured interaction energies are purely depletion-induced. Fig.3c shows the dependence of the cantilever velocity v on the measured interaction energies. In the control measurements, no influence of the velocity could be seen. On the contrary, a dependence of the velocity could be observed in the dextran measurements. We do not have a conclusive explanation for this dependence, but we assume that higher interaction energies lead to larger viscoelastic effects while deforming the RBCs. Due to the higher velocity, the RBCs are deformed to greater extent, and this might lead to higher apparent interaction energies. Up to a certain velocity, the effect of velocity can be neglected; e.g., for DEX70 this effect begins at velocities only higher than 9μm/s. At high velocities, in the DEX150 measurements, this effect can be significant; while, for moderate velocities, this effect is still less than the error measurement. As mentioned above, it is necessary to minimize the contact time such that any bridging effects can be excluded; i.e., the cantilever velocity must not be too small. Therefore, in all measurements, the cantilever velocity was chosen as $v = 5\mu$m/s.

Fig.4 shows the dependence of the adhesion force and the interaction energy on the dextran concentration. Each data point represents an average of 100 force curves for the same cell. The measured interaction energies are in excellent agreement with the predicted interaction energies given by Neu et al. [9],who used an analytical approach to calculate the depletion interaction energy E_D between two RBCs [9]:

$$E_D = -2\pi(\Delta - d/2 + \delta - p) \qquad (1)$$

where π is the osmotic pressure, Δ is thickness of the depletion layer, d is the separation distance between adjacent surfaces, δ is the glycocalyx thickness and p is the depth of polymer penetration into the glycocalyx. Their model combines electrostatic repulsion due to RBC surface charge and osmotic attractive forces due to polymer depletion near the RBC surface. The theory considers the soft surfaces of RBCs and the subsequent penetration depth p of polymers into the surface. This penetration depth p depends on the polymer type, concentration, and molecular size and is expected to be larger for small molecules and to increase with increasing polymer concentration due to increasing osmotic pressure π. With increasing osmotic pressure, the penetration of macromolecules into the soft RBCs deepens, impeding the depletion of macromolecules between both cells and hence reducing the interaction energy. Above a threshold concentration this effect becomes dominant, and this decreases the interaction energy, even though the concentration of macromolecules is increasing further. Taking the depletion effect and the soft surfaces of the RBCs into account, a bell-shaped dependence of the interaction energy on the dextran concentration was calculated (the solid line in Fig.4b).

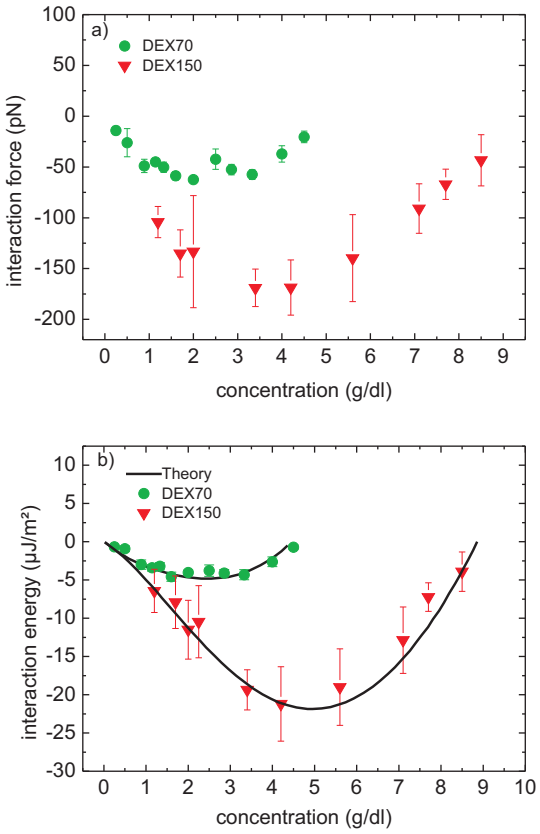

FIG. 4: a) The measured adhesion forces of the dextrans and the concentrations used. The maximum interaction strengths were observed at 2g/dl (DEX70) and 4g/dl (DEX150). b) the dependence of the interaction energy of two red blood cells on the concentrations of two dextran types. The solid line represents the curve calculated by Neu et al. [9].

In conclusion, we have presented single cell force spectroscopy measurements on dextran-induced red blood cell aggregation. The presence of dextran mimics the plasma molecules that lead to the formation of rouleaux under physiological conditions. Our findings are in excellent agreement with previous studies [9], and they can be described by a model based on the depletion effect. For contact times longer than a few seconds we find a slight tendency towards stronger adhesion energies. We can not conclusively decide whether this is due to bridging of the macromolecules between two cells or due to some other effect. One would need a sideview [22] of the adhesion areas while performing the adhesion tests to analyze this effect in greater detail.

ACKNOWLEDGEMENTS

This work was supported by the German graduate school GRK 1276 and the Nanoscience Foundation. We thank JPK Instruments for preliminary help with the experiments.

REFERENCES

[1] R. Fahraeus, Physiological Reviews **9, No. 2**, 241 (1929).
[2] M. Rampling, H. Meiselman, B. Neu, and O. Baskurt, Biorheology **41**, 91 (2004).
[3] P. Steffen, A. Jung, D. Nguyen, T. Mueller, I. Bernhardt, L. Kaestner, and C. Wagner, Cell Calcium **50**, 54 (2011).
[4] A. Pribush, D. Zilberman-Kravits, and N. Meyerstein, Eur. Biophys. J. **36**, 85 (2007).
[5] Z. Marton, G. Kesmarky, J. Vekasi, A. Cser, R. Russai, B. Horvath, and K. Toth, Clin. Hemorheol. Microcirc. **24**, 75 (2001).
[6] D. Brooks, *Mechanism of red cell aggregation, in Blood Cells, Rheology and Aging* (Springer-Verlag, 1988).
[7] S. Chien and L. Lang, Clin. Hemorheol. **7**, 71 (1987).
[8] D. Brooks, J. Colloid Int. Sci. **43**, 714 (1973).
[9] B. Neu and H. Meiselman, Biophys. J. **83**, 2482 (2002).
[10] B. Neu and H. Meiselman, Bioch. Biophys. Acta **1760**, 1772 (2006).
[11] H. Meiselmann, Biorheology **46**, 1 (2009).
[12] H. Baeumler, E. Donath, A. Krabi, W. Knippel, A. Budde, and H. Kiesewetter, Biorheology **33**, 333 (1996).
[13] J. Armstrong, H. Meiselman, and T. Fisher, Biorheology **36**, 433 (1999).
[14] S. Asakura and F. Oosawa, J. Polym. Sci. **33**, 183 (1958).
[15] K. Buxbaum, E. Evans, and D. Brooks, Biochemistry **21**, 3235 (1982).
[16] J. Friedrichs, J. Helenius, and D. J. Muller, Nat. Protocols **5**, 1353 (2010).
[17] S. Santos, D. Zanette, H. Fischer, and R. Itri, J. Colloid Int. Sci. **262**, 400 (2003).
[18] K. Khairy, J. Foo, and J. Howard, Cell. and Molec. Bioeng. **1**, 173 (2008).
[19] A. Jay, Biophys. J. **15**, 205 (1975).
[20] A. Williams, Bioch. Biophys. Acta. **307**, 58 (1973).
[21] P. H. Bronkhorst, J. Grimbergen, G. Brakenhoff, R. Heethaar, and J. Sixma, Br. J. Haematology **96**, 256 (1997).
[22] E. Canetta, A. Duperray, A. Leyrat, and C. Verdier, Biorheology **42**, 321 (2005).

Bioelectrochemistry xxx (2011) xxx–xxx

Contents lists available at SciVerse ScienceDirect

Bioelectrochemistry

journal homepage: www.elsevier.com/locate/bioelechem

Lysophosphatidic acid induced red blood cell aggregation in vitro

Lars Kaestner [a,b,*], Patrick Steffen [c], Duc Bach Nguyen [d], Jue Wang [a,b], Lisa Wagner-Britz [d], Achim Jung [c], Christian Wagner [c], Ingolf Bernhardt [d]

[a] Institute for Molecular Cell Biology, School of Medicine, Saarland University, Building 61, 66421 Homburg/Saar, Germany
[b] Research Center for Molecular Imaging and Screening, Saarland University, 66421 Homburg/Saar, Germany
[c] Experimental Physics Department, Building E2 6, Saarland University, 66123 Saarbrücken, Germany
[d] Biophysics Laboratory, Saarland University, Building A2 4, 66123 Saarbrücken, Germany

ARTICLE INFO

Article history:
Received 22 June 2011
Received in revised form 8 August 2011
Accepted 9 August 2011
Available online xxxx

Keywords:
Erythrocyte adhesion
Fluorescence imaging
Holographic optical tweezers
Calcium signaling
Phosphatydylserine exposure

ABSTRACT

Under physiological conditions healthy RBCs do not adhere to each other. There are indications that RBCs display an intercellular adhesion under certain (pathophysiological) conditions. Therefore we investigated signaling steps starting with transmembrane calcium transport by means of calcium imaging. We found a lysophosphatidic acid (LPA) concentration dependent calcium influx with an EC^{50} of 5 μM LPA. Downstream signaling was investigated by flow cytometry as well as by video-imaging comparing LPA induced with "pure" calcium mediated phosphatidylserine exposure and concluded the coexistence of two branches of the signaling pathway. Finally we performed force measurements with holographic optical tweezers (HOT): The intercellular adhesion of RBCs (aggregation) exceeds a force of 25 pN. These results support (i) earlier data of a RBC associated component in thrombotic events under certain pathophysiological conditions and (ii) the concept to use RBCs in studies of cellular adhesion behavior, especially in combination with HOT. The latter paves the way to use RBCs as model cells to investigate molecular regulation of cellular adhesion processes.

1. Introduction

Adhesion between cells is a vital property that is essential for multicell organism. This holds true all the way from primitive cell clusters to mammals that can be regarded as the most complex organisms known. Most organs of the human body form tissues that rely on cell to cell adhesion. The adhesion processes are complex and versatile ranging from direct cell–cell contacts, like occluding junctions, desmosomes or gap junctions, to processes involving extracellular matrix proteins. One of the few organs, where the constitutive cells instead of adhering to each other form a complex liquid, is the blood. The predominant cell type in the blood is the red blood cell (RBC). Although the normal physiological function of RBCs is devoid of intercellular adhesion, there are conceptual reviews proposing the active involvement of RBCs in aggregation processes [1,2].

Already more than 30 years ago, Evan Evans studied intercellular adhesion of RBC on the level of individual cell using micropipettes [3]. Such early studies were based either on hydrodynamic interaction forces or interaction mediated by macromolecules [4] — both of them being reversible. The nature of these effects is based on "physical adhesion" and is therefore different from cross bridging or binding associated "biological adhesion", although the borderline in-between is blurred.

However, experimental evidence for an involvement of RBC aggregation in vivo was published recently [5]. Our own previous work connected intercellular RBC adhesion to an increase in intracellular Ca^{2+} [6]. Therefore RBC adhesion is both a relevant (patho) physiological process and a model system to study particular aspects of the adhesion process.

Here we investigate several aspects of the RBC aggregation in greater detail ranging from the stimulation of the calcium increase to the cellular signaling cascade.

2. Material and methods

2.1. RBC preparation and fluorescence microscopy

For experiments fresh blood from healthy donors was obtained by a fingertip needle prick or human venous blood was drawn from healthy donors. Heparin or EDTA was used as an anticoagulant. The obtained blood was used within one day. The cells were washed three times by centrifugation (2000 *g*, 3–5 min) in a HEPES buffered solution of physiological ionic strength containing the following (in mM): 145 NaCl, 7.5 KCl, 10 glucose and 10 HEPES, pH 7.4, at room temperature. The buffy coat and plasma were removed by aspiration. For Ca^{2+} imaging, RBCs were loaded with 4–5 μM Fluo-4 AM (Molecular Probes, Eugene, USA) from a 1 mM stock solution in

* Corresponding author at: Institute for Molecular Cell Biology, Building 61, 66421 Homburg/Saar, Germany. Tel.: +49 68411626103; fax: +49 68411626104.
E-mail address: lars_kaestner@me.com (L. Kaestner).

1567-5394/$ – see front matter © 2011 Elsevier B.V. All rights reserved.
doi:10.1016/j.bioelechem.2011.08.004

dimethyl sulfoxide with 20% Pluronic (F-127, Molecular Probes). Loading was performed in 1 mL of solution of physiological ionic strength at an RBC hematocrit of approximately 1% for 45 min at 37 °C. The cells were washed by centrifugation once more and equilibrated for de-esterification for 15 min. LPA, prepared from a stock solution of 1 mM in distilled water, and the Ca^{2+} ionophore 4-bromo-A23187, prepared from a stock solution of 1 mM in ethanol, were obtained from Sigma-Aldrich (St. Louis, USA). To investigate phosphatidylserine (PS) exposure, cells were stained with annexin V-FITC (Molecular Probes). Annexin V-FITC was delivered in a unit size of 500 μL containing 25 mM HEPES, 140 mM NaCl, 1 mM EDTA, pH 7.4, and 0.1% bovine serum albumin. Five hundred microliters of annexin binding buffer (10 mM HEPES, 140 mM NaCl, 2.5 mM $CaCl_2$, pH 7.4) was added to 1 μL of washed, packed RBCs previously treated with LPA or A23187. Afterwards, 5 μL annexin V-FITC was added, and the cells were mixed gently. The probes were incubated at room temperature in the dark. Finally, the cells were placed on coverslips to perform the microscopy recordings. The measurements were obtained from images taken with CCD cameras, Imago (TILL, Photonics, Gräfelfing, Germany) and CCD97 (Photometrics, Tucson, USA) for Ca^{2+} imaging and annexin V imaging, respectively.

2.2. Flow cytometry

Washed RBCs were suspended in a physiological solution containing (mM): NaCl 145, KCl 7.5, glucose 10, HEPES 10, $CaCl_2$ 2 (pH 7.4) at an haematocrit of 0.1%. The Ca^{2+} ionophore 4-bromo-A23187, from a stock solution of 1 mM in absolute ethanol, was added to give a final concentration of 2 μM. The cell suspensions were incubated at 37 °C for different time intervals. The RBCs were washed by quick centrifugation (20 s, 12 000 *g*) in cold PBS buffer (mM): NaCl 140, KCl 3, Na_2HPO_4 7.5, and KH_2PO_4 1.5 (pH 7.4).

To investigate PS exposure, cells were stained with annexin V-FITC (Molecular Probes). A volume of 500 μL of annexin binding buffer (10 mM HEPES, 140 mM NaCl, 2.5 mM $CaCl_2$, pH 7.4) was added to 1 μL of washed, packed RBCs previously treated with 4-bromo-A23187. 5 μL of annexin V-FITC was then added, and the cells were mixed gently. The probes were incubated at room temperature in the dark for 15 min. Subsequently, the samples were washed once in annexin binding buffer by quick centrifugation (20 s, 12 000 *g*) to remove unbound annexin V-FITC and resuspended in 500 μL of the same buffer and placed on ice. RBCs showing PS exposed on their outer membrane leaflet were measured in the FL-1 channel using an argon laser at 488 nm of a fluorescence-activated flow cytometer (FACSCalibur, BD Biosciences, Franklin Lakes, New Jersey). The setting of the negative fluorescent gate was obtained in the absence of the Ca^{2+} ionophore 4-bromo-A23187 (negative control). The annexin V-FITC positive RBCs can be calculated in percentage by comparing the number of positive and negative signal events with the control. CellQuest Pro (BD Biosciences) software was used for data acquisition and analysis. The experiment was repeated three times on blood from different donors. For each experiment, 30 000 events were counted. The data are presented as mean values ± SD. For statistical comparison unpaired, two tailed *t*-test was performed (Prism5, GraphPad Software, La Jolla, USA).

2.3. Holographic optical tweezers (HOT)

The set-up of the holographic optical tweezers (HOT) was previously described [6]. In short: A Nd:YAG infrared laser (Ventus, Laser Quantum, Stockport, UK) with a beam width of 2.5 mm was coupled for coarse alignment with a visible He–Ne laser via a dichroic mirror. Both beams were expanded five-fold (BM.X, Linos Photonics, Göttingen, Germany) to overfill the 8 mm back aperture of the microscope objective (CFI Plan Fluor 60× oil immersion, Nikon Corp., Tokyo, Japan). The optics were integrated into an inverted fluorescence microscope (TE-2000, Nikon Corp.). This allowed for combined trapping and fluorescence or differential interference contrast measurements. Images were taken with an electron multiplication CCD camera (Cascade 512F, Roper Scientific, Trenton, USA) with a typical frame rate of 100 Hz. The optical setup was placed on active vibration isolation elements (Vario Series, Halcyonics, Göttingen, Germany). The phase of the laser's electric field was modified using a spatial light modulator (PPM X8267-15, Hamamatsu Photonics, Hamamatsu City, Japan) to create the desired trap pattern in the focal plane of the microscope objective. In order to test for RBC adhesion after stimulation, a suitable configuration of independently movable optical traps was created (cp. Fig. 3A). The laser power in each trap was approximately 5 mW. Cells could be moved against one another by replaying a series of kinoforms on the computer-controlled spatial light modulator.

3. Results and discussion

3.1. Lysophosphatidic acid (LPA) induced Ca^{2+} entry

Although it is known for more than 10 years that LPA opens a calcium permeable channel in RBCs [7,8], the molecular identity of the channel is still not resolved [9]. From other cell types it is known that there are in principle five different isoforms of LPA receptors [10]. If the LPA induced Ca^{2+} entry in RBCs is receptor mediated one would expect a clear dose response relationship. The results of concentration dependent experiments are depicted in Fig. 1. The EC_{50} of LPA towards the amplitude of the Ca^{2+} entry is 5 μM, which is compatible with previous studies on cloned LPA receptors [11]. This clear concentration dependent behavior speaks for a receptor mediated signaling and against detergent like effects that should anyway occur only at concentrations above 70 μM [12]. Concerning the present knowledge of LPA receptors, it is fair to assume that their activation translates into the activation of G-proteins [10]. However, the mechanism from G-protein activation to Ca^{2+} entry remains to be elucidated in RBCs.

At a LPA concentration of 10 μM we observe a shape transformation to spherocytes that does not occur at lower LPA concentrations, although there was no difference in the adhesion behavior between 2.5 and 10 μM LPA stimulation [6]. The spherical shape of RBC makes them an ideal object for laser tweezer calibration (see below).

3.2. Exposure of phosphatidylserine (PS) to the outer membrane leaflet

Although it is known, that LPA induces PS exposure in RBC, there are conflicting reports about the mechanism. While Chung et al. [13] claim it is a totally Ca^{2+}-independent process, we could show that Ca^{2+} alone is sufficient to get a PS exposure in RBCs [6]. Therefore we aimed for a comparison of the temporal course of pure Ca^{2+}-induced and LPA induced PS exposure. The results of this investigation are displayed in Fig. 2. The first difference is that A23187 treated cells could be reliably investigated over a time period of 24 h, while cells treated with LPA beyond 2 h showed such a significant hemolysis that further investigations were impossible. Based on the results presented in Fig. 1 we can assume that the average Ca^{2+} concentration in A23187 treated RBCs is higher compared to LPA-treated cells. Opposite to that, the image series propose that LPA stimulated cells depict a faster and more intense PS exposure than a "pure" Ca^{2+} increase (compare Fig. 2A and C). This notion is supported by the flow cytometry measurements. Thirty min after stimulation 17.29 ± 1.38% of A23187 treated cells exposed PS in the outer membrane leaflet (Fig. 2B), while for 30 min LPA stimulation the responding cells were determined to show a percentage of 35.05 ± 6.66. This is a significant difference ($p = 0.01$).

These observations suggest the coexistence of two pathways leading to LPA induced PS exposure. One of the pathways is well known involving Ca^{2+}-induced flippase inhibition [14] and scramblase activation [15]. The other one was suggested to involve Ca^{2+}-

Please cite this article as: L. Kaestner, et al., Lysophosphatidic acid induced red blood cell aggregation in vitro, Bioelectrochemistry (2011), doi:10.1016/j.bioelechem.2011.08.004

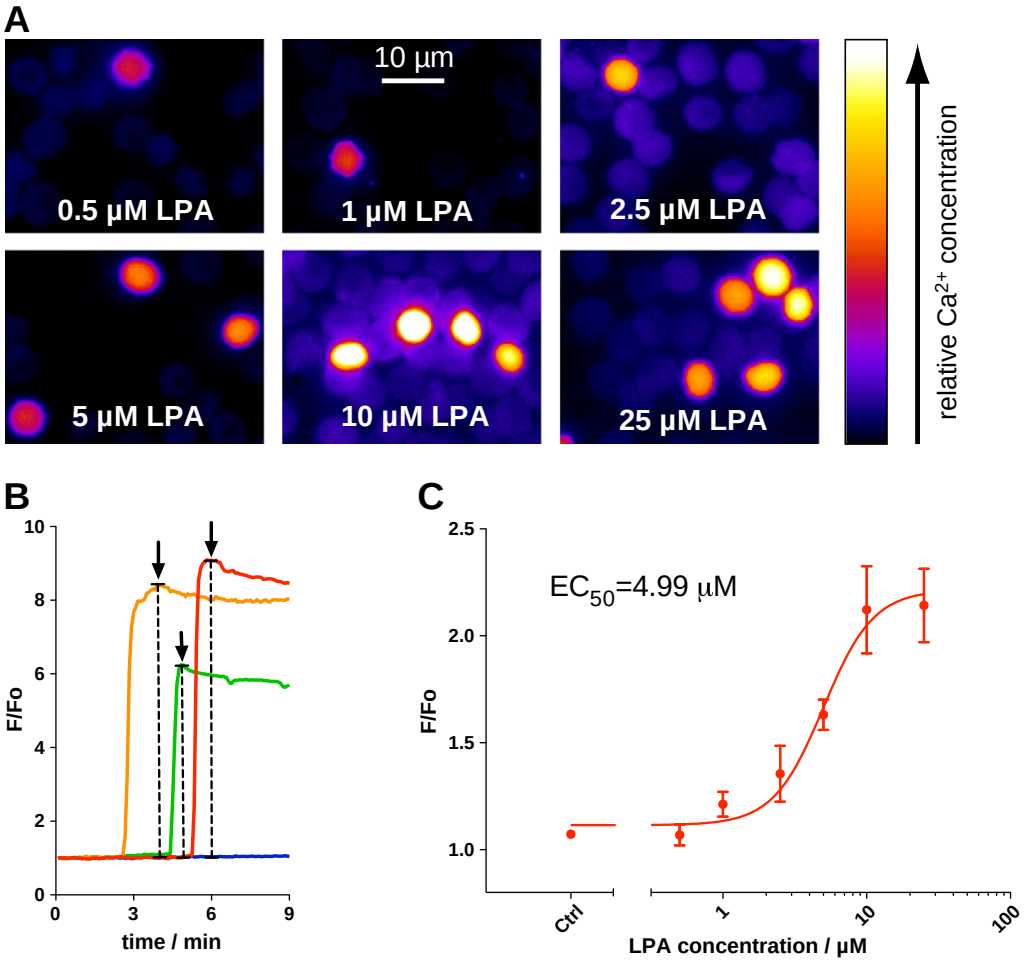

Fig. 1. Dose response relationship between lysophosphatidic acid (LPA) concentration and Ca^{2+} influx in RBCs. Panel A shows intensity images of Fluo-4 loaded cells 14 min after stimulation with the given LPA concentration. The time course of LPA stimulation was followed for 15 min. Panel B depicts intensity traces for 3 example RBCs. The amplitude of the Ca^{2+} signal for each cell is highlighted by the arrows and was taken for analysis. To determine the dose–response relationship as illustrated in panel C, the maximum amplitude from at least 158 cells per condition out of three independent experiments were analyzed. The self-ratio of the fluorescence F/F_o was plotted against the LPA concentration and the Hill slope of the non-linear fit revealed a mean effective concentration (EC_{50}) of 5 µM.

independent protein kinase C (PKC) isoforms [13]. Since RBCs also contain the Ca^{2+} dependent PKC_α [16], a cross-linking of both signaling pathways seems reasonable. However, further studies need to be performed to refine the signaling pathways and to elucidate their interconnection.

3.3. RBC adhesion forces

In a previous study atomic force microscopy (AFM) was used to determine the adhesion force between RBCs after LPA stimulation and was found to be in the range of $F_{AFM} = 100 \pm 84$ pN [6]. However control experiments in the same study gave an average separation force of 29 ± 9 pN. This high value is supposed to be an artifact caused by the inherent operation mode of the AFM, which requires an initial pressure to push the cells together. To overcome this potential artifact we aimed on using holographic optical tweezers (HOT) to estimate the adhesion power. Therefore two cells were captured with two independent traps of the HOT and they were brought into contact in an oscillatory manner. Cells that were not treated with LPA did not show any adhesive properties within our experimental force resolution, while LPA treated cells did adhere so strongly to each other that they could not be separated with the HOT. In order to quantify the adhesion forces occurring between adhering RBCs, the HOT needs to be force calibrated. The force F acting on the RBC in the optical trap is defined by the gradient intensity. Using a Gaussian shaped laser intensity profile, the force obeys a Hookian spring law:

$$F \propto \kappa x \tag{1}$$

where x is the displacement of the particle from the center of the trap. There are many calibration methods commonly used to determine the trap stiffness κ of optical tweezers [17]. Using identical experimental conditions the probe chamber as a whole is brought under oscillatory displacement with amplitude A_0. In that way a hydrodynamic force acts on the blood cells that can be approximated using the Stokes force relation [18]:

$$x(t) = \Re\left(\frac{A_0 \nu}{\sqrt{\nu^2 + \nu_0^2}} e^{-(i2\pi\nu t + \varphi)}\right) \tag{2}$$

with $\Re()$ denominating the real part and

$$\varphi = -tan^{\frac{\nu_0}{\nu}}, \tag{3}$$

where

$$\nu = \frac{\kappa}{2\pi\beta} \tag{4}$$

Please cite this article as: L. Kaestner, et al., Lysophosphatidic acid induced red blood cell aggregation in vitro, Bioelectrochemistry (2011), doi:10.1016/j.bioelechem.2011.08.004

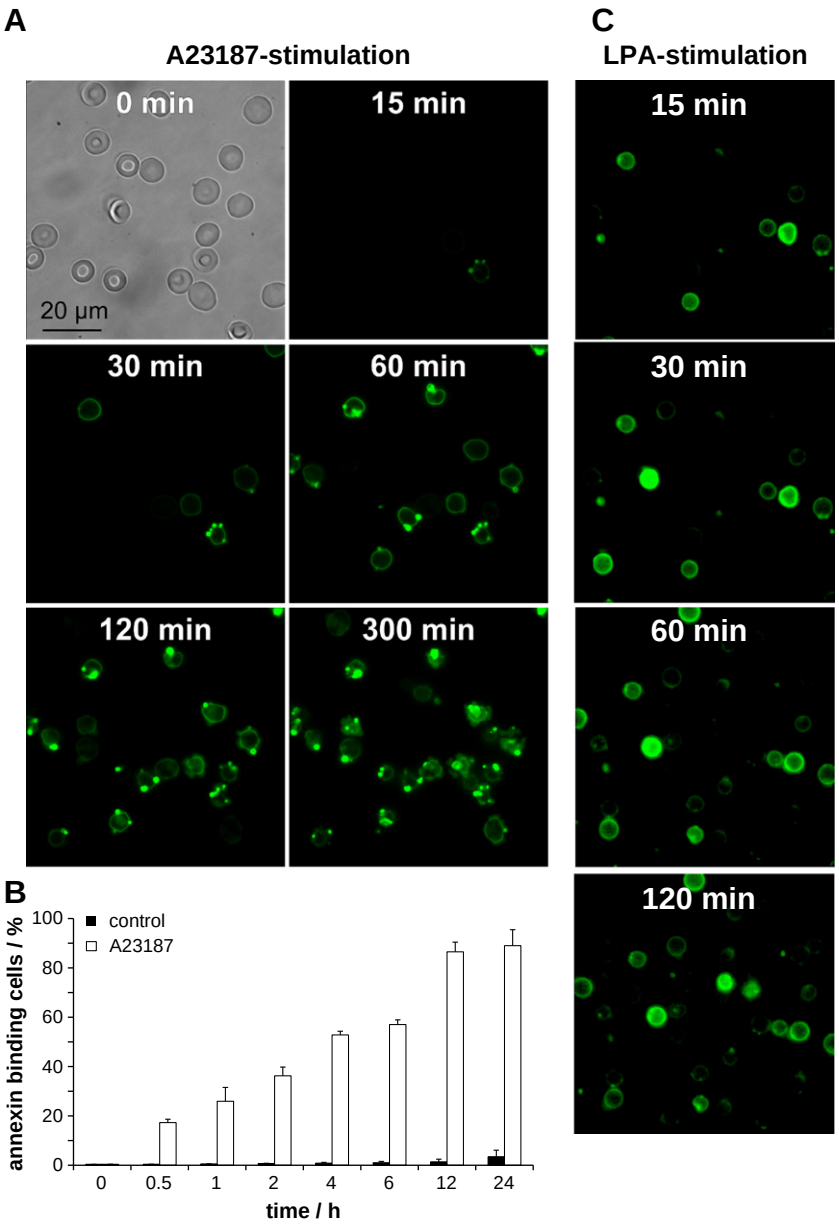

Fig. 2. Investigation of phosphatydylserine (PS) exposure to the outer membrane leaflet of RBCs. Panel A depicts an image series of RBCs that ware stimulated with the Ca^{2+}-ionophore bromo-A23187 (2 µM) and simultaneously incubated with FITC labeled annexin V. The first image is a white light image to show the integrity of the cells, while all other images are fluorescence based. The procedure of the PS exposure was followed over 5 h and accompanied with a strong vesicle constriction. Additionally the long term rate (up to 24 h) of PS exposing cells was followed by flow cytometry and is given in panel B. Images of the PS exposure of RBCs stimulated with 2.5 µM LPA are given in panel C. LPA stimulation was restricted to 2 h, since longer stimulations led to significant haemolysis.

the characteristic frequency of the trap. The latter is generally much higher than the driving frequency, i.e. the system is over-damped with damping coefficient β leaving Eq. (2) to be

$$x(t) \approx \frac{A_0 \nu}{\nu_0} \sin 2\pi \nu t. \tag{5}$$

Fig. 3C shows a plot of the mean displacement of 12 RBCs. Peak hydrodynamic forces have been calculated from the Stokes relation assuming spherical RBCs (see above) with a diameter of 5.6 µm. This corresponds to a sphere with a total volume comparable to that of the native cells (90 μm^3). The resulting cell displacements are determined from the center of mass in video microscopy. However, small force displacements are more likely due to membrane deformations and not simple displacements as for the case of rigid beads. This is substantiated by comparing the trap strength $\kappa = 5.85 \pm 0.01$ pN/µm calculated from the initial slope to typical values for RBC elastic moduli [19]. In any case, from these measurements a mean escape force $F_{HOT} = 14 \pm 3$ pN required for cells to leave the trap can be determined. The strength of the observed adhesion of LPA treated cells turned out to be larger than the maximum force applicable using the optical traps. However, we can also conclude that the untreated cells did not show any adhesive force within the measurement resolution of 3 pN. This confirms our original assumption that the adhesion forces for untreated cells, measured with the AFM, are due to instrumental artifacts or due to the strong contact pressure.

We also applied another method to quantify the adhesion forces that is (i) less invasive than the AFM and (ii) based on HOT, but a low trapping strength is sufficient. The method is based on the Young–Dupré relation [20] by taking into account the equilibrium adhesion

Please cite this article as: L. Kaestner, et al., Lysophosphatidic acid induced red blood cell aggregation in vitro, Bioelectrochemistry (2011), doi:10.1016/j.bioelechem.2011.08.004

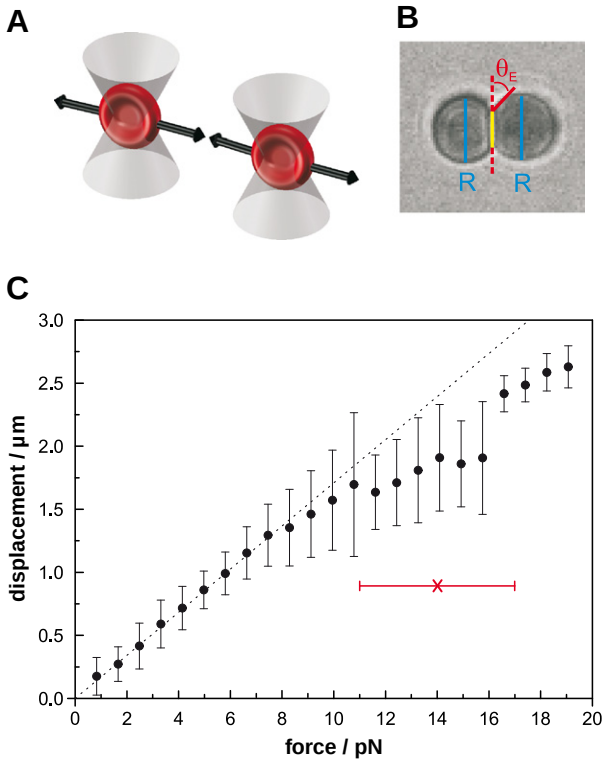

Fig. 3. The use of holographic optical tweezers (HOT) to determine the adhesion force. Panel A illustrates the how the holographic optical tweezers were used. The kinoforms on a spatial light modulator generated two foci, which could trap two RBCs. These cells could be independently moved and such brought in contact with each other in an oscillating manner. Panel B shows a picture of two adhering cells (spherocytes), held with two traps. The strength of the traps was weakened so that their influence on the contact angle μ establishment can be neglected. R is given by the diameter of the cell. Panel C depicts the resulting plot of the mean displacement of 12 RBCs. At small displacements the average of all cells is shown, at larger displacements more and more cells did escape from the trap and averaging was only done with the remaining cells. The red bar indicates the mean force and standard deviation at escape from the trap. The trap stiffness can be calculated from the initial slope, while in our measurements only the escape force was used. (For interpretation of the references to color in this figure legend, the reader is referred to the web version of this article.)

contact area geometry as shown in Fig. 3B [21–23]. In the absence of external forces cell–cell adhesion energies W_{adh} are given by the equilibrium angle of contact θ_e and the cell surface tension γ via Young–Dubré relation of capillary forces:

$$W_{adh} = \gamma(1 - \cos\theta_e) \quad (6)$$

in which both cells are considered to be identical in their physical properties [24]. In particular, the surface tension that is given by the shear modulus of the cell must be known *a priori*. Separation forces can be derived from the Derjaguin approximation [25]:

$$F_s = -2\pi W_{adh} R \quad (7)$$

where

$$R = \frac{R_1 R_2}{R_1 + R_2} \quad (8)$$

is the mean radius on the apex. In these measurements the strength of the traps has been weakened so that their influence on the membrane and contact angle establishment can be neglected, i.e. the zero external force condition is well approximated. The traps serve as weak pinpoints to hold the cells in the focal plane of observation. An equilibrium contact angle of $\theta \approx 45°$ was established where the diameter on apex is identically $D = 6.70 \pm 0.27$ µm for both cells. Values for surface tension may be obtained from Hilbert phase microscopy and are taken from the literature. There is a difference in the values obtained from discocytes compared to spherocytes due to morphological changes in the RBC cytoskeleton [26]. Spherocytes occur to some extend in samples from healthy donors, and for those a value $\gamma = 8.25 \pm 1.6 \times 10^{-6}$ N/m has been reported [27]. The resulting separation force in our study is then $F_{YD} = 25.0 \pm 6.0$ pN. For now, we cannot tell if the literature value for the surface tension holds for the LPA treated spherocytes, but our impression is that they are significantly stiffer than the discocytes and their surface tension and thus the adhesion forces might be even larger. Indeed, an independent measurement of the surface tension would allow for a more accurate determination of the adhesion energy. However, already with a reasonable factor of four for the surface tension one would get adhesion forces with this method in the order of 100 pN which is similar to what we get from the AFM measurements [6].

We can now compare the measured adhesion forces to typical shear stresses in the blood flow. Supposing a RBCs cross section surface of 50 µm^2 of discocytes of 8 µm we find a maximum sustainable shear strain of $\tau = F_{HOT}/c \approx 2.8 \pm 0.6$ N/m^2 from the Stokes force calibration and $\tau \approx 5.0 \pm 1.2$ N/m^2 from the contact angle, respectively. c is a characteristic constant taking into account the random orientation of cell doublets when tumbling in the vascular flow [28]. The values mentioned are above those from measurements on depletion mediated rouleaux formation and mostly above shear strain typically found in veins ($\tau = 1$–6 N/m^2) or aortas ($\tau = 0.5$–2 N/m^2). Thus the RBC adhesion should resist most shear forces in the vascular system.

4. Conclusion

The present study allowed us to refine and extend previous studies about the action of LPA on RBCs [6–8,13], although the molecular mechanism from LPA-receptor activation in RBC to Ca^{2+} entry (most probably by a non-selective ion channel) still needs to be elucidated. Here we are now presenting a hypothesis of a cellular signaling scheme reaching from LPA stimulation to RBC aggregation as depicted in Fig. 4. Although not all steps are completely resolved, we believe this is a general scheme, where the LPA receptor mediated Ca^{2+} entry can be substituted by other Ca^{2+} permeable channels, such as NMDA receptors [29] or prostaglandin E_2 activated pathways [30,31]. This points to a relevance of this pathway in pathophysiological situations like sickle cell anemia, thalassemia or complications after blood transfusion.

Furthermore we show that the RBCs and holographic optical tweezers are complementary to investigate intercellular adhesion. This system can be utilized to explore the molecular mechanism of adhesion processes. Such investigations are very promising, especially for the low force range since HOT is a very sensitive tool — providing a force resolution of approximately 3 pN in the range up to 25 pN. Estimates on the adhesion forces based on a Young Dupré approach were within in the range of the results of the HOT and AFM measurements. HOT in combination with microfluidics [6] even allows probing two different cell populations, e.g. differently treated RBCs. Additionally, HOT can be combined with fluorescence microscopy and such a multi parameter read-out can be performed to refine results.

Acknowledgments

The research leading to these results has received funding from the DFG Graduate School (GRK 1276), the European Community's Seventh Framework Program (FP7 2007–2013) under grant agreement nr. NMP3-SL-2008-214032 and the Ministry of Economy and Sciences of the Saarland. The study was approved by the ethics committee of the Medical Association of the Saarland (reference number 132/08).

Please cite this article as: L. Kaestner, et al., Lysophosphatidic acid induced red blood cell aggregation in vitro, Bioelectrochemistry (2011), doi:10.1016/j.bioelechem.2011.08.004

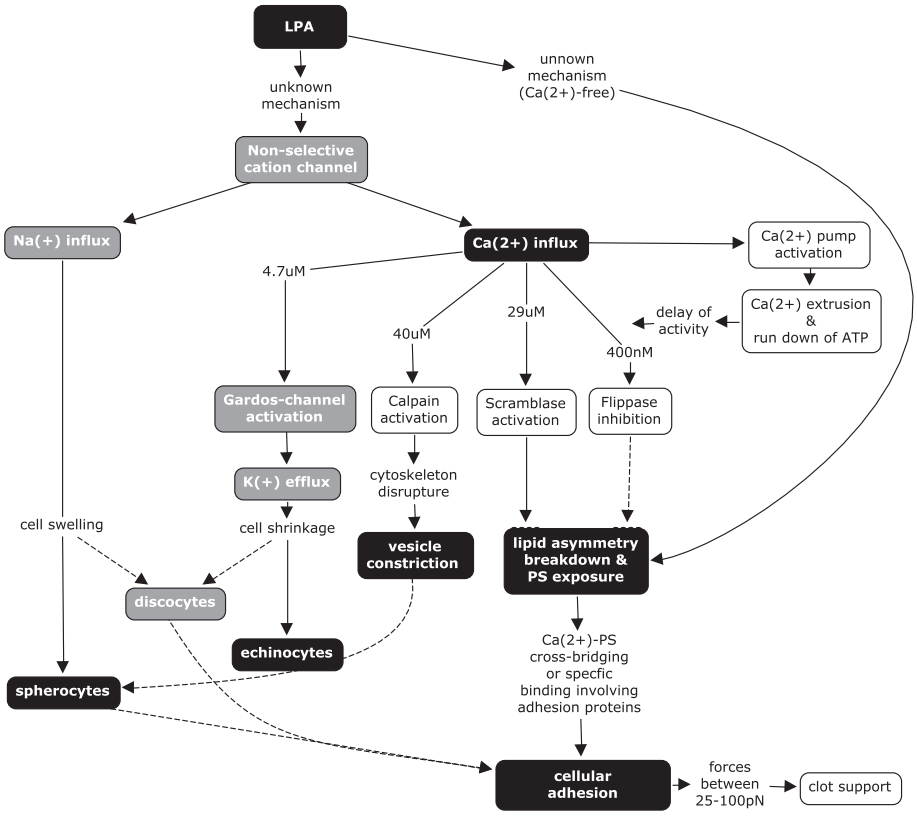

Fig. 4. Hypothesis of the signaling cascade in human red blood cells upon LPA stimulation. The black boxes depict observations and results from the current paper. The gray boxes represent previously published results by the authors, whereas the information in the white boxes is retrieved from scientific literature. LPA activates a non-selective cation channel [7,8]. This channel is permeable to Na^+ as well as to Ca^{2+} [32,33]. The Ca^{2+} influx is presented in Fig. 1. This influx leads to a concentration dependent switching process of the Ca^{2+} pump [34], the flippase inhibition [14], the scramblase activation [15], the calpain activation [35] and the Gardos channel activation [36]. The shape changes RBCs undergo after stimulation with LPA and the consecutive Ca^{2+} influx are well described [2,13,29]. The cell changes are accompanied by the encapsulation of microvesicles, which can be seen in Fig. 2. The mechanism behind the shape transformation is a Ca^{2+} influx upon the activation of the non-selective cation channel, what activates the Gardos channel. A K^+ loss-induced shrinkage of the cells leads to the formation of echinocytes. Caused by the Ca^{2+}-activated calpain the RBC cytoskeleton is breaking down. This triggers the microvesicle constriction and the consecutive formation of spherocytes. The lipid asymmetry breakdown and phosphatidylserine exposure is mediated by the inhibition of the flippase and the activation of the scramblase. There is a second Ca^{2+}-independent pathway involved, which is LPA mediated and leads to PS exposure. For a discussion about the relation of these two pathways see main text. Finally the signaling results in adhesion properties occurring between RBCs that were determined to result in forces greater than 25 pN (Fig. 3) but can reach values around 100 pN [6].

References

[1] D.A. Andrews, P.S. Low, Role of red blood cells in thrombosis, Curr. Opin. Hematol. 6 (1999) 76–82.
[2] L. Kaestner, A. Juzeniene, J. Moan, Erythrocytes-the “house elves” of photodynamic therapy, Photochem. Photobiol. Sci. 3 (2004) 981–989.
[3] E.A. Evans, Minimum energy analysis of membrane deformation applied to pipet aspiration and surface adhesion of red blood cells, Biophys. J. 30 (1980) 265–284.
[4] P. Snabre, G. Grossmann, P. Mills, Effects of dextran polydispersity on red blood-cell aggregation, Colloid Polym. Sci. 263 (1985) 478–483.
[5] J. Noh, K. Lim, O. Bae, S. Chung, S. Lee, K. Joo, S. Lee, J. Chung, Procoagulant and prothrombotic activation of human erythrocytes by phosphatidic acid, Am. J. Physiol. Heart Circ. Physiol. 299 (2010) H347–H355.
[6] P. Steffen, A. Jung, D.B. Nguyen, T. Müller, I. Bernhardt, L. Kaestner, C. Wagner, Stimulation of human red blood cells leads to Ca^{2+}-mediated intercellular adhesion, Cell Calcium 50 (2011) 54–61.
[7] L. Yang, D.A. Andrews, P.S. Low, Lysophosphatidic acid opens a Ca(++) channel in human erythrocytes, Blood 95 (2000) 2420–2425.
[8] L. Kaestner, W. Tabellion, E. Weiss, I. Bernhardt, P. Lipp, Calcium imaging of individual erythrocytes: problems and approaches, Cell Calcium 39 (2006) 13–19.
[9] L. Kaestner, Cation channels in erythrocytes — historical and future perspective, Open Biol. J. 4 (2011) 27–34.
[10] J.W. Choi, D.R. Herr, K. Noguchi, Y.C. Yung, C. Lee, T. Mutoh, M. Lin, S.T. Teo, K.E. Park, A.N. Mosley, J. Chun, LPA receptors: subtypes and biological actions, Annu. Rev. Pharmacol. Toxicol. 50 (2010) 157–186.
[11] K. Bandoh, J. Aoki, A. Taira, M. Tsujimoto, H. Arai, Lysophosphatidic acid (LPA) receptors of the EDG family are differentially activated by LPA species: structure–activity relationship of cloned LPA receptors, FEBS Lett. 478 (2000) 159–165.
[12] T. Eichholtz, K. Jalink, I. Fahrenfort, The bioactive phospholipid lysophosphatidic acid is released from activated platelets, Biochem. J. 291 (1993) 677–680.
[13] S.M. Chung, O.N. Bae, K.M. Lim, J.Y. Noh, M.Y. Lee, Y.S. Jung, J.H. Chung, Lysophosphatidic acid induces thrombogenic activity through phosphatidylserine exposure and procoagulant microvesicle generation in human erythrocytes, Arterioscler. Thromb. Vasc. Biol. 27 (2007) 414–421.
[14] M. Bitbol, P. Fellmann, A. Zachowski, P.F. Devaux, Ion regulation of phosphatidylserine and phosphatidylethanolamine outside–inside translocation in human erythrocytes, Biochim. Biophys. Acta 904 (1987) 268–282.
[15] L.A. Woon, J.W. Holland, E.P. Kable, B.D. Roufogalis, Ca^{2+} sensitivity of phospholipid scrambling in human red cell ghosts, Cell Calcium 25 (1999) 313–320.
[16] R.B. Govekar, S.M. Zingde, Protein kinase C isoforms in human erythrocytes, Ann. Hematol. 80 (2001) 531–534.
[17] K.C. Neuman, S.M. Block, Optical trapping, Rev. Sci. Instrum. 75 (2004) 2787–2809.
[18] S. Grover, R. Gauthier, A. Skirtach, Analysis of the behaviour of erythrocytes in an optical trapping system, Opt. Express 7 (2000) 533–539.
[19] E.A. Evans, Structure and deformation properties of red blood cells: concepts and quantitative methods, Methods Enzymol. 173 (1989) 3–35.
[20] A. Pribush, D. Zilberman-Kravits, N. Meyerstein, The mechanism of the dextran-induced red blood cell aggregation, Eur. Biophys. J. 36 (2007) 85–94.
[21] Z.W. Zhang, B. Neu, Role of macromolecular depletion in red blood cell adhesion, Biophys. J. 97 (2009) 1031–1037.
[22] S. Pierrat, F. Brochard-Wyart, P. Nassoy, Enforced detachment of red blood cells adhering to surfaces: statics and dynamics, Biophys. J. 87 (2004) 2855–2869.
[23] Y. Chu, S. Dufour, J.P. Thiery, E. Perez, F. Pincet, Johnson–Kendall–Roberts theory applied to living cells, Phys. Rev. Lett. 94 (2005) 028102.
[24] S. Bailey, S. Chiruvolu, J. Israelachvili, Measurements of forces involved in vesicle adhesion using freeze-fracture electron microscopy, Langmuir 6 (1990) 1326–1329.
[25] B. Derjaguin, V. Muller, Effect of contact deformations on the adhesion of particles, J. Colloid Interface Sci. 53 (1975) 314–326.
[26] G. Lim H.W., M. Wortis, R. Mukhopadhyay, Stomatocyte–discocyte–echinocyte sequence of the human red blood cell: evidence for the bilayer — couple hypothesis from membrane mechanics, Proc. Nat. Acad. Sci. U.S.A. 99 (2002) 16766–16769.
[27] G. Popescu, T. Ikeda, K. Goda, C. Best-Popescu, Optical measurement of cell membrane tension, Phys. Rev. Lett. 97 (2006) 218101–218104.
[28] P. Snabre, M. Bitbol, P. Mills, Cell disaggregation behavior in shear flow, Biophys. J. 51 (1987) 795–807.

Please cite this article as: L. Kaestner, et al., Lysophosphatidic acid induced red blood cell aggregation in vitro, Bioelectrochemistry (2011), doi:10.1016/j.bioelechem.2011.08.004

[29] A. Makhro, J. Wang, J. Vogel, A.A. Boldyrev, M. Gassmann, L. Kaestner, A. Bogdanova, Functional NMDA receptors in rat erythrocytes, Am. J. Physiol. Cell Physiol. 298 (2010) C1315–C1325.
[30] L. Kaestner, I. Bernhardt, Ion channels in the human red blood cell membrane: their further investigation and physiological relevance, Bioelectrochemistry 55 (2002) 71–74.
[31] L. Kaestner, W. Tabellion, P. Lipp, I. Bernhardt, Prostaglandin E_2 activates channel-mediated calcium entry in human erythrocytes: an indication for a blood clot formation supporting process, Thromb. Haemost. 92 (2004) 1269–1272.
[32] L. Kaestner, C. Bollensdorff, I. Bernhardt, Non-selective voltage-activated cation channel in the human red blood cell membrane, Biochim. Biophys. Acta 1417 (1999) 9–15.
[33] L. Kaestner, P. Christophersen, I. Bernhardt, P. Bennekou, The non-selective voltage-activated cation channel in the human red blood cell membrane: reconciliation between two conflicting reports and further characterisation, Bioelectrochemistry 52 (2000) 117–125.
[34] H. Schatzmann, Calcium movements across the membrane of human red cells, J. Physiol. 201 (1969) 369–395.
[35] C.P. Berg, I.H. Engels, A. Rothbart, K. Lauber, A. Renz, S.F. Schlosser, K. Schulze-Osthoff, S. Wesselborg, Human mature red blood cells express caspase-3 and caspase-8, but are devoid of mitochondrial regulators of apoptosis, Cell Death Differ. 8 (2001) 1197–1206.
[36] G. Gardos, The permeability of human erythrocytes to potassium, Acta Physiol. Hung. 10 (1956) 185–189.

Please cite this article as: L. Kaestner, et al., Lysophosphatidic acid induced red blood cell aggregation in vitro, Bioelectrochemistry (2011), doi:10.1016/j.bioelechem.2011.08.004

Original Paper

Cellular Physiology and Biochemistry

Cell Physiol Biochem 2011;28:847-856

Accepted: October 28, 2011

Regulation of Phosphatidylserine Exposure in Red Blood Cells

Duc Bach Nguyen[1,2], Lisa Wagner-Britz[1], Sara Maia[1], Patrick Steffen[3], Christian Wagner[3], Lars Kaestner[4] and Ingolf Bernhardt[1]

[1]Laboratory of Biophysics, Faculty of Natural and Technical Sciences III, Saarland University, Building A2 4, Saarbruecken, [2]Department of Molecular Biology, Faculty of Biotechnology, Hanoi University of Agriculture, Ngo Xuan Quang, Gia Lam, Hanoi, [3]Department of Experimental Physics, Saarland University, Building E2 6, Saarbruecken, [4]Institute for Molecular Cell Biology, School of Medicine, Saarland University, Building 61, Homburg

Key Words

Red blood cells • Lysophosphatidic acid • Scramblase • Flippase • Calcium concentration • Phosphatidylserine • Fluorescence imaging

Abstract

The exposure of phosphatidylserine (PS) on the outer membrane leaflet of red blood cells (RBCs) serves as a signal for eryptosis, a mechanism for the RBC clearance from blood circulation. The process of PS exposure was investigated as function of the intracellular Ca^{2+} content and the activation of PKCα in human and sheep RBCs. Cells were treated with lysophosphatidic acid (LPA), 4-bromo-A23187, or phorbol-12 myristate-13 acetate (PMA) and analysed by flow cytometry, single cell fluorescence video imaging, or confocal microscopy. For human RBCs, no clear correlation existed between the number of cells with an elevated Ca^{2+} content and PS exposure. Results are explained by three different mechanisms responsible for the PS exposure in human RBCs: (i) Ca^{2+}-stimulated scramblase activation (and flippase inhibition) by LPA, 4-bromo-A23187, and PMA; (ii) PKC activation by LPA and PMA; and (iii) enhanced lipid flop caused by LPA. In sheep RBCs, only the latter mechanism occurs suggesting absence of scramblase activity.

Introduction

Phospholipids are asymmetrically distributed in the plasma membrane of most, if not all, biological cells. Sphingomyelin (SM) and phosphatidylcholine (PC) are found predominantly in the outer leaflet of the membrane bilayer, while phosphatidylserine (PS) and phosphatidylethanolamine (PE) are located mostly in the inner leaflet [1]. The distribution of the membrane phospholipids is regulated by three proteins: flippase [2], floppase, and scramblase [3-5]. PS exposure on the outer leaflet of the membrane has been described as a marker for apoptosis in nucleated cells [5]. Although the apoptosis of RBCs is still under discussion, they undergo suicidal death with signs of apoptosis such as PS exposure, membrane blebbing and vesicle formation [6]. This process was termed eryptosis by Lang et al. [7].

KARGER

Fax +41 61 306 12 34
E-Mail karger@karger.ch
www.karger.com

1015-8987/11/0285-0847$38.00/0

Accessible online at:
www.karger.com/cpb

Ingolf Bernhardt
Universität des Saarlandes, Naturwiss.-Techn. Fakultät III
Zentrales Isotopenlabor / AG Biophysik, Gebäude A2.4
P.O.Box 151150, 66041 Saarbrücken (Germany)
Tel. +49 681 3026689, E-Mail i.bernhardt@mx.uni-saarland.de

Based on a correlation between decreased haematocrit and longer bleeding times [8] and experiments of Andrews and Low [9], an active role of RBCs in thrombus formation has been proposed [9]. Kaestner et al. published a more detailed signalling cascade based on Ca^{2+} uptake via a non-selective cation channel that could be activated by prostaglandin E_2 (PGE_2) [10, 11]. This channel was believed to be a voltage-activated non-selective cation channel [12, 13]. Recent considerations [14] propose the PGE_2 receptor-activated non-selective cation channel [10, 11] and the voltage activated cation channel [12, 13] are of different identity. Ca^{2+} entry can also be caused by a mechanical deformation of RBCs as described by Dyrda et al. [15].

PGE_2 and LPA are local mediators released by platelets after their activation within the coagulation cascade and, in case of PGE_2, are released by RBCs under mechanical stress [16]. Moreover, in recent reports, we showed that PS exposure induced by LPA was associated with cell-cell adhesion of human RBCs [17, 18]. PS exposure at the outer leaflet of the RBC membrane is of importance for the adhesion of RBCs to endothelium in some diseases such as sickle cell anaemia, malaria, and diabetes [19].

Although it is known that in RBCs LPA induces PS exposure at the outer membrane leaflet, there are conflicting reports about its mechanism. While Chung et al. [20] claim that it is a totally Ca^{2+}-independent process, we showed that Ca^{2+} alone is sufficient to induce PS exposure in human RBCs [17]. Woon et al. found that an increase of the intracellular Ca^{2+} level in RBCs results in the exposure of PS to the outer membrane leaflet due to activation of the scramblase and inhibition of the flippase [21]. Protein kinase Cα (PKCα) has been also described to be involved in the PS exposure on RBCs [20, 22, 23]. In human RBCs, in addition to PKCα, only a limited number of PKC isoforms (ζ, λ/ι, and μ) have been detected [24]. The molecular mechanisms for the participation of these proteins in the Ca^{2+} uptake and/or in the PS exposure remain to be elucidated.

Here, we investigated the parameters regulating PS exposure at the outer membrane leaflet of human RBCs by addressing Ca^{2+} content manipulated by an ionophore and PKC activation by phorbol-12 myristate-13 acetate (PMA). For comparison, sheep RBCs were studied because these cells have a completely different membrane phospholipid distribution. Like in human RBCs, PS and PE are present at the inner membrane leaflet, however, sheep RBC membranes lack PC and the outer layer consists exclusively of SM [25, 26].

Materials and Methods

Blood and solutions

Human venous blood from healthy donors was obtained from the Institute of Clinical Haematology and Transfusion Medicine of Saarland University Hospital. Sheep blood samples were obtained from the sheep farm Ernst in Blieskastel, Germany. Citrate or EDTA (for human blood) or heparin (for sheep blood) were used as anticoagulants. Freshly drawn blood samples were stored at 4 °C and used within one day.

Blood was centrifuged at 2,000 g for 5 min at room temperature (RT) and the plasma and buffy coat was removed by aspiration. Subsequently, RBCs were washed 3 times in HEPES-buffered physiological solution (HPS) containing (mM): NaCl 145, KCl 7.5, glucose 10, HEPES 10, pH 7.4, under the same conditions. Finally, RBCs were re-suspended in HPS and kept at 4 °C. To assess the effect of cell volume, the last wash was done in a high-K^+ solution (mM): NaCl 2.5, KCl 150, glucose 10, HEPES 10, pH 7.4.

Intracellular Ca^{2+} content

The application of fluo-4 for Ca^{2+} measurements in intact RBCs has been reported elsewhere [27]. It has been also shown that fura-2 or indo-1 cannot be applied for those measurements due to quenching by haemoglobin [27].

RBCs were loaded with 5 μM fluo-4 AM from a 1 mM stock solution in dimethyl sulfoxide (DMSO) with 20% Pluronic F-127 in 1 ml HPS at a haematocrit of 1% for 45 min at 37 °C in the dark. Cells were washed 3 times by centrifugation (20 s, 12,000 g) in HPS and finally equilibrated for de-esterification for 15 min at a haematocrit of 0.5% at RT.

Intracellular free Ca^{2+} levels of single RBCs were monitored using an inverted fluorescence microscope (Eclipse TE2000-E, Nikon, Tokyo, Japan). A diluted RBC suspension (approximately 0.025% haematocrit), prepared in HPS with 2 mM $CaCl_2$, was placed on a cover slip coated with poly-L-lysine 5 min before the start of the imaging procedure. Ca^{2+} ionophore 4-bromo-A23187 (the non-fluorescent variant of A23187, thereafter named A23187), LPA, and PMA were added immediately before the start of the imaging procedure. The experiments were performed at RT in a dark room. Control conditions consisted of the same procedure but cells were re-suspended in the presence of respective amounts of reagent solvents (ethanol, water, or DMSO).

Our experimental approach was designed to provide a quantitative assessment of fluorescence intensity while maintaining identical imaging parameters under all conditions. This was accomplished by taking images with an electron multiplication CCD camera (CCD97, Photometrics, Tucson, USA) using a 100×1.4 (NA) oil immersion lens with infinity corrected optics. An image was taken every 20 s (exposure time 500 ms) for a 30 min experiment using the imaging software Metavue (Universal Imaging Corp., Marlow, UK).

Fluo-4 was excited with a xenon lamp-based monochromator (Visitron Systems, Puchheim, Germany) at a centre wavelength of 488 nm. Emission was recorded at 520/15 nm. The background corrected fluorescence signals were normalized to the initial fluorescence (F_o). For each experiment 20 - 30 cells

were analysed from each sample and at least three different blood samples were used.

Additionally, the intracellular free Ca^{2+} content of RBCs was measured by flow cytometry (FACS Calibur and Cell Quest Pro software, Becton Dickinson Biosciences, Franklin Lakes, USA). Preparation of cells, solutions and experimental conditions were the same as described above (except that samples were analysed after 12 min). Ca^{2+} content was measured in the FL-1 channel and analysed using the mean value of the relative fluorescence of 30,000 cells from each blood sample. For each experiment at least three different blood samples were used.

PS exposure

PS exposure on the outer membrane leaflet of RBCs was evaluated by annexinV-FITC binding to this phospholipid. RBCs prepared as described above were treated with A23187, LPA, or PMA or with ethanol, water, or DMSO (for controls) in HPS with 2 mM $CaCl_2$ at 37 °C for 30 min (0.1% haematocrit). Cells were washed in the ice-cold HPS with 2 mM $CaCl_2$ by centrifugation (20 s, 12,000 g). Approximately 10^6 cells were incubated with 5 µl of annexin V-FITC in 500 µl of annexin binding buffer containing (mM): NaCl 145, HEPES 10, $CaCl_2$ 2.5, pH 7.4, for 15 min at RT. Annexin V-FITC was delivered in unit size of 500 µl containing 25 mM HEPES, 140 mM NaCl, 1 mM EDTA, pH 7.4, and 0.1% bovine serum albumin. After incubation, samples were kept on ice and analysed immediately by flow cytometry (FACS Calibur and Cell Quest Pro software). PS exposure was measured in the FL-1 channel excited by an argon laser at 488 nm. Control conditions for the negative fluorescent gate were obtained in the absence of A23187, LPA, or PMA. Annexin V positive RBCs were determined as percentage by relating positive and negative signal events to the control condition. For each experiment at least three different blood samples were used and 30,000 events for each sample were counted.

The kinetics of PS exposure was recorded using a fluorescence microscope (the same as described above for Ca^{2+} measurements). A diluted RBC suspension (approximately 0.025% haematocrit) was prepared in the HPS with 2 mM $CaCl_2$ and 5 µl annexin V-FITC and transferred to a cover slip (coated with poly-L-lysine) 5 min before the start of the imaging procedure. A23187, LPA, and PMA (or the solvents ethanol, water, or DMSO, for controls) were added immediately before the start of the imaging procedure. Experiments were performed at RT in a dark room. An image was taken every 30 s (exposure time 500 ms).

Double labelling experiments

To evaluate the relationship between the intracellular Ca^{2+} content and the PS exposure, RBCs were labelled with both fluo-4 AM and annexin V-alexa 568. Briefly, cells loaded with fluo-4 AM as described before were induced for PS exposure using A23187, LPA, or PMA. After washing in the HPS at RT, cells were incubated with annexin V-alexa 568 for 15 min at RT. The double labelling experiments were carried out using the confocal laser scanning fluorescence microscope LSM 510 META (Carl Zeiss AG, Jena, Germany). Samples were scanned with an argon laser (488 nm) for fluo-4 and HeNe laser (543 nm) for annexin V-alexa 568.

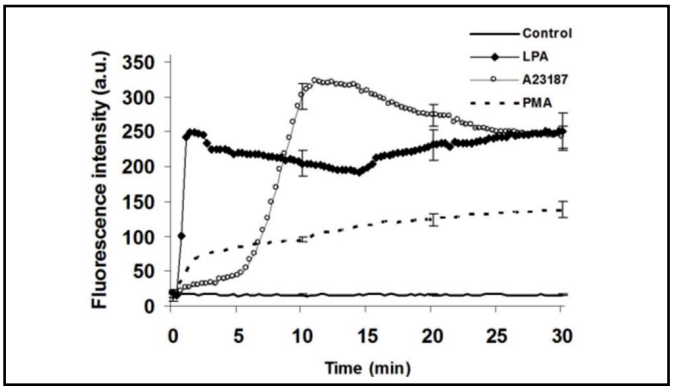

Fig. 1. Fluo-4 AM fluorescence intensity (arbitrary units) of human RBC for Ca^{2+} content after treatment with 2.5 µM LPA, 2 µM A23187 or 6 µM PMA in the presence of 2 mM extracellular Ca^{2+} measured with single cell fluorescence microscopy over a time interval of 30 min. Curves show the mean values of at least 60 RBCs from 3 different blood samples. Error bars represent 25% of SD.

Reagents

All chemicals used (except fluorescent dyes and Pluronic F-127) were purchased from Sigma-Aldrich (Munich, Germany). Fluo-4 AM, annexin V-FITC, and Pluronic F-127 were obtained from Molecular Probes (Eugene, USA) and annexin V-alexa from Roche Diagnostics GmbH (Mannheim, Germany). Stock solutions for A23187 (1 mM), LPA (1 mM), and PMA (10 mM) were dissolved in ethanol, water, and DMSO, respectively.

Statistical significance

Data are presented as mean values ± SD of at least 3 independent experiments. The significance of differences was tested by Student's *t*-test. Statistical significance of the data was defined as follows: $p > 0.05$ (n.s.), $p = 0.05$ (*); $p = 0.01$ (**), $p = 0.001$ (***).

Results

An increased intracellular Ca^{2+} content of RBCs results in the activation of several processes, important for PS exposure: (i) activation of the scramblase and inhibition of flippase [4], (ii) activation of the Ca^{2+}-activated K^+ channel leading to loss of KCl and water, causing cell shrinkage [28-30], (iii) activation of PKCα [22], and (iv) activation of calpain resulting in cytoskeleton destruction, membrane blebbing, and micro-vesiculation [31, 32]. In addition, elevated intracellular Ca^{2+} activates the Ca^{2+} pump.

In order to correlate between increased intracellular Ca^{2+} content and PS exposure of human RBCs, we focussed on LPA treatment shown to increase the intra-

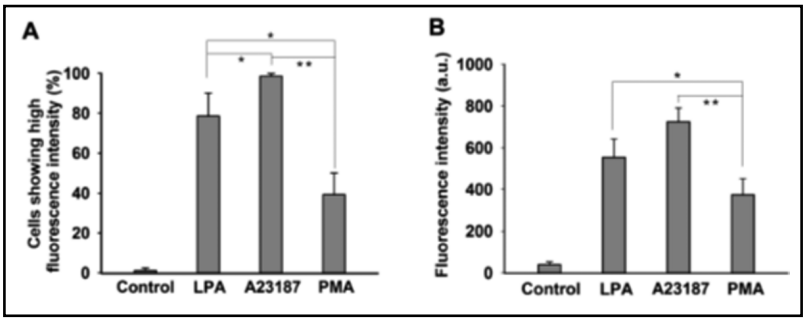

Fig. 2. Flow cytometric analysis of human RBC Ca^{2+} content after treatment with 2.5 µM LPA, 2 µM A23187 or 6 µM PMA in the presence of 2 mM extracellular Ca^{2+} after 12 min of incubation. Mean values of 3 different blood samples (with 30,000 cells per sample) are shown. Error bars represent SD, p = 0.05 (*); p = 0.01 (**), p = 0.001 (***). Control measurements were done in the presence of solvents (ethanol, water, or DMSO, see Material and Methods). All data measured in the presence of the reagents are significantly different from control, p = 0.001. A: Percentage of RBCs showing a significant higher Ca^{2+} content compared to control after treatment with LPA, A23187 or PMA. B: Increase of Ca^{2+} content of RBCs in response to LPA, A23187 or PMA treatment shown as arbitrary units (a.u.) of fluorescence intensity analysed in cells with higher Ca^{2+} content.

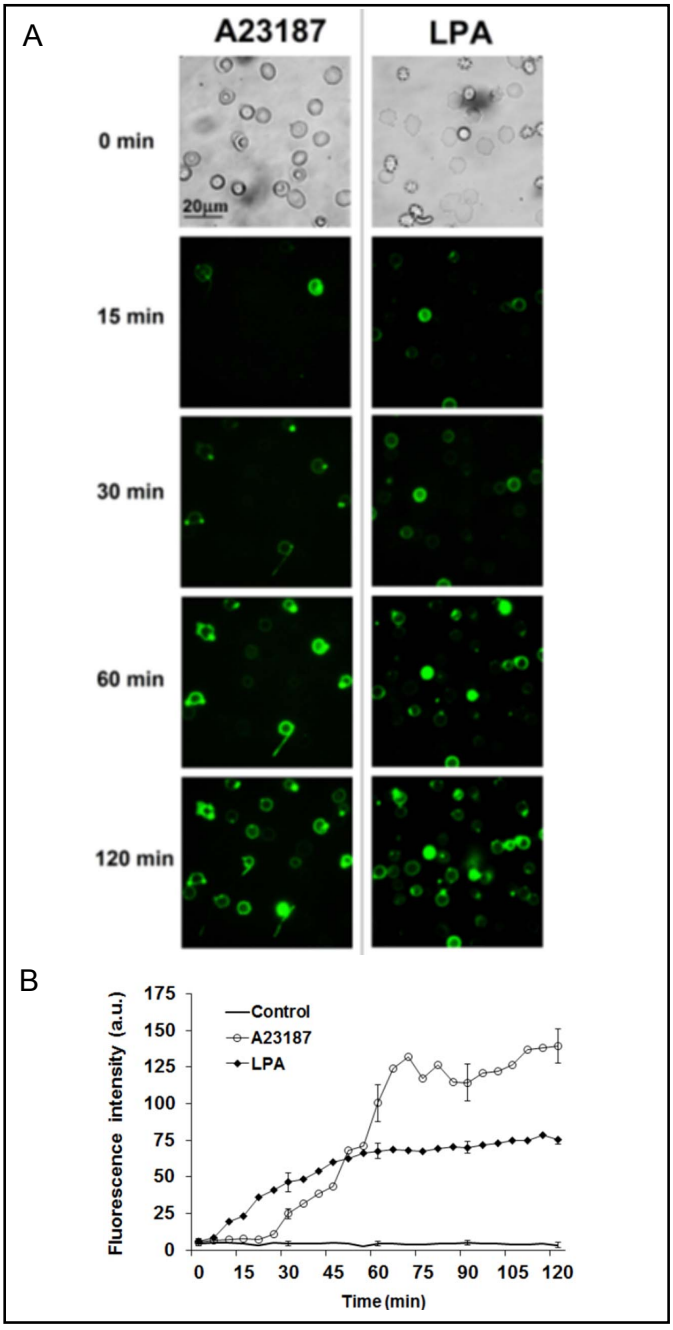

Fig. 3. PS exposure evaluation of human RBCs treated with 2 µM A23187 or 2.5 µM LPA in the presence of 2 mM extracellular Ca^{2+} up to 120 min and labelled with annexin V-FITC using fluorescence microscopy. A: Representative images out of 3 independent experiments. Note that blood samples from different donors are presented. B: Kinetics of fluorescence intensity shown as arbitrary units (a.u.); curves show the mean values of at least 30 RBCs from 3 different blood samples. Error bars represent SD.

cellular Ca^{2+} content [17, 18, 20, 22, 27]. For comparison, we used the Ca^{2+} ionophore A23187. In addition, we treated the RBCs with PMA, a known activator of the Ca^{2+}-dependent conventional PKC (cPKC) isoforms (α, βI, βII, γ) and the Ca^{2+}-independent novel PKC (nPKC) isoforms (δ, ε, η, θ) but not the Ca^{2+}-independent, non phorbol ester-binding atypical PKC (aPKC) isoforms (ζ, λ/ι, µ) [33, 34]. As mentioned before, PKCα [22] as well as PKCζ [24], and PKCλ/ι [24] are present in human RBCs and may play a role in PS exposure. So far no nPKC isoforms were detected in RBCs.

Fig. 1 shows the kinetics of Ca^{2+} uptake after treating RBCs with LPA, A23187, or PMA measured by fluorescence video imaging. Addition of 2.5 µM LPA immediately led to an increase of the intracellular Ca^{2+} content that remains relatively constant up to 30 min. At higher LPA concentrations (3.5 - 10 µM) the rate of haemolysis continuously increased (data not shown). Treatment with 2 µM A23187 significantly increased the Ca^{2+} content but only after a delay of about 5 min. The final fluorescence intensity, i.e. the intracellular Ca^{2+} content, was the same under both conditions after 30 min. At higher concentrations (up to 10 µM) the lag phase was reduced without affecting the maximal fluorescence intensity (data not shown). Similar to the treatment with LPA, exposure to 6 µM PMA, a recommended concentration to activate cPKCs and nPKCs [22], increased the Ca^{2+} content with-

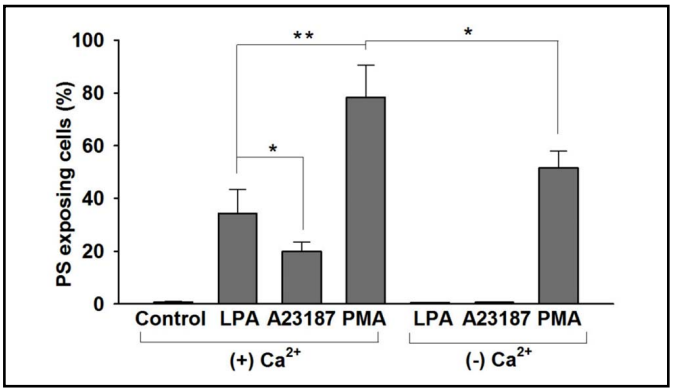

Fig. 4. Flow cytometry analysis of human RBCs showing a significant higher percentage PS exposure compared to control after a 30 min treatment with 2.5 µM LPA, 2 µM A23187 or 6 µM PMA in the presence of 2 mM extracellular Ca^{2+} [(+) Ca^{2+}]. For comparison cells were treated in the absence of extracellular Ca^{2+} (presence of 1 mM EGTA) [(-) Ca^{2+}]. Bars show mean value of 3 different blood samples (30,000 cells of each blood sample were analysed). Error bars represent SD, $p \leq 0.05$ (*); $p \leq 0.01$ (**). Control measurements were done in the presence of solvents (ethanol, water, or DMSO) and extracellular Ca^{2+} (see Material and Methods). LPA or A23187 treatments in the absence of extracellular Ca^{2+} were not significantly different from control. All data measured in the presence of reagents were significantly different from control, $p \leq 0.001$.

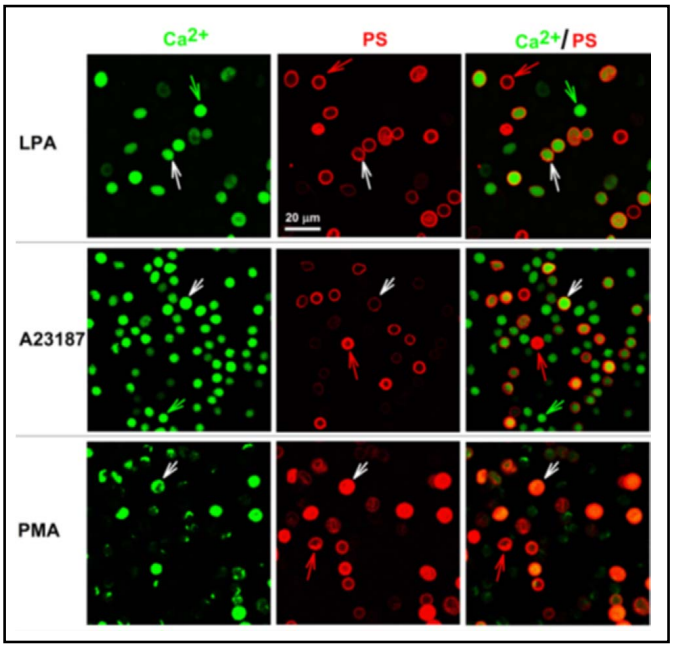

Fig. 5. Human RBCs double labelled with fluo-4 and annexin V-alexa 568 (Ca^{2+}/PS double scan, green and red, right column) after stimulated to increase Ca^{2+} content (green, left column) and PS exposure (red, middle column), respectively. Upper panels - 2.5 µM LPA, middle panels - 2 µM 23187, lower panels - 6 µM PMA. White arrows indicate cells with both, elevated Ca^{2+} content and an increased PS exposure, green arrows cells with increased Ca^{2+} content only, and red arrows cells with externalised PS only. These are representative images out of 3 independent experiments.

out a lagphase, but failed to reach comparably high fluorescence intensities.

Comparable experiments were carried out using flow cytometry analysis and results are represented in Fig. 2. Fig. 2A depicts the percentage of cells with an elevated Ca^{2+} content after LPA, A23187, or PMA treatment in comparison to control conditions after 12 min when the fluorescence intensity after A23187 treatment had reached maximal values (see Fig. 1). Fig. 2B shows the corresponding fluorescence intensities of the reacting cells, i.e. a significantly enhanced Ca^{2+} content after stimulation by the three substances. Fig. 2A shows that in 99.2% of the cells there was a significant increase of Ca^{2+} content in response to A23187. In the presence of LPA about 80% of the cells raised their Ca^{2+} content, comparable to the Ca^{2+} ionophore treatment. With PMA only about 40% of the cells increased their Ca^{2+} content reaching only half the fluorescence intensity as compared to A23187 or LPA (Fig. 2B). With 10 µM PMA, the number of cells reacting by exposing PS increased significantly, reaching a value of about 70%, although the Ca^{2+} content was not enhanced under these conditions (not shown in Fig. 2, but cf. with fluorescence microscopy results presented in Fig. 1). It should be mentioned that on average only 1.3% of control cells had about 5-fold

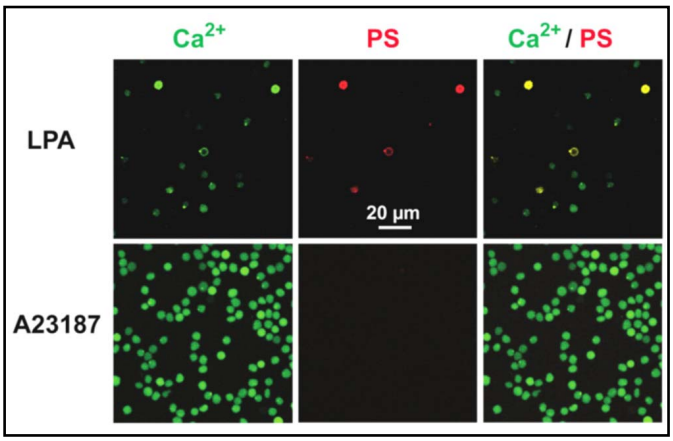

Fig. 6. Sheep RBCs double labelled with fluo-4 and annexin V-alexa 568 (Ca^{2+}/PS double scan, green and red, right column) after stimulation to increase Ca^{2+} content (green, left column) and PS exposure (red, middle column), respectively. Upper panels - 2.5 µM LPA, lower panels - 2 µM A23187. There are two cells with elevated Ca^{2+} content and increased PS exposure. Representative images out of 3 independent experiments.

higher fluo-4 fluorescence intensity compared to the non-reacting control cells (for non-reacting cells data not shown).

The PS exposure was studied in LPA- and A23187-treated cells over a time period of 120 min using fluorescence microscopy (Fig. 3). At times longer than 120 min in LPA treated RBCs haemolysis occurred. In contrast, no significant haemolysis was seen with A23187-treated cells at longer incubation times (up to 24 h). PMA treatment also did not result in a significant haemolysis after long time incubation (up to 6 h, data not shown). The images of treatments with LPA and A23187 (Fig. 3A) as well as PMA (not shown) reveal that vesiculation occurred. The kinetic of PS exposure of human RBCs treated with LPA or A23187 is presented in Fig. 3B. It can be seen that the process of PS exposure is faster and more pronounced in case of LPA compared to A23187. Although the kinetics is a convolution of the annexin V binding to PS and the PS exposure rate, we can deduct from the comparison of Fig. 1 and Fig. 3B that the PS exposure is a slower process than the Ca^{2+} entry.

PS exposure was additionally measured by flow cytometry 30 min after incubation of RBCs with LPA, A23187, or PMA and results are presented in Fig. 4. The number of annexin V-positive cells after LPA treatment in the presence of Ca^{2+} was about 35% and significantly higher as compared to the A23187 treatment (20%). Also, PMA induced the highest PS exposure in human RBCs. It should be stated that these measurements using fluorescence microscopy (Fig. 3B) represent integrated values of the fluorescence intensity whereas the data obtained from the flow cytometry experiments depict the numbers of PS exposing cells (in %).

Based on the data obtained from flow cytometry experiments (quadrant analysis), we estimated the number of vesicles detached from the RBC membrane after 30 min. In case of LPA, A23187, or PMA treatment the number of vesicles per 30,000 RBCs was estimated as 10,698 ± 2,363 (n = 3), 6,626 ± 2,898 (n = 4), and 15,509 ± 6,382 (n = 4), respectively.

Experiments were also carried out after treating human RBCs with LPA, A23187, or PMA in the absence of extracellular Ca^{2+} (presence of 1 mM EGTA). In case of LPA and A23187, there were no significant differences in the PS exposure between treatment and control conditions (Fig. 4, (-) Ca^{2+}). Only in the case of PMA treatment, about 50% of RBCs showed PS exposure (compared to about 80% in the presence of Ca^{2+}, see Fig. 4, (+) Ca^{2+}). The data obtained for control conditions in the presence of Ca^{2+} shown in Fig. 4 were not significantly different from the control conditions in the absence of Ca^{2+} (data not shown).

Table 1. FACS analysis of RBCs showing a significant higher PS exposure compared to control conditions (in %) after treatment with 2.5 µM LPA, 2 µM A23187 or 6 µM PMA in the presence of 2 mM extracellular Ca^{2+} in HPS (7.5 mM KCl) or in a high K^+ solution (150 mM KCl). Mean values ± SD of 3 different blood samples (30,000 cells of each blood sample were analysed).

	7.5 mM KCl [%]	150 mM KCl [%]
LPA	36.3 ± 7.3	23.1 ± 2.9
4-bromo-A23187	27.7 ± 7.7	10.8 ± 5.5
PMA	78.5 ± 6.0	76.9 ± 8.8

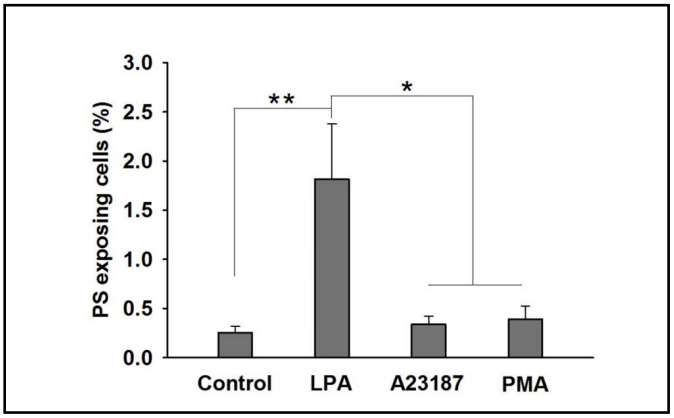

Fig. 7. Flow cytometry analysis of sheep RBCs showing a significant higher PS exposure compared to control (in %) after treatment with 2.5 µM LPA, 2 µM A23187 or 6 µM PMA in the presence of 2 mM extracellular Ca^{2+} (incubation time 30 min). Columns show mean value of 3 different blood samples (30,000 cells of each blood sample were analysed). Error bars represent SD, $p \leq 0.05$ (*); $p \leq 0.01$ (**). Control measurements were done in the presence of solvents only (ethanol, water, or DMSO) and extracellular Ca^{2+} (see Material and Methods). Data for treatments with A23187 or PMA are statistically not significantly different from control.

Comparing the results of Figs. 2 and 4 it is evident that there is no correlation between the number of cells showing an elevated Ca^{2+} content and increased PS exposure. It should be noted that the threshold for the forward scatter in the flow cytometry measurements was set at a value so that only events based on the size of intact cells were counted, since micro-vesicle formation occurred after treatment with all 3 substances (see Fig. 3).

A lack of correlation between Ca^{2+} content and PS exposure was further supported by confocal fluorescence microscopy with double labelling experiments (for both, intracellular Ca^{2+} and PS in the outer membrane leaflet). The upper panels of Fig. 5 show the effect of LPA treat-

ment. Most of the cells exhibited both, an elevated Ca^{2+} content and external PS exposure (Fig. 5, upper panels, white arrows). However, some cells displayed an increased Ca^{2+} level, but no PS exposure (Fig. 5, upper panels, green arrows), whereas other cells externalise PS without a higher Ca^{2+} content (Fig. 5, upper panels, red arrows). The same observation was found for A23187-treated cells (middle panels of Fig. 5) although it should be noted that PS exposure without high Ca^{2+} content is relatively rare in both cases. The lower panels of Fig. 5 show that after PMA treatment PS exposure was more prevalent at low Ca^{2+} content in agreement with the findings presented in Figs. 2 and 4.

Experiments after PMA treatment, but in the complete absence of external Ca^{2+} (presence of 1 mM EGTA), were carried out using confocal fluorescence microscopy and double labelling of the cells (for Ca^{2+} and PS). In agreement with the flow cytometry measurements, many cells revealed PS exposure but none increased Ca^{2+} (data not shown). In addition, the presence of 1 mM *o*-vanadate to inhibit the Ca^{2+} pump failed to produce further significant changes (data not shown).

To consider a possible effect of cell volume alteration on PS exposure, experiments were carried out with the HPS replaced by a solution containing 150 mM KCl plus 2.5 mM NaCl instead of 145 mM NaCl plus 7.5 mM KCl. Under these conditions no net K^+ efflux occurs through the Ca^{2+}-dependent K^+ channel and hence no KCl loss and accompanying cell shrinkage. Table 1 reveals that a substantial part of the PS exposure in the presence of LPA or A23187 was due to volume decrease which was confirmed by analysing the forward scatter (FSC) by flow cytometry recordings (data not shown). Note that the PS exposure data in HPS (7.5 mM KCl) presented in Table 1 were not identical to the data shown in Fig. 4 since different blood samples were analysed for both investigations.

In comparison, in sheep RBCs (Fig. 6) LPA (upper panels) also increased the Ca^{2+} content. However, in comparison to human RBCs only very few cells showed PS exposure (see Fig. 5, upper panels). For A23187 (Fig. 6, lower panels) and PMA treatment (data not shown) there was no PS exposure although the intracellular Ca^{2+} content was increased in both cases in comparison to control conditions. These results were confirmed by flow cytometry and are depicted in Fig. 7. Only 2% of sheep RBCs treated with LPA expose PS on the outer membrane leaflet whilst A23187 and PMA treatment failed to induce PS exposure (Fig. 7), thus differing significantly from those obtained with human RBCs (see Fig. 4).

Discussion

The main idea was to investigate the process of PS exposure as a function of the intracellular Ca^{2+} content and the activation of PKCα in human and sheep RBCs. Flow cytometry, single cell fluorescence microscopy, and confocal fluorescence microscopy were used.

In HPS, the Ca^{2+} permeability of the RBC membrane is very low [35] and the basal level of free cytoplasmic Ca^{2+} is in the range of 60 nM maintained by the activity of the Ca^{2+} pump [36]. Our data reveal a fast uptake of Ca^{2+} by LPA stimulation (Fig. 1). This effect is probably mediated by a specific pathway rather than a non-specific leak since it has been proposed that a non-selective cation channel is activated by a still unclear mechanism [17, 27]. Other Ca^{2+} permeable cation channels in the RBC membrane also may be involved [7, 32, 37] (for a recent review see [14]). Furthermore the Ca^{2+} entry showed a clear LPA dose-dependent response [18].

Ca^{2+} uptake mediated by A23187 reached the same levels as LPA treatment after 30 min, although a delay in the response of about 5 min occurred, probably because A23187 partitions into the membrane before acting as ionophore. The effect of PMA (even at 10 μM) was fast at the beginning of the experiment without ever inducing high levels of intracellular Ca^{2+}, as compared to LPA and A23187 treatments. Flow cytometry experiments (Fig. 2B) performed at 12 min (when the Ca^{2+} content reached the maximum values, cf. Fig. 1) are consistent with data obtained by fluorescence microscopy. The mechanism by which PMA increases intracellular Ca^{2+} is different from the LPA and A23187 stimulations. Andrews et al. [38] assume that PMA activates PKC isoforms that in turn opens a ω-agatoxin-TK-sensitive, Cav2.1-like (P/Q-type) Ca^{2+} channel. It has been proposed that this channel may be identical with the voltage-activated non-selective cation channel [14]. PKC activation by PMA is Ca^{2+}-independent, whereas the channel opening leads to an increase of the intracellular Ca^{2+} content. In addition, PMA may activate the Ca^{2+} pump [34] and inhibit the Ca^{2+}-activated K^+ channel [34, 39].

From the images depicting PS exposure at different time points presented in Fig. 3, one can see that the increased Ca^{2+} content also leads to a vesiculation of the cells, in agreement with findings reported in literature [31, 32]. Calpain, a calcium-dependent proteolytic enzyme, cleaves spectrin and actin, leading to cytoskeleton breakdown [40-42], and therefore may be involved in vesiculation.

PMA induced a greater PS exposure in comparison to LPA and A23187 (Fig. 4, (+) Ca^{2+}). PS exposure was not directly correlated with the Ca^{2+} content since RBCs stimulated with PMA, at the same time point (30 min), displayed two-fold lower Ca^{2+}-dependent fluorescence when compared to LPA and A23187 treatment (cf. Figs. 1 and 4).

These findings were further supported by the results of the double labelling experiments presented in Fig. 5. After treatment with LPA or A23187 many cells (in case of LPA most of the cells) showed an increased Ca^{2+} content and external PS exposure. However, in both cases some cells had an increased Ca^{2+} level but no PS exposure and, vice versa, some cells depicted externalised PS in the absence of an increased Ca^{2+} content. This situation was rare in both cases and it cannot be ruled out that, after 30 min of incubation, a reduction of the intracellular Ca^{2+} content due to the activation of the Ca^{2+} pump occurred in some cells, in agreement with the findings shown in Fig. 1 (i.e. a sub-population of cells behaved different from others). In case of the PMA treatment, some cells displayed an enhanced Ca^{2+} content and PS exposure. Interestingly, more cells as compared to LPA or A23187 treated cells, show PS exposure without having an elevated Ca^{2+} content. In a control experiment, i.e. in the absence of external Ca^{2+} (Fig. 4), some cells showed PS exposure. Thus the primary cause of PS exposure stimulated by PMA is different from the LPA or A23187 stimulation. Finally, the cell volume seems to be important for PS exposure in agreement with findings of Lang et al. [43, 44] but only in case of LPA or A23187 treatment. However, we cannot rule out the possibility that the extracellular K^+ concentration might contribute to the observed volume effect on the PS exposure in case of LPA or A23187 treatment, which would be in agreement with the results of Wolfs et al. [45].

Surprisingly, comparable experiments with sheep RBCs did not show PS exposure after treatment with the Ca^{2+} ionophore or PMA although the intracellular Ca^{2+} content was enhanced. However, treatment with LPA resulted in a very small number of cells externalising PS. These effects can be explained by assuming absence of scramblase activity. In turn, LPA had an additional but minor effect on PS exposure (see below). The presumed absence of the scramblase activity in sheep RBCs is supported by findings of the group of A. Herrmann (Humboldt University, Berlin) applying spin-labelled lipids and investigating the PS movement across the RBC membrane of a great variety of animal species by electron spin resonance (A. Herrmann, personal communication). Indeed, data mining using the scramblase amino acid sequences against protein databases failed to show any match with proteins from sheep. Furthermore, the external leaflet of the sheep RBC membrane contains 100% SM and no PC [25, 26]. SM is transported across the membrane very slowly (even slower than PC) [46] and therefore no need for the presence of the scramblase exists in sheep RBCs.

Based on the findings of this paper, it seems reasonable to assume at least 3 different mechanisms being responsible for the PS exposure in human RBCs:

First, a Ca^{2+}-stimulated scramblase activation (and flippase inhibition) [4, 6, 7, 47, 48] brought about by LPA, A23187, or PMA treatment inducing Ca^{2+} uptake by different pathways. LPA activates the non-selective cation channel [14] whereas PMA opens the ω-agatoxin-TK-sensitive, Cav2.1-like (P/Q-type) Ca^{2+} channel [38]. This first mechanism is a rather general one that can occur under various pathological conditions, e.g. by activation of NMDA receptors in sickle cell disease as discussed by Makhro et al. [49].

Second, PMA directly activates PKCα involved in PS exposure in human RBCs [22, 23]. In addition, LPA activates in human RBCs both the PKCα (Ca^{2+}-dependent) and the PKCζ (Ca^{2+}-independent) [20]. Whether there is a direct activation of the scramblase in human RBCs by PKCα and/or PKCζ remains to be shown. The more pronounced effect of PS exposure after treatment of RBCs with PMA as compared to LPA can be explained by assuming that PMA activates all available PKCα whereas LPA stimulation triggers a signalling cascade [50] resulting only in partial activation of the PKCα pool.

Third, an additional mechanism has to be taken into consideration in the case of sheep RBCs. LPA may insert into the membrane (more pronounced in the presence of Ca^{2+} since it becomes more hydrophobic) stimulating the flop of PS from the inner to the outer membrane leaflet. Such an event would explain the higher rate of haemolysis after LPA treatment as compared to A23187 or PMA treatment. In comparison to the first and second mechanisms, this third effect only plays a minor role in the PS exposure which may be due to the fact that the LPA concentration used was far below the micelle forming concentration [51].

How the 3 pathways are interconnected remains to be elucidated in further investigations. The situation is even more challenging since other parameters, not being addressed here, are also known to affect the PS exposure in human RBCs. For instance, it has been shown

that activation of caspases, production of ceramides, oxidative stress as well as ATP depletion increase the PS exposure [7, 31, 32, 52]. ATP depletion is a Ca^{2+}-dependent process because at higher intracellular Ca^{2+} levels the Ca^{2+} pump is activated and will consume more ATP. It has also been demonstrated that the intracellular K^+ content and the cell shape can affect the PS exposure in RBCs [45, 53]. Furthermore, it has been demonstrated that RBCs show an increased PS exposure after long-term storage and induced by hyperosmotic shock [54].

Conclusion

PS exposure in RBCs is a complex process involving at least 3 mechanisms. A variety of Ca^{2+}-dependent as well as Ca^{2+}-independent parameters play a substantial role for PS exposure (see e.g. [52, 55, 56]). Since the Ca^{2+}-dependent and Ca^{2+}-independent mechanisms are not additive, an interaction between those pathways can be assumed. Cell volume and probably the Ca^{2+} pump modulate the signalling cascade leading to PS exposure. Furthermore, the majority of PS is transported to the outer membrane leaflet mediated by scramblase activity but an additional minor effect based on lipid flop has to be taken into consideration.

Externalisation of PS to the outer membrane leaflet is important for the adherence of RBCs to endothelium [19, 57, 58] as well as for the RBC-RBC adhesion [9, 17, 18]. Knowledge of the underlying mechanisms is important for clincial prevention of thrombus formation.

Acknowledgements

This work has been supported by a grant to DBN from the German Academic Exchange Service (DAAD) and the Ministry of Economy and Sciences of the Saarland. Part of the research leading to these results has received funding from the European Community's Seventh Framework Programme (FP7 2007-2013) under grant agreement nr NMP3-SL-2008-214032 and the DFG Graduate School (GRK 1276). The study was approved by the ethics committee of the Medical Association of the Saarland (reference No 132/08).

References

1 Haest CWM: Distribution and movement of membrane lipids; in Bernhardt I, Elorry JC (eds): Red cell membrane transport in health and disease. Berlin, Springer, 2003, pp 1-25.

2 Devaux PF, Herrmann A, Ohlwein N, Kozlov MM: How lipid flippases can modulate membrane structure. Biochim Biophys Acta 2008;1778:1591-1600.

3 Bevers EM, Comfurius P, Dekkers DW, Zwaal RF: Lipid translocation across the plasma membrane of mammalian cells. Biochim Biophys Acta 1999;1439:317-330.

4 Daleke DL: Regulation of phospholipid asymmetry in the erythrocyte membrane. Curr Opin Hematol 2008;15:191-195.

5 Zwaal RF, Comfurius P and Bevers EM: Surface exposure of phosphatidylserine in pathological cells. Cell Mol Life Sci 2005;62:971-988.

6 Lang F, Gulbins E. Lerche H, Huber SM, Kempe DS, Foller M: Eryptosis, a window to systemic disease. Cell Physiol Biochem 2008;22:373–380.

7 Lang F, Lang KS, Lang PA, Huber SM, Wieder T: Mechanisms and significance of eryptosis. Antioxid Redox Signal 2006;8:1183-1192.

8 Hellem AJ, Borchgrevink CF, Ames SB: The role of red cells in haemostasis: the relation between haematocrit, bleeding time and platelet adhesiveness. Br J Haematol 1961;7:42-50.

9 Andrews DA, Low PS: Role of red blood cells in thrombosis. Curr Opin Hematol 1999;6:76-82.

10 Kaestner L, Bernhardt I: Ion channels in the human red blood cell membrane: their further investigation and physiological relevance. Bioelectrochemistry 2002;55:71-74.

11 Kaestner L, Tabellion W, Lipp P, Bernhardt I: Prostaglandin E_2 activates channel-mediated calcium entry in human erythrocytes: an indication for a blood clot formation supporting process. Thromb Haemost 2004;92: 1269-1272.

12 Kaestner L, Bollensdorff C, Bernhardt I: Non-selective voltage-activated cation channel in the human red blood cell membrane. Biochim Biophys Acta 1999;1417: 9-15.

13 Kaestner L, Christophersen P, Bernhardt I, Bennekou P: The non-selective voltage-activated cation channel in the human red blood cell membrane: reconciliation between two conflicting reports and further characterisation. Bioelectrochemistry 2000;52:117-125.

14 Kaestner L: Cation channels in erythrocytes - historical and future perspective. Open Biol J 2011;4:27-34.

15 Dyrda A, Cytlak U, Ciuraszkiewicz A, Lipinska A, Cueff A, Bouyer G, Egee S, Bennekou P, Lew VL, Thomas SLY: Local membrane deformations activate Ca^{2+}-dependent K^+ and anionic currents in intact human red blood cells. PLoS One 2010;5:e9447.

16 Oonishi T, Sakashita K, Ishioka N, Suematsu N, Shio H, Uyesaka N: Production of prostaglandins E_1 and E_2 by adult human red blood cells. Prostaglandins Other Lipid Mediat 1998;56:89-101.

17 Steffen P, Jung A, Nguyen DB, Mueller T, Bernhardt I, Kaestner L, Wagner C: Stimulation of human red blood cell leads to Ca^{2+}-mediated intercellular adhesion. Cell Calcium 2011;50:54-61.

18 Kaestner L, Steffen P, Nguyen DB, Wang J, Wagner-Britz L, Jung A, Wagner C, Bernhardt I: Lysophosphatidic acid induced red blood cell aggregation in vitro. Bioelectrochemistry 2011;in press.

19 Closse C, Dachary-Prigent J, Boisseau MR: Phosphatidylserine-related adhesion of human erythrocytes to vascular endothelium. Br J Haematol 1999;107: 300-302.

20 Chung SM, Bae ON, Lim KM, Noh JY, Lee MY, Jung YS, Chung JH: Lysophosphatidic acid induces thrombogenic activity through phosphatidylserine exposure and procoagulant microvesicle generation in human erythrocytes. Arterioscler Thromb Vasc Biol 2007;27:414-421.
21 Woon LA, Holland JW, Kable EP, Roufogalis BD: Ca^{2+} sensitivity of phospholipid scrambling in human red cell ghosts. Cell Calcium 1999;25:313-320.
22 De Jong K, Rettig MP, Low PS, Kuypers FA: Protein kinase C activation induces phosphatidylserine exposure on red blood cells. Biochemistry 2002;41:12562-12567.
23 Klarl BA, Lang PA, Kempe DS, Niemoeller OM, Akel A, Sobiesiak M, Eisele K, Podolski M, Huber SM, Wieder T, Lang F: Protein kinase C mediates erythrocyte "programmed cell death" following glucose depletion. Am J Physiol 2006;290:C244-C253.
24 Govekar RB, Zingde SM: Protein kinase C isoforms in human erythrocytes. Ann Hematol 2001;80:531-534.
25 Van Dijck PW, De Kruijff B, Van Deenen LL, De Gier J, Demel RA: The preference of cholesterol for phosphatidylcholine in mixed phosphatidylcholine-phosphatidylethanolamine bilayers. Biochim Biophys Acta 1976;455:576-587.
26 Saito M, Tanaka Y, Ando S: Thin-layer chromatography-densitometry of minor acidic phospholipids: application to lipids from erythrocytes, liver, and kidney. Anal Biochem 1983;132:376-383.
27 Kaestner L, Tabellion W, Weiss E, Bernhardt I, Lipp P: Calcium imaging of individual erythrocytes: problems and approaches. Cell Calcium 2006;39:13-19.
28 Gardos G: The permeability of human erythrocytes to potassium. Acta Physiol Hung 1956:10:185-189.
29 Hoffman JF, Joiner W, Nehrke K, Potapova O, Foye K, Wickrema A: The hSK4 (KCNN4) isoform is the Ca^{2+}-activated K^+ channel (Gardos channel) in human red blood cells. Proc Natl Acad Sci USA 2003;100:7366-7371.
30 Lang PA, Kaiser S, Myssina S, Wieder T, Lang F, Huber SM: Role of Ca^{2+}-activated K^+ channels in human erythrocyte apoptosis. Am J Physiol 2003;285:C1553-C1560.
31 Lang KS, Lang PA, Bauer C, Duranton C, Wieder T, Huber SM, Lang F: Mechanisms of suicidal erythrocyte death. Cell Physiol Biochem 2005;15:195-202.
32 Foeller M, Huber SM, Lang F: Erythrocyte programmed cell death. IUBMB Life 2008;60:661-668.
33 Lord JM, Pongracz J: Protein kinase C: a family of isoenzymes with distinct roles in pathogenesis. Clin Mol Pathol 1995;48:M57-M64.
34 Fathallah H, Sauvage M, Romero JR, Canessa M, Giraud F: Effects of PKC alpha activation on Ca^{2+} pump and K(Ca) channel in deoxygenated sickle cells. Am J Physiol 1997;273:C1206-C1214.
35 Tiffert T, Bookchin RM, Lew VL: Calcium homeostasis in normal and abnormal human red cells; in Bernhardt I, Elorry JC (eds): Red cell membrane transport in health and disease. Berlin, Springer, 2003, pp 373-405.
36 Gilboa H, Chapman BE, Kuchel PW: 19F NMR magnetization transfer between 5-FBAPTA and its complexes. An alternative means for measuring free Ca^{2+} concentration, and detection of complexes with protein in erythrocytes. NMR Biomed 1994;7:330-338.
37 Duranton C, Huber S, Tanneur V, Lang K, Brand V, Sandu C, Lang F: Electrophysiological properties of the plasmodium falciparum-induced cation conductance of human erythrocytes. Cell Physiol Biochem 2003;13:189-198.
38 Andrews DA, Yang L, Low PS: Phorbol ester stimulates a protein kinase C-mediated agatoxin-TK-sensitive calcium permeability pathway in human red blood cells. Blood 2002;100:3392-3399.
39 Del Carlo B, Pellegrini BM, Pellegrino M: Modulation of Ca^{2+}-activated K^+ channels of human erythrocytes by endogenous protein kinase C. Biochim Biophys Acta 2003;1612:107-116.
40 Anderson DR, Davis JL, Carraway KL: Calcium-promoted changes of the human erythrocyte membrane. Involvement of spectrin, transglutaminase, and a membrane-bound protease. J Biol Chem 1977;252:6617-6623.
41 Hatanaka M, Yoshimura N, Murakami T, Kannagi R, Murachi T: Evidence for membrane-associated calpain I in human erythrocytes. Detection by an immunoelectrophoretic blotting method using monospecific antibody. Biochemistry 1984;23:3272-3276.
42 Lofvenberg L, Backman L: Calpain-induced proteolysis of beta-spectrins. FEBS Lett 1999;443:89-92.
43 Lang F, Lang KS, Wieder T, Myssina S, Birka C, Lang PA, Kaiser S, Kempe D, Duranton C, Huber SM: Cation channels, cell volume and the death of an erythrocyte. Pflügers Arch 2003;447:121-125.
44 Lang F, Gulbins E, Szabo I, Lepple-Wienhues A, Huber SM, Duranton, C, Lang KS, Lang PA, Wieder T: Cell volume and the regulation of apoptotic cell death. J Mol Recognit 2004;17:473-480.
45 Wolfs JLN, Comfurius P, Bekers O, Zwaal RFA, Balasubramanian K, Schroit AJ, Lindhout T, Bevers EM: Direct inhibition of phospholipid scrambling activity in erythrocytes by potassium ions. Cell Mol Life Sci 2009;66:314-323.
46 Van Meer G, Holthuis JC: Sphingolipid transport in eukaryotic cells. Biochim Biophys Acta 2000;1486:145-170.
47 Williamson P, Kulick A, Zachowski A. Schlegel RA, Devaux PF: Ca^{2+} induces transbilayer redistribution of all major phospholipids in human erythrocytes. Biochemistry 1992;31:6355-6360.
48 Daleke DL: Regulation of phospholipid asymmetry in the erythrocyte membrane. Curr Opin Hematol 2008;15:191-195.
49 Makhro A, Wang J, Vogel J, Boldyrev AA, Gassmann M, Kaestner L, Bogdanova A: Functional NMDA receptors in rat erythrocytes. Am J Physiol Cell Physiol 2010;298:C1315-C1325.
50 Choi JW, Herr DR, Noguchi K, Yung YC, Lee C, Mutoh T, Lin M, Teo ST, Park KE, Mosley AN, Chun J: LPA receptors: subtypes and biological actions. Annu Rev Pharmacol Toxicol 2010;50:157-186.
51 Eichholtz T, Jalink K, Fahrenfort I: The bioactive phospholipid lysophosphatidic acid is released from activated platelets. Biochem J 1993;291:677-680.
52 Mandal D, Moitra PK, Saha S, Basu J: Caspase 3 regulates phosphatidylserine externalization and phagocytosis of oxidatively stressed erythrocytes. FEBS Lett 2002;513:184-188.
53 Wolfs JLN, Comfurius P, Bevers EM, Zwaal RFA: Influence of erythrocyte shape on the rate of Ca^{2+}-induced scrambling of phosphatidylsrine. Mol Membr Biol 2003;20:83-91.
54 Bosman GJCGM, Cluitmans JCA, Groenen YAM, Were JM, Willekens FLA, Novotny VMJ: Susceptibility to hyperosmotic stress-induced phosphatidylserine exposure increases during red blood cell storage. Transfusion 2011;51:1072-1087.
55 Lang PA, Kempe DS, Tanneur V, Eisele K, Klarl BA, Myssina S, Jendrossek V, Ishii S, Shimizu T, Waidmann M, Hessler G, Huber SM, Lang F, Wieder T: Stimulation of erythrocyte ceramide formation by platelet-activating factor. J Cell Sci 2005;118:1233-1243.
56 Kiedaisch V, Akel A, Niemoeller OM, Wieder T, Lang F: Zinc-induced suicidal erythrocyte death. Am J Clin Nutr 2008;87:1530-1534.
57 Telen MJ: Red blood cell surface adhesion molecules: their possible roles in normal human physiology and disease. Semin Hematol 2000;37:130-142.
58 Setty BN, Kulkarni S, Stuart MJ: Role of erythrocyte phosphatidylserine in sickle red cell-endothelial adhesion. Blood 2002;99:1564-1571.

List of Figures

Bibliography

[1] B. Alberts, A. Johnson, J. Lewis, M. Raff, K. Roberts, and P. Walter, *Molecular biology of the cell*, Garland Science, Taylor and Francis Group, 2002.

[2] D.A. Andrews and P.S. Low, *Role of red blood cells in thombosis*, Current Opinion Hematology **6** (1999), no. 2, 76.

[3] J.K. Armstrong, R.B. Wenby, H.J. Meiselman, and T.C. Fisher, *The hydrodynamic radii of macromolecules and their effect on red blood cell aggregation*, Biophysical Journal **87** (2004), no. 6, 4259–4270.

[4] S. Asakura and F. Oosawa, *Interactions between particles suspended in solutions of macromolecules*, Journal of Polymer Science **33** (1958), no. 126, 183–192.

[5] A. Ashkin, *Acceleration and trapping of particles by radiation pressure*, Physical Review Letters **24** (1970), no. 4, 156–159.

[6] A. Ashkin, *Trapping of atoms by resonance radiation pressure*, Physical Review Letters **40** (1978), no. 12, 729–732.

[7] A. Ashkin, *Applications of laser radiation pressure*, Science **4474** (1980), no. 4474, 1081–1088.

[8] A. Ashkin, *Observation of a singe-beam gradient force optical trap for dielectric particles.*, Optical Letters **11** (1986), no. 5, 288–290.

[9] A. Ashkin, *Forces of a single-beam gradient laser trap on a dielectric sphere in the ray optics regime*, Biophysical Journal **61** (1992), no. 2, 569–582.

[10] A. Ashkin and J.M. Dziedzic, *Optical levitation by radiation pressure*, Applied Physics Letters **19** (1971), no. 8, 283–285.

[11] A. Ashkin and J. J.M. Dziedzic, *Optical levitation of liquid drops by radiation pressure*, Science **4181** (1975), 1073–1075.

[12] M. Babicova and E. Machova, *Dextran enhances calcium-induced aggregation of phyosphatidylserine liposomes: possible implications for exocytosis*, Physiological Research **48** (1999), no. 4, 319–321.

[13] K. Balasubramanian and A.J. Schroit, *Aminophospholipid asymmetry: A matter of life and death*, Annual Review of Physiology **65** (2003), 701–734.

[14] F. Basse, J.G. Stout, P.J. Sims, and T. Wiedmer, *Isolation of an erythrocyte membrane protein that mediates ca^{2+}-dependent transbilayer movement of phospholipid*, Journal of Biological Chemistry **271** (1996), no. 19, 17205–17210.

[15] H.R. Baumgartner, *The role of blood flow in platelet adhesion, fibrin deposition, and formation of mural thrombi*, Microvascular Research **5 Issue 2** (1973), no. 2, 167–179.

[16] P. Bennekou and P. Christopherson, *Ion channels*, Red Cell Membrane Transport in Health and Disease, Springer, 2003, pp. 139–152.

[17] M. Benoit, D. Gabriel, G. Gerisch, and H.E. Gaub, *Discrete interactions in cell adhesion measured by single-molecule force spectroscopy*, Nature Cell Biology **2** (2000), 313–317.

[18] M. Benoit and H.E. Gaub, *Measuring cell adhesion forces with the atomic force microscope at the molecular level*, Cells Tissues Organs **172** (2002), no. 3, 174–189.

[19] C. Berg, I. engels, A. Rothbart, K. Lauber, A. Renz, S. Schlosser, K. Schulze-Osthoff, and S. Wesselborg, *Human mature red blood cells express caspase-3 and caspase-8, but are devoid of mitochondrial regulators of apoptosis*, Cell Death and Differentiation **8** (2001), no. 12, 1197–1206.

[20] A. Bershadsky, M. Kozlov, and B. Geiger, *Adhesion-mediated mechanosensitivity: a time to experiment, and a time to theorize*, Current Opinion in Cell Biology. **18** (2006), no. 5, 472–481.

[21] M. Bitbol, P. Fellmann, A. Zachowski, and P.F. Devauy, *Ion regulation of phosphatidylserine and phosphatidylethanolamine outside inside translocation in human erythroctyes*, Biochimica et Biophysica Acta **904** (1987), no. 2, 268–282.

[22] S.M. Block, *Making light work with optical tweezers*, Nature **360** (1992), 493–495.

[23] A. Bogdanova, A. Makhro, J. Goede, J. Wang, A. Boldyrev, and M. gassmann abd L. kaestner, *Nmda receptors in mammalian erythrocytes*, Clinical Biochemistry **42** (2009), 1858–1859.

[24] M. Boynard and J.C. Lelievre, *Size determination of red blood cell aggregates induced by dextran using ultrasound backscattering phenomenon*, Biorheology **27** (1990), no. 1, 39–46.

[25] P.J. H. Bronkhorst, J. Grimbergen, G.J. Brakenhoff, R.M. Heethaar, and J.J. Sixma, *The mechanism of red blood cell (dis)aggregation investigated by means of direct cell manipulation using multiple optical trapping*, British Journal of Haematology **96** (1997), no. 2, 256–258.

[26] D.E. Brooks, *The effect of neutral polymers on the electrokinetic potential of cells and other charged particles: Iv. electrostatic effects in dextran-mediated cellular interactions*, Journal of Colloid and Interface Science **43** (1973), 714–726.

[27] D.E. Brooks, *Mechanism of red cell aggregation, in blood cells, rheology and aging*, Springer-Verlag, 1988.

[28] D.E. Brooks, R.G. Grieig, and J. Jansen, *Erythrocyte mechanics and blood flow*, ch. Mechanism of Erythrocyte Aggregation, pp. 119–140, New York:A.R. Liss;, 1980.

[29] K. Brummel, S. Butenas, and K.G. Mann, *An intergrated study of fibrinogen during blood coagulation*, Journal of Biological Chemistry **274** (1999), no. 32, 2286222870.

[30] H. Bumler, E. Donath, A. Krabi, W. Knippel, A. Budde, and H. Kiesewetter, *Electrophoresis of human red blood cells and platelets: evidence for depletion of dextran*, Biorheology **33** (1996), no. 4-5, 333–351.

[31] H.J. Butt and M. Jaschke, *Calculation of thermal noise in atomic force microscopy*, Nanotechnology **6** (1995), no. 1, 1–7.

[32] K. Buxbaum, E. Evans, and D.E. Brooks, *Quantitation of surface affinities of red-blood-cells in dextran solutions and plasma*, Biochemistry **21** (1982), no. 13, 3235–3239.

[33] C.J. Campbell and B.A.Grzybowski, *Microfuidic mixers: from microfabricated to self-assembling devices*, Philosophical Transactions of the Royal Society **362 no. 1818** (2004), no. 1818, 1069–1086.

[34] M.E. Carr and Y. Hauge, *Enhancement of red blood cell washout from blood clots by alteration of gel pore size and red cell flexibility*, American Journal of Physiology - Heart and Circulatory Physiology **259** (1990), no. 5, H1528.

[35] P.C. Chaumet and M. Nieto-Vesperinas, *Coupled dipole method determination of the electromagnetic force on a particle over a flat dieelctric substrate*, Physical Review B **61** (2000), no. 20, 14119–14127.

[36] P.C. Chaumet and M. Nieto-Vesperinas, *Time-averaged total force on a dipolar sphere in n an electromagnetic field*, Optics Letters **25** (2000), no. 15, 1065–1067.

[37] S. Chien, *Biophysical behavior of red cells in suspensions*, The Red Blood Cell, Academic Press, 1975.

[38] S. Chien, R.J. Dellenback, S. Usami, D.A. Burton, P.F. Gustavson, and V. Magazinovic, *Blood volume, hemodynamic and metabolic changes in hemorrhagic shock in normal and splenectomized dogs*, American Journal of Physiology **225** (1973), no. 4, 866–879.

[39] S. Chien and L.A. Jan, *Ultrastructural basis of the mechanism of rouleaux formation*, Microvascular Research **5** (1973), no. 2, 155–166.

[40] S. Chien and L.A. Lang, *Physiochemical basis and cllinical implications of red cell aggregation*, Clinical Hemorheology **7** (1987), 71–91.

[41] S. Chien, A.S. Lanping, K. Syngcuk, A. M. Burke, and U. Shunichi, *Determination of aggregation force in rouleaux by fluid mechanical technique*, Microvascular Research **13** (1977), no. 3, 327333.

[42] A.P. Chikkatur, Y. Shin, A.E. Leanhardt, D. Kielpinsky, E. Tsikata, T.L. Gustavson, D.E. Pritchard, and W. Ketterle, *A continious source of bose einstein condensed atoms*, Science **296** (2002), no. 5576, 2193–2195.

[43] P. Christopherson and P. Bennekou, *Evidence for a voltage-gated, non selective cation channel in the human red-cell membrane*, Biochimica et Biophysica Acta **1065** (1991), no. 1, 103–106.

[44] S. Chu, *Laser manipulation of atoms and particles*, Science **253** (1991), no. 5022, 861–866.

[45] S.M. Chung, O.N. Bae, K.M. Lim, J.Y: Noh, M.Y. Lee, Y.S. Jung, and J.H. Chung, *Lysophosphatidic acid induced thrombogenic activity through phosphatidylserine exposure and procoagulant microvesicle generation in human erythrocytes*, Arteriosclerosis Thrombosis and Vasular Biology **27** (2007), 414–421.

[46] C. Closse, J. Dachary-Prigent, and M.R. Boisseau, *Phosphatidylserine related adhesion of human erythroctyes to vascular endothelium*, British Journal of Haematology **107** (1999), 300.

[47] A. Cueff, R. Seear, A. Dydra, G. Bouyer, S. Egee, A. Esposito, J. Skepper, T. Tiffert, V.L. Lew, and S.L. Thomas, *Effects of elecated intracellular calcium on the osmotic fragility of human red blood cells*, Cell Calcium **47** (2010), no. 1, 29–36.

[48] P.G. DeGennes, *Scaling concepts in polymer solutions*, Cornell University Press, 1979.

[49] D.W.C. Dekkers, P. Comfurious, E.M. Bevers, and R.F.A. Zwaal, *Comparison between ca^{2+}-induced scrambling of various fluorescently labelled lipid analogues in red blood cells*, Biochemical Journal **362** (2002), no. 3, 741–747.

[50] W. Demtrder, *Experimentalphysik 1*, Springer, 2006.

[51] W. Demtrder, *Experimentalphysik 2*, Springer, 2006.

[52] B. Deuticke, *Membrane lipids and proteins as a basis of red cell shape and its alterations*, Red Cell Membrane Transport in Health and Disease, Springer, 2003, pp. 27–60.

[53] P.F. Devaux, *Static and dynamic lipid asymetry in cell membranes*, Biochemistry **30** (1991), no. 5, 1163–1173.

[54] R. Dixon, K. Young, and N. Brunskill, *Lysophosphatidic acid-induced calcium mobilization and proliferation in kidney proximal tubular cells*, American Journal of Physiology **276** (1999), no. 2, F191–F198.

[55] D.C. Duffy, H.L. Gillis, J. Lin, N.F. Sheppard, and G.J. Kellogg, *Microfabricated centrifugal microfluidic systems: Characterization and multiple enzymatic assays*, Analytical Chemistry **71** (1999), no. 20, 4669–4678.

[56] W.W. Duke, *The relation of blood platelets to hemorrhagic disease*, JAMA **55** (1910), no. 14, 1185.

[57] T. Eichholtz, K. Jalik, I. Fahrenfort, and W.H. Moolenaar, *The bioactive phospholipid lysophosphatidic acid is released from activated platelets*, Biochemical Journal **291** (1993), no. 3, 677–680.

[58] A. Eldor and E.A. Rachmilewitz, *The hypercoagulable state in thalassemia*, Blood **99** (2002), no. 1, 36–43.

[59] L.E. Eriksson, *On the shape of human red blood cells interacting with flat artificial surfaces–"the glass effect"*, Biochimica et Biophysica Acta **1036** (1990), 193–201.

[60] E. Evans and K. Ritchie, *Dynamic strength of molecular adhesion bonds*, Biophysical Journal **72 (4)** (1997), no. 4, 15411555.

[61] E. Evans, K. Ritchie, and R. Merkel, *Sensitive force technique to probe molecular adhesion and structural linkages at biological interfaces*, Biophysical Journal **68,** (1995), no. 6, 2580–2587.

[62] E.A. Evans and R. Skalak, *Mechanics and thermodynamics of biomebranes*, CRC Press Inc., 1980.

[63] R. Fahraeus, *The suspension stability of the blood*, Physiological Reviews **9, No. 2** (1929), no. 2, 241–274.

[64] H. Felgner, O. Mller, and M. Schliwa, *Calibration of light forcecs in optical tweezers*, Applied Optics **34** (1995), no. 6, 977–982.

[65] G.J. Fleer, H.M.H. Scheutjens, and B. Vincent, *The stability of dispersions of hard spherical particles in the presence of nonadsorbing polymer*, Polymer Adsorption and Dispersion Stability (E.D. Goddard and B. Vincent, eds.), Washington, DC: ACS, 1984, pp. 245–263.

[66] P.J. Flory, *Principles of polymer chemistry*, NY: Cornell University Press, 1953.

[67] J. Friedrichs, J. Helenius, and D. J. Muller, *Quantifying cellular adhesion to extracellular matrix components by single-cell force spectroscopy*, Nature Protocols **5** (2010), 1353–1361.

[68] J. Friend and L. Yeo, *Fabrication of microfluidic devices using polydimethylsiloxane*, Biomicrofluidics / **4** (2010), no. 2, http://dx.doi.org/10.1063/1.3259624.

[69] F. Gaits, O. Fourcade, F. LeBalle, G. Gueguen, B. Gaige, A. GassamaDiagne, J. Fauvel, J. Salles, G. Mauco, M. Simon, and H. Chap, *Lysophosphatidic acid as a phospholipid mediator: pathways of systhesis*, FEBS Letters **410** (1997), no. 1, 54–58.

[70] A.J. Garcia, P. Ducheyne, and D. Boettiger, *Quantification of cell adhesion using a spinning disk device and application to surface-reactive materials*, Biomaterials **18** (1997), no. 16, 1091–1098.

[71] G. Gardos, *The function of calcium in the potassium permeability of human erythrocytes*, Biochemica et Biophysica Acta **30** (1958), no. 3, 653–654.

[72] P. Garstecki, M.J. Fuerstman, M. A. Fischbach, S.K.S. Whitesides, and G.M. Whitesides, *Mixing with bubbles: a practical technology for use with portable microfluidic devices*, Lab Chip **6** (2006), no. 2, 207–212.

[73] L.P. Ghislain, N.A. Switz, and W.W. Webb, *Measurement of scmall forces using an optical trap*, Review of Scientific Instruments **65** (1994), no. 9, 2762–2768.

[74] F. Gittes and C.F. Schmidt, *Signals and noise in micromechanical measurements*, Methods in Cell Biology **55** (1998), 129–156.

[75] R.B. Govekar and S.M. Zingde, *Protein kinase c isoforms in human erythrocytes*, Annals of Hematology **80** (2001), no. 9, 531–534.

[76] A.G. Hadd, D.E. Raymond, J.W. Halliwell, S.C. Jacobson, and J.M. Ramsey, *Microchip device for performing enzyme assays*, Analytical Chemistry **69** (1997), no. 17, 3407–3412.

[77] C.W.M. Haest, *Red cell membrane transport in health and disease*, ch. Distribution and movement of membrane lipids, pp. 1–25, Springer, 2003.

[78] Y. Harada and T. Asakura, *Radiation forces on a dielectric sphere in the rayleigh scattering regime*, Optics Communications **124** (1996), no. 5-6, 529–541.

[79] J. Helenius, C.P. Heisenberg, H.E. Gaub, and D. J. Muller, *Single-cell force spectroscopy*, Journal of Cell Science **121** (2008), 1785–1791.

[80] A.J. Hellem, C.F. Borchgrevink, and S.B. Ames, *The role of red cells in haemostasis: the relation between haematocrit, bleeding time and platelet adhesiveness*, British Journal of Haematology **7** (1961), no. 1, 42–50.

[81] J.F. Hoffman, W. joiner, K. Nehrke, O. Potapova, K. Foye, and A. Wickrema, *The hsk4 (kcnn4) isoform is the ca^{2+}-activated k^+ channel (gardo channel) in human erythroctyes*, Proceedings of the National Academy of Sciences of the United States of America **100** (2003), no. 12, 7366–7371.

[82] D.R. Holland, M. I. Steinberg, and W. Armstrong, *23187: a calcium ionophore that directly increases cardiac contractility*, Proceedings of the Society for Experimental Biology and Medicine **148** (1975), no. 4, 1141–1145.

[83] Mc D.K. Horne, A.M. Cullinane, P.K. Merryman, and E.K. Hodeson, *The effect of red blood cells on thrombin generation*, British Journal of Haematology **133** (2006), no. 4, 403.

[84] J.L. Hutter, *Comment on 'tilt of atomic force microscope cantilevers: effect on spring constant and adhesion measurements*, Langmuir **21** (2005), no. 6, 26302632.

[85] J.L. Hutter and J. Bechhoefer, *Calibration of atomic-force microscope tips*, Review of Scientific Instruments **64** (1993), no. 7, 18681873.

[86] J. Janzen and D.E. Brooks, *Do plasma proteins asorb to red cells?*, Clincal Hemorheology **9** (1989), 695–714.

[87] J. Janzen and D.E. Brooks, *A critical reevaluation of the nonspecific adsorption of plasma proteins and dextrans to eythroctyes and the role of these in rouleaux formation*, Interfacial Phenomena in Biological Systems (M. Bender, ed.), New York: Marcel Dekker, 1991, pp. 193–250.

[88] A.W.L. Jay, *Geometry of the human erythrocyte. i. effect of albumin on cell geometry*, Biophysical Journal **15** (1975), no. 3, 205–222.

[89] A. Jones and B. Vincent, *Depletion flocculation in dispersions of sterically-stabilized particles. 2. modifications to theory and further studies*, Colloids and Surfaces **42** (1989), no. 1-2, 113–138.

[90] A. Jung, *Untersuchung einer ca^{2+}- induzierten erythrocytenadhaesion mittels holographischer optischer pinzetten*, Ph.D. thesis, Universitt des Saarlandes, 2009.

[91] L. Kaestner, *Cation channels in erythrocytes- historical and future perspective*, The Open Biology Journal **4** (2011), no. 4, 27–34.

[92] L. Kaestner and I. Bernhardt, *Ion cahnnels in the human red blood cell membrane: their further investigation and physiological relevance*, Bioelectrochemistry **55** (2002), no. 1-2, 71–74.

[93] L. Kaestner, C. Bollensberg, and I. Bernhardt, *Non-selective voltage-activated cation channel in the human red blood cell membrane*, Biochimica et Biophysica Acta **1417** (1999), no. 2, 9–15.

[94] L. Kaestner, P. Christopherson, I.Bernhardt, and P. Benekou, *The non-selective voltage-activated cation channel in the human red blood cell membrane: reconciliation between two conflicting reports and further characterisation*, Bioelectrochemistry **52** (2000), 117–125.

[95] L. Kaestner, A. Juzeniene, and Moan J, *Erythrocytes- the "house elves" of photodynamic therapy*, Photochemical & Photobiological Sciences **3** (2004), no. 11-12, 981–989.

[96] L. Kaestner, P. Steffen, D.B. Nguyen, J. Wang, L. Wagner-Britz, A. Jung, C. Wagner, and I. Bernhardt, *Lysophosphatidic acid induced red blood cell aggregation in vitro*, Bioelectrochemistry **in press.** (2011).

[97] L. Kaestner, W. Tabellion, P. Lipp I., and Bernhardt, *Prostaglandin e_2 activates chanelle-mediated calcium entry in human erythrocytes: an indication for a blood clot formation supporting process*, Thrombosis and Haemostasis **92** (2004), 1269–1272.

[98] L. Kaestner, W. Tabellion, E. Weiss, I. Bernhardt, and P. lipp, *Calcium imaging of individual erythrocytes: Problems and aproaches*, Cell Calcium **39** (2006), no. 1, 13–19.

[99] A. E. Kamholz, B.H. Weigl, B.A. Finlayson, and P. Yager, *Quantitative analysis of molecular interaction in a microfluidic channel: The t-sensor*, Analytical Chemistry **71** (1999), no. 23, 5340–5347.

[100] A.E. Kamholz, E.A. Schilling, and P. Yager, *Optical measurement of transverse molecular diffusion in a microchannel*, Biophysical Journal **80** (2001), no. 4, 1967–1972.

[101] G. Kaplanski, C. Farnarier, O. Tissotand A. Pierres, A.M. Benoliel, M.C. Alessi, S. Kaplanski, and P. Bongrand Analysis of transient binding event, *Granulocyte-endothelium initial adhesion. analysis of transient binding events mediated by e-selectin in a laminar shear flow*, Biophysical Journal **64** (1993), no. 6, 1922–1933.

[102] K. Khairy, J. Foo, and J. Howard, *Shapes of red blood cells: Comparison of 3d confocal images with the bilayer-couple model*, Cellular and Molecular Bioengineering **1** (2008), no. 2-3, 173–181.

[103] B.A. Klarl, P.A. lang, D.S. Kempe, O. M. Niemoeller, A. Akel, M. Sobiesiak, K. Eisele, M. Podolski, S.M. Huber, T. Wieder, and F. Lang, *Protein kinase c*

mediates erythroctye "programmed cell death" following glucose depletion, American Journal of Physiology - Cell Physiology **290** (2006), no. 1, C244–C253.

[104] R.J. Klebe, *Isolation of a collagen-dependent cell attachment factor*, Nature **250** (1974), no. 463, 248–251.

[105] P. Kleinbongard, R. Schulz, M. Muench, T. Rassaf, T. lauer, A. Goedecke, and M. Kelm, *Red blood cells express a functional endothelial nitric oxide synthase*, European Heart Journal **27** (2006), no. 7, 127.

[106] F.A. Kuypers, R.A. Lewis, M. Hua, M.A. Schott, D. Discher, J.D. Ernst, and B.H. Lubin, *Detection of altered membrane phospholipid asymmetry in subpopulations of human red blood cells using fluorescently labeled annexinv*, Blood **87** (1996), no. 3, 1179–1187.

[107] K.S. Lang, P.A. Lang, C. Bauer, C. Duranton, T. Wieder, S.M. Huber, and F. Lang, *Mechanisms of suicidial erythrocyte death*, Cellular Physiology and Biochemistry **15** (2005), no. 5, 195–202.

[108] M.J. Lang and S.M. Block, *Resource letter: Lbot-1 laser based optical tweezers*, American Journal of Optics **71** (2003), no. 3, 201–215.

[109] P.A. Lang, S. Kaiser, S. Myssina, T. Wieder, F. Lang, and S.M. Huber, *Role of* ca^{2+}*- activated* k^+ *channels in human erythrocyte apoptosis*, American Journal of Physiology- Cell Physiology **285** (2003), no. 6, C1553–C1560.

[110] J. Lansman and D.H. Haynes, *Kinetics of a* ca^{2+}*-triggered membrane aggregation reaction of phospholipid membranes*, Biochimica et Biophysica Acta **394** (1975), no. 3, 335–347.

[111] T. Leinders, R.G.D.M. Vankleef, and H.P.M. Vijverberg, *Single* ca^{2+}*-activated* k^+ *channels in human erythroctyes:* ca^{2+} *dependencce of opening frequency but not of open lifetimes*, Biochimica et Biophysica Acta **1112** (1992), 67–74.

[112] V.L. Lew, N. Daw, D. Perdomo, Z. Etzion, R.M. Bookchin, and T. Tiffert, *Distribution of plasma membrane* ca^{2+} *pump activity in normal human red blood cells*, Blood **102** (2003), no. 12, 4206–4213.

[113] Q. Li, V. Jungmann, A. Kiyatkin, and P.S. Low, *Prostaglandin* e_2 *stimulates a* ca^{2+}*- dependen* k^+ *channel in human erythrocytes and alters cell volume and filterability*, Journal of Biological Chemistry **271** (1996), 18651–18656.

[114] H.W.G. Lim, M. Wortis, and R. Mukhopadhyay, *Stomatocyte-discocyte-echinocyte sequence of the human red blood cell: Evidence for the bilayer-couple hypothesis from membrane mechanics*, Proceedings of the National Academy of Sciences of the United States of America **99** (2002), no. 26, 16766–16769.

[115] R.I. Litvinov, H. Shuman, J.S. Bennett, and J.W. Weisel, *Binding strength and activation state of single fibrinogen-integrin pairs on living cells*, Proceedings of the National Academy of Sciences of the United States of America **99** (2002), no. 11, 7426–7431.

[116] M. Livio, E. Gotti, D. Marchesi, G. Mecca, G. Remuzzi, and G. de Gaetano, *Uraemic bleeding: role of anaemia and beneficial effect of red cell transfusions*, Lancet **2** (1982), no. 8306, 1013–1015.

[117] D. Lominadze and W. L. Dean, *Involvement of fibrinogen specific binding site in erythrocyte aggregation*, FEBS Letters **517** (2002), no. 1-3, 41–44.

[118] L. Lu, K.S. Ryu, and C. Liu, *A magnetic microstirrer and array for microfluidic mixing*, Journal of Microelectromechanical Systems **11 Issue 5** (2002), no. 5, 1057–7157.

[119] V. Luvira, S. Chamnanchamnunt, V. Thanachartwet, W. Phumratanaprapin, and A. Viriyavejakul, *Cerebral venous sinus thrombosis in severe malaria*, The Southeast Asian Journal of Tropical Medicine and Public Health **40** (2009), no. 5, 893–897.

[120] N. Mackman, *Triggers, teargets and treatments for thrombosis*, Nature **7181** (2008), 914–918.

[121] K. Macounova, C.R. Cabrera, M.R. Holl, and P. Yager, *Generation of natural ph gradients in microfluidic channels for use in isoelectric focusing*, Analytical Chemistry **72** (2000), no. 16, 3745–3751.

[122] A. Makhro, J. Wang, J. vogel, A.A. Bioldyrev, M. gassmann, L. Kaestner, and A. Bogdanova, *Functional nmda receptors in rat erythrocytes*, American Journal of Physiology - Cell Physiology **298** (2010), no. 6, C1315–1325.

[123] A.B. Mandoori, G.A. Barabino, B.H. Lubin, and F.A. Kuypers, *Adherence of phosphatidylserine-exposing erythrocytes to endothelial matrix thrombospondin*, Blood **95** (2000), no. 4, 1293.

[124] Z. Marton, G. Kesmarky, J. Vekasi, A. Cser, R. Russai, B. Horvath, and K. Toth, *Red blood cell aggregation measurements in whole blood and in fibrinogen solutions by different methods*, Clinical Hemorheology and Microcirculation **24** (2001), no. 2, 75–83.

[125] G.A. Matei, E.J. Thoreson, J.R. Pratt, D.B. Newell, and N.A. Burnham, *Precision and accuracy of thermal calibration of atomic force microscopy cantilevers*, Review of Scientific Instruments **77** (2006), 083703–1–083703–6.

[126] K. Meerschaert, V. De Corte, Y. De Ville, J. Vandekerckhove, and J. Gettemans, *Gelsolin and functionally similar actin-binding proteins are regulated by lysophosphatidic acid*, EMBO **17** (1998), no. 20, 5923–5932.

[127] U.K. Messmer and J. Pfeilschifter, *New insights into the mechanism for clearance of apoptotic cells*, Bioessays **22** (2000), no. 10, 878–881.

[128] M.Tomishige, Y. Sako, and A. Kusumi, *Regulation mechanism of the lateral diffusion of band 3 in erythrocyte membranes by the membrane skeleton*, Journal of Cell Biology **142** (1998), no. 4, 989–1000.

[129] T. Murakama, M. Hatanaka, and T. Murachi, *The cytosol of human-erythrocytes contains a highly ca^{2+}-sensitive thiol protease (calpain 1) and its specific inhibitor protein (calpastatin)*, The Journal of Biochemistry **90** (1981), no. 6, 1809–1816.

[130] G.B. Nash, R.b. Wendy, S.O. Sowemimo-Coker, and H.J. Meiselman, *Influence of cellular properties on red blood cell aggregation*, Clinical Hemorheology and Microcirculation **7** (1987), no. 4, 93–108.

[131] B. Neu and H.J. Meiselman, *Depletion mediated red blood cell aggregation in polymer solutions*, Biophysical Journal **83** (2002), no. 5, 2482–2490.

[132] K.C. Neuman and S.M. Block, *Optical trapping*, Review of Scientific Instruments **75** (2004), no. 9, 2787–2809.

[133] D.B. Nguyen, *Phosphatidylserine exposure in red blood cells: A suggestion for the active role of red blood cells in blood clot formation*, Ph.D. thesis, Saarland University, 2010.

[134] D.B. Nguyen, L. Wagner-Britz, S. Maia, P. Steffen, C. Wagner, L. Kaestner, and I. Bernhardt, *Regulation of phosphatidylserine exposure in red blood cells*, Cellular Physiology and Biochemistry **28** (2011), 847–56.

[135] J.Y. Noh, K.M Lim, O.N Bae, S.M. Chung, S.W. Lee abnd K.M. Joo, S.D. Lee, and J.H. Chung, *Procoagulant and prothrombotic activation of human erythroctyes by phosphatidic acid*, American Journal of Physiology - Heart and Circulatory Physiology **299** (2010), H347–H355.

[136] O.Baskurt, B. Neu, and H. H.J. Meiselman, *Red blood cell aggregation*, CRC Press taylor and Francis Group, 2012.

[137] S. Ohki, N. Duzgunes, and K. Leonards, *Phospholipid vesicle aggregation: effect of monovalent and divalent ions*, Biochemistry **21** (1982), no. 9, 2127–2133.

[138] Y.N. Ohshima, H. Sakagami, K. Okumoto, Tokoyoda A, T. Igarashi, K.B. Shintaku, S. Toride, H. Sekino, K. kabuto, and I. Nishio, *Direct measurment of infinitisemal depletion force in a colloid-polymer mixture by laser radiation pressure*, Physical Review Letters **20** (1978), no. 20, 3963–2966.

[139] T. Oonishi, K. Sakashita, N. Ishioka, N. Suematsu, H. Shio, and N.Uyesaka, *Production of prostaglandins e_1 and e_2 by adult human red blood cells*, Prostaglandin and other Lipid Mediators **56** (1998), no. 2-3, 89–101.

[140] P.Comfurius, P. Williamson, E.F. Smeets, R.A. Schlegel, E.M. Bevers, and R.F.A. Zwaal, *Reconstitution of phospholipid scramblase activity from human blood platelets*, Biochemistry **35** (1996), no. 24, 7631–7634.

[141] G. Popescu, T. Ikeda, K. Goda, C.A. Best-Popescu, M. Laposata, S. Manley, R.R. Dasari, K. Badizadegan, and M.S. Feld, *Optical measurement of cell membrane tension*, Physical Review Letters **21** (2006), no. 21, 218101.

[142] A. Pralle, M. Prummer, E.L. Florin, E.H.K. Stelzer, and J.K.H. Horber, *Three-dimensional high-resolution particle tracking for optical tweezers by forward scattered light*, Microscopy Research and Technique **44** (1999), no. 5, 378–386.

[143] B. C. Pressman, *Biological applications of ionophores*, Annual Review of Biochemistry **45** (1976), 501–530.

[144] A. Pribush, D. Zilberman-Kravits, and N. Meyerstein, *The mechanism of the dextran-induced red blood cell aggregation*, European Biophysics Journal **36** (2007), no. 2, 85–94.

[145] P.Steffen, C. Verdier, and C.Wagner, *Quantification of depletion induced adhesion of red blood cells*, submitted.

[146] P.H. Puech, K. Poole, D. Knebel, and D.J. Muller, *A new technical approach to quantify cell-cell adhesion forces by afm*, Ultramicroscopy **106,** (2006), no. 8-9, 637–644.

[147] S. Rad and B. Neu, *Impact of cellular properties on red-cell affinitiy in plasma like suspensions*, European Physical Journal **E30** (2009), no. 2, 135–140.

[148] M. W. Rampling, *"rouleaux formation -its causes, estimation and consequences"*, Doga Turkish Journal of Medical Sciences **14** (1990), 447–453.

[149] M.W. Rampling, *Red cell aggregation and yield stress*, Clinical Blood Rheology (G.D.O. Lowe, ed.), FL: CRC Press., 1988.

[150] S. Raphael, *Practice of hematology lynch's medical labratory technology*, Philadephia: W.B. Saunders Co., 1983.

[151] A. Rohrbach and E.H.K. Stelzer, *Optiocal trapping of dielectric particles in arbitrary fields*, Journal of the Optical Society of America **18** (2001), no. 4, 839–853.

[152] A. Rohrbach and E.H.K. Stelzer, *Three-dimensional position detection of optically trapped particles*, Journal of Apllied Physics **91** (2002), no. 5474, 5474–5488.

[153] A. Rohrbach and E.H.K. Stelzer, *Trapping forces, force constants, and potential depths for dielectric spheres in the peresence of spherical abberations*, Applied Optics **41** (2002), no. 13, 2494–2507.

[154] S.F. Santos, D. Zanette, H. Fischer, and R. Itri, *A systematic study of bovine serum albumin (bsa) and sodium dodecyl sulfate (sds) interactions by surface tension and small angle x-ray scattering*, Journal of Colloid and Interface Science **262** (2003), no. 2, 400–408.

[155] H.J. Schatzmann, *Atp-dependent ca^{2+}-extrusion from human red cells*, Experentia **22** (1966), 364–365.

[156] H. Schmid-Schnbein, R. Wells, and R. Schildkraut, *Microscopy and viscometry of blood flowing under uniform shear rate*, Journal of Applied Physiology **26** (1969), no. 5, 674–678.

[157] A.J. Schroit, J.W. Madsen, and Y. tanaka, *In vivo recognition and clearance of red blood cells containing phosphatidylserine in their plasma membranes*, Journal of Biological Chemistry **260** (1985), no. 8, 5131–5138.

[158] G.V.F. Seaman, *Electrokinetic behavior of red cells*, The Red Blood Cell, Ney York: Academic press, 1975, pp. 1135–1229.

[159] M. Seigneuret and P.F. Devaux, *Atp-dependent asymmetric distribution of sopinlabeled phospholipids in the erythrocyte membrane: Realtion to changes*, Proceedings of the National Academy of Sciences of the United States of America **12** (1984), 3751–3755.

[160] M.P. Sheetz and S.J. Singer, *Biologiocal membranes as bilayer couples. a molecular mechanism of drug-erythrocyte interactions*, Proceedings of the National Academy of Sciences of the United States of America **71** (1974), no. 11, 4457–4461.

[161] S.J. Singer and G.L. Nicolson, *Fluid mosaic model of structure of cell-membranes*, Science **4023** (1972), no. 4023, 720–731.

[162] J.B. Smith, C. Ingerman, J.J. Kocsis, and M.J. Silver, *Formation of prostaglandins during the aggregation of human blood platelets*, Journal of Clinical Investigations **52** (1973), no. 4, 965–969.

[163] P. Snabre, M. Bitbol, and P. Mills, *Cell disaggregation behavior in shear flow*, Biophysical Journal **51** (1987), no. 5, 795–807.

[164] P. Snabre and P. Mills, *Effect of dextran polymer on glycocalyx structure and cell electrophoretic mobility*, Colloid and Polymer Science **263** (1985), no. 6, 494–500.

[165] P. Steffen, *Charakterisierung der zell-zell-adhaesion roter blutzellen mittels holographischer optischer pinzetten*, Master's thesis, Universitt des Saarlandes, 2009.

[166] P. Steffen, A. Jung, D.B. Nguyen, T.Mller, I. Bernhardt, L. Kaestner, and C. Wagner, *Stimulation of human red blood cells leads to ca^{2+}-mediated intercellular adhesion*, Cell Calcium **50** (2011), no. 1, 54–61.

[167] J.G. Stout, Q.S. Zhou, T. Wiedmer, and P.J. Sims, *Change in the conformation of plasma membrane phospholipid scramblase induced by occupany of its ca^{2+} building site*, Biochemistry **37** (1998), no. 42, 14860–14866.

[168] K. Svoboda and S.M. Block, *Biological applications of optical forces*, Annual Review of Biophysics and Biomolecular Structure **23** (1994), 247–285.

[169] W. Tabellion, *Untersuchung des ca^{2+}-transports durch die membran einzelner erythrocyten mithilfe einen fluoreszenztz-imaging-systems*, Master's thesis, Universitt des Saarlandes, 2005.

[170] A.T. Taher, Z.K. Otrock, and M.D. Cappellini, *Thalassemia and hypercoagulability*, Blood Reviews **22** (2008), no. 5, 283–292.

[171] Y. Tanaka and A.J. Schroit, *Insertion of fluorescent phosphatidylserine into the plasma membrane of red blood cells- recogniction by autologous macrophages*, Journal of Biological Chemistry **258** (1983), no. 18, 1335–1343.

[172] M. Thie, R. Rospel, W. Dettmann, M. Benoit, M. Ludwig, H.E. Gaub, and H.W. Denker, *Interactions between trophoblast and uterine epithelium: monitoring of adhesive forces*, Human Reproduction **13** (1998), no. 11, 3211–3219.

[173] T. Tiffert, R.M. Bookchin, and V.L. Lew, *Calcium homeostasis in normal and abnormal human red cells*, Red Cell Membrane Transport in Health and Disease, Springer Verlag, 2003, pp. 373–405.

[174] M. Tomishige, Y. Sako, and A. Kusumi, *Regulation mechanism of the lateral diffusion of band 3 in eerythrocyte membranes by the membrane skeleton*, Journal of Cell Biology **142** (1998), no. 4, 989–1000.

[175] E.K. Tullius, P. Williamson, and R.A. Schlegel, *Effects of transbilayer phospholipid distribution on erythrocyte fusion*, Bioscience Reports **9** (1989), no. 5, 623–633.

[176] H.C. van de Hulst, *Light scattering by small particles*, Dover Publication Inc., New York, 1981.

[177] B. Vincent, *The calculation of depletion layer thickness as a function of bulk polymer concentration*, Colloids and Surfaces **50** (1990), 241–249.

[178] B. Vincent, J. Edwards, S. Emmett, and A. Jones, *Depletion flocculation in dispersions of sterically-stabilized particles ("soft spheres")*, Colloids and Surfaces **18** (1986), no. 2-4, 261–281.

[179] B.H. Weigl and P. Yager, *Silicon-microfabricated diffusion-based optical chemical sensor*, Sensors and Actuators B-Chemical **39** (1997), no. 1-3, 452–457.

[180] Wikipedia, *http://de.wikipedia.org/wiki/cantilever-(mikroskop).*

[181] Wikipedia, *http://de.wikipedia.org/wiki/zellmembran.*

[182] A.R. Williams, *The effect of bovine and human serum albumins on the mechanical properties on human erythrocyte membranes.*, Biochimica et Biophysica Acta **307** (1973), 58–64.

[183] P. Williamson, E.M. Bevers, E.F. Smeets, P. Comfurius, R.A. Schlegel, and R.F.A. Zwaal, *Continious analysis of the mechanism of activated transbilayer lipid movement in platelets*, Biochemistry **34** (1995), no. 33, 10448–10455.

[184] P. Williamson, A. Christie, T. kohlin, R.A. Schlegel, P. Comfurius, M. Harmsma, R.F.A. Zwaal, and E.M. Bevers, *Phospholipid scramblase activation pathways in lymphocytes*, Biochemistry **40** (2001), no. 27, 8065–8072.

[185] P. Williamson, A. Kulick, A. Zachowski, R.A. Schlegel, and P. P.F. Devaux, *ca^{2+} induces transbilayer redistribution of all major phospholipids in human erythrocytes*, Biochemistry **31** (1992), no. 27, 6355–6360.

[186] J.L.N. Wolfs, P. Comfurius, J.T. Rasmussen, J.F.W. Keuren, T. Lindhout, R.F.A. Zwaal, and E.M. Bevers, *Activated scramblase and inhibited aminophospholipid tranmslocase cause phosphatidylserine exposure in a distinct platelet fraction*, Cellular and Molecular Life Science **62** (2005), no. 13, 1514–1525.

[187] C. B. Wollheim, B. Blondel, P. A. Trueheart, A. E. Reynold, and G. W. G. Sharp, *Calcium-induced insulin release in monolayer culture of the endocrine pancreas*, The Journal of Biological Chemistry **250** (1975), no. 4, 1354–1360.

[188] B.L. Wood, D.F. Gibson, and J.F. Tait, *Increased erythrocyte phosphatidylserine exposure in sickle cell disease: Flow-cytometric measurement and clinical associations*, Blood **88** (1996), no. 5, 1873–1880.

[189] L.A. Woon, J.W. Holland, E.P.W. Kable, and B.D. Roufogalis, *ca^{2+} sensitivity of phospholipid scrambling in human red cell ghosts*, Cell Calcium **25** (1999), no. 4, 313–320.

[190] P. Worner and R. Brossmer, *Platelet aggregation and the release reaction induced by ionophores for divalent cations*, Thrombosis Research **6** (1975), no. 4, 295–305.

[191] L. Yang, D.A. Andrews, and P.S. Low, *Lysophosphatidic acid opens a ca^{2+} channel in human erythroctyes*, Blood **95** (2000), no. 7, 2420–2425.

[192] Y.Z. Yoon, J. Kotar, and P. Cicuta, *Non-linear mechanical response of the red blood cell*, Physical Biology **5** (2008), Issue 3.

[193] R.F.A. Zwaal, P. Comfurius, and E.M. Bevers, *Surface exposure of phosphatidylserine in pathological cells*, Cellular and Molecular Life Science **62** (2005), no. 9, 971–988.

[194] R.F.A. Zwaal and A.J. Schroit, *Pathophysiologic implications of membrane phospholipid asymmetry in blood cells*, Blood **89** (1997), no. 4, 1121–1132.

Danksagung

An Erster Stelle möchte ich mich bei Prof. Dr. Christian Wagner für die Aufnahme in seine Arbeitsgruppe und das interessante Thema meiner Doktorarbeit bedanken. Des Weiteren möchte ich mich für die hervorragende Betreuung, sowie für Anregungen und sehr hilfreiche Gespräche bedanken.

Bei Prof. Dr. Ingolf Bernhardt, Dr. Claude Verdier und Dr. Lars Kästner möchte ich mich für anregende Diskussionen im Rahmen unserer Kooperationen bedanken.

Ein besonderer Dank gilt den gesamten Arbeitsgruppen von Prof. Dr. Wagner und Dr. P.Huber für ein hervorragendes Arbeitsklima, welches in dieser Form wohl nur selten zu finden ist.

Ein großer Dank geht an die mechanische Werkstatt unter Leitung von Herrn M. Schmidt.

Ich möchte mich zudem bei allen Menschen bedanken, die mich während meines Studiums und meiner Promotion begleitet haben und es auf diese Weise zu einer unvergesslichen Erfahrung gemacht haben.

Danken möchte ich zudem Silvia Mommenthal und Oscar Elias für das Korrekturlesen meiner Arbeit.

Danke Silvia. Danke, dass du bei mir bist.

Ein nicht in Worte zu fassender Dank gilt meiner Mutter. Ohne ihre unglaubliche Aufopferung während meines gesamten Studiums, wäre es mir niemals möglich gewesen so weit zu kommen.

Eidesstattliche Versicherung

Hiermit versichere ich an Eides statt, dass ich die vorliegende Arbeit selbständig und ohne Benutzung anderer als der angegebenen Hilfsmittel angefertigt habe. Die aus anderen Quellen oder indirekt Übernommenen Daten und Konzepte sind unter Angabe der Quelle gekennzeichnet.
Die Arbeit wurde bisher weder im In- noch im Ausland in gleicher oder ähnlicher Form in einem Verfahren zur Erlangung eines akademischen Grades vorgelegt.

Saarbrücken,

Patrick Steffen